2012-04-18

Passive Resistance of Abutments with MSE Wingwalls

Nathanael G. Bingham
Brigham Young University - Provo

Passive Resistance of Abutments with MSE Wingwalls

Nathanael G. Bingham

A thesis submitted to the faculty of
Brigham Young University
in partial fulfillment of the requirements for the degree of

Master of Science

Kyle M. Rollins, Chair
Kevin W. Franke
Fernando S. Fonseca

Department of Civil and Environmental Engineering

Brigham Young University

June 2012

ABSTRACT

Passive Resistance of Abutments with MSE Wingwalls

Nathanael G. Bingham
Department of Civil and Environmental Engineering, BYU
Master of Science

Large scale static lateral load tests were performed on a pile cap under varying sand backfill configurations: no backfill, full-width dense sand backfill, dense sand slip plane confined backfill, and two configurations of dense sand MSE wall confined backfills. Efforts were made to maintain the relative compaction of the backfills for each of the tests near the same value. The MSE wall panel arrangement was varied to determine the effect of different reinforcement configurations on the passive resistance and wall panel displacement. Passive force-displacement curves were generated from each test.

It was found that the MSE design manual provided reasonable estimates of pullout resistance of bar mats in dense sand, and that the passive resistance of a soil backfill confined by MSE walls can be calculated with an increased friction angle using a log-spiral approach. Also, the amount the triaxial friction angle can be increased depends on how much the MSE wall panels displace outward.

Correlations were developed between the pressure on the pile cap and that on the MSE wall panels near the pile cap. Generally, the pressure on the wall panels was less than 10% of that which was on the adjacent pile cap, and decreased as the distance from the pile cap increased.

Finally, it was found that while limiting the backfill width decreases the ultimate passive resistance of the backfill, if the backfill is confined in a plane strain configuration the passive resistance per unit width is higher than that for an unconfined backfill.

Keywords: passive force, MSE walls, abutments, pile caps, lateral resistance

ACKNOWLEDGMENTS

I wish to acknowledge and thank my graduate committee chair and advisor, Dr. Kyle M. Rollins. He has provided countless hours of help with this research and supported me throughout my efforts as a graduate student. I also would like to thank the other members of my graduate committee, Dr. Kevin W. Franke and Dr. Fernando S. Fonseca. Their insights and expertise were much appreciated. Fellow students Alec Strassburg, Joshua Pruett, and Richard Christensen contributed significantly to the work and research completed, with other staff and students who participated in the testing completed at the airport. I appreciate their contributions. I would also like to thank Dr. Travis M. Gerber for his help in this research and in my studies.

In addition, I would like to thank my family and friends for their love and support throughout my graduate studies.

This research was supported by the California, Montana, New York, Oregon, and Utah Department of Transportation through a Federal Highway Administration (FHWA) pooled-fund arrangement under Contract Number 069148 "Dynamic Passive Pressure on Abutments and Pile Caps," the National Science Foundation (NSF) under Award Number CMS-0421312, and the George E. Brown, Jr. Network for Earthquake Engineering Simulation (NEES) which operates under NSF Award Number CMS-0402490. This support was greatly appreciated. The Utah Dept. of Transportation served as the lead agency for the pooled-fund study with Daniel Hsiao as the project manager.

The opinions, interpretations, and recommendations in this report are those of the author and do not necessarily represent those of the sponsors.

TABLE OF CONTENTS

LIST OF TABLES

LIST OF FIGURES

1 Introduction

1.1 Background

In the design of bridges, it is important to consider the inertial forces that could develop in an earthquake event. The columns and bridge abutments must be sized appropriately to transfer these loads to the ground. Larger loadings result in larger columns and larger and deeper piles, and in turn, higher costs. However, commonly placed adjacent to each side of a bridge is a soil backfill which can be counted on to transfer some of this load, lowering the engineering and construction cost of the other components of the bridge. While the maximum passive pressure of a soil backfill can be determined using the Rankine, Coulomb, or log-spiral theories, how the passive pressure develops as a function of deflection is less well defined. Research has been performed to determine the development of passive resistance with deflection (Cole and Rollins, 2006; Duncan and Mokwa, 2001), but limited research is available on the development of passive pressure in a soil backfill in the presence of mechanically-stabilized earth (MSE) walls.

In addition to earthquake applications, there are also applications in shorter bridges without expansion joints. In such a bridge, the abutments are expected to deflect as the bridge expands. It is important to know what load the backfill is placing on the bridge as a function of the displacement of the abutments.

1.2 Objective of Research

The research was undertaken to accomplish the following objectives:

1. Develop typical passive force vs. displacement curves for abutments with MSE wingwalls.
2. Evaluate the effect of MSE wall pull-out resistance on passive force-displacement curves.
3. Determine the additional force on MSE reinforcements produced by transverse loading.
4. Determine the appropriateness of using plane strain friction properties in computing ultimate passive force for abutments with MSE wingwalls
5. Compare passive force-displacement response for 3D and 2D conditions and evaluate correction factors for 3D shearing effects.

1.3 Scope

This thesis is limited to relations between MSE walls and backfill with side isolation. To accomplish the objectives of the research, a series of tests were performed which consisted of laterally loading a full-scale pile cap with varying backfill conditions. These backfills consisted of a plain sand backfill, sand backfill with plywood side isolation, and three MSE wall setups, with varying soil densities and arrangements of reinforcing.

Equipment was set up to monitor lateral displacements of the cap, walls, and backfill. Outward movement of the walls was monitored, as was strain in selected bar mats. Elevations of the backfill surface were taken to monitor heave and settlement after the testing, and the

development of cracks on the surface of the backfill was monitored and mapped incrementally throughout the testing process. Data gathered was analyzed to determine whether relationships existed between the backfill conditions; the results of this analysis and the interpretation thereof are presented herein.

2 Literature Review

2.1 Determination of Ultimate Passive Force

Rankine Method

The Rankine method of determining the passive earth force calculates the passive pressure acting on a surface assuming a frictionless interface between the surface and the soil. If the backfill is level, the soil cohesionless, and the surface is at 90° from horizontal, then the equation for determining the ratio of effective stresses, K_p, is shown in Equation 2-1. This ratio is multiplied by the vertical effective stress to determine the horizontal passive pressure at any depth along the surface. The passive force is determined from this using basic soil mechanics, as shown in Equation 2-2.

$$K_p = \tan^2\left(45 + \frac{\phi'}{2}\right) \tag{2-1}$$

where K_p is the ratio of effective stresses
ϕ' is the friction angle from effective stress

$$P_p = \frac{1}{2} K_p \gamma H^2 \tag{2-2}$$

where K_p is the ratio of effective stress
γ is the unit weight of the soil
H is the height of the surface

Coulomb Method

The Coulomb method of determining passive earth forces is more complex than the Rankine method. The determination of K_p using the Coulomb method is shown in Equation 2-3.

$$K_p = \frac{\cos^2(\phi'+\theta)}{\cos^2\theta\cos(\delta'-\theta)\left[1-\sqrt{\frac{\sin(\phi'+\delta')\sin(\phi'+\alpha)}{\cos(\delta'-\theta)\cos(\alpha-\theta)}}\right]^2} \tag{2-3}$$

where K_p is the ratio of effective stress
ϕ' is the friction angle from effective stress
θ is the angle of wall batter from vertical
δ' is the angle of friction between the soil and the wall
α is the angle of backfill slope

However, if the wall is vertical ($\theta = 0$) and the backfill is flat ($\alpha = 0$) Equation 2-3 simplifies to Equation 2-4. The passive force is determined in the same way as was used in the Rankine method, using Equation 2-2.

$$K_p = \frac{\cos^2\phi'}{\cos\delta'\left[1-\sqrt{\frac{\sin(\phi'+\delta')\sin\phi'}{\cos\delta'}}\right]^2} \tag{2-4}$$

Log-Spiral Method

The Log-Spiral method of determining the ultimate passive force involves a Prandtl section and a Rankine section. The determination of the ratio of effective stress is difficult using the Log-Spiral method, but can be simplified by using charts, such as the chart from the US

2.2 Determination of Passive Force as a Function of Deflection

CalTrans

The Caltrans method of determining passive force versus deflection was based on tests performed at UC Davis (Maroney, 1995). Equations were derived for the initial stiffness of an abutment backfill and for the ultimate resistance, and are shown in Equation 2-5 and Equation 2-6.

$$K_{abut} = 20kips/in/ft * w_{abut} * \left(\frac{h}{5.5ft} \right) \tag{2-5}$$

$$P_{ult} = 5.0ksf * A_{abut} * \left(\frac{h}{5.5ft} \right) \tag{2-6}$$

where K_{abut} is the initial stiffness
P_{ult} is the ultimate force
w_{abut} is the width of the abutment (ft)
h is the height of the abutment (ft)
A_{abut} is the area of the abutment (ft^2)

The force develops linearly from 0 to the ultimate force P_{ult} at a slope equal to the initial stiffness K_{abut}. At this point the force remains at the ultimate value for any displacement. The dimensions of the abutment are considered in this method, but the soil properties of the backfill are not considered at all.

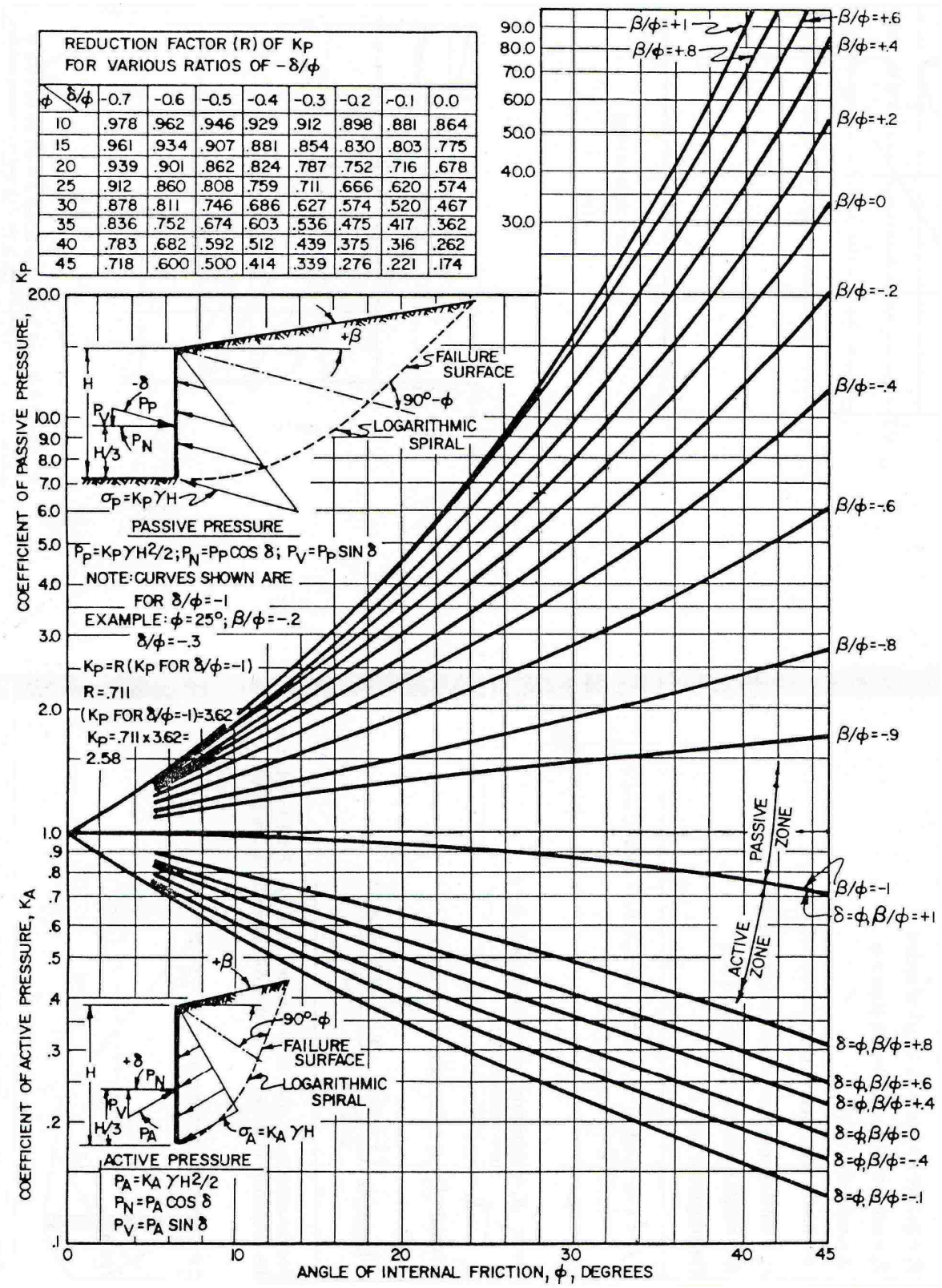

Figure 2-1: Active and passive coefficients with wall friction (US Navy Manual, 1982).

AASHTO LRFD (Log-Spiral)

The AASHTO LRFD Bridge Design Specifications, 5th Edition (2010) specifies the use of Log-Spiral charts to determine the passive resistance acting on the pile cap. Table C3.11.1-1 says that for dense sand the movement required to develop the ultimate passive resistance is only 1% of the wall height, 4% for loose sand. However, the commentary on page 3-105 states that for loose sand a displacement of 5% of the wall height may be needed to fully develop the passive resistance; for dense sand, the displacement is less than 5% of the wall height, but 5% represents a conservative estimate. The AASHTO Guide Specifications for LRFD Seismic Bridge Design (2009) states that a wall friction of 2/3 of the friction angle should be used when using this method.

Duncan and Mokwa/PYCAP

PYCAP is a Microsoft Excel Spreadsheet developed by Duncan and Mokwa (2001) to estimate the passive resistance of a soil backfill. It uses a log-spiral approach, with a hyperbolic displacement model as shown in Figure 2-2. The spreadsheet includes an Ovesen-Brinch-Hansen correction factor that has a maximum value of 2, to account for end effects near the edge of the pile cap. A solution is obtained iteratively by varying the location of the log spiral center until a minimum resistance is found. Equation 2-7 shows how the ultimate passive resistance is calculated, while Equation 2-8 shows how the resistance develops as a function of displacement.

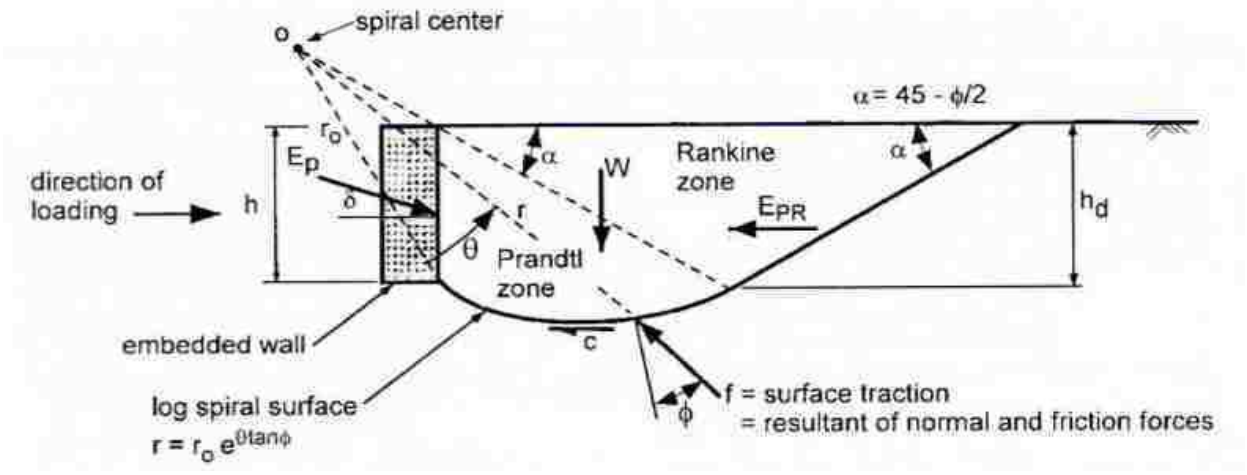

Figure 2-2: Log spiral failure mechanism (Duncan and Mokwa, 2001).

#

$$P_{ult} = (E_p)(M)(b) \tag{2-7}$$

$$P = \frac{y}{\left[\frac{1}{K_{\max}} + R_f \frac{y}{P_{ult}}\right]} \tag{2-8}$$

where P_{ult} is the total passive resistance on the structure (units of force)
E_p is the passive resistance per unit length (units of force/length)
M is the Ovesen-Brinch Hansen correction factor for 3D effects (dimensionless)
b is the length of structure perpendicular to plane of analysis (units of length)
P is the passive resistance (units of force)
y is the deflection (units of length)
$K_{\max}$ is the initial stiffness, which is the initial slope of the load-deflection curve (units of force/length)
R_f is the failure ratio, and is equal to P_{ult} /hyperbolic asymptote (dimensionless)

$K_{\max}$ is based on the elastic half-space developed by Douglas and Davis (1964). The development of the force versus deflection as calculated in Equation 2-8 is shown in Figure 2-3.

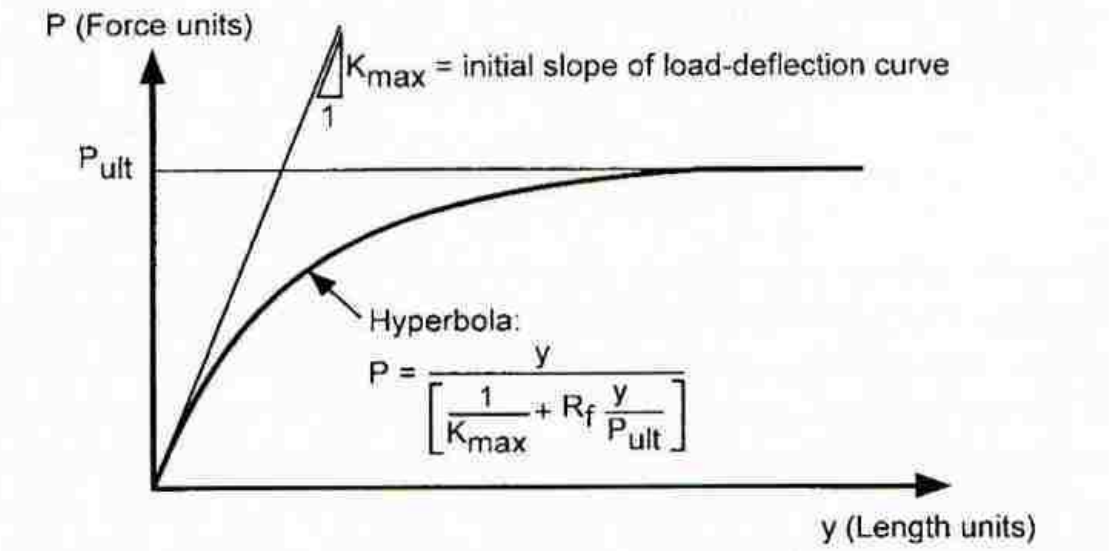

Figure 2-3: Hyperbolic load-deflection curve (Duncan and Mokwa, 2001).

Shamsabadi/ABUT

Shamsabadi et al (2007) developed a program to predict the passive resistance of a backfill based on a log-spiral hyperbolic model (LSH). The program uses a log-spiral wedge and a hyperbolic stress-strain relationship model to estimate the load-displacement curve for a given geometry and soil. The input parameters are the soil weight, friction angle, soil to wall friction angle, cohesion, adhesion, failure ratio, poisson ratio, surcharge, and surface geometry. In addition, a strain at 50%, ε_{50}, of the failure strength is required.

The program methodology is to divide the backfill soil into slices, and then solve the force-based equilibrium equations for mobilized logarithmic spiral failure surfaces, as shown in Figure 2-4. The results of the program match well the data from tests performed by Cole (2003) as shown in Figure 2-5. The values of ε_{50} recommended by Shamsabadi for the program are shown in Table 2-1.

Table 2-1: Recommended Values of ε50 (Shamsabadi et at, 2007)

	ε_{50}	
Predominant Value	Range	Presumptive value
Gravel	0.001-0.005	
Clean sand (0-12% fines)[a]	0.002-0.003	0.0035
Silty sands (12-50% fines)[a]	0.003-0.005	
Silt	0.005 (nonplastic)-0.007 (plastic	
Clay	0.0075	0.007

[a]Fines is the percentage by weight of soil grain sizes smaller than 0.075 mm.

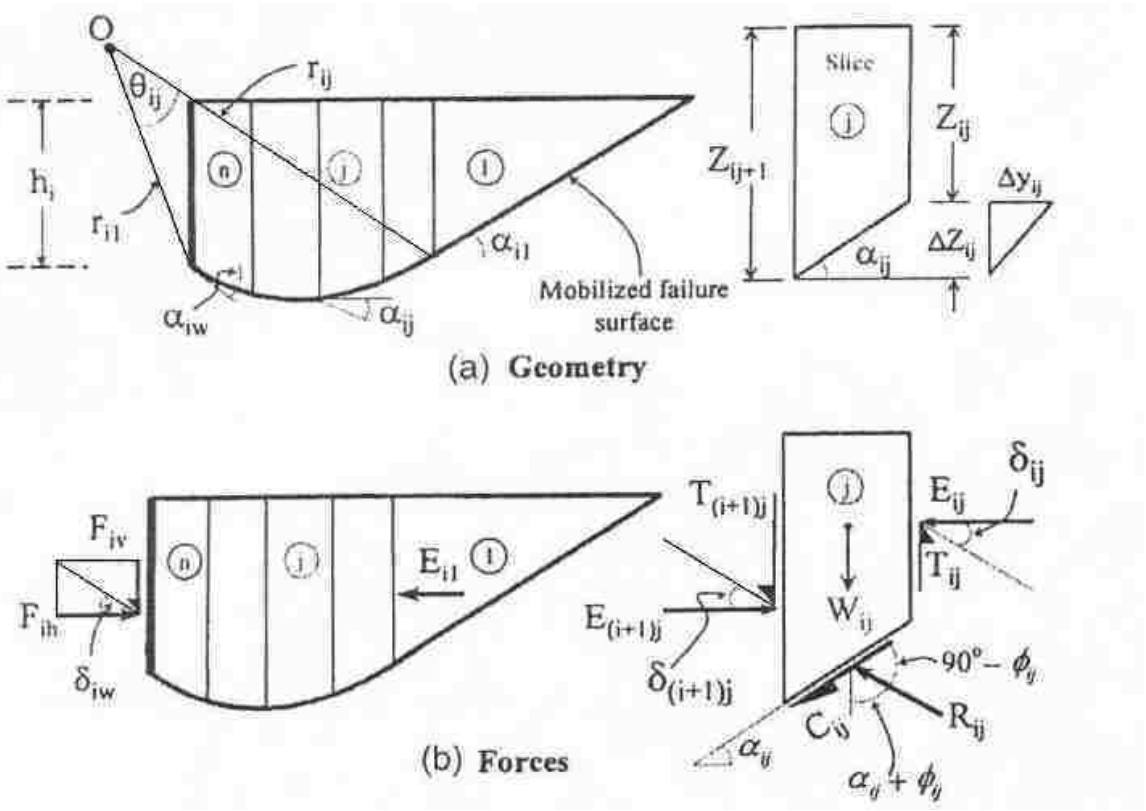

Figure 2-4: Mobilized logarithmic-spiral passive wedge (Shamsabadi et at, 2007).

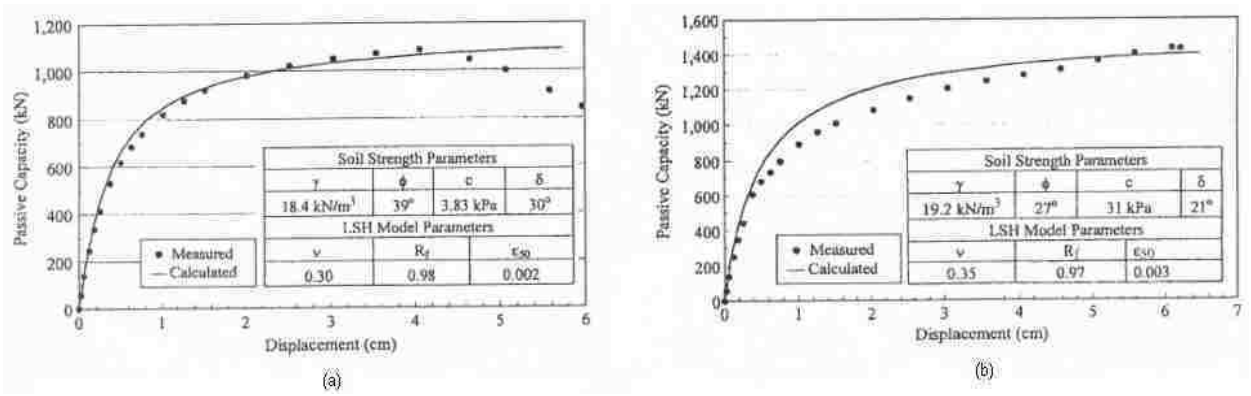

Figure 2-5: Comparison of measured and LSH predicted passive pressure for (a) clean sand and (b) silty sand (Shamshabadi et al, 2007).

2.3 Plane Strain Friction Angle

Rowe (1969) demonstrates that the direct shear friction angle can be increased to account for plane strain loading conditions. A relationship is established between the direct shear and plane strain friction angles; this is shown in Equation 2-9. This demonstrates a basis for changing the friction angle for differing loading scenarios.

$$\tan \phi_{ds} = \sin \phi_{ps} \tag{2-9}$$

where ϕ_{ds} is the friction angle from direct shear
ϕ_{ps} is the friction angle from plane strain

Ladd et al (1977) produced a plot that is shown in Figure 2-6. He states that the triaxial friction angle can be increased to account for plane strain loading conditions, 2° to 4° for loose sands, and 4° to 9° for dense sands.

The Manual on Estimating Soil Properties for Foundation Design cites the preceding two articles, and summarizes them by stating that the triaxial friction angle can be increased by 7 to 18 percent to account for plane strain loading conditions, with an average of 12 percent. Figure 2-7 is taken from this manual; from this figure it appear that for dense sands, the triaxial friction angle can be increased from 10 to 18 degrees to account for plain strain loading conditions.

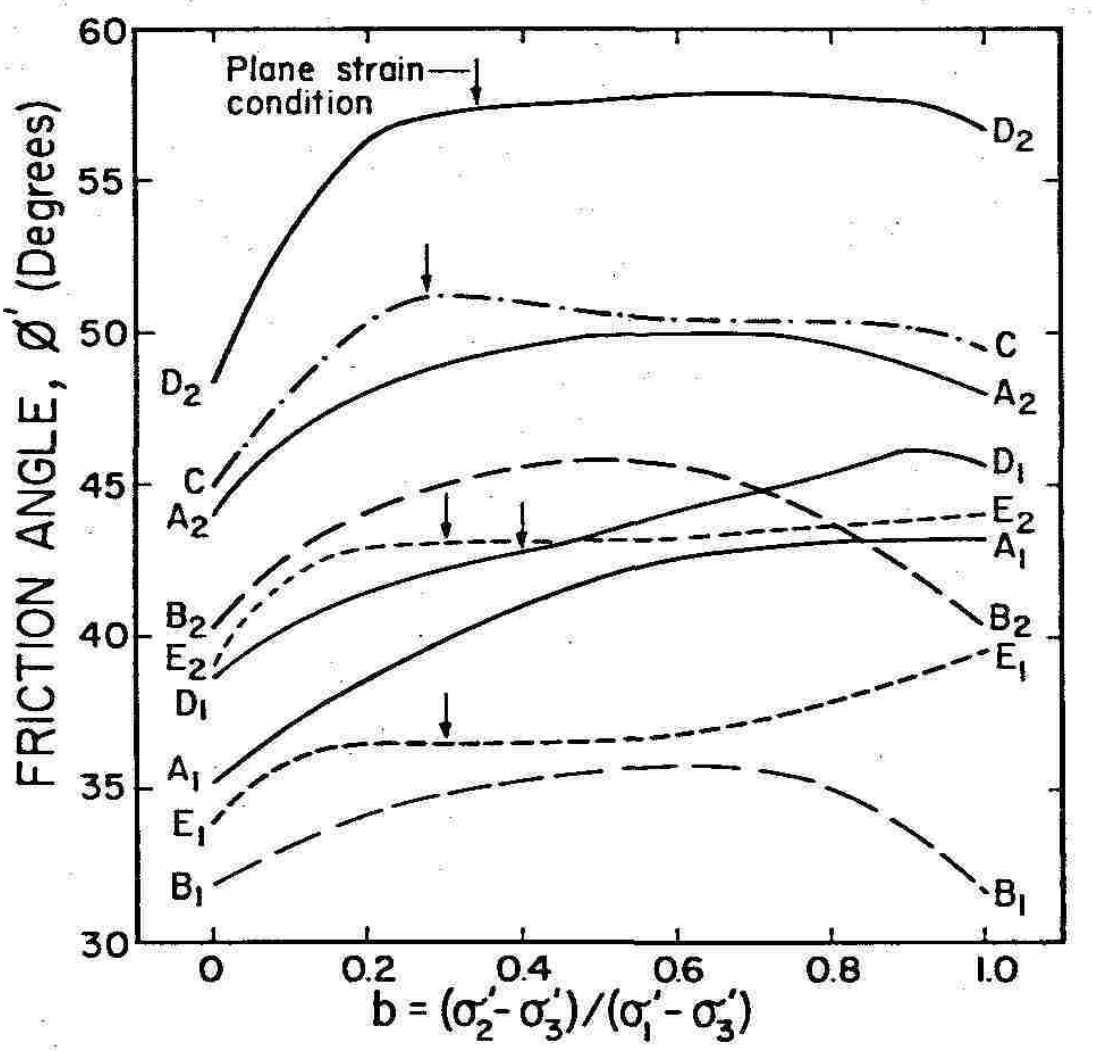

Figure 2-6: Friction angle versus b (Ladd et al, 1977).

2.4 Design of and Tests With MSE Walls

The MSE walls used in the tests with MSE walls were designed for internal stability according to the AASHTO Simplified Method described in the manual Mechanically Stabilized Earth Walls and Reinforced Soil Slopes, Design and Construction Guidelines, produced by the Federal Highway Administration (2001). This manual provides a design pullout value for the mats.

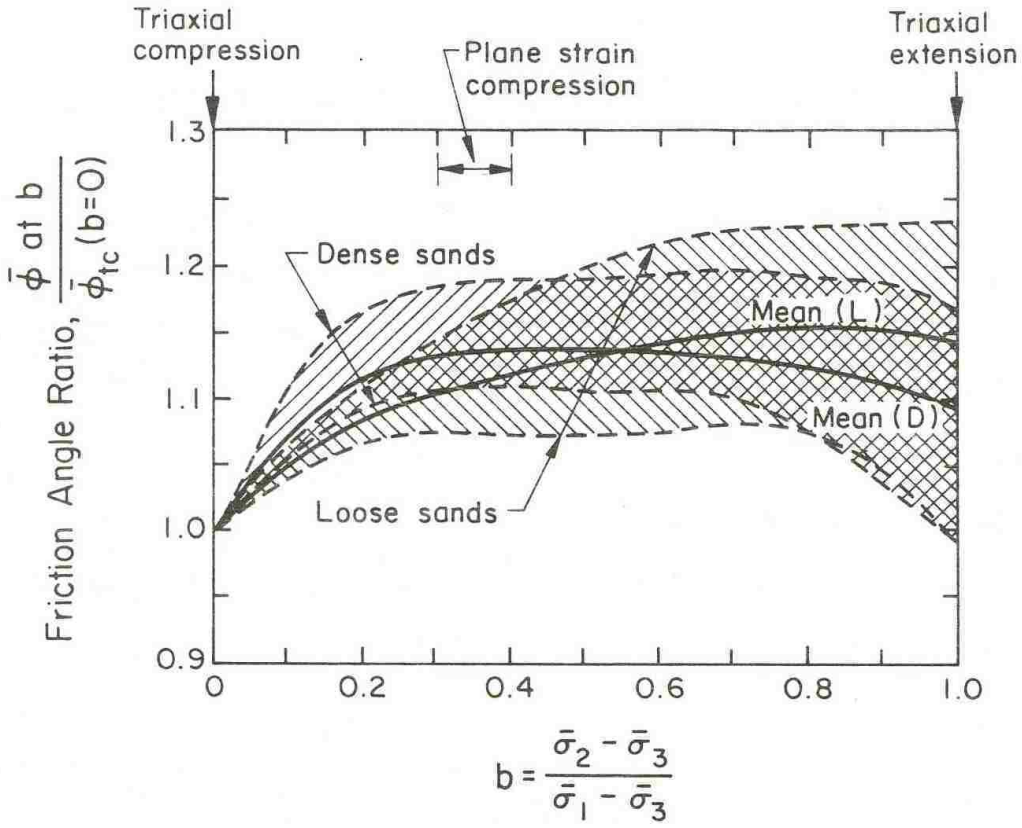

Figure 2-7: Increase in friction angle as a function of intermediate effective pricnciple stress factor (Kulhawy and Mayne, 1990).

Bathurst, Nernheim, and Allen (2009) analyzed the AASHTO Simplified Method using an expanded database of information and statistics to determine whether it is reasonably accurate

in predicting loads in steel reinforcement. Their results showed that with bar mats the AASHTO Simplified Method design procedure is slightly conservative.

Tests performed by Rollins and Heiner (2010) were the first to confine the backfill using MSE wingwalls. The tests reported in this thesis are intended to further explore the research performed. Rollins and Heiner found that despite pullout of the MSE wall panels, the passive force per effective width was 28 kips/ft versus 25 kips/ft of effective width obtained with an unconfined backfill.

Mitchell and Villet (1987) present the results of pullout tests performed with VSL bar mats, and give an anchorage factor for various tests. The anchorage factor is a similar concept to the pullout resistance factor used in the FHWA manual. Results from testing performed will be compared to the results presented by Mitchell and Villet.

3 Geotechnical Site Conditions

3.1 Existing Conditions

The test site is located about 1000 ft (300 meters) north of the air traffic control tower at the Salt Lake City airport. The location of the site is shown in Figure 3-1. The original site consisted of 5 ft of densely compacted sandy gravel fill over alternating layers of silty clay and sand to a depth of 100 ft. In 2004, the gravel and 3 ft of silty clay were excavated and replaced with compacted sand to a depth of about 8 ft. This site is ideally suited for tests because it is flat and open, allowing access of heavy equipment needed to handle the test equipment and materials. In addition, there are no overhead obstructions or subsurface utilities.

Tests have been performed at this site over the past 15 years. Because of this, many geotechnical investigations have been performed, and a wealth of information is available about the site soil characteristics. Boreholes and cone penetration soundings in the vicinity of the site are shown in Figure 3-2. The CPT sounding that shows the soil conditions best is CPT-06-M, shown in Figure 3-3.

Tests have been performed on undisturbed samples from the boreholes. Other in-situ tests have been performed on the site, including vane shear tests, pressuremeter tests, shear wave velocity tests, and dilatometer tests. The information on these tests can be found in Rollins and Peterson (1996), Snyder (2003), and Christensen (2006).

Figure 3-1: Location of test site.

Most of the support of laterally-loaded piles comes from the top 5 to 10 pile diameters. As a result, detailed soil information for this zone is of greatest interest. The native surface materials consist of low-plasticity silts and clays, classified as ML, CL-ML, or CL according to the Unified Soil Classification System (USCS). Hydrometer tests performed on the soil show that 50%-75% of the soil consists of silt-sized particles, while 10%-25% consists of clay-size particles. Figure 3-4 shows the shear strength, shear wave velocity, and soil stress, along with the soil profile. As can be seen, the undrained shear strength is generally from 500 to 1000 psf, though test results show values as high as 2000 psf. The higher strengths near the ground surface are a result of overconsolidation due to desiccation. The soil is overconsolidated to a depth of

about 30 ft, but the overconsolidation ratio decreases with depth. Throughout the tests the water table remained at a depth of 5 to 5.5 ft.

3.2 Backfill Soil

The average particle-size distribution is shown in Figure 3-5. This is an average of sieve analyses performed at various dates throughout the testing period. Multiple tests were performed to account for any addition of external materials that could have been mixed into the sand during the cycles of excavation and backfill. The onsite compaction results for each of the tests are shown in Figure 3-6 through Figure 3-9. As can be seen in these figures, the median onsite compaction was close to the 96% of modified Proctor compaction target, with the largest difference between median density and 96% of modified Proctor density being about 1.6 pcf. The densities in these figures are dry densities. The results of laboratory testing to determine the friction angle are summarized in Table 3-1. The triaxial friction angle of 43.1° was used and increased to account for plane strain loading, as was explained in Section 2.3.

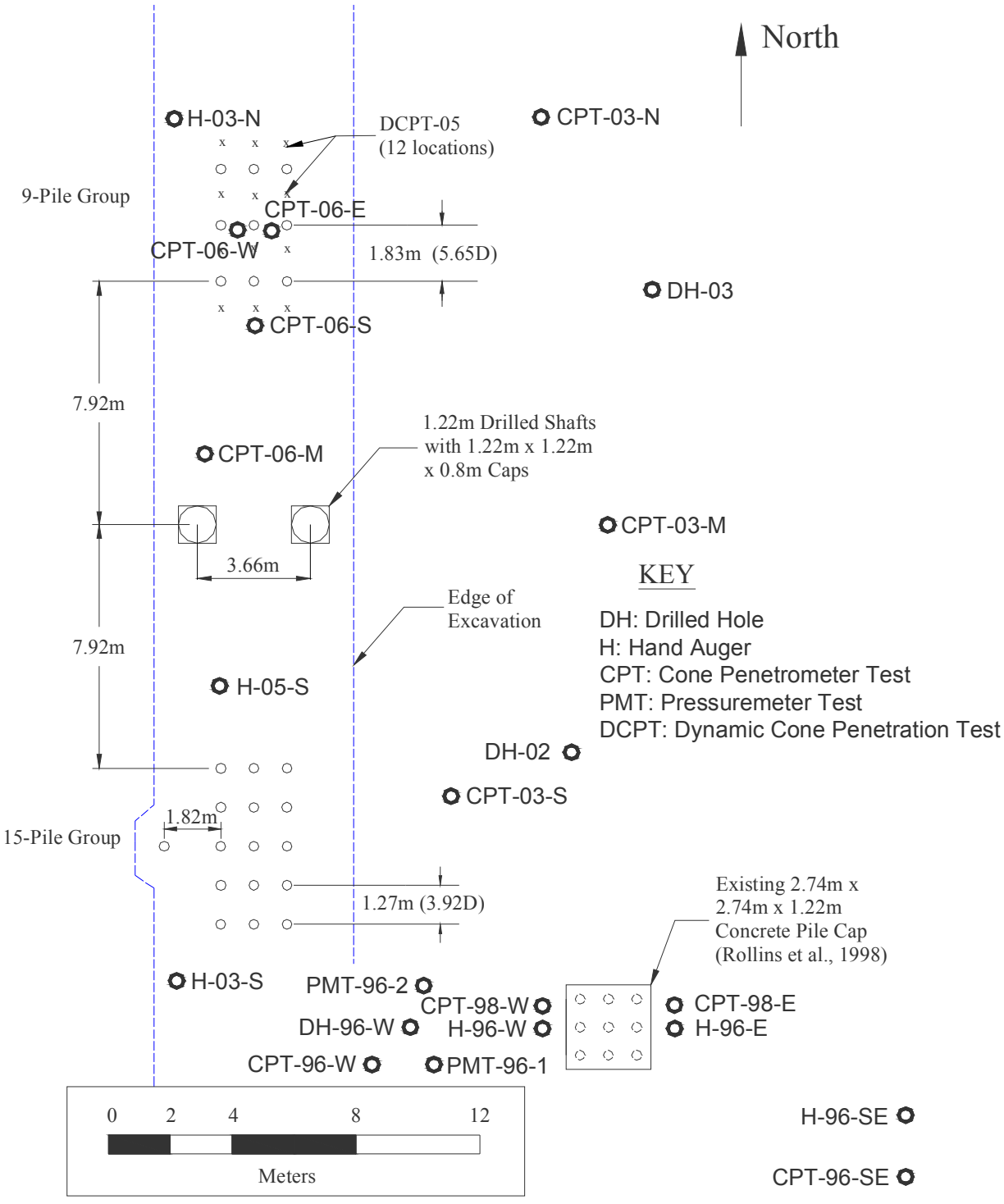

Figure 3-2: Locations of geotechnical investigations.

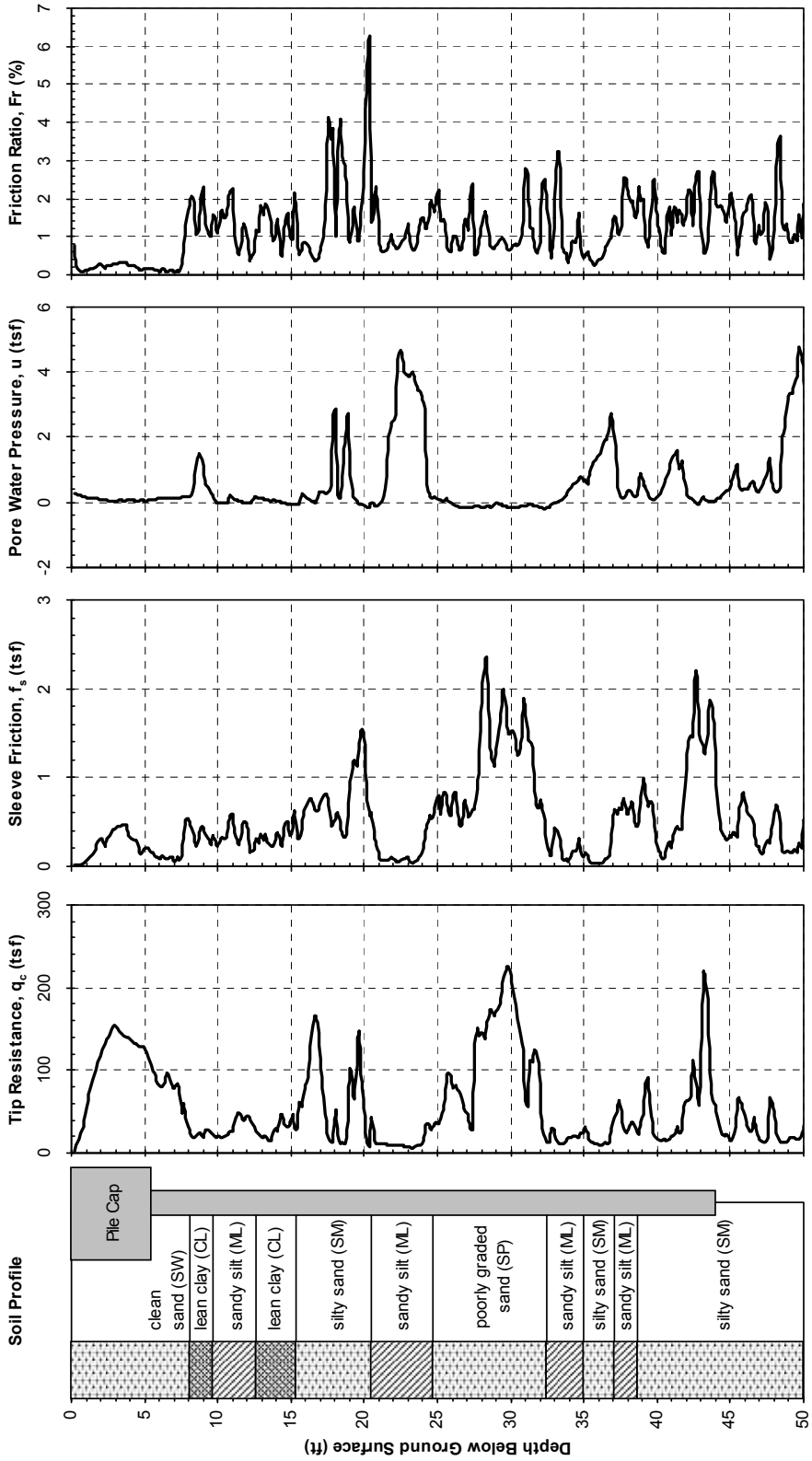

Figure 3-3: CPT-06-M.

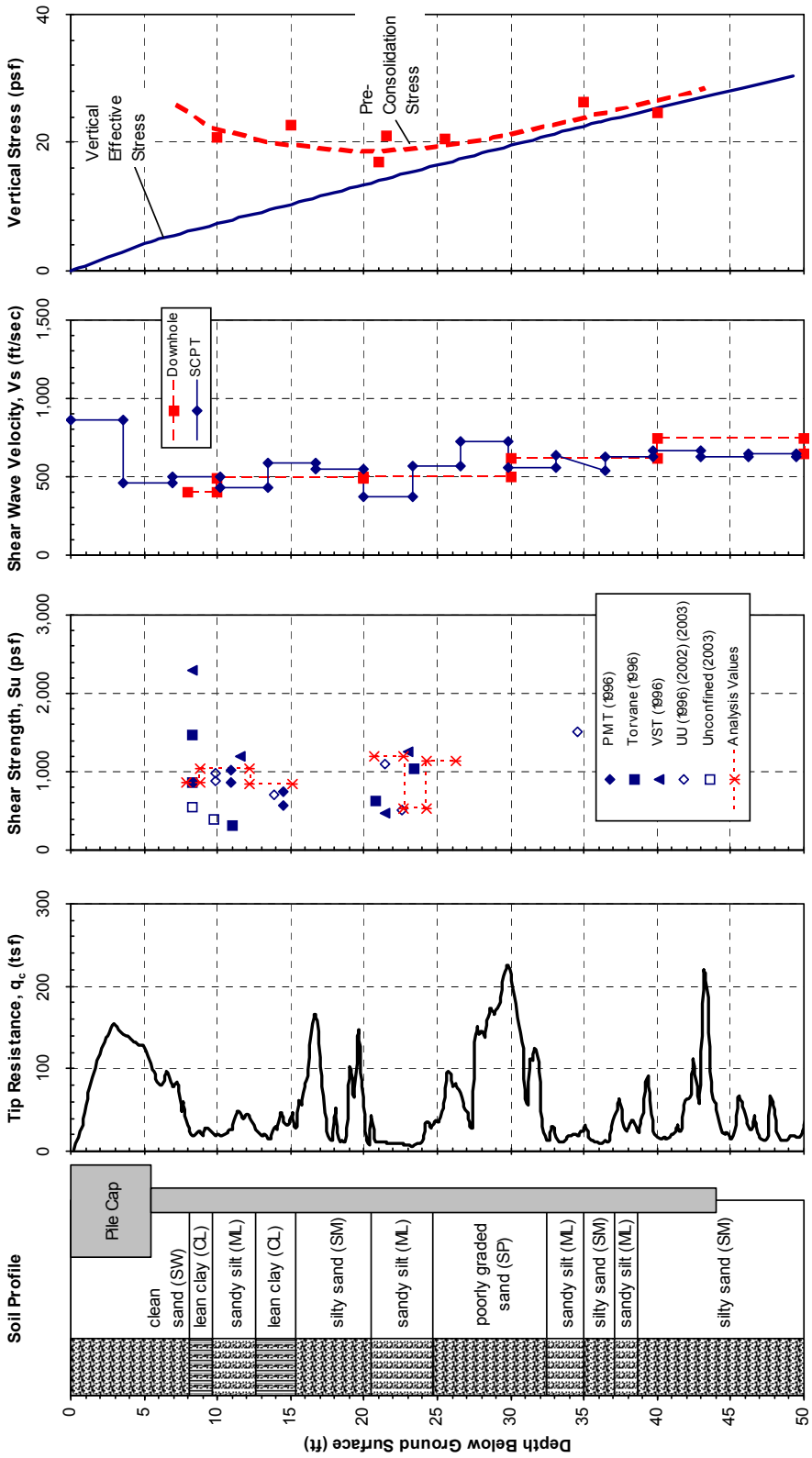

Figure 3-4: Soil properties.

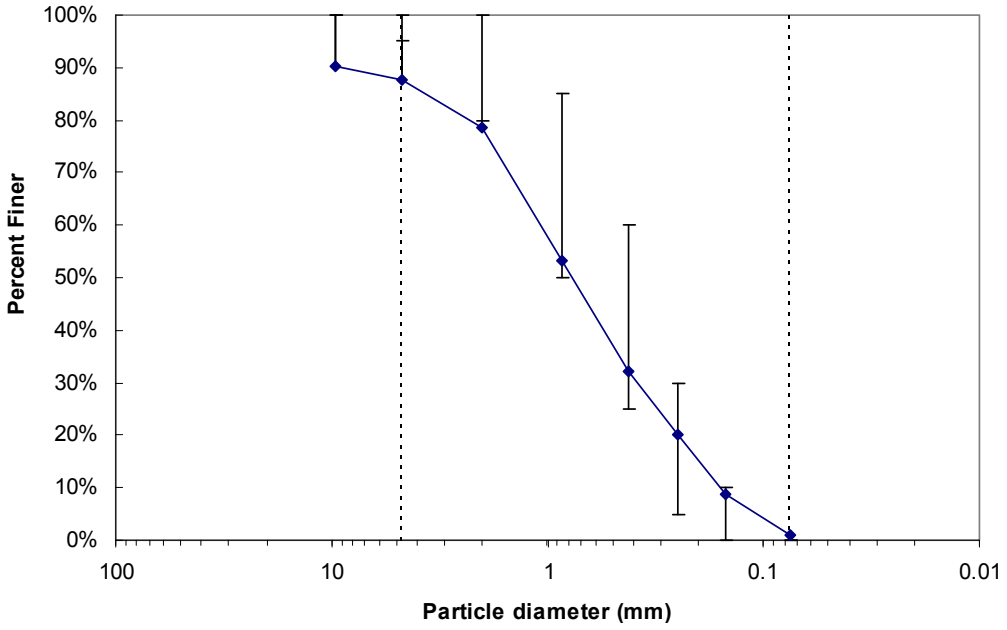

Figure 3-5: Particle-size distribution.

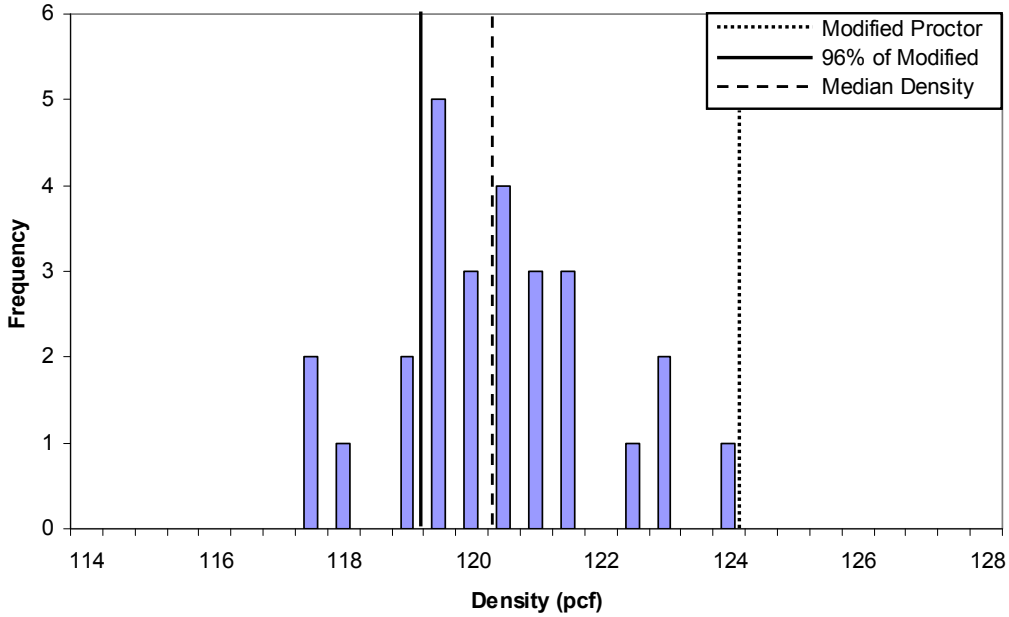

Figure 3-6: Unconfined dense sand backfill compaction testing results.

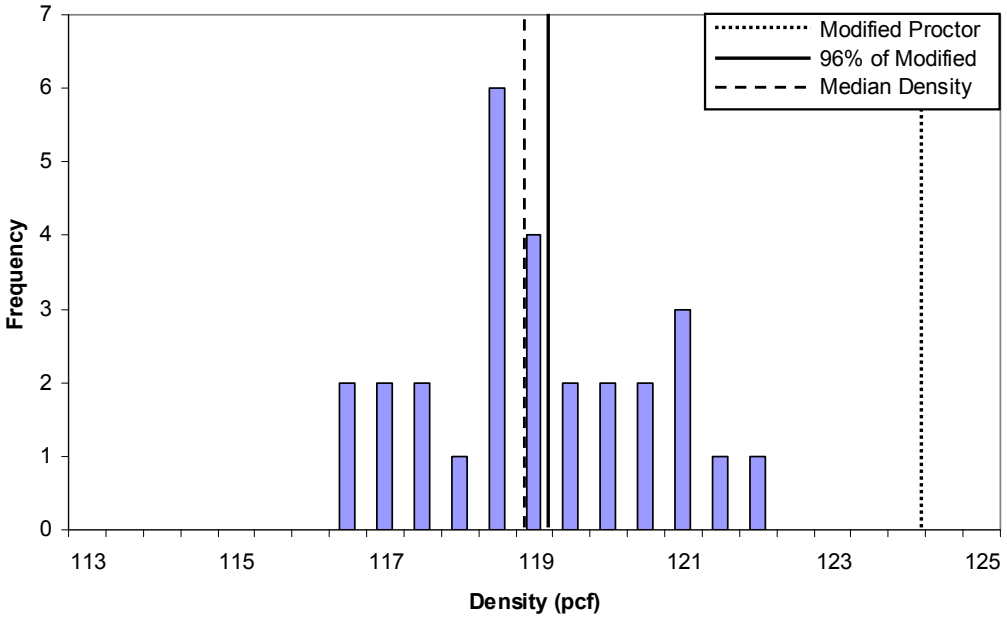

Figure 3-7: 2D slip planes compaction testing results.

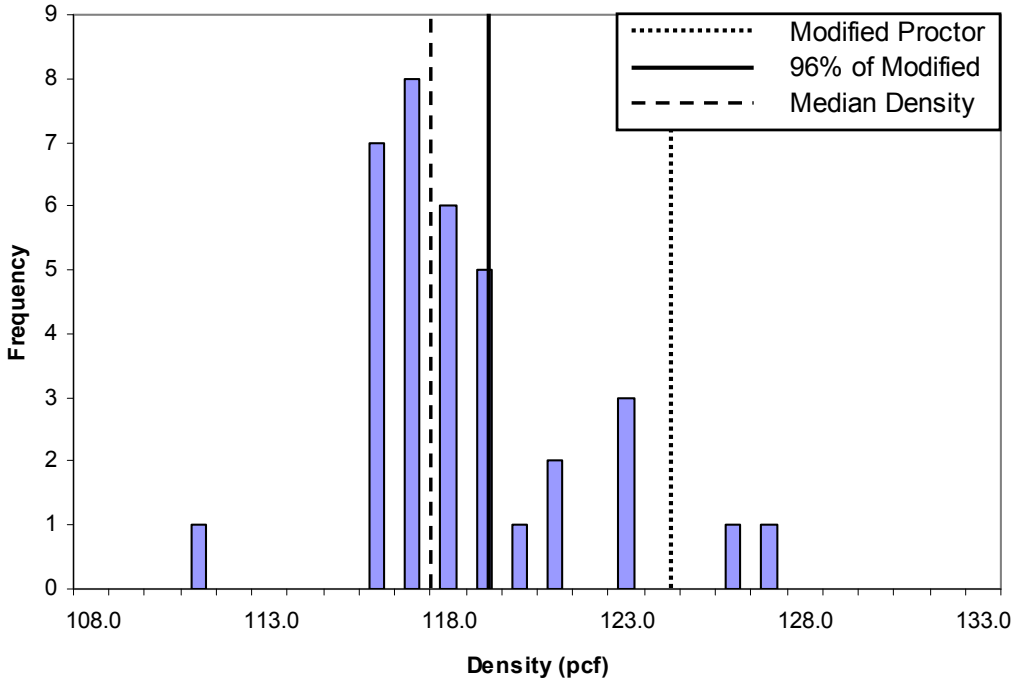

Figure 3-8: MSE test 1 compaction testing results.

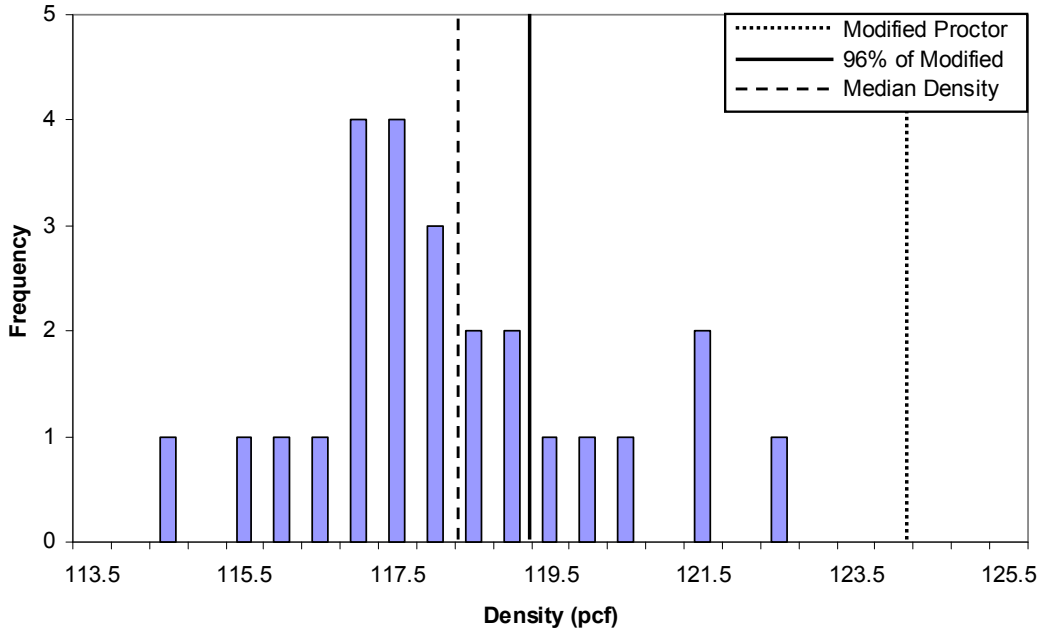

Figure 3-9: MSE test 2 compaction testing results.

Table 3-1: Summary of Soil Friction Angle Testing

	Peak		Ultimate	
Source of Test Result	φ (deg)	c (psf)	φ (deg)	c (psf)
Direct Shear (full range)	48	1020	37.3	15.9
Direct Shear (full range, zero cohesion)	50.9	0	37.4	0
Direct Shear (250 psf to 3000 psf)	52.2	751	36.2	47.4
Direct Shear (250 psf to 3000 psf, zero cohesion)	58.8	0	36.7	0
Direct Shear (6000 psf to 12000 psf)	44.3	2280	36.7	204
Direct Shear (6000 psf to 12000 psf, zero cohesion)	50.5	0	37.4	0
Triaxial	43.1	823	40.6	459
Triaxial (zero cohesion)	47.6	0	43.5	0

4 Site Layout And Instrumentation

This chapter provides a description of the basic layout of the load testing equipment and instrumentation on the site which were common for each of the tests performed. In addition, a description is provided of the basic instrumentation used for each of the MSE wall setups.

4.1 Instrumentation and Test Layout Common to all Load Tests

The basic equipment setup consists of a pile cap, which is loaded laterally using two hydraulic actuators reacting against a load frame, as shown in Figure 4-1. An independent reference frame is setup between the load frame and pile cap to enable the measurement of displacements and rotations of the pile cap. The following discussion provides additional information regarding each component of the load testing system.

4.1.1 Loading System and Reaction Piles

The lateral load on the pile cap is applied by two MTS actuators. Each actuator is capable of applying 600 kips of force in compression and 450 kips tension. The actuators react against a load frame consisting of two 28 ft long beams which are 5 ft 4 inches deep. The beams are connected to two-4 ft diameter drilled shafts and a sheet pile wall with eight 2.5 inch diameter high strength threaded bars tensioned to 100 kips each. The drilled shafts are 12 ft on center. The west shaft extends to a depth of 55.2 ft, while the east shaft is 70 ft deep.

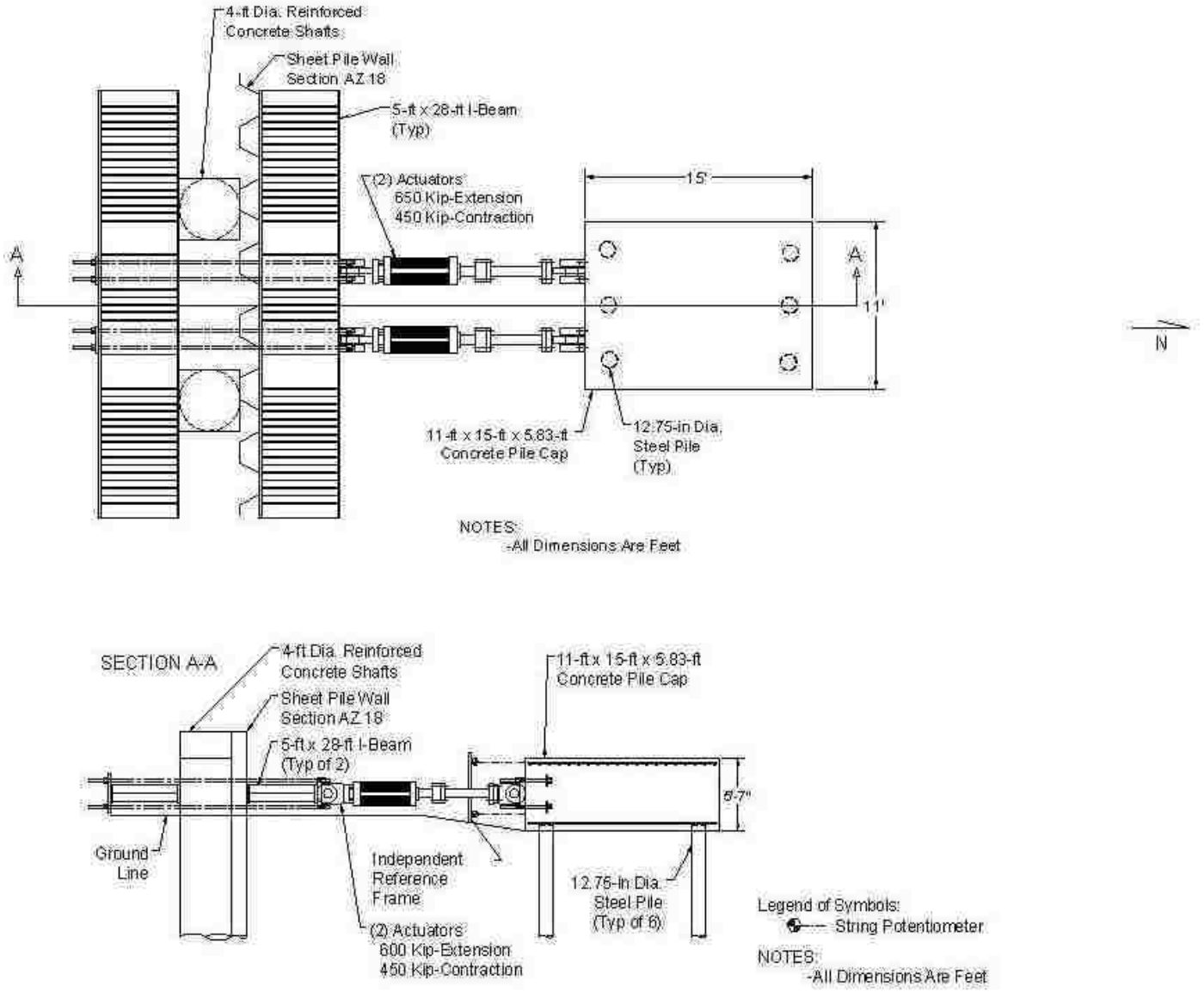

Figure 4-1: Basic layout of site

Both shafts are reinforced with eighteen #11 vertical bars extending 35 ft below ground; half of the vertical bars extend to a depth of 55 ft. Spiral reinforcement consisting of #5 bars is wrapped around the vertical bars at a pitch of 3 inches to a depth of 35 ft, and at a 12 inch pitch to 55 ft. The clear cover of concrete over the reinforcement is 4.75 inches. The top 2 ft of each shaft consists of a 4 ft square cap, which facilitates load application. The concrete in the drilled shafts has a compressive strength of 6000 psi.

The sheet pile extends to depths of 33.6 to 35.6 ft, and consists of AZ-18 sheet piling, constructed of ASTM A-572, Grade 50 steel. These were selected from materials readily available in the area, and installed with a vibratory hammer. The purpose of the sheet piling was to increase the lateral capacity of the frame and help tie the drilled shafts together. As such, they were installed as flush to the face of the drilled shafts as possible.

Two string potentiometers (string pots) were attached from the reference frame to the reaction beam, as shown in Figure 4-2. The potentiometers were Ametek model P-20 A units with a range of 20 inches, a tolerance of +/- 0.10%, and a linearity of 0.03% of full scale. They were located at the elevation of the load point and at 8 ft from the east and west ends of the beam, so as to line up with the drilled shafts.

4.1.2 Pile Cap

The pile cap rests on six 12.75 in. diameter driven piles made of ASTM A252 Grade 2 (57 ksi yield strength) with a wall thickness of 3/8 inch. The piles are closed end and extend to a depth of 43 ft below existing ground surface. When originally constructed, nine piles were driven three piles wide by three long, at 3.5 ft center-to-center spacing east to west and 6 ft center-to-center spacing north to south. Before the pile cap was constructed, the middle three piles orthogonal to the direction of loading were removed, leaving the arrangement shown in

Figure 4-1. The remaining piles were cut off, leaving the piles embedded 6 inches into the pile cap.

The piles were filled with 6000 psi concrete and connected to the pile cap using a rebar cage. This cage consisted of six #8 vertical bars, with spiral reinforcing consisting of #4 rebar wrapped at a 6 inch pitch. The cages extended about 13.2 ft into the piles, and 4.8 ft into the pile cap. The upper mat of horizontal reinforcement in the pile cap is supported on top of these rebar cages. Inclinometer tubes are integrally cast in the center piles on both the north and south rows of pile and extend up through the cap. The cap is 15 ft long (in the direction of loading), 11 ft wide, and 66 inches tall, and is constructed of 6000 psi concrete. Transverse and longitudinal reinforcement is located in the top and bottom of the cap. This reinforcement consists of #6 rebar spaced at 8 inches on center.

Figure 4-2: Picture of string pots from reference frame to load frame.

Pile cap displacements were monitored using string pots attached to an independent reference frame and to the corners of the pile cap. These string pots were Ametek model P-20 A units with a range of 20 inches, a tolerance of +/- 0.10%, and a linearity of 0.03% of full scale. String pots were attached at 3 and 51 inches from the top of the pile cap on the east and west edges of the south side of the pile cap. This string pot arrangement also made it possible to determine the rotation of the pile cap about horizontal and vertical axes.

Slotted Inclinometer casings were installed within the middle pile in the front and back rows of the piles prior to testing. The casings had 2.32 inches inside diameter and 2.75 inches outside diameter, and extended to a depth of 47-48 ft from the top of the pile cap. Inclinometer readings were taken before each test and at the maximum extent of each loading. This was done by extending the inclinometer within the slots to the bottom of the casing, and taking readings at 2 ft intervals while removing the inclinometer. The inclinometer was then rotated 180° about the long axis, and the process was repeated to reduce error. This was done in both inclinometer casings. These measurements provide displacement versus depth profiles and can also be used to calculate bending moment and generate bending moment versus depth profiles.

4.1.3 Backfill Soil

As indicated previously, the backfill soil consisted of dense compacted concrete sand. Details regarding the material properties of the sand and the relative compaction test results are provided in Chapter 3.

String pots were placed on the pile cap to monitor the surface displacement of the backfill test area at distances of 2, 4, 6, 9, 12, 15, 18, and 24 ft from the North face of the pile cap. A piece of angle iron 10 ft long was bolted to the top of the pile cap, near the backfill edge, oriented normal to the direction of loading. The string pots were attached to this angle using C-

clamps, as shown in Figure 4-3. The string pots were located 10 inches back from the face of the pile cap. The string pots located at 2, 4, 6, 9, and 12 ft were Ametek Model P-20A units with a range of 20 inches, a tolerance of +/- 0.10%, and a linearity of 0.03% of full scale. The string pots placed to measure the displacement at 15, 18, and 24 ft were UniMeasure Model P1010-5-S15 units with a range of 10 and 5 inches, and a linearity of 0.18% of full scale. Steel stakes were driven into the backfill soil at the indicated distances, and the other end of the string pots were attached to these stakes.

Figure 4-3: String pots from pile cap to backfill soil.

A 2 ft grid was painted over the ground surface prior to testing. A surveying level was used to take elevations of the surface both before loading and at the maximum displacement of the pile cap on the intersection of the 2 ft grid. Surface cracking was monitored at 0.25 inch nominal displacements of the pile cap throughout the test. This was done by holding the pile cap displacement constant and visually inspecting the surface of the soil backfill for the presence of cracks. Cracks were painted using marking paint and the development of the crack pattern was noted on grid paper, using a different color to note the location on the paper for each displacement increment. The paint made distinction of cracks from one displacement increment to the next possible.

4.1.4 Soil Pressures (Pressure Plates)

The soil pressure on the face of the cap was measured using pressure plates, embedded into the face of the cap as shown in Figure 4-4. The plates were recessed into the front face of the cap, so as to be flush with the concrete surface. The same pressure plates were previously cast integrally into the face of the pile cap, and were replaced in the same locations for a proper fit. They were placed at depths of 5.5, 16.5, 27.5, 38.5, 49.5, and 60.5 inches to the center of the plates. The plates were designed with a reinforced steel back to reduce the effects of point loading. The plates use an electrical resistance type strain gauge system to measure accurately the total pressure.

The tests performed and the dates they were performed are shown in Table 4-1. This thesis will include data from all of the dense sand tests performed, or all of the backfilled tests performed from June 22, 2009 to July 9, 2009.

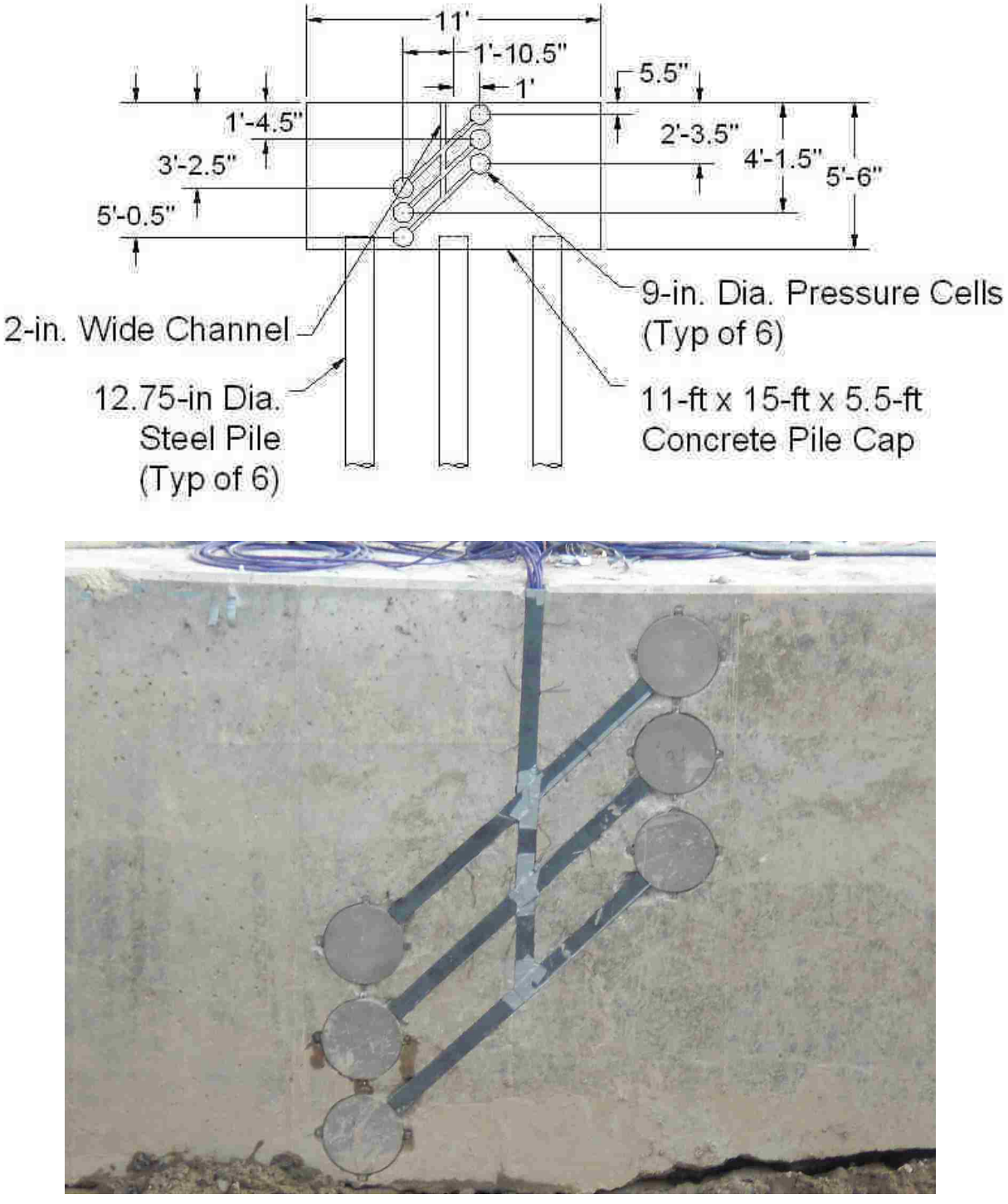

Figure 4-4: Pressure plates installed in the front face of the pile cap.

Table 4-1: Tests Performed

Test Number	Test Date	Test Description
1	3-Jun-2009	No Backfill (Free Response)
2	4-Jun-2009	No Backfill (Free Response)
3	8-Jun-2009	Loosely Compacted Sand Full Width (3D - No Walls)
4	12-Jun-2009	Loosely Compacted Sand Plane Strain (2D - Plywood Walls w/ Plastic Sheeting)
5	18-Jun-2009	Loosely Compacted Sand MSE
6	22-Jun-2009	Densely Compacted Sand MSE 1
7	24-Jun-2009	No Backfill (Free Response)
8	26-Jun-2009	Densely Compacted Sand MSE 2
9	2-Jul-2009	Densely Compacted Sand Plane Strain (2D - Plywood Walls w/ Plastic Sheeting)
10	9-Jul-2009	Densely Compacted Sand Full Width (3D - No Walls)

4.2 Layout and Instrumentation for Unconfined Backfill Test

The unconfined backfill test had all the instrumentation described in previous sections. The difference between this test and the tests that follow was the width of the backfill zone. Whereas the other tests were limited to the width of the pile cap, the unconfined backfill test was excavated 6 ft beyond each side of the cap, to ensure the 3D failure zone was captured in the backfill. Performing 3D tests allowed for a comparison of the results of our other tests to tests that have been performed by other researchers (Duncan and Mokwa, 2001, Rollins and Cole, 2006). The layout of the unconfined test is shown in Figure 4-5.

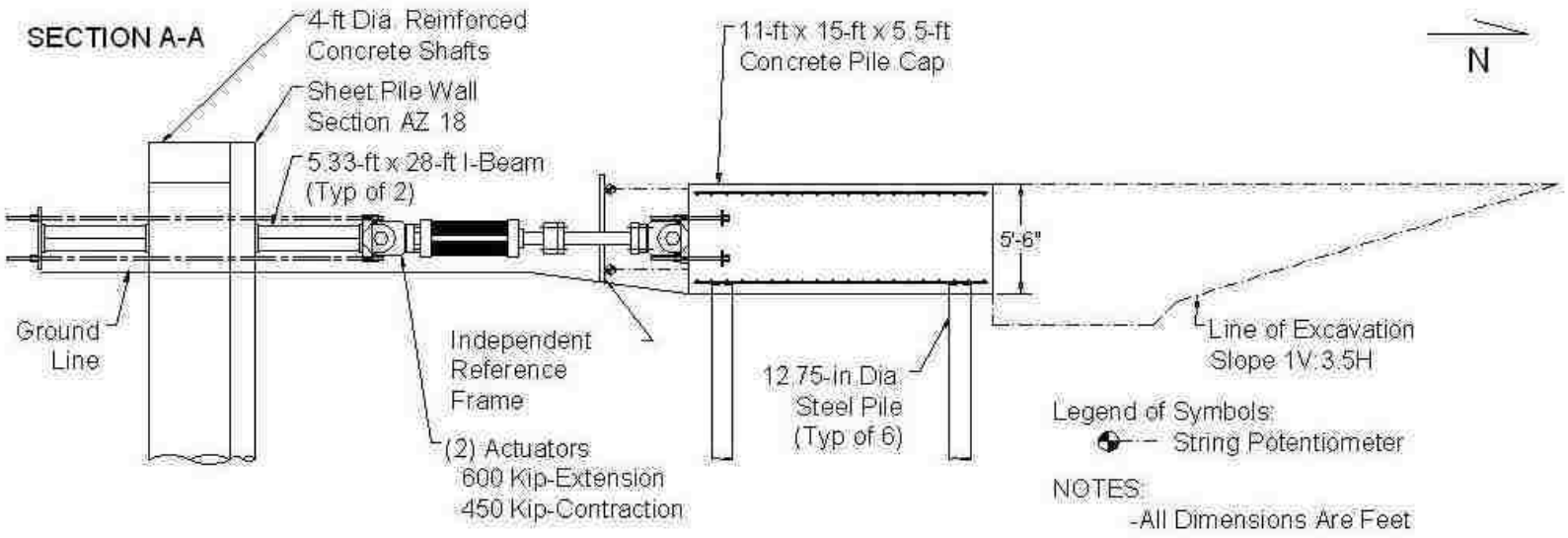

Figure 4-5: Layout of unconfined .

4.3 Layout and Instrumentation Details for Plane Strain (2D) Load Test

This test layout was designed to approximate a plane strain or 2D failure surface. Plywood sheets (isolation panels) covered with plastic sheeting were placed parallel to the sides of the pile cap to prevent the shear planes from extending beyond the edge of the cap and to minimize shearing on the sides of the failure mass. Photos of the plane strain load test during construction are shown in Figure 4-6 through Figure 4-8. The plywood wall panels were 5/8 inch thick, 4 ft x 8 ft sheets. The panels were placed vertically side by side to a distance of 24 ft into the backfill zone. They were connected by two rows of 2x4's, one about 4 ft from the bottom and the other near the top of the sheets, all on the outside of the panels. The two panels nearest the cap on each side of the cap were placed 18 inches lower than the rest of the panels, to account for the deeper excavation and failure surface. Sand was compacted on the outside of the panels at the same time as it was compacted inside the panels in an effort to balance the normal stress on the wall. In addition, the plywood panels were supported at ground level (5.5 ft above the base of the cap), during construction with 2x4 kickers, which were removed when the backfill was about halfway up the panels to permit access for the compaction equipment around the panels. The panels were installed with emphasis on keeping them vertical, level and parallel with the pile cap. The inside face of the plywood was covered with two layers of plastic sheathing (Visqueen) to create a low-friction interface between the backfill material and panels. This created a two-dimensional failure geometry that should approximate a plane strain condition. Figure 4-9 provides plan and profile drawings of the test layout.

Figure 4-6: Picture of side isolation panels.

Figure 4-7: Installation of side isolation panels.

Figure 4-8: Picture of side isolation panels being backfilled.

In addition to the common instrumentation described previously (Section 4.1), the first 18 ft of wall panels on the west were instrumented with string pots just above the ground surface to monitor the outward displacement of the panels as shown in Figure 4-10. These were attached to metal stakes placed outside of the backfill zone about 6 ft from the panels to go beyond potential soil movement. Four string pots were used, placed at distances of 2, 6, 12 and 18 ft from the pile cap face. These were UniMeasure Model P1010-5-S15 string pots, with a range of 5 and 10 inches, and a linearity of 0.18% of full scale.

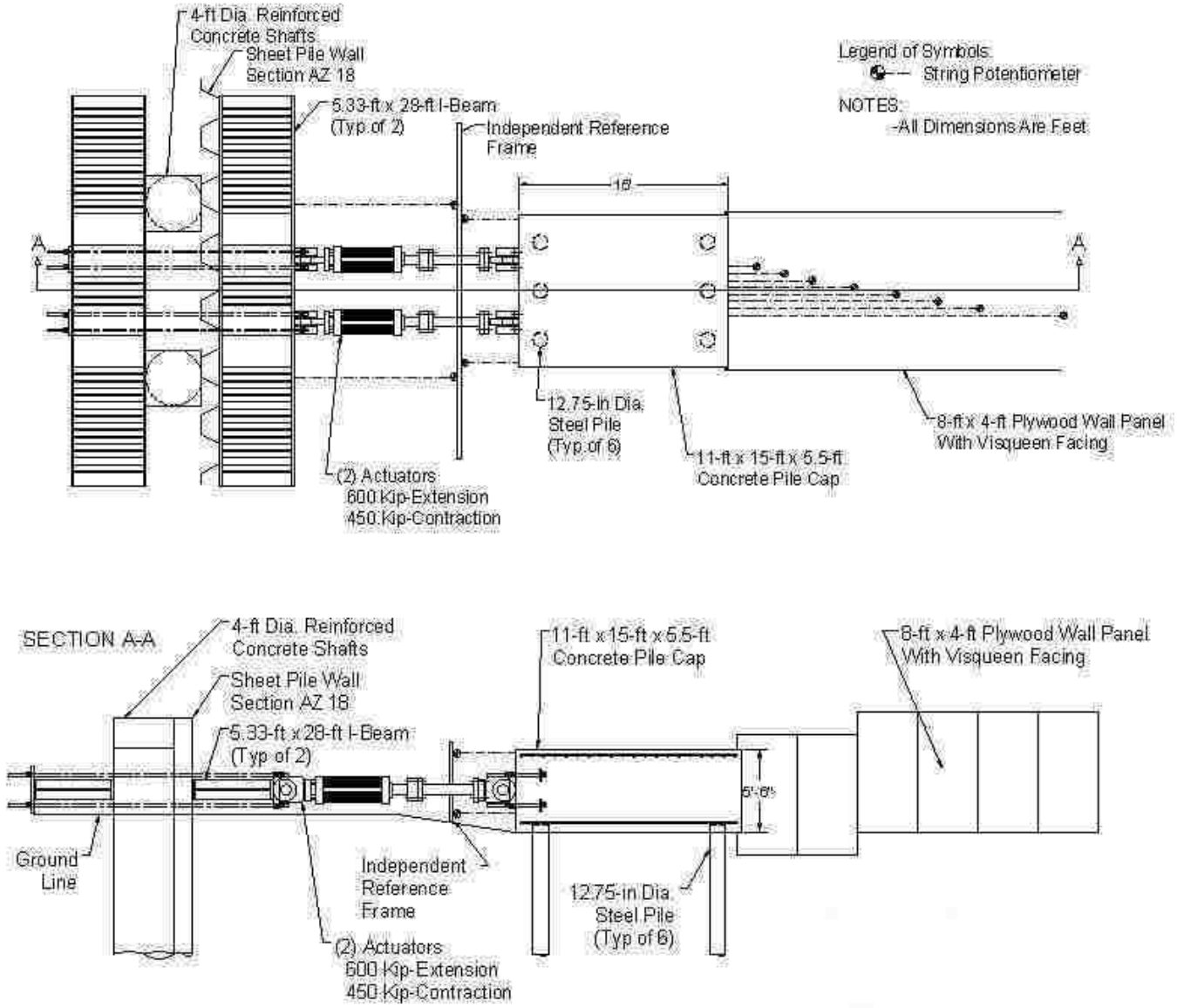

Figure 4-9: Layout for plane .

Figure 4-10: String pots on side isolation panels.

4.4 MSE Test One

The first test with MSE wall panels consisted of four panels arranged as shown in Figure 4-11. These panels were 12 ft x 5 ft, and included 2 x 8 wood planks on top to increase the depth of the backfill by 0.5 ft. The panels were set on 4 x 4 leveling pads. Structural details of typical wall panels are shown in Figure 4-12 and Figure 4-13.

This test was designed to have an average static factor of safety against pullout of 1.5, with an actual average design factor of safety of 1.65, different from the factor of safety of the second MSE test. The upper bar mats were designed to resist 2140 lbs per bar mat with a design capacity of 3467 lbs. The lower bar mats were designed to resist 3856 lbs per bar mat with a design capacity of 6410 lbs.

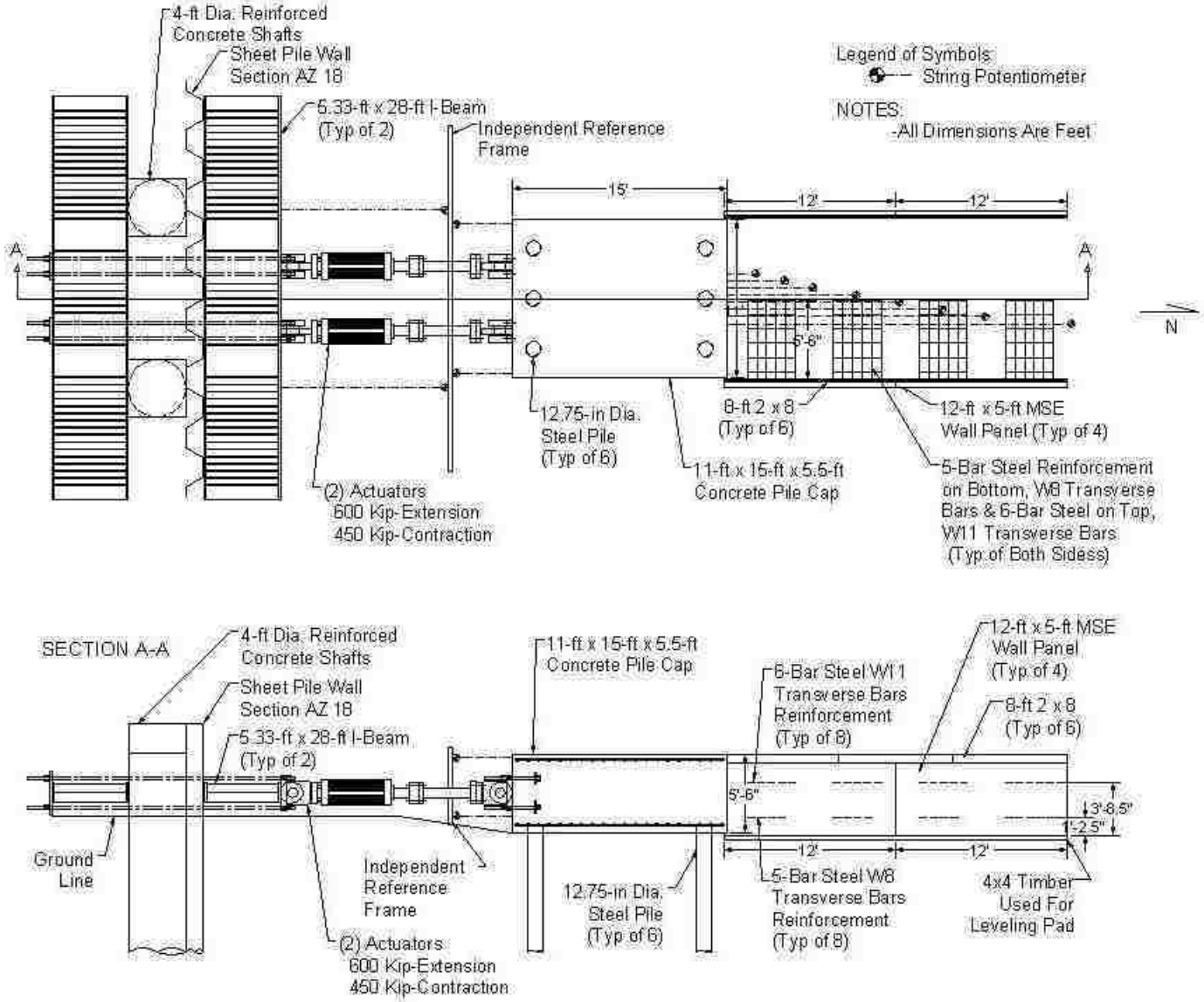

Figure 4-11: Layout of MSE test .

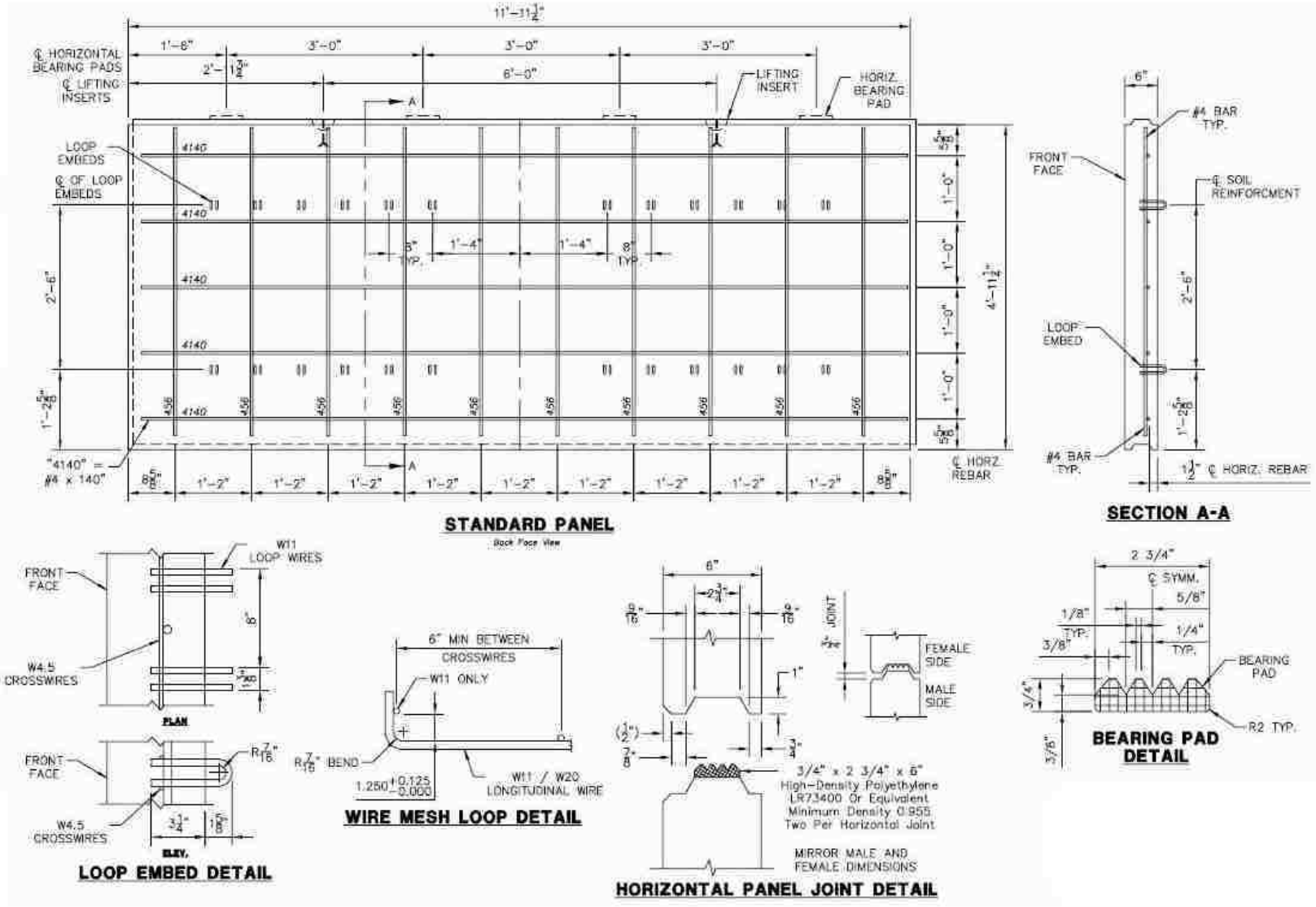

Figure 4-12: Wall panel .

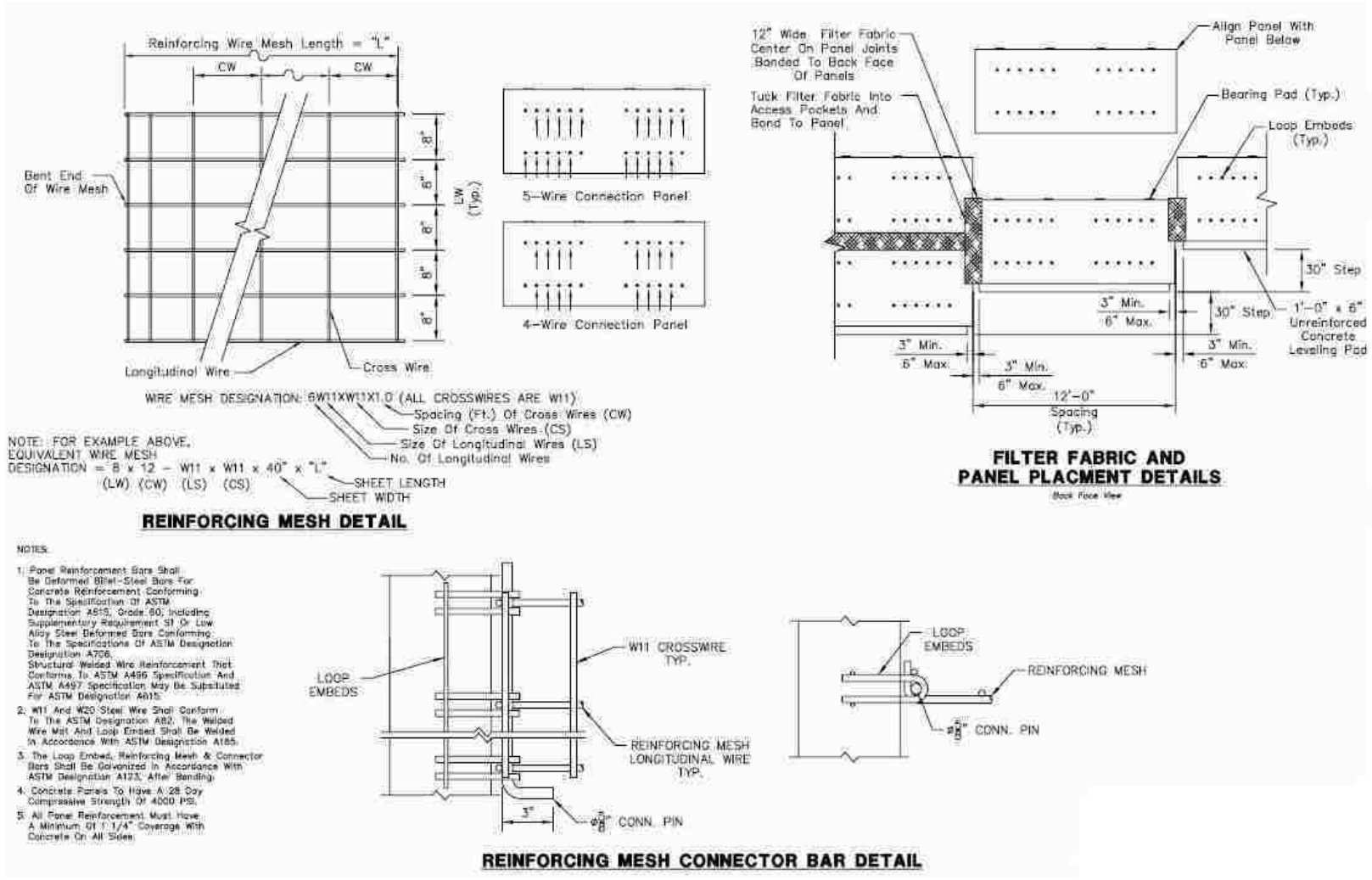

Figure 4-13: Wall panel .

Two sizes of bar mats were used to reinforce the panel. The upper mats had six W20 longitudinal bars, with W11 cross bars spaced 1 ft on center. The lower mats had five W11 longitudinal bars, with W8 cross bars spaced 1 ft on center. Both types of mats were 5.5 ft long, with longitudinal bars spaced 8 inches on center. Drawings of both types of mats can be seen in Figure 4-14. The upper bar mats were placed at a depth of 21.5 inches, the lower bar mats at 51.5 inches. This corresponds to 3 ft 8.6 inches and 14.5 inches from the bottom of the MSE wall panel, respectively.

Each bar mat was instrumented with FLA-2-11 strain gauges on the center longitudinal bar on the mats with five longitudinal bars, and the bar north of center on mats made of six longitudinal bars. The tolerance of the gauges was +/-0.85 μm/m/°C, with a gauge factor of 2.11+/-1.0%, and a coefficient of 11.8x10^-6/°C. These gauges were placed at distances of 2, 5, 9, 19.5, 28, 37, 47, and 56 inches from the wall face. Gauges were placed on both the top and bottom of the longitudinal bars, to eliminate bending effects. This was done to monitor the development of force in the mat, and relate this to load on the wall panel. The four mats reinforcing the southeast wall panel (closest to the pile cap) were the only mats instrumented for this test. Proper procedure was followed to affix the strain gauges to the bar mats. The section of bar to be instrumented was sanded with successively finer grit sandpaper to remove any protective coating and to smooth the surface. Following sanding, the bar was cleaned using acetone to remove any dust and contaminants that might interfere with the gauges bonding to the steel. Scotch tape was placed around the bar next to the intended gauge location (to separate the wires from the steel) and on the back of the strain gauge, and a drop of glue was placed on the bar. The gauge was placed on the bar and held in place for 1 minute. After the glue had cured a protective epoxy coating was placed over the gauge and exposed wire and electrical tape was

wrapped around the gauges, wires, and bar along the length of the bar to protect the assembly from moisture and damage.

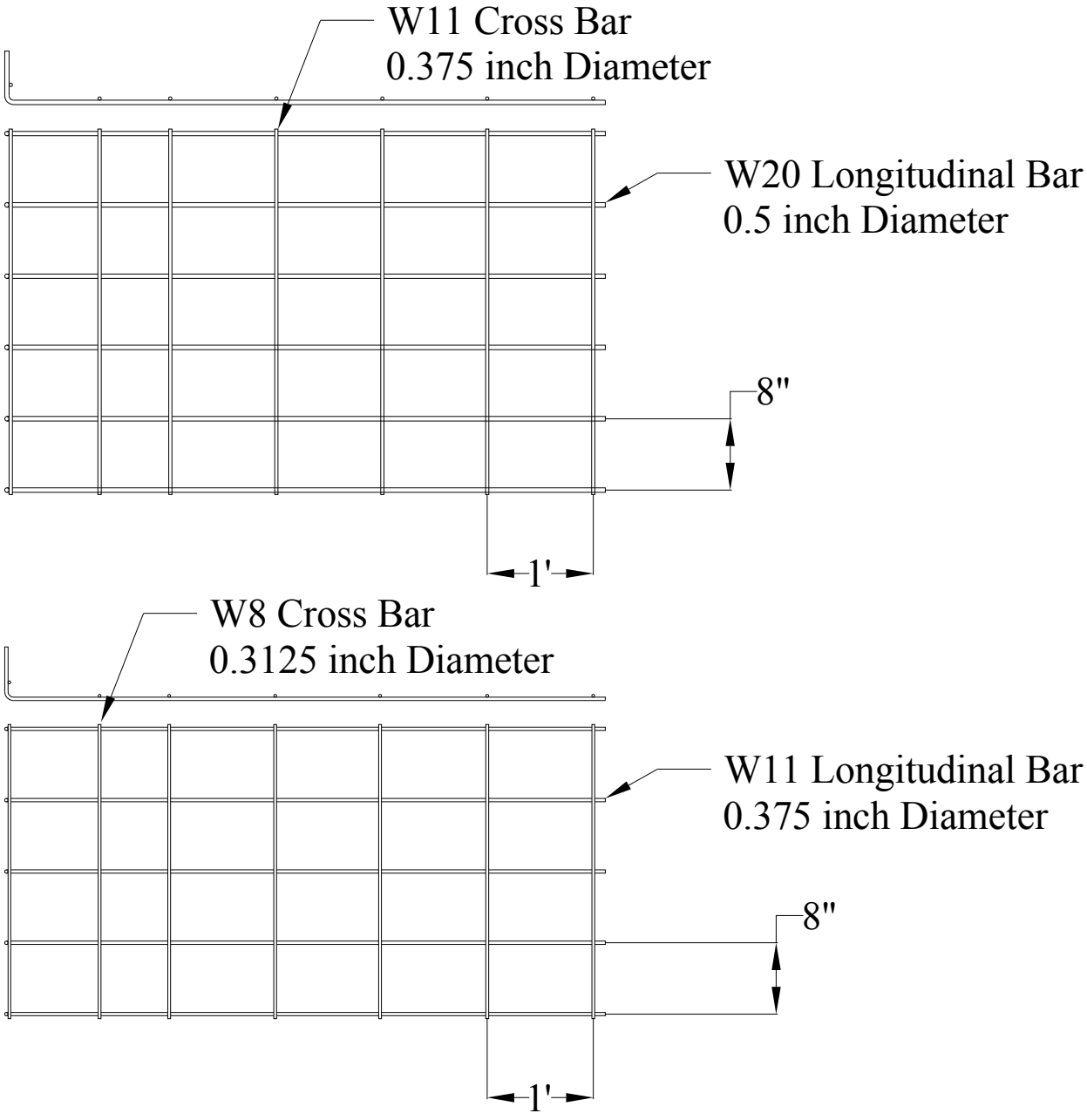

Figure 4-14: Bar mat schematic.

To define the displacement and rotation of the wall during the load test, four string pots were placed on the outside of the southeast wall panels, at heights of 14 and 44 inches from the bottom of the wall panel and at distances of 20.5 and 102.5 inches from the face of the pile cap, as shown in Figure 4-15. These string pots were placed to correspond to the approximate centers of the bar mats reinforcing the backfill, and were used to monitor the pullout of these mats. The string pots were UniMeasure Model P1010-5-S15 units with a range of 5 and 10 inches and a linearity of 0.18% of full scale. The end of the string pots were attached to T-posts placed in the excavation and reinforced against movement with cabling. Measurements of the wall location relative to the pile cap were taken before and after the test.

Figure 4-15: String pots to measure wall deflection.

4.5 MSE Test Two

Different wall panels were used for the second MSE wall test, along with more reinforcing mats. These wall panels were 12 ft long and 6.25 ft tall, so 2 x 8's were not needed at the top as with the first test. The depth of backfill was the same to allow for comparisons between the tests. Six mats were placed for each wall panel. These mats were placed at depths of 6, 36, and 58.5 inches below the backfill (60, 30, and 7.5 inches, respectively, from the bottom of the panel). The top and middle mats were consisted of six W20 longitudinal bars spaced 8 inches on center, with W11 cross bars spaced 1 ft on center. The bottom mats had five W11 longitudinal bars spaced 8 inches on center, with W8 cross bars spaced 1 ft on center. Drawings of these mats can be seen in Figure 4-14. The test setup is shown in Figure 4-16. A drawing of the wall panels used in this test indicating wall dimensions and locations of connection hoops is shown in Figure 4-17.

This test was designed to have an average static factor of safety against pullout of 2.5, with an actual average design factor of safety of 2.6. The upper bar mats were designed to resist 356 lbs per bar mat with a design capacity of 1001 lbs. The middle bar mats were designed to resist 2491 lbs per bar mat with a design capacity of 5838 lbs. The lower bar mats were designed to resist 2736 lbs per bar mat with a design capacity of 7685 lbs.

LVDT's were used to measure the outward displacement of the wall panel instead of string pots as shown in Figure 4-18. These were Schaevitz Model GA-HD GCD-121-1000 LVDT's with a range of 2 inches and a linearity of 0.12% of full range, and were placed at heights of 47.25, 20, 50.75, and 20 inches from the bottom of the wall panel and 16, 13, 99, and 96 inches from the pile cap, respectively, so as to correspond as closely as possible to the locations of the top and bottom bar mats in the southeast panel. It was not possible to locate

them right at the bar mats, due to the need to have the LVDT's in grooves in the wall panel, in case the wall moved.

The method of mat instrumentation and location of strain gauges on these mats was identical to the mats from MSE wall test 1; however, instead of four instrumented bar mats, all six bar mats attached to the southeast wall panel were instrumented.

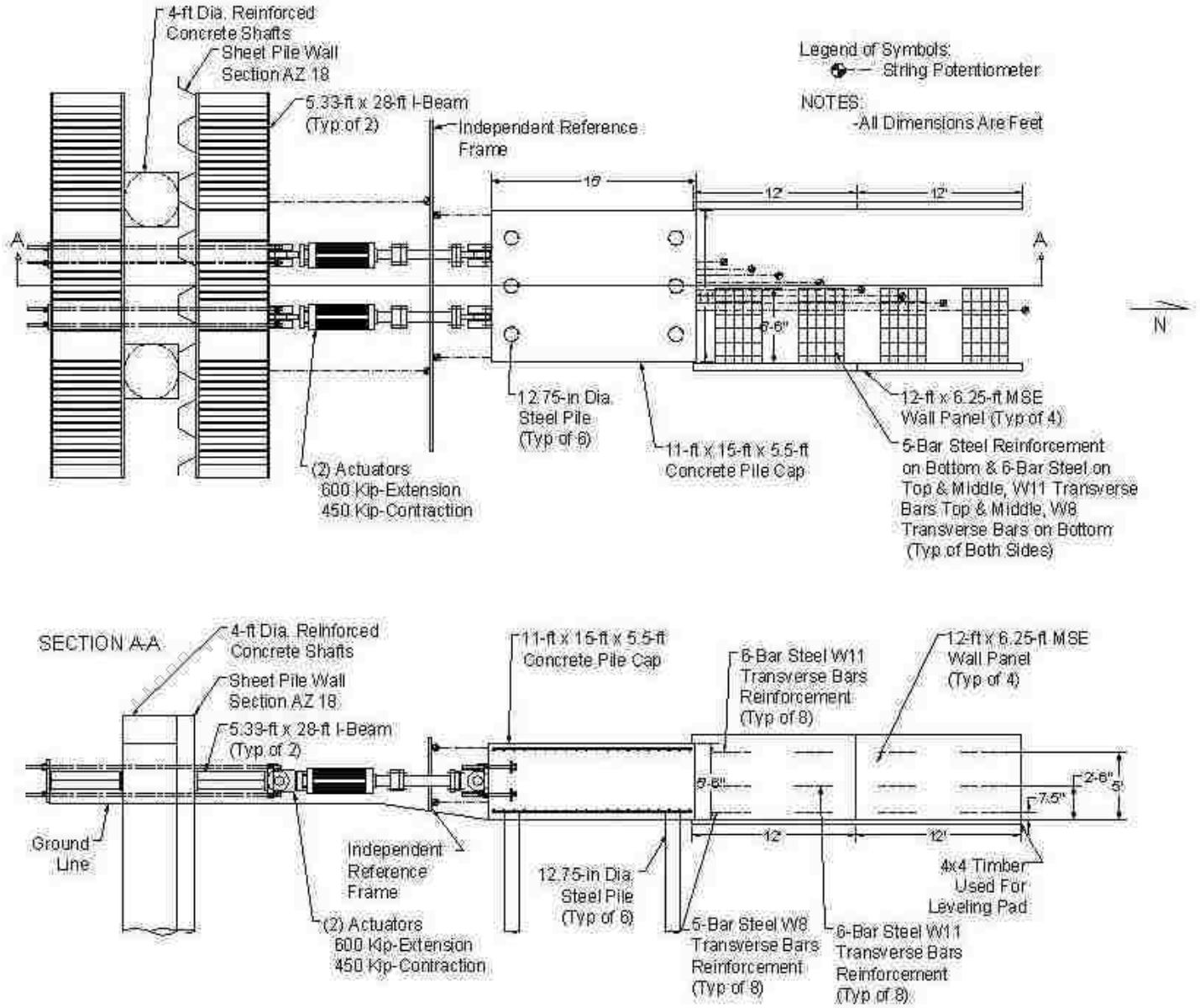

Figure 4-16: MSE 2 test .

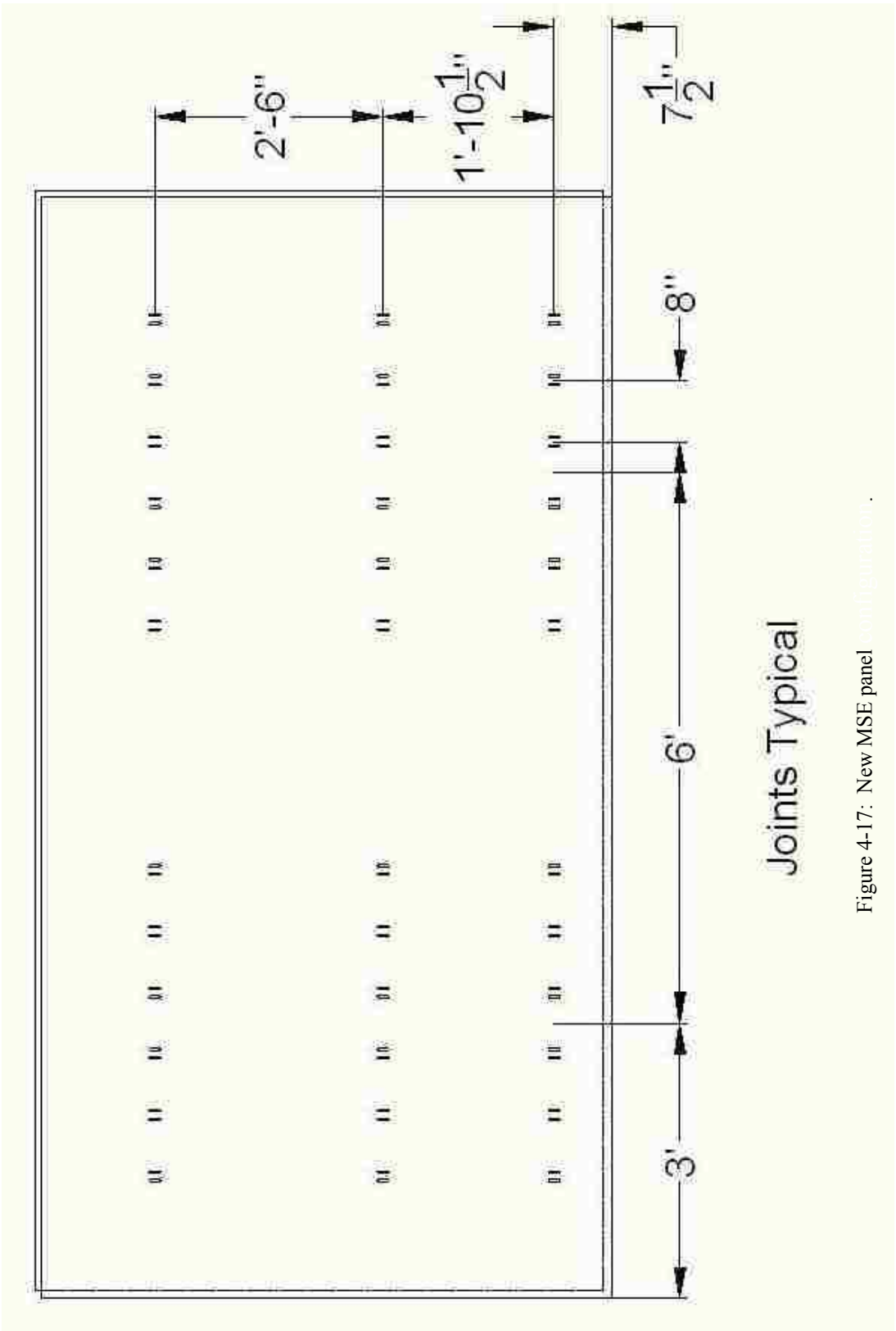

Figure 4-17: New MSE panel

Figure 4-18: LVDT's to measure wall deflection.

5 Unconfined (3D) Backfill

This chapter presents the results of the unconfined sand backfill test. These results are broken down into the following areas: force-displacement (force measured from actuators), force-displacement (force measured from pressure cells), inclinometer data, backfill displacement, and heave and cracking.

5.1 Load-Displacement Results

The measured total resistance versus deflection of the pile cap is shown in Figure 5-1. The graph was obtained by plotting the measured total force from the actuators versus the average displacement of the pile cap corresponding to the peak load. The displacement was taken as the median value of the four string pots attached to the pile cap. Figure 5-2 also shows the total measured response, along with the baseline response and the passive earth response. The baseline results were obtained by running the test with no backfill present. This allows researchers to subtract the resistance contributed by factors other than the backfill passive response (such as lateral pile resistance and base shears) from the total response measured during the test. The baseline curve is relatively linear with a stiffness of approximately 117 kips/in. In contrast, the passive resistance versus displacement curve exhibits a hyperbolic shape and approaches an ultimate resistance of about 780 kips asymptotically.

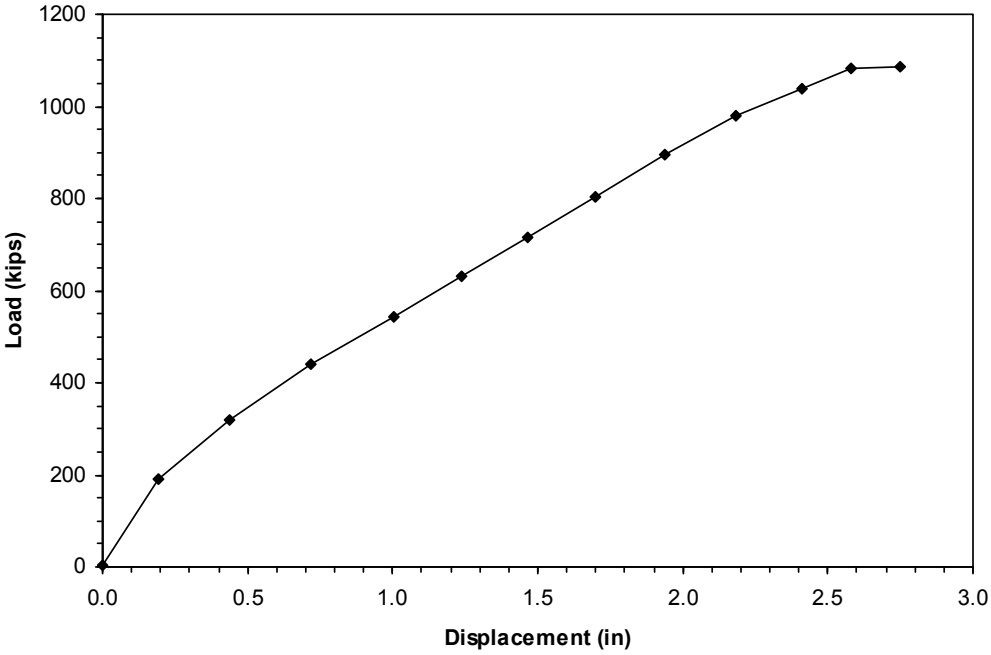

Figure 5-1: Total measured response versus displacement.

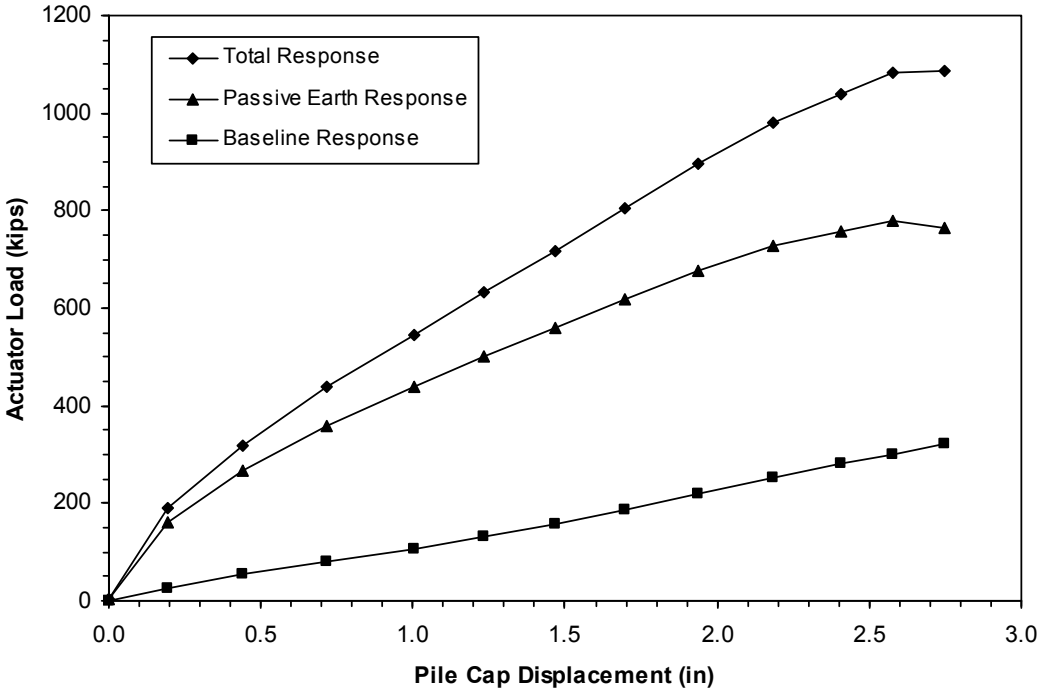

Figure 5-2: Passive resistance versus pile cap displacement.

5.2 Load-Displacement Results from Pressure Cells

Figure 5-3 shows the development of pressure on the pile cap face, with each reading corresponding to each displacement increment. Each point going down the pile cap face indicates the location of a pressure cell. The pressure in this test develops evenly in the top half of the pile cap, but much greater pressure develops in the bottom half. Some of the values at depths of 0.46 and 2.30 ft reach a peak value, and then begin to drop off toward the end of the test. These values have been adjusted to equal the maximum value reached at that depth; this is shown in Figure 5-4.

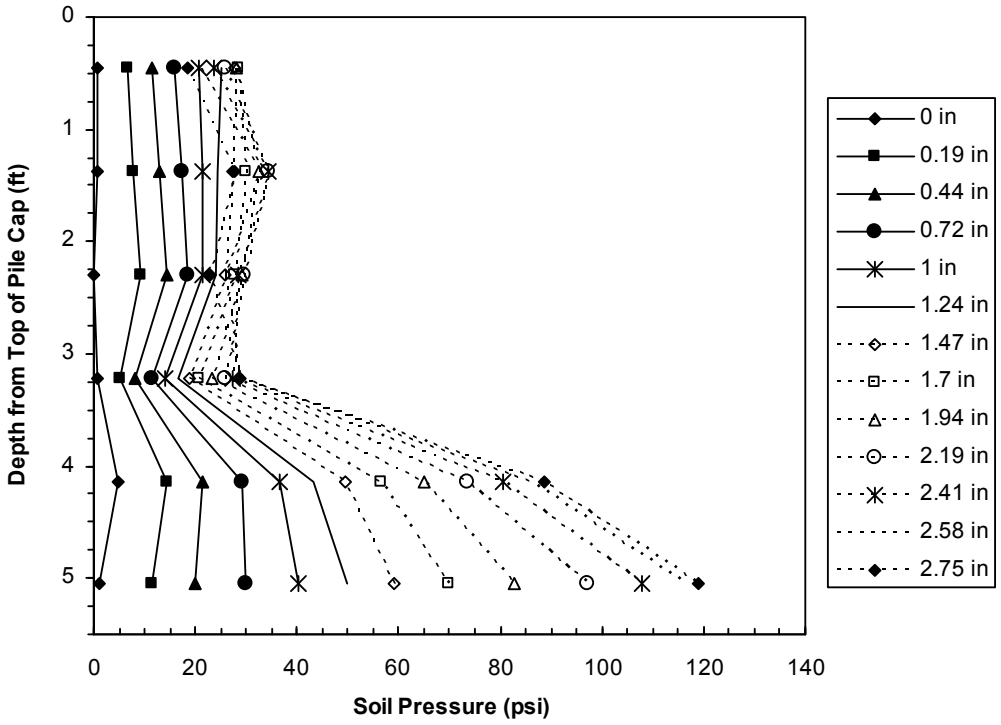

Figure 5-3: Development of pressure cell readings versus displacement.

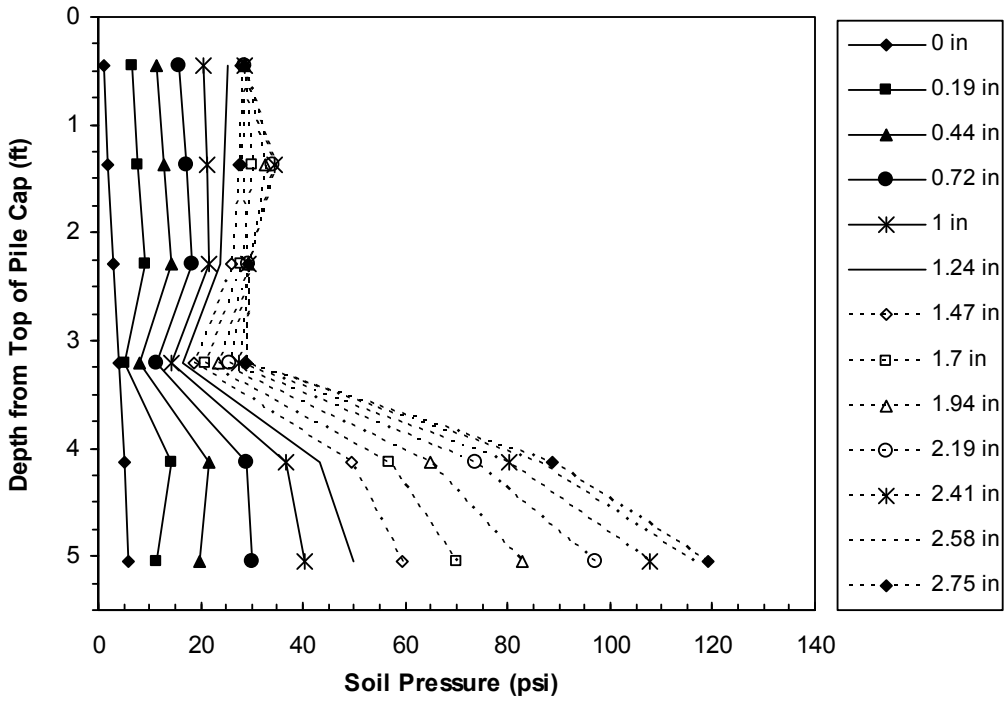

Figure 5-4: Development of pressure cell readings versus displacement, adjusted.

Figure 5-5 provides a comparison of the passive force-displacement curves obtained from the pressure cells with that from the actuators. The passive force from pressure cells was obtained by multiplying the measured pressure of each cell (as shown in Figure 5-4) by its tributary area. The tributary area is the distance from either the top of the pile cap or halfway to the adjacent pressure cell above the cell to the bottom of the pile cap or halfway to the adjacent pressure cell below the cell multiplied by the width of the pile cap. The passive force as measured from the pressure cells was typically 30-40% lower than that measured from the actuators. The difference is likely due to the assumption of uniform pressure across the width of the pile cap. In reality, stress concentrations occur near the edge of the pile cap. The pressure cells were placed near the center of the pile cap, resulting in the passive pressure being underestimated.

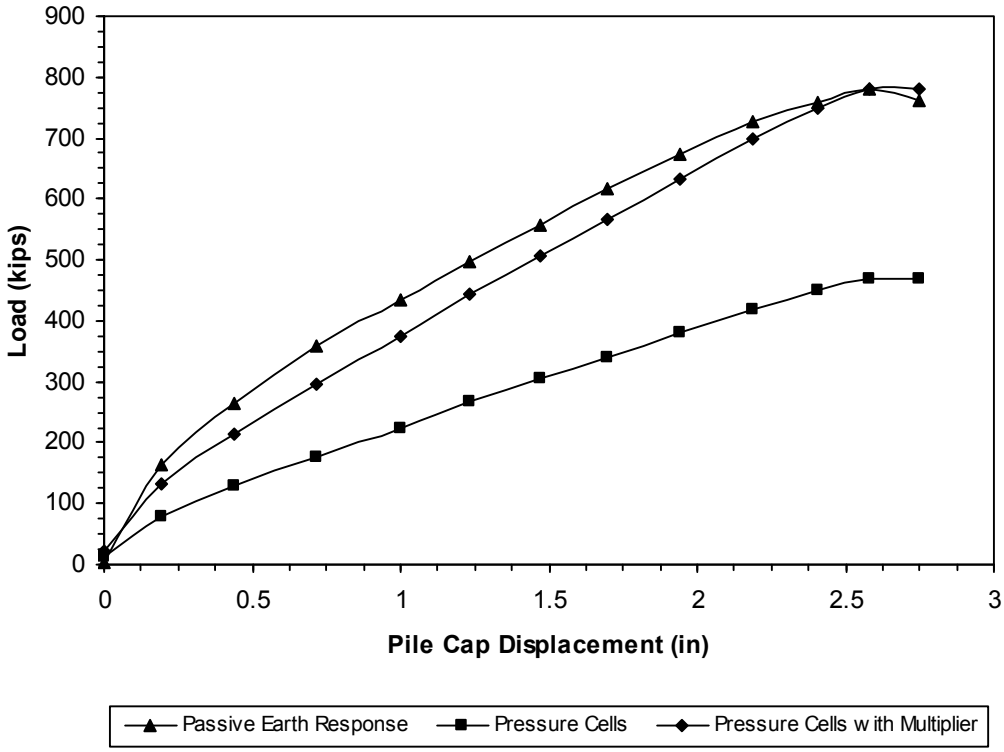

Figure 5-5: Load versus displacement from pressure cells.

The measured passive earth response from the pressure cells is multiplied by a factor of 1.67 to account for end effects; these values are shown as the pressure cells with multiplier in Figure 5-5. This multiplier is to produce a best fit; in the plane strain and both MSE tests this multiplier is 1.3. The difference may be due to the end effects produced on the pile cap with an unconfined loading configuration being more pronounced. The passive earth response in the figure is the measured curve obtained from the actuators. As can be seen, the values for load from pressure cells with multiplier lies just below the passive earth response obtained from actuator measurements for most of the development portion of the curve. The ultimate measured passive resistance is reached by the pressure cells with multiplier curve near the end of the testing. This reinforces the values obtained from the actuators alone, and increases the confidence in results obtained from the actuators. It also qualifies the method of subtracting

baseline response from total measured resistance to obtain the passive earth response described in Section 5.1.

Throughout all the tests, the pressure cell located at a depth of 5.5 inches reached a peak value and then recorded decreasing pressures. In all the tests except MSE test 2, the pressure cells located at depths of 16.5, 27.5, and 38.5 inches either did the same thing as was mentioned occurred to the pressure cell at 5.5 inches, or acted unexpectedly in some other manner, whether it be reaching a peak value and no longer rising, or increasing dramatically.

5.3 Inclinometer Data

As discussed in Section 4.1.2, inclinometer readings were taken for each test. Figure 5-6 shows the deflection versus depth from these readings in both the north and south inclinometer casings. The curve represents change in deflection of the inclinometer tubes in the direction of loading, (the baseline reading was subtracted from the reading taken at the maximum displacement of the pile cap). A depth of zero corresponds to the top of the pile cap. The curves from both the north and the south match each other very well as would be expected. Also shown in this figure is the displacement of the pile cap as measured by the string pots that were attached to the pile cap. As can be seen the displacement measured by the inclinometer matches the displacement measured from the string pots. The deflection in the pile reaches zero at a depth of about 20 ft, which corresponds to nearly 19 pile diameters. The points within the cap translate horizontally and remain nearly vertical, indicating very little rotation of the pile cap. This is consistent with a fixed head boundary condition.

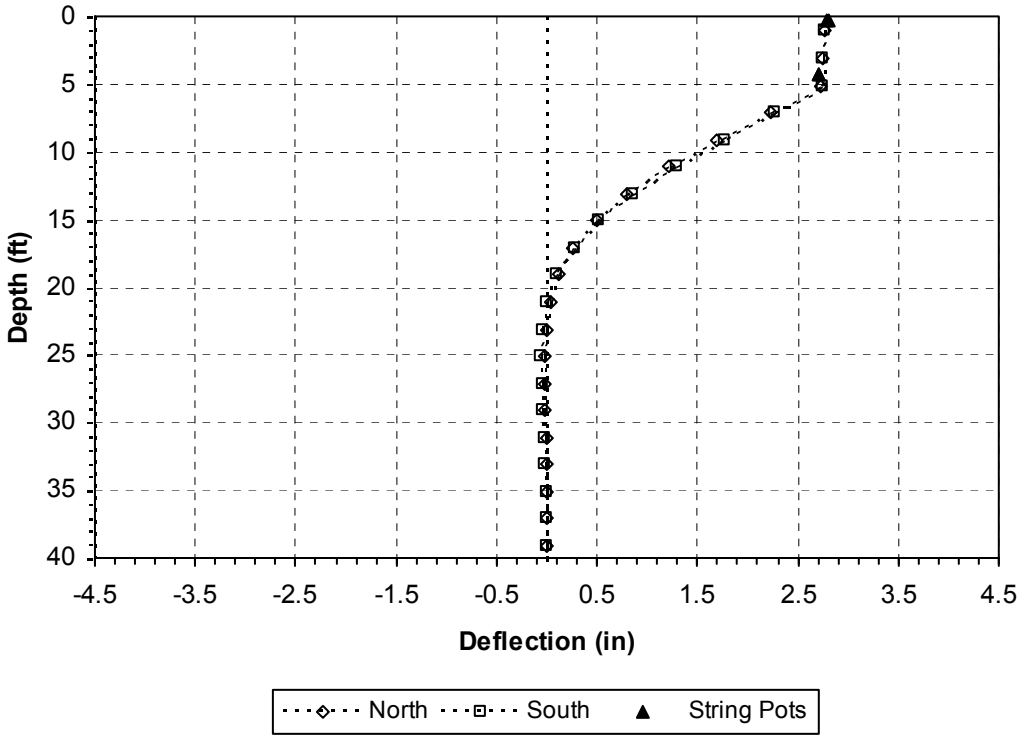

Figure 5-6: Deflection versus depth.

5.4 Backfill Soil Displacements

Figure 5-7 shows the absolute displacement of the backfill soil. The arrangement of string pots and stakes was discussed in section 4.1.3. These values were obtained by subtracting the displacement measured by each backfill string pot from the pile cap displacement at that loading increment. For example, if the backfill string pot at a distance of 2 ft from the face of the pile cap measured a displacement of 1 inch, and the loading increment was 2 inches, the value shown in Figure 5-7 would be 1 inch at 2 ft.

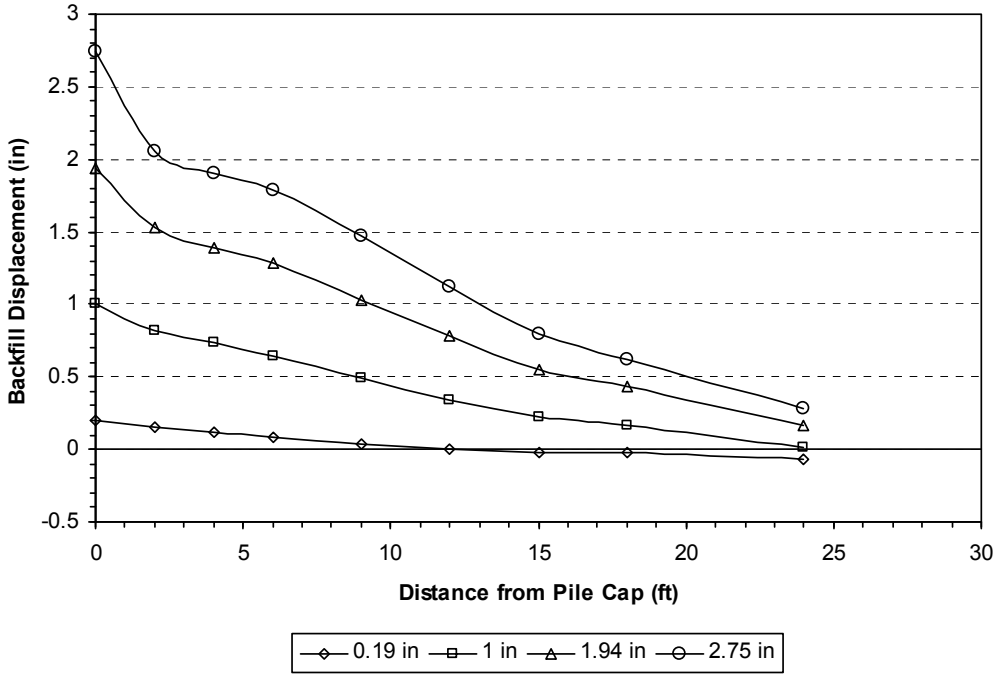

Figure 5-7: Displacement of backfill soil.

The compressive strain of the backfill is shown in Figure 5-8. In this figure each of the lines represents the compressive strain obtained from the corresponding string pot and stake. The strain values were obtained using the equation

$$\varepsilon = \Delta L / L \tag{5-1}$$

where

ΔL = change in length from adjacent string pot
L = distance between adjacent stakes

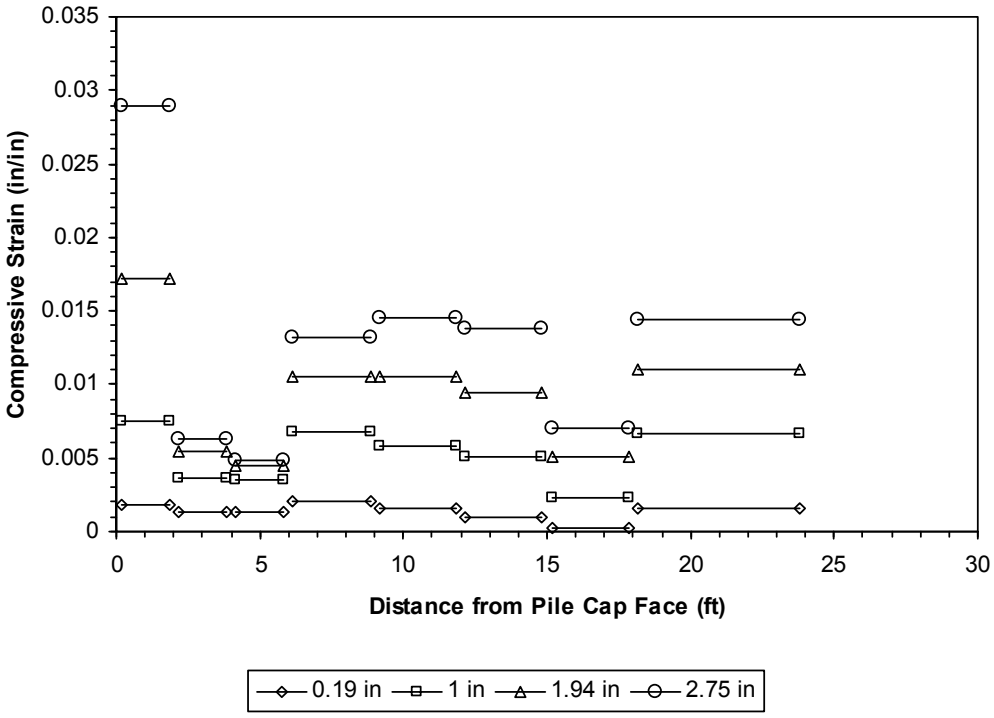

Figure 5-8: Compressive soil strain in backfill as a function of distance behind the cap for several displacement increments.

To simplify presentation of these results, only the first displacement increment, the nominal inch displacement increments, and the final displacement increment are shown in this figure. As can be seen, the greatest compressive strain occurs within the first couple ft of the cap face. In this test, the compressive strain is fairly uniform beyond 6 ft, except in the 15 to 18 ft range. The predicted log-spiral failure profile surfaces at about 24.6 ft from the face of the pile cap. The compressive strain remains fairly constant to this distance.

5.5 Heave and Cracking of Soil Backfill

This section will present the data gathered regarding heaving and cracking of the backfill soil profile during and after testing. The methods used to gather this data are discussed in section 4.1.3. Figure 5-9 shows the soil heave profile for the test. The values represent the change in

elevation from before the test to the largest displacement of the pile cap and are in inches. Positive values indicate upward movement, while negative indicates downward movement (settlement). The dashed lines are set up in a 2 ft by 2 ft grid, consistent with the grid that was painted on the soil surface before the test was performed. As can be seen from this figure, the maximum heave occurs from about 4 to 8 ft from the face of the pile cap. The shape of the heave contour lines is circular.

Figure 5-10 is a map showing the development of cracks observed for each pile cap displacement increment, with cracks for each displacement increment identified by a separate color. The process by which cracks were mapped is described in greater detail in section 4.1.3. The cracks tend to go from the corners of the pile cap at about 45° from the face of the cap, and at about 7 ft from the cap face angle back in toward the center, converging at about 14 ft from the face of the cap. The overall shape formed by the cracks is circular, and looks like the heave contour lines from Figure 5-9.

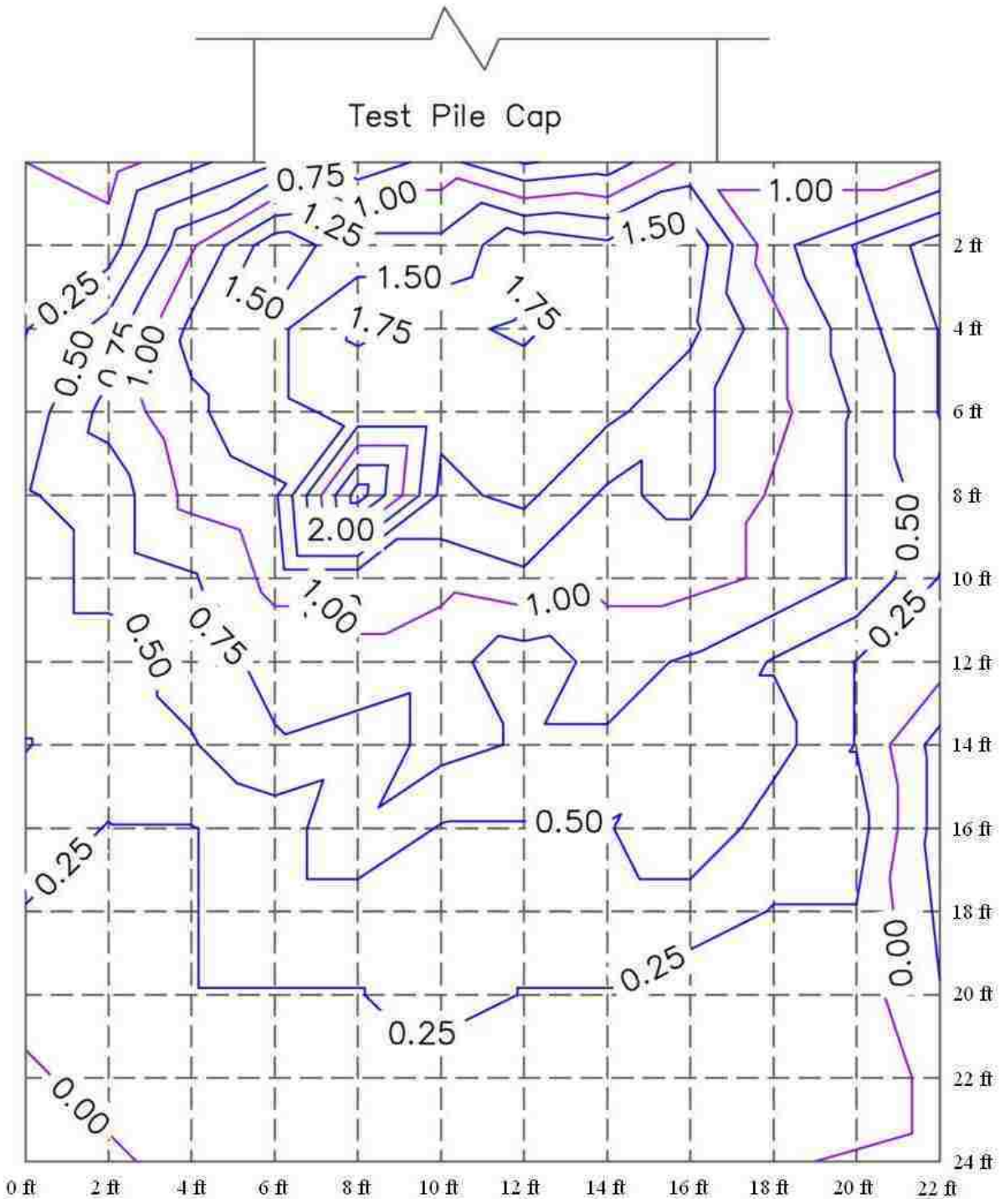

Figure 5-9: Soil heave contours (inches) for the backfill behind pile cap.

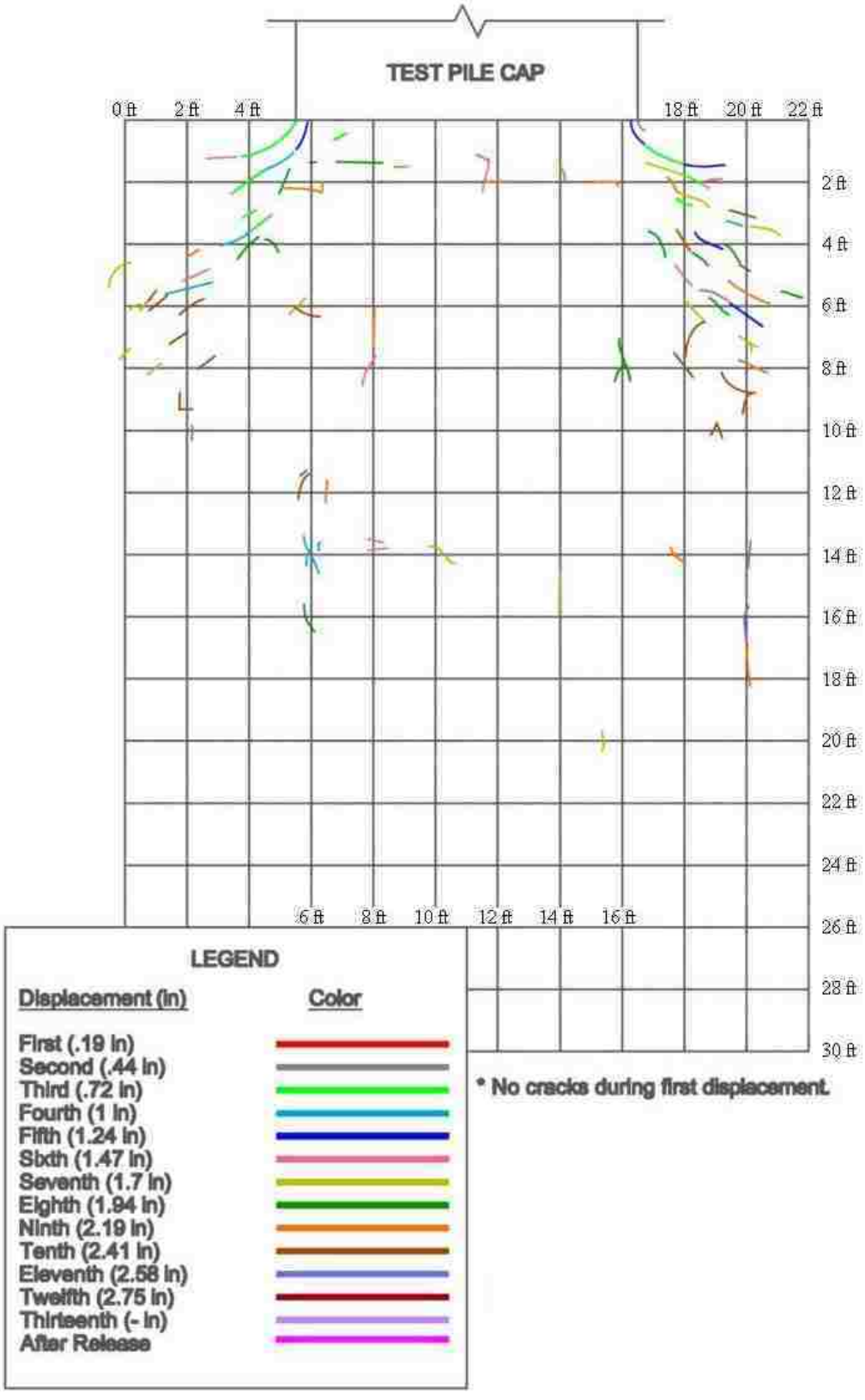

Figure 5-10: Crack map for the soil backfill for each displacement increment.

6 Plane Strain (2D Slip Planes)

This chapter presents the results of the dense plane strain (2D) test. These results are broken down into the following areas: force-displacement (force measured from actuators), force-displacement (force measured from pressure cells), inclinometer data, backfill displacement, transverse wall displacement, and heave and cracking.

6.1 Load-Displacement Results

The measured total resistance versus deflection of the pile cap is shown in Figure 6-1. The graph was obtained by plotting the measured total force from the actuators versus the average displacement of the pile cap corresponding to the peak load. The displacement was taken as the median value of the four string pots attached to the pile cap. Figure 6-2 also shows the total measured response, along with the baseline response and the passive earth response. The baseline results were obtained by running the test with no backfill present. This allows researchers to subtract the resistance contributed by factors other than the backfill passive response (such as lateral pile resistance and base shears) from the total response measured during the test. The baseline curve is relatively linear with a stiffness of approximately 118.4 kips/in. In contrast, the passive resistance versus displacement curve exhibits a hyperbolic shape and approaches an ultimate passive resistance of about 650 kips asymptotically.

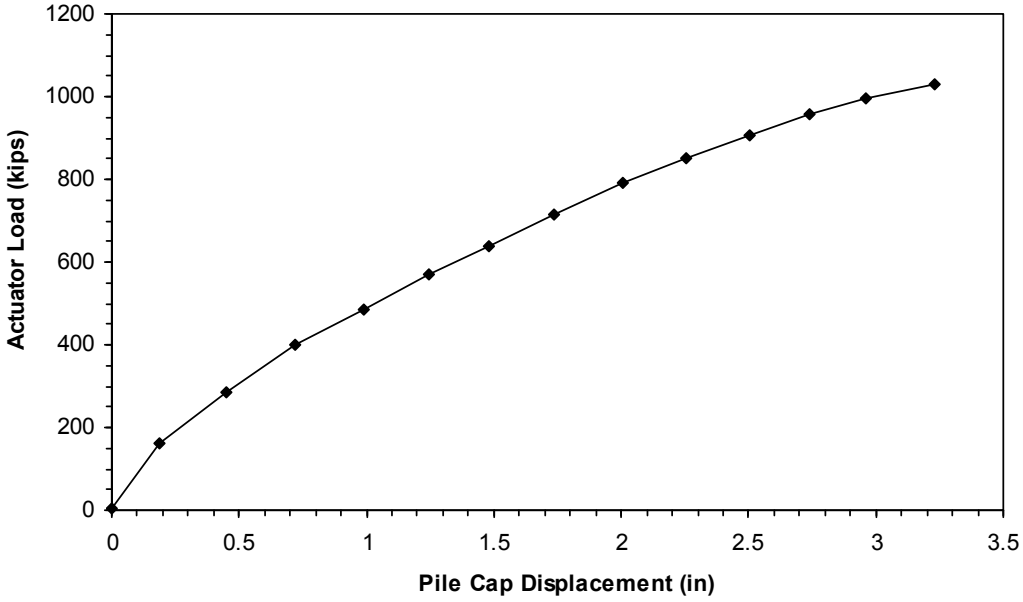

Figure 6-1: Total measured response versus displacement.

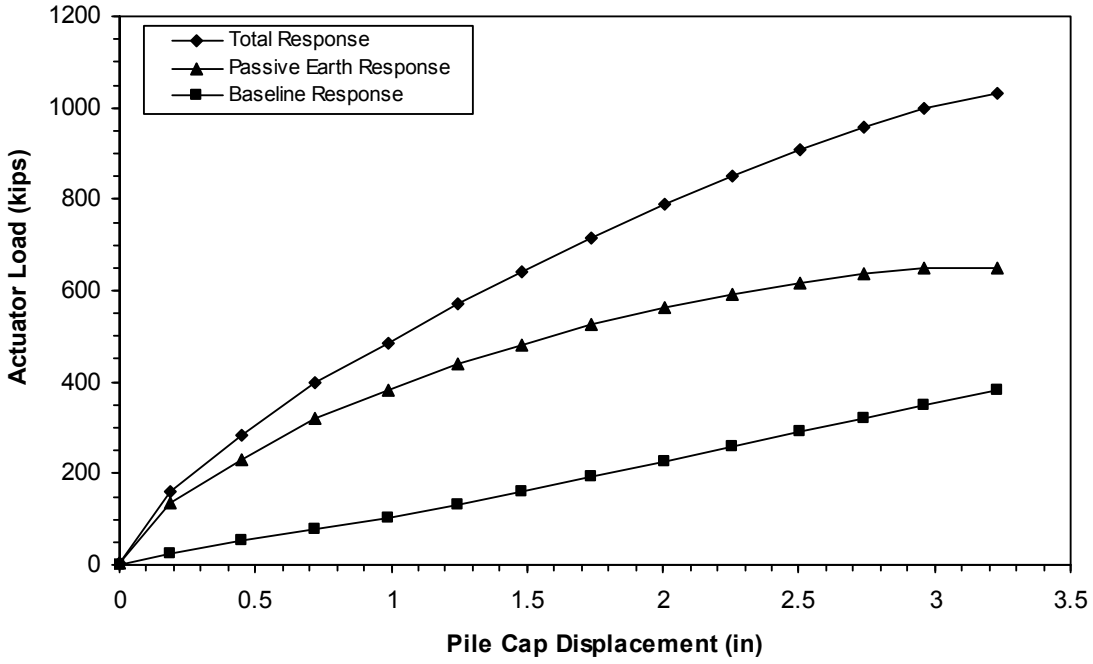

Figure 6-2: Passive resistance versus pile cap displacement.

6.2 Load-Displacement Results from Pressure Cells

Figure 6-3 shows the development of pressure on the pile cap face, with each reading corresponding to each displacement increment. Each point going down the pile cap face indicates the location of a pressure cell. The pressure in this test develops evenly in the top half of the pile cap, but much greater pressure develops in the bottom half. There is a tendency for the values at all depths to drop off near the end of testing, but the values at depths of 0.46, 1.38, 2.30, and 5.05 ft do this much earlier, at about the 2 inch nominal displacement of the pile cap, and drop off a lot more. These values have been adjusted to equal the maximum value reached at that depth; this is shown in Figure 6-4.

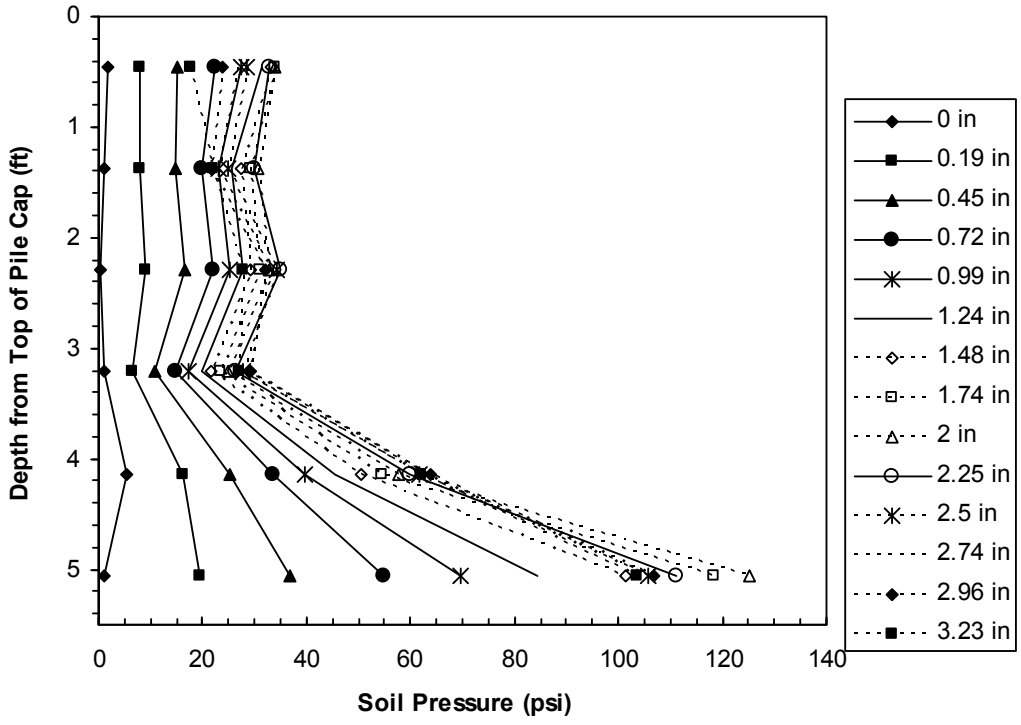

Figure 6-3: Development of pressure cell readings versus displacement.

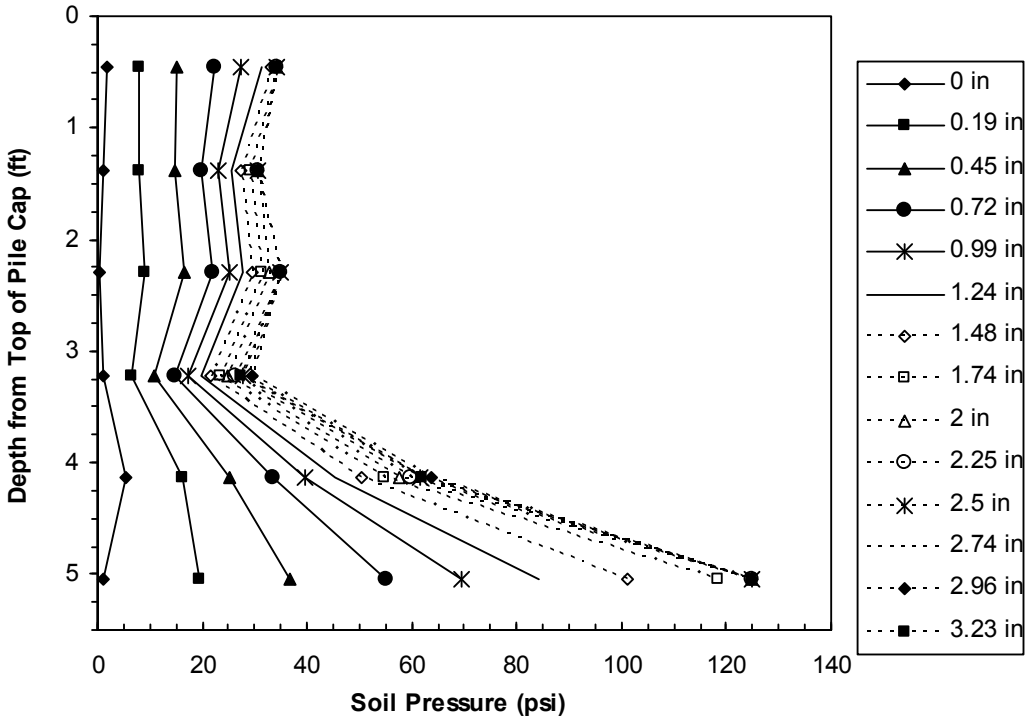

Figure 6-4: Development of pressure cell readings versus displacement, adjusted.

Figure 6-5 provides a comparison of the passive force-displacement curves obtained from the pressure cells with that from the actuators. The passive force from pressure cells was obtained by multiplying the measured pressure of each cell (as shown in Figure 6-4) by its tributary area. The tributary area is the distance from either the top of the pile cap or halfway to the adjacent pressure cell above the cell to the bottom of the pile cap or halfway to the adjacent pressure cell below the cell multiplied by the width of the pile cap. The passive earth response is the measured curve obtained from the actuators. The measured passive earth response from the pressure cells is multiplied by a factor of 1.3 to account for the end effects discussed in Section 5.2; these values are shown as the pressure cells with multiplier in Figure 6-5. As can be seen, the values for load from pressure cells with multiplier provides an excellent match to the load measured from the actuators for the initial part of the curve, then rises slightly above this curve

and then flat lines, falling below the ultimate passive resistance measured from the actuators. The flat line is due to the load being set to equal the maximum value a pressure cell reaches as was discussed, so after this point there is little to no increase in the overall measured resistance. The portion that matches the actuator curve reinforces the values obtained from the actuators alone, and increases the confidence in results obtained from the actuators. It also qualifies the method of subtracting baseline response from total measured resistance to obtain the passive earth response described in Section 6.1.

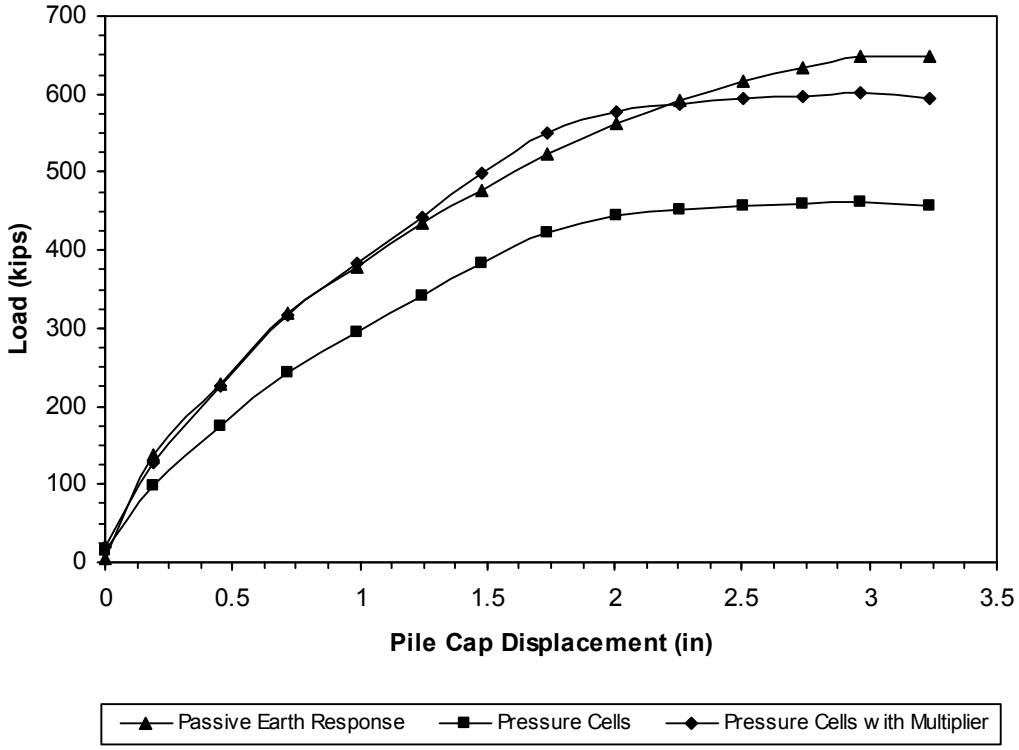

Figure 6-5: Load versus displacement from pressure cells.

6.3 Inclinometer Data

As discussed in Section 4.1.2, inclinometer readings were taken for each test. Figure 6-6 shows the deflection versus depth from these readings in both the north and south inclinometer casings. The curve represents change in deflection of the inclinometer tubes in the direction of loading, (the baseline reading was subtracted from the reading taken at the maximum displacement of the pile cap). A depth of zero corresponds to the top of the pile cap. The curves from both the north and the south match each other very well as would be expected. Also shown in this figure is the displacement of the pile cap as measured by the string pots that were attached to the pile cap. As can be seen the displacement measured by the inclinometer matches the displacement measured from the string pots. The deflection in the pile reaches zero at a depth of about 21 ft, which corresponds to nearly 20 pile diameters. The points within the cap translate horizontally and remain nearly vertical, indicating very little rotation of the pile cap. This is consistent with a fixed head boundary condition.

6.4 Backfill Soil Displacements

Figure 6-7 shows the absolute displacement of the backfill soil. The arrangement of string pots and stakes was discussed in section 4.1.3. These values were obtained by subtracting the displacement measured by each backfill string pot from the pile cap displacement at that loading increment. For example, if the backfill string pot at a distance of 2 ft from the face of the pile cap measured a displacement of 1 inch, and the loading increment was 2 inches, the value shown in Figure 6-7 would be 1 inch at 2 ft.

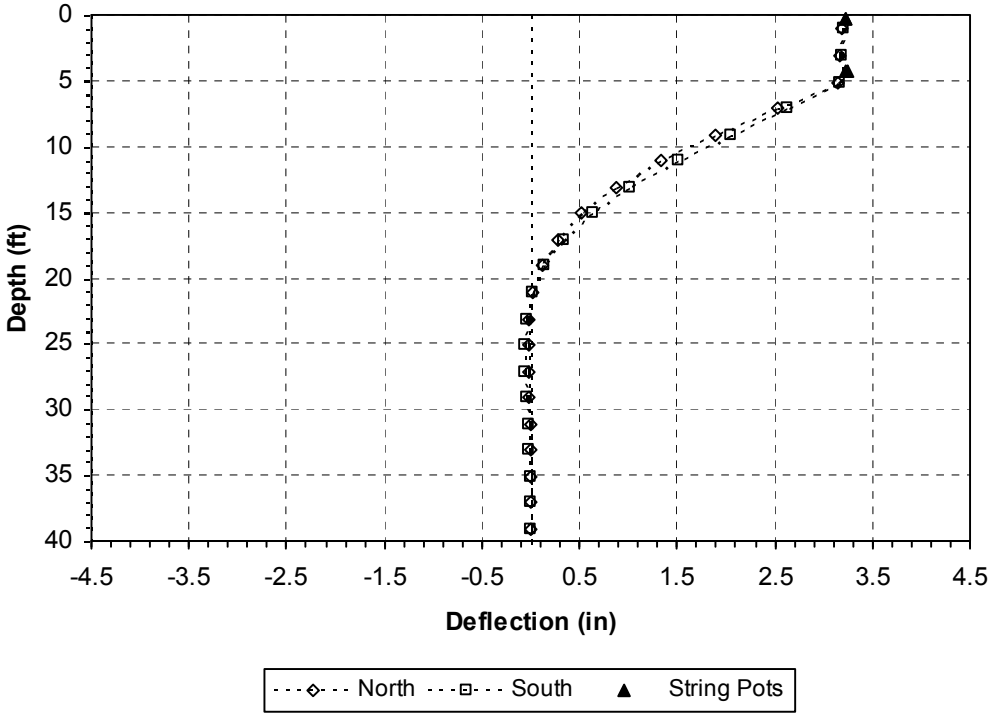

Figure 6-6: Deflection versus depth.

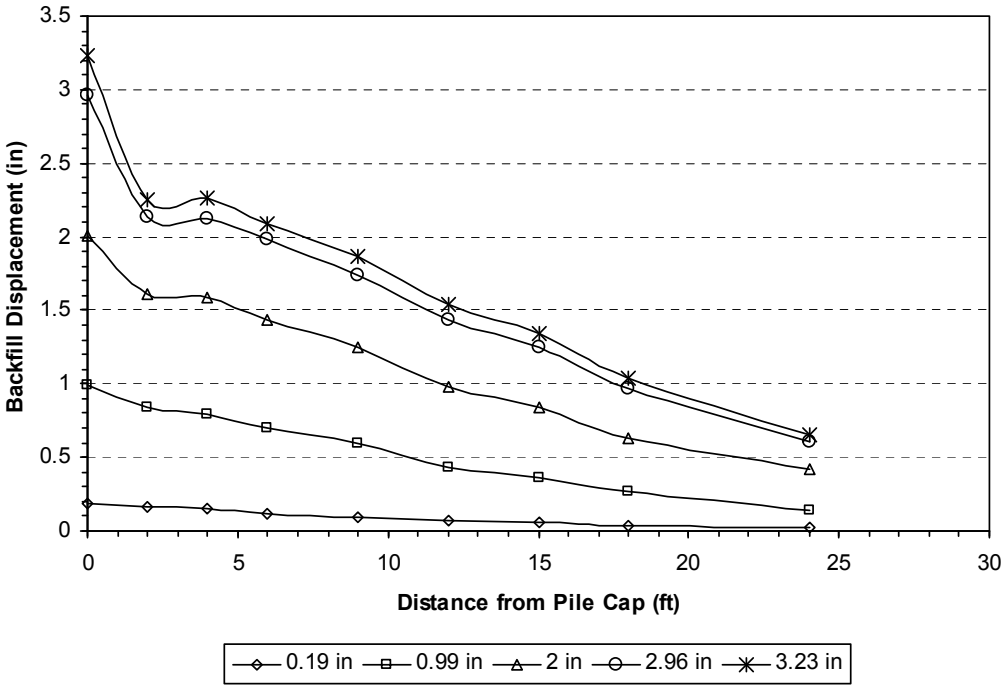

Figure 6-7: Displacement of backfill soil.

The compressive strain of the backfill is shown in Figure 6-8. In this figure each of the lines represents the compressive strain obtained from the corresponding string pot and stake. The strain values were obtained using the equation

$$\varepsilon = \Delta L / L \tag{6-1}$$

where ΔL = change in length from adjacent string pot
L = distance between adjacent stakes

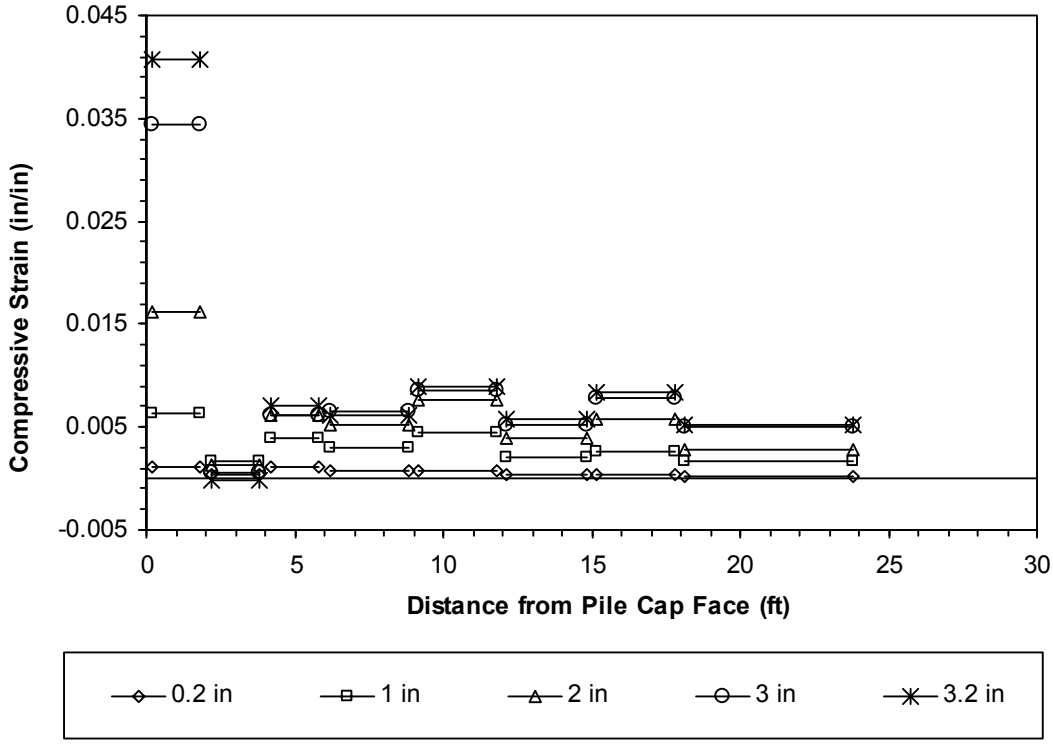

Figure 6-8: Compressive soil strain in backfill as a function of distance behind the cap for several displacement increments.

To simplify presentation of these results, only the first displacement increment, the nominal inch displacement increments, and the final displacement increment are shown in this figure. As can be seen, the greatest compressive strain occurs within the first couple feet of the cap face. In this test, the compressive strain is fairly uniform beyond 4 ft, with slightly higher strains occurring from 9 to 12 ft and again from 15 to 18 ft. The predicted log-spiral failure profile surfaces at about 24.6 ft from the face of the pile cap. The compressive strain remains fairly constant to this distance.

6.5 Transverse Displacement of Wall Panels

Figure 6-9 shows the outward movement of the top of the wall panels versus distance from the face of the pile cap. These plots represent the data obtained from the string pots located at 2, 6, 12, and 18 ft from the face of the pile cap. The graph is shown as if a viewer were above the test, with the west wall in front of them, and the pile cap to their left, with the face of the pile cap at 0 on the horizontal axis. Each line represents values from selected displacement increments, as indicated. For clarity, data from the first pile cap displacement, each nominal inch, and the last pile cap displacement are shown. This plot indicates that the wall is moving out fairly evenly, though a bulge appears in the wall from 2 to 12 ft from the face of the pile cap. The displacement of the string pots located at 2 and 6 ft from the face of the pile cap have been averaged to lessen this bulge. This line is shown as the dashed line that flattens the appearance of the bulge, though this isn't done for the 0.25 inch pile cap displacement, as the bulge doesn't appear here. The reason for averaging the two string pots is to lessen the bulge that appears in the center of a sheet of plywood. However, the appearance of the bulge may not be wrong, as the maximum difference from the center of the sheet of plywood to the edges (from 4 to 8 ft,

edge to edge locations) is only three-hundredths of an inch, or about 1/32 of an inch. This is well within reasonable flexure values. The flexure of the entire wall system from 2 to 18 ft is about 0.0565 in, or just under 1/16 of an inch. Also, the maximum outward displacement of the wall panels is about 1/4 of an inch. From this it is reasonable to state that while the test approximated plane strain conditions, it wasn't true plane strain. Despite this, plane strain is the term that will continue to be used throughout this research.

Figure 6-10 shows the displacement of the wall panels versus the actuator load. As can be seen, during the first of the load, the panels displace very little, and then the wall panels displace uniformly, as can be seen by the same slope of the straight-portions of each of the lines.

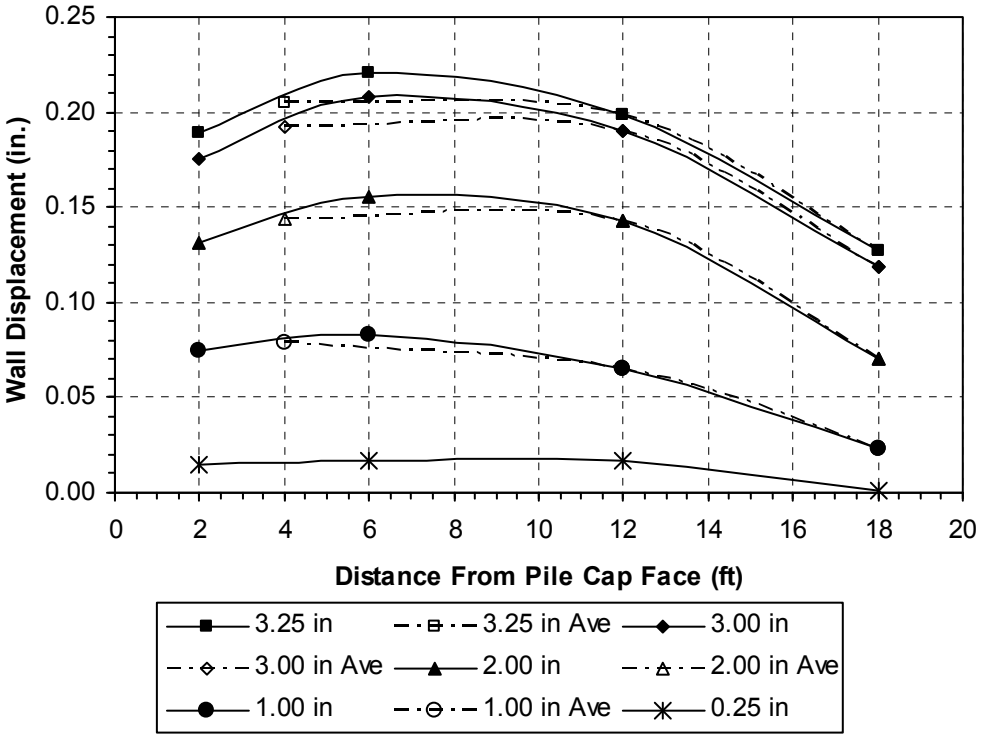

Figure 6-9: Outward movement of wall panel, plan view, near the top of the wall panel.

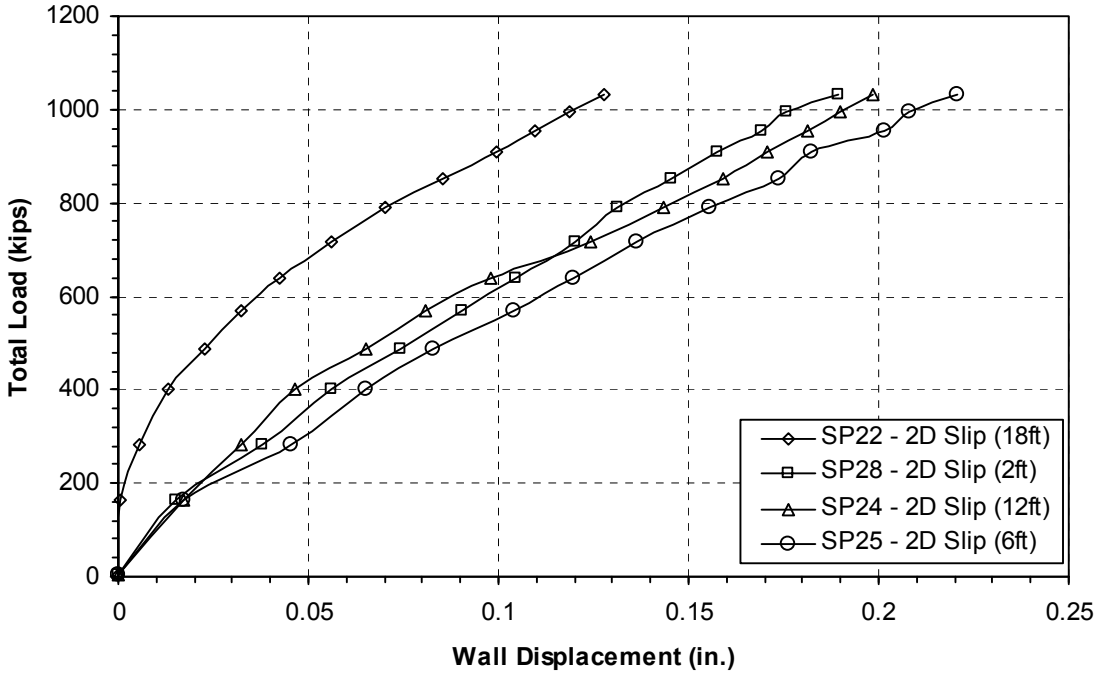

Figure 6-10: Outward displacement of wall panel versus actuator load.

6.6 Heave and Cracking of Soil Backfill

This section will present the data that was gathered regarding heaving and cracking of the backfill soil profile during and after testing. The methods that were used to gather this data are discussed in section 4.1.3. Figure 6-11 shows the soil heave profile for the test. The values represent the change in elevation from before the test to the largest displacement of the pile cap and are in inches. Positive values indicate upward movement, while negative indicates downward movement (settlement). The dashed lines are set up in a 2 ft by 2 ft grid, consistent with the grid that was painted on the soil surface before the test was performed. As can be seen from this figure, the maximum heave occurs from about 4 to 6 ft from the face of the pile cap. The shape of the heave contour lines is circular, as occurs with a plain soil backfill (no MSE walls), and appear as though they would continue outside the side confinement.

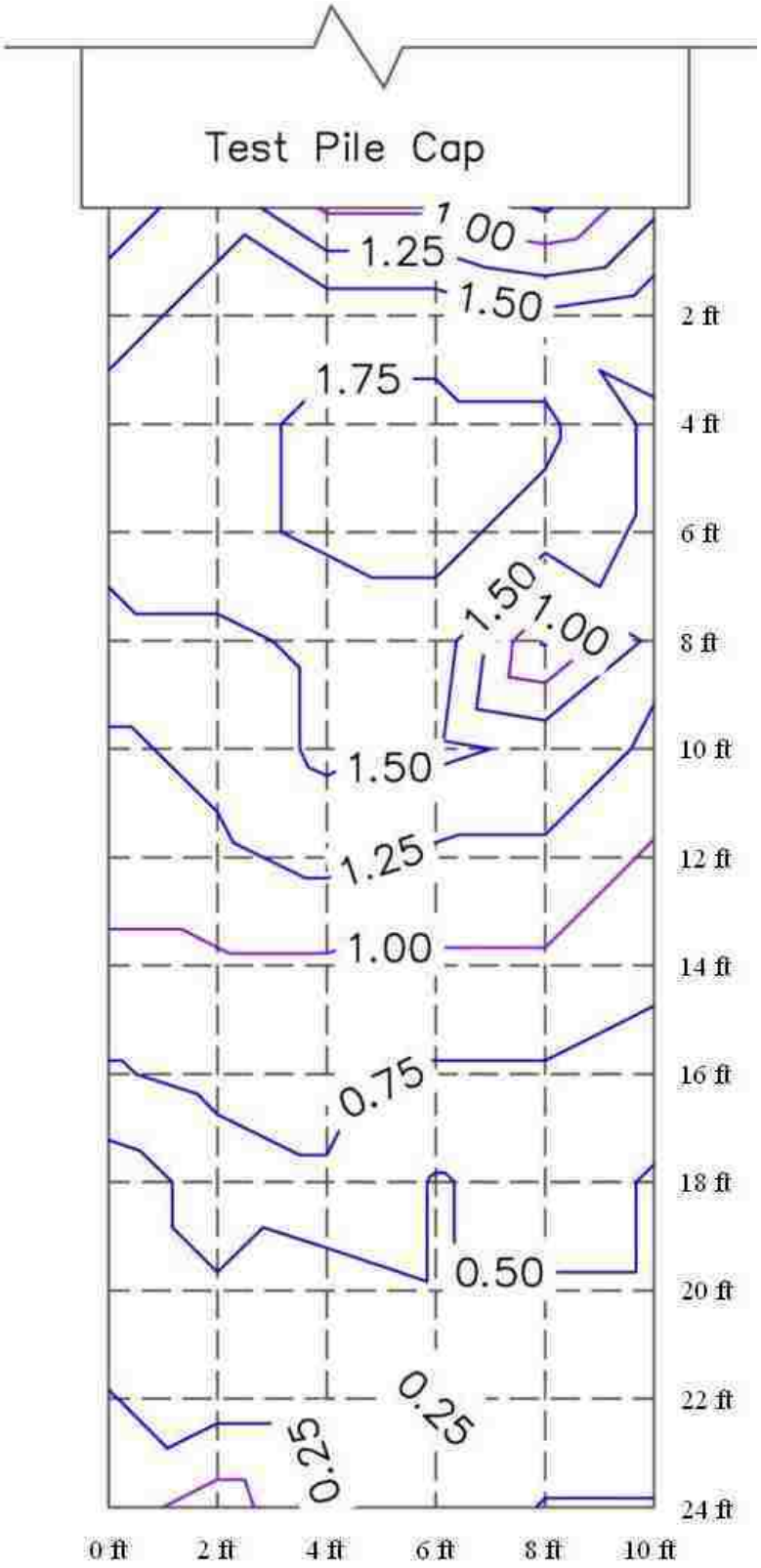

Figure 6-11: Soil heave profile.

Figure 6-12 is a map showing the development of cracks observed for each pile cap displacement increment, with cracks for each increment identified by a separate color. The process by which cracks were mapped is described in greater detail in section 4.1.3. The cracking in this test appears to have been minimal, with the majority of crack during testing running perpendicular to the face of the pile cap or parallel to the wall panels.

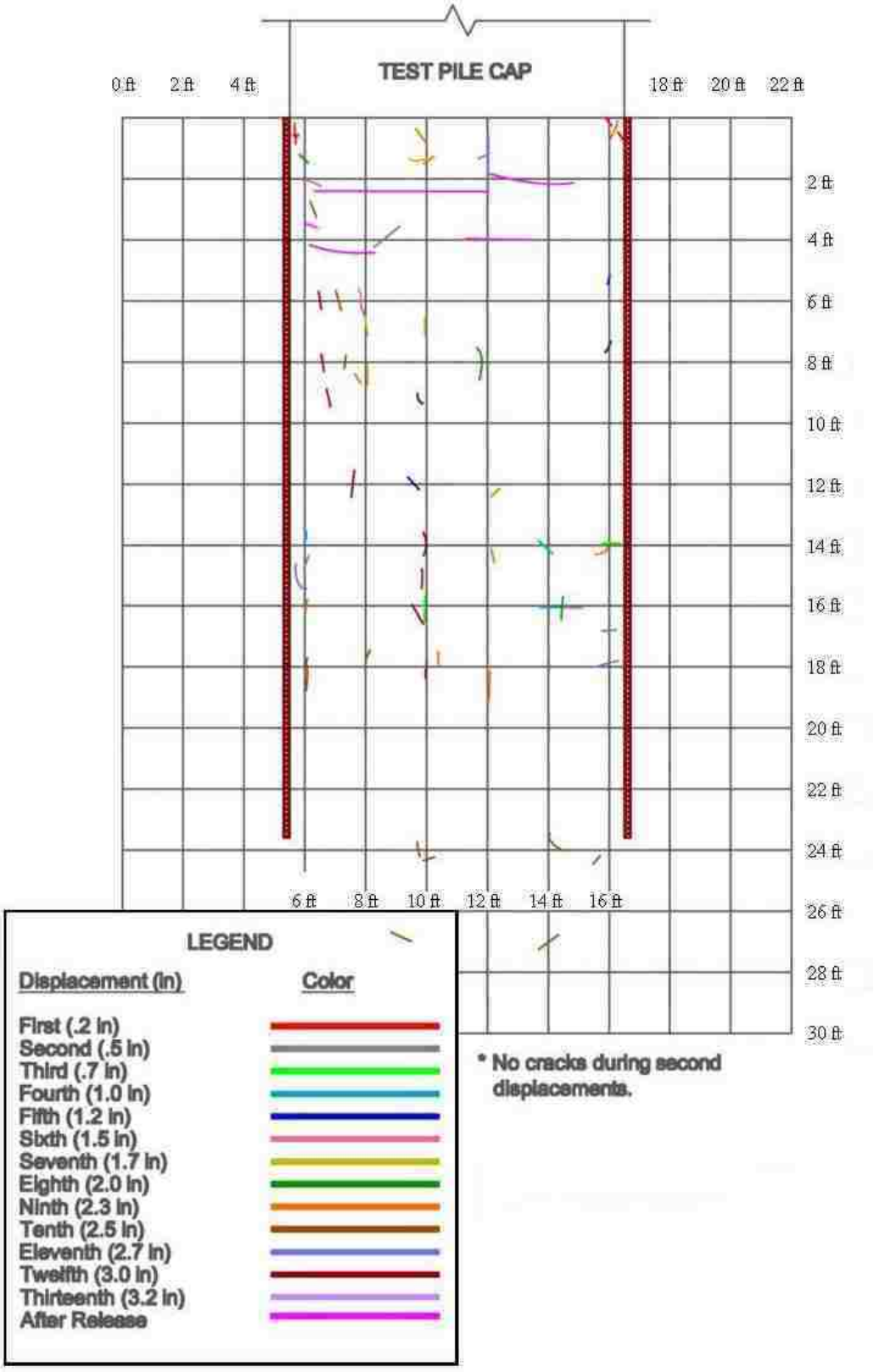

Figure 6-12: Crack map.

7 MSE Test 1 Results

This chapter presents the results of the first MSE test. These results are broken down into the following areas: force-displacement (force measured from actuators), force-displacement (force measured from pressure cells), inclinometer data, backfill displacement, transverse wall displacement, heave and cracking, and mat strains/forces. This test was designed to have an average static factor of safety against pullout of 1.5, different from the factor of safety of the test in Chapter 8. The results from this test will be compared with other test results in this study and with test results from Heiner (2010) in a later chapter.

7.1 Load-Displacement Results

The measured total resistance versus deflection of the pile cap is shown in Figure 7-1. The graph was obtained by plotting the measured total force from the actuators versus the displacement of the pile cap corresponding to the peak load. The displacement was taken as the median value of the four string pots attached to the pile cap. Figure 7-2 also shows the total measured response, along with the baseline response and the passive earth response. The baseline results were obtained by running the test with no backfill present. This allows researchers to subtract the resistance contributed by factors other than the backfill passive response (such as lateral pile resistance and base shears) from the total response measured during the test. The baseline curve is relatively linear with a stiffness of approximately 118 kips/in. In

contrast, the passive resistance versus displacement curve exhibits a hyperbolic shape and approaches an ultimate resistance of about 590 kips asymptotically.

7.2 Load-Displacement Results from Pressure Cells

Figure 7-3 shows the development of pressure on the pile cap face, with each reading corresponding to each displacement increment. Each point going down the pile cap face indicates the location of a pressure cell. The pressure in this test develops evenly in the top half of the pile cap, but much greater pressure develops in the bottom half. The values from the pressure plate at a depth of 1.38 ft drop off beginning at about the 1.75 inch nominal pile cap displacement increment. The values that begin to decrease have been fixed to equal the maximum value reached at that depth. The values from the pressure plate located at a depth of 2.30 ft increases much more than any values around it. These values have been set to a value that is an interpolation of the values from adjacent pressure plates; these two changes are reflected in Figure 7-4.

Figure 7-5 provides a comparison of the passive force-displacement curves obtained from the pressure cells with that from the actuators. The passive force from pressure cells was obtained by multiplying the measured pressure of each cell (as shown in Figure 7-4) by its tributary area. The tributary area is the distance from either the top of the pile cap or halfway to the adjacent pressure cell above the cell to the bottom of the pile cap or halfway to the adjacent pressure cell below the cell multiplied by the width of the pile cap. The passive earth response is the measured curve obtained from the actuators. The measured passive earth response from the pressure cells is multiplied by a factor of 1.3 to account for the end effects discussed in Section 5.2; these values are shown as the pressure cells with multiplier in Figure 7-5.

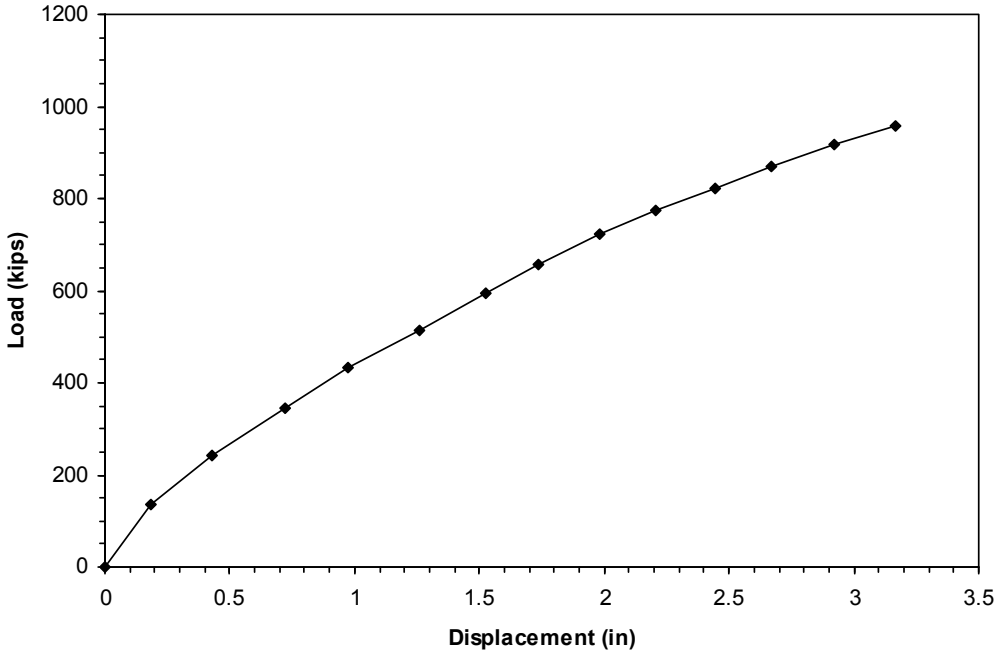

Figure 7-1: Total measured response versus displacement.

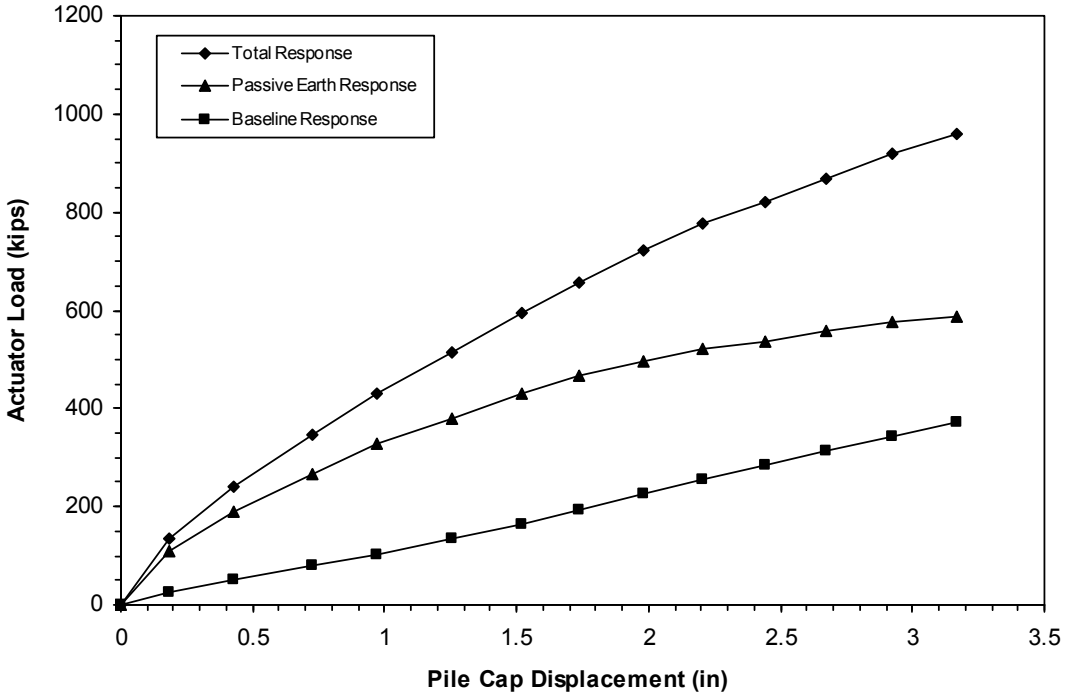

Figure 7-2: Passive resistance versus pile cap displacement.

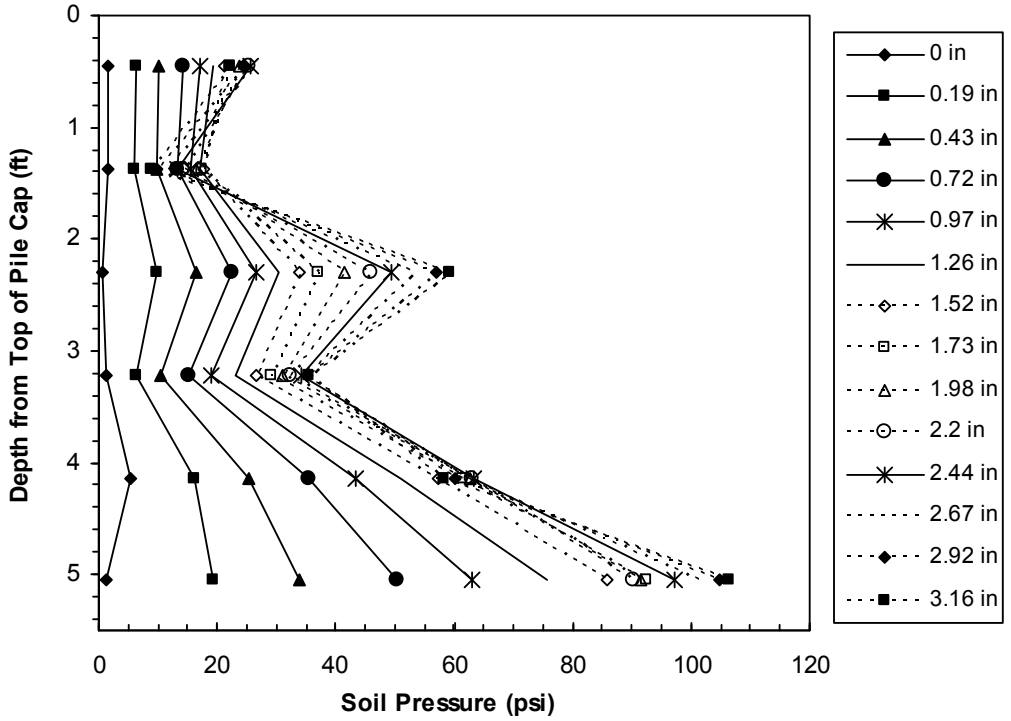

Figure 7-3: Development of pressure cell readings versus displacement.

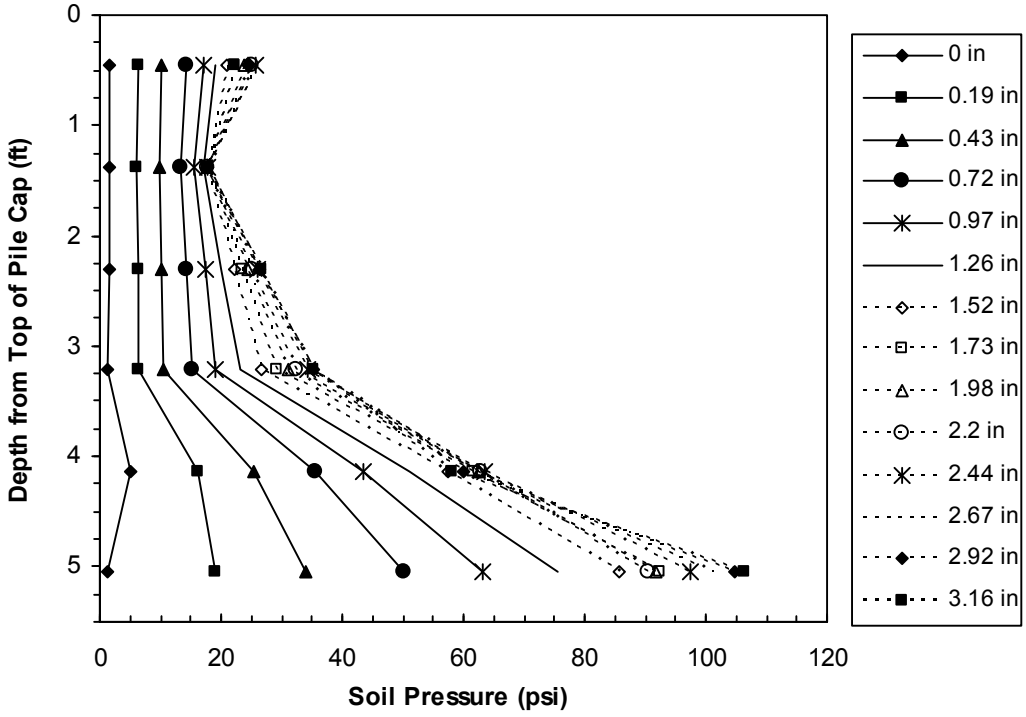

Figure 7-4: Development of pressure cell readings versus displacement, adjusted.

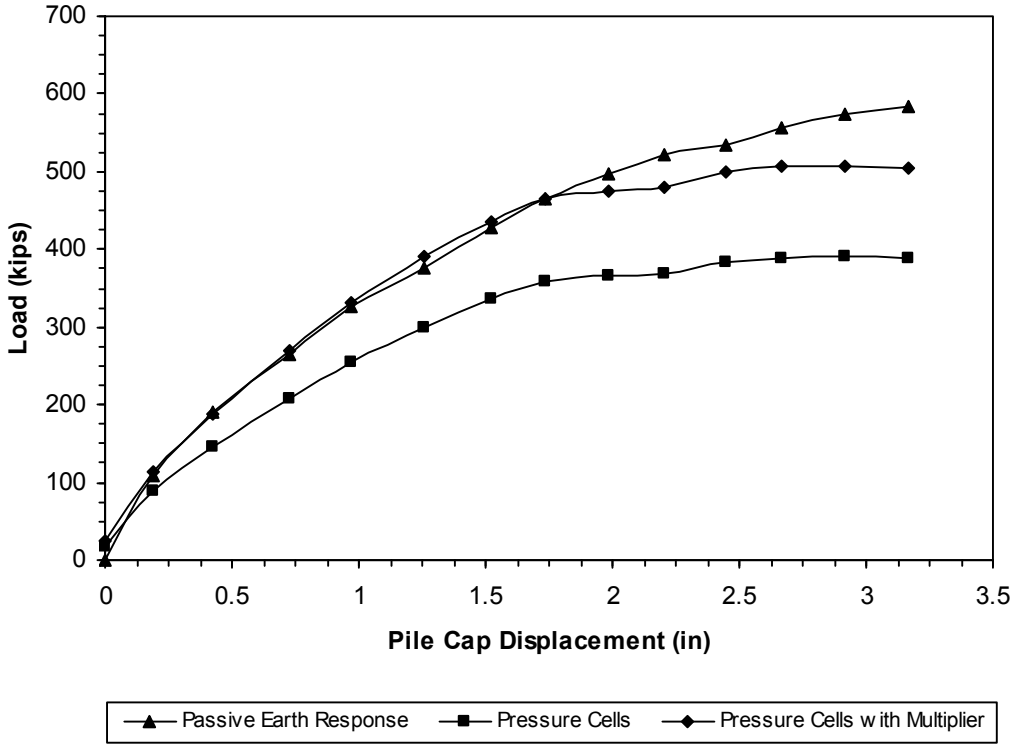

Figure 7-5: Load versus displacement from pressure cells.

As can be seen, the values for load from pressure cells with multiplier provides an excellent match to the load measured from the actuators for the initial part of the curve, then flat lines, falling below the ultimate passive resistance measured from the actuators. The portion that matches the actuator curve reinforces the values obtained from the actuators alone, and increases the confidence in results obtained from the actuators. It also qualifies the method of subtracting baseline response from total measured resistance to obtain the passive earth response described in Section 7.1.

7.3 Inclinometer Data

As discussed in Section 4.1.2, inclinometer readings were taken for each test. Figure 7-6 shows the deflection versus depth from these readings in both the north and south inclinometer

casings. The curve represents change in deflection of the inclinometer tubes in the direction of loading, (the baseline reading was subtracted from the reading taken at the maximum displacement of the pile cap). A depth of zero corresponds to the top of the pile cap. The curves from both the north and the south match each other very well as would be expected. Also shown in this figure is the displacement of the pile cap as measured by the string pots that were attached to the pile cap. As can be seen the displacement measured by the inclinometer matches the displacement measured from the string pots. The deflection in the pile reaches zero at a depth of about 21 ft, which corresponds to nearly 20 pile diameters. The points within the cap translate horizontally and remain nearly vertical, indicating very little rotation of the pile cap. This is consistent with a fixed head boundary condition.

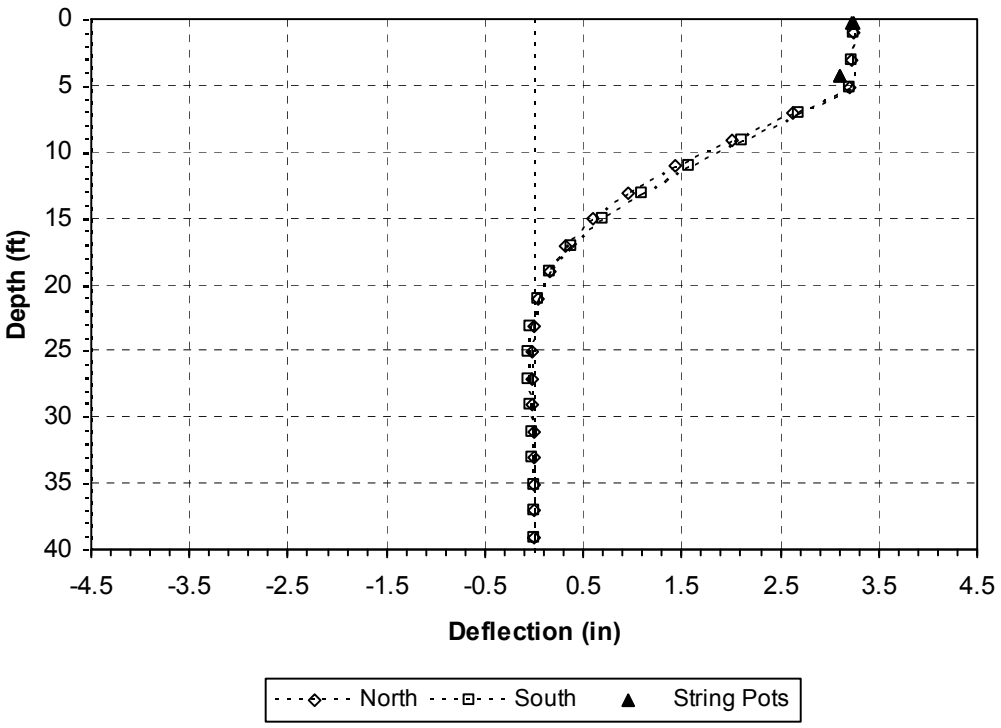

Figure 7-6: Deflection versus depth.

7.4 Backfill Soil Displacements

Figure 7-7 shows the absolute displacement of the backfill soil. The arrangement of string pots and stakes was discussed in section 4.1.3. These values were obtained by subtracting the displacement measured by each backfill string pot from the pile cap displacement at that loading increment. For example, if the backfill string pot at a distance of 2 ft from the face of the pile cap measured a displacement of 1 inch, and the loading increment was 2 inches, the value shown in Figure 7-7 would be 1 inch at 2 ft.

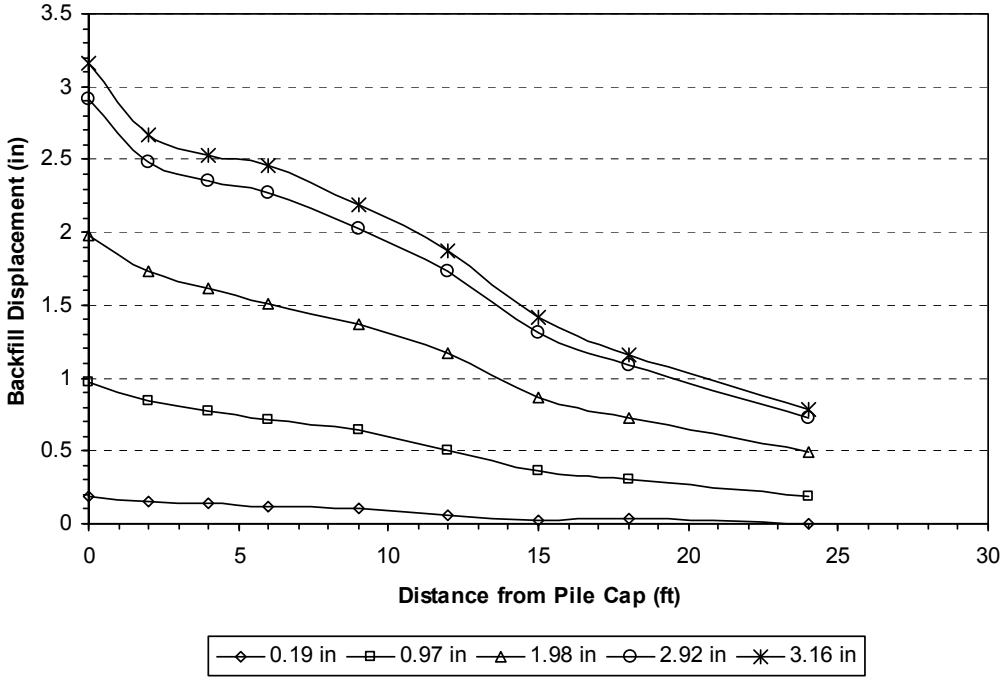

Figure 7-7: Displacement of backfill soil.

The compressive strain of the backfill is shown in Figure 7-8. In this figure each of the lines represents the compressive strain obtained from the corresponding string pot and stake. The strain values were obtained using the equation

$$\varepsilon = \Delta L / L \tag{7-1}$$

where ΔL = change in length from adjacent string pot
L = distance between adjacent stakes

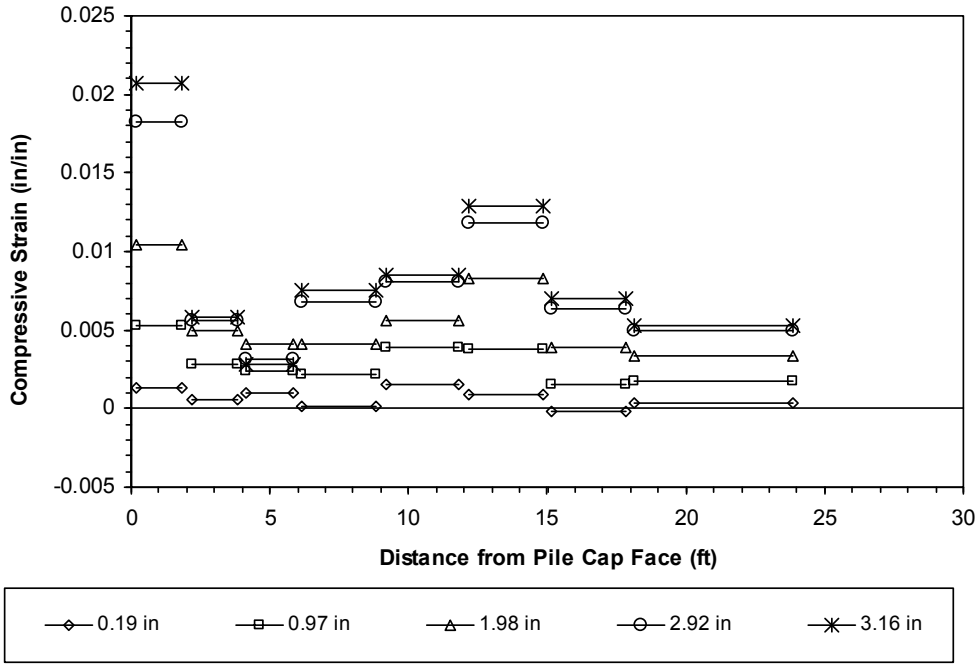

Figure 7-8: Compressive soil strain in backfill as a function of distance behind the cap for several displacement increments.

To simplify presentation of these results, only the first displacement increment, the nominal inch displacement increments, and the final displacement increment are shown in this figure. As can be seen, the greatest compressive strain occurs within the first couple feet of the cap face. A minimum value of compressive strain is reached from 4 to 6 ft from the face of the pile cap, then the compressive strain increases to reach a local maximum value at 12 to 15 ft from the face of the pile cap, and decreases toward the back edge of the backfill zone. The predicted log-spiral failure profile surfaces at about 28.2 ft from the face of the pile cap. This appears consistent with the measured backfill strain in this figure.

7.5 Transverse Displacement of Wall Panels

Figure 7-9 shows the outward movement of the wall panel. This plot represents the data obtained from the string pots 102.5 inches (8.54 ft) from the face of the pile cap. Data from one of the string pots located 20.5 inches from the wall face was faulty. The data was extrapolated linearly to demonstrate the movement of the wall from top to bottom, while the point on each line represents the location of each string pot. Each line represents values from each displacement increment, as indicated. The top of the wall is located at a depth of 0 inches. This plot shows that the top of the wall is displacing outward more than the bottom, resulting in rotation of the wall. This result can be expected, as the bottom reinforcing has about 1230 lb capacity per bar mat available beyond the construction load.

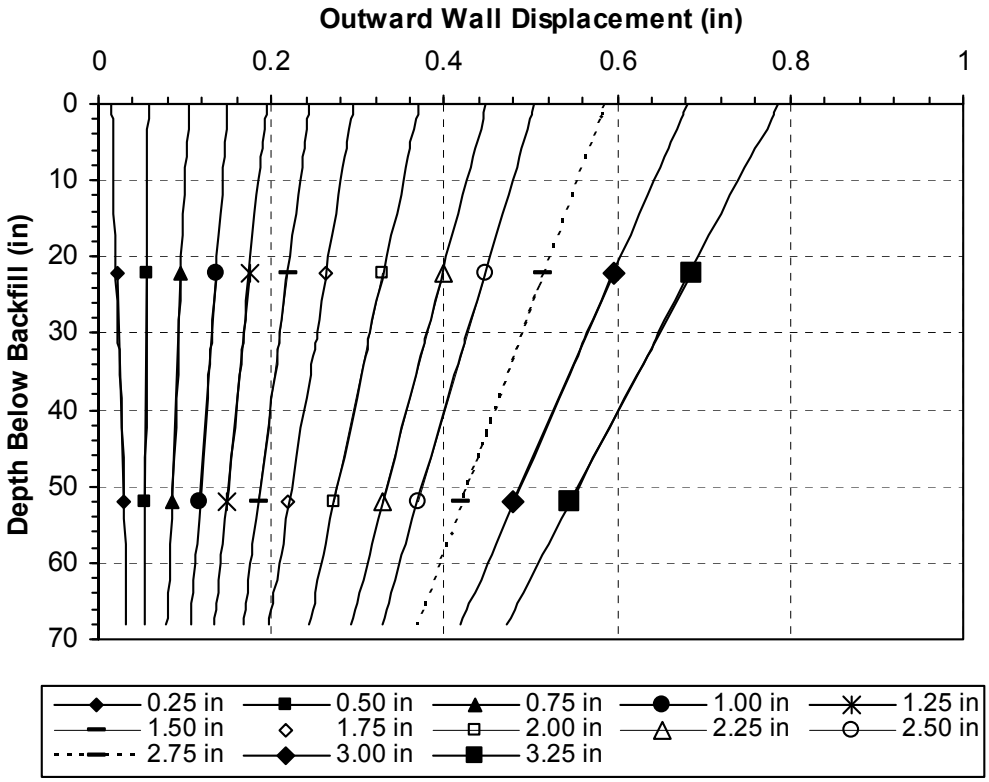

Figure 7-9: Outward movement of wall panel, top to bottom, 102.5 inches from pile cap face.

Figure 7-10 shows the rotation of the wall panel versus the actuator load. This is the measured rotation at a distance of 102.5 inches (8.54 ft) from the face of the pile cap. As can be seen, for the first two displacement increments, very little rotation occurs at this distance. However, as the test develops the rotation of the wall panel increases more rapidly.

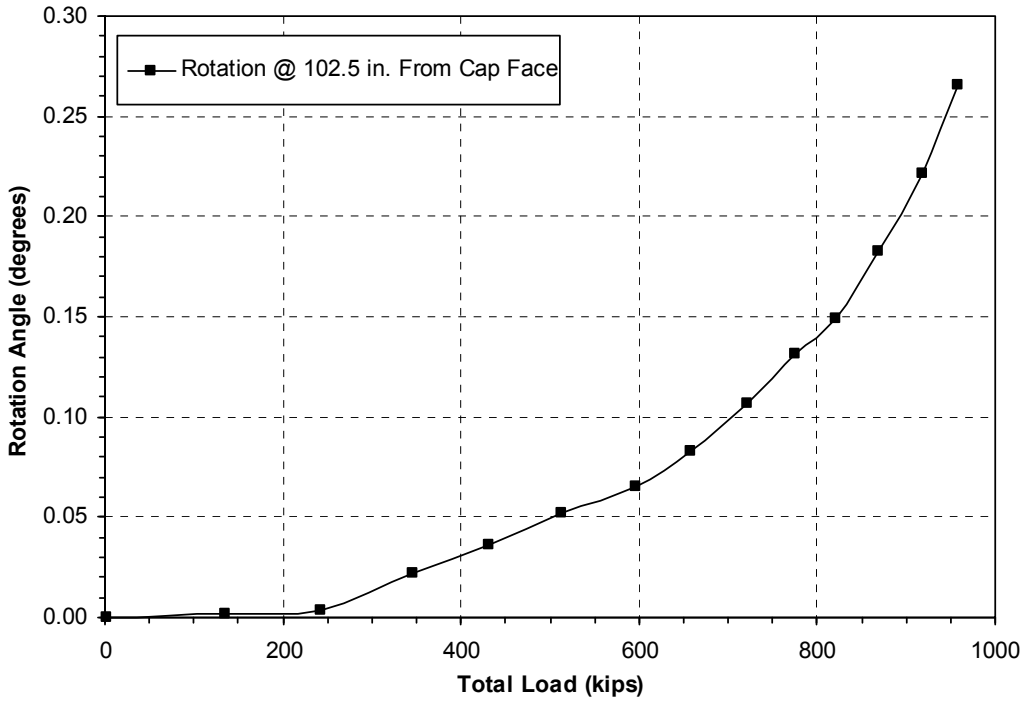

Figure 7-10: Rotation of wall panel versus actuator load.

Figure 7-11 shows the outward movement of the wall versus distance from the pile cap. While Figure 7-9 can be pictured as one standing at the end of the wall and looking along the wall (an elevation), Figure 7-11 is seen from above (plan view). For clarity, only data from every half inch of displacement is shown. This plot indicates that the point where the wall panels join is moving outward much more than the end of the wall panel near the pile cap. The points on this plot indicate the location of the string pots.

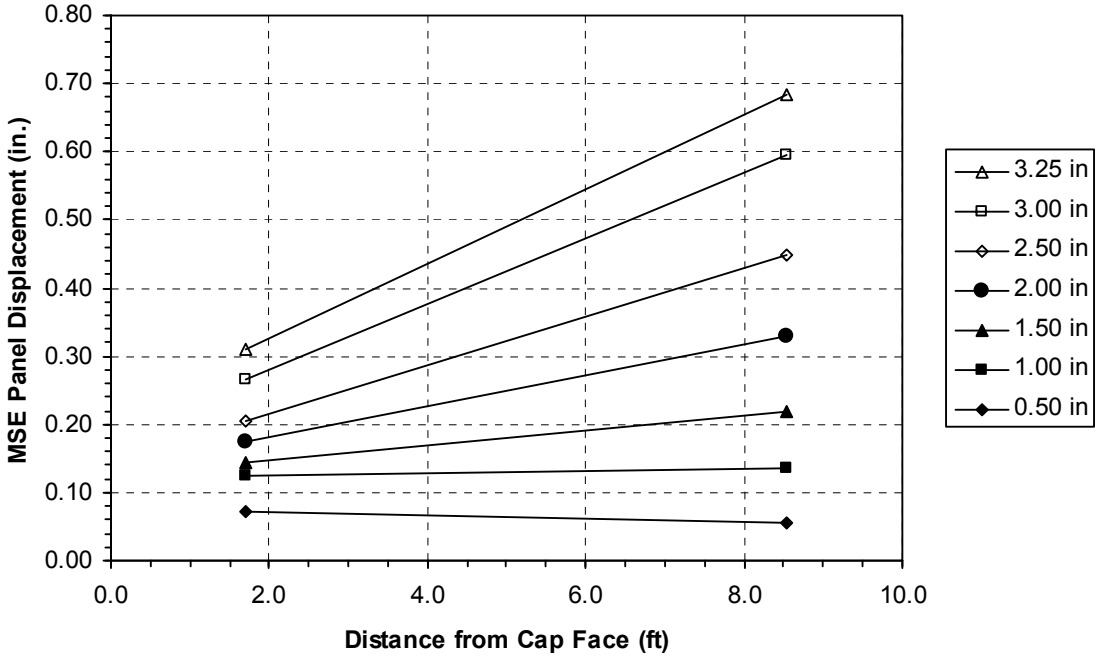

Figure 7-11: Outward movement of wall panel versus distance from pile cap.

Shown in Figure 7-12 is the outward movement of the top of the wall panel versus the measured load from the actuator. As can be seen from the shape of this plot, the wall begins to displace more rapidly, indicating diminishing returns from the wall panels. This data is from the top of the wall at a distance of 102.5 inches from the pile cap face.

Figure 7-13 shows the transverse displacement of the wall panel versus the incremental displacement of the pile cap during the loading sequence. The displacement is for the top of the wall panels at a distance of 102.5 inches from the pile cap face. This also indicates that the rate at which the wall panels are displacing outward is increasing. If the rate were constant, the line in Figure 7-13 would be linear. Instead, it is concave upward, indicating that the rate at which the MSE wall panels move outward is increasing as the test progresses.

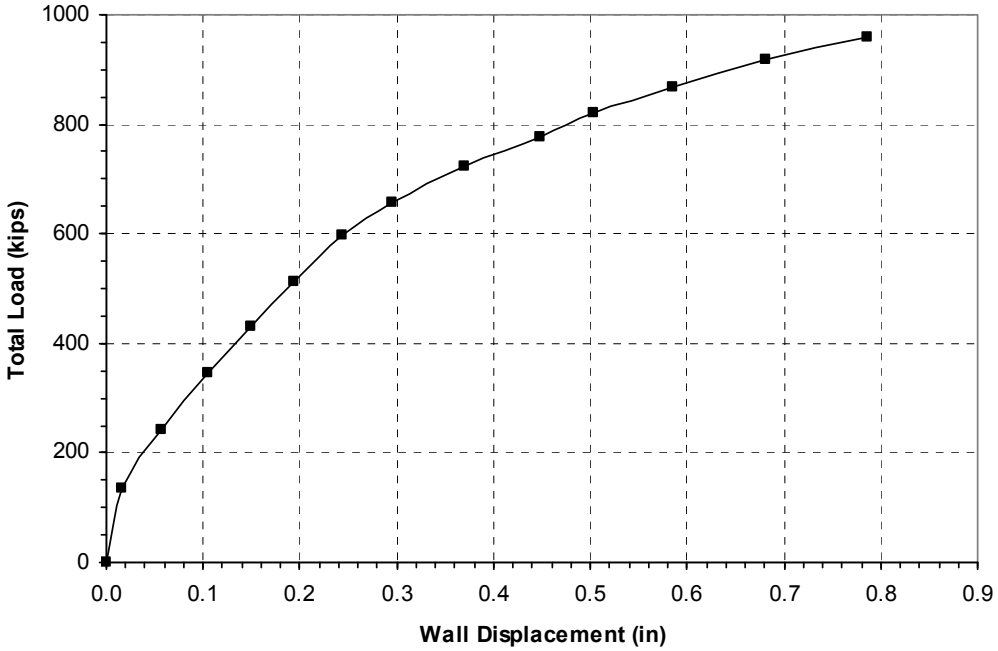

Figure 7-12: Outward displacement of wall panel versus actuator load.

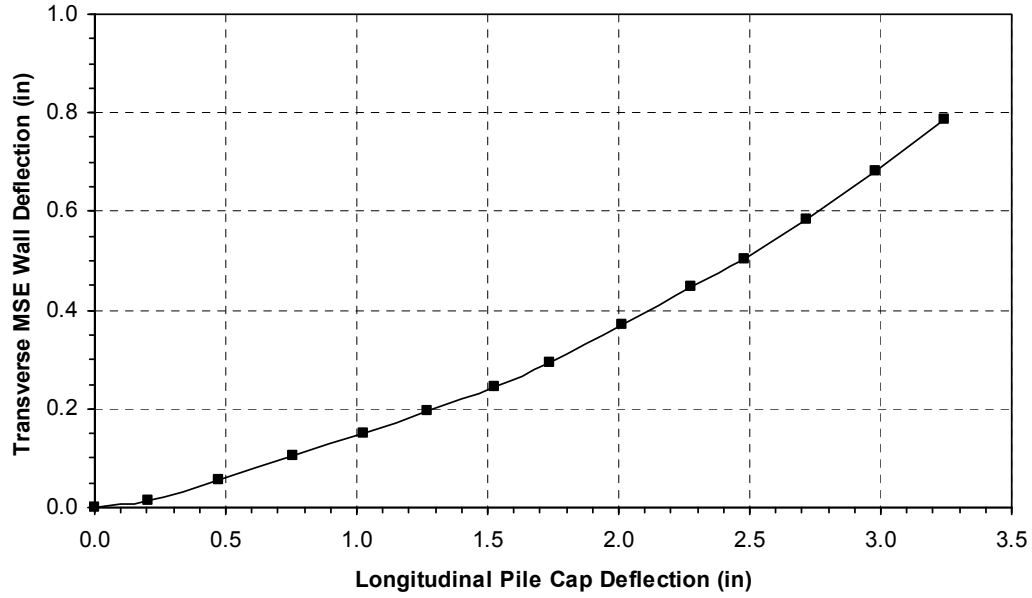

Figure 7-13: Transverse deflection versus longitudinal deflection.

7.6 Heave and Cracking of Soil Backfill

This section will present the data gathered regarding heaving and cracking of the backfill soil profile during and after testing. The methods that were used to gather this data are discussed in section 4.1.3. Figure 7-14 shows the soil heave profile for the test. The values represent the change in elevation from before the test to the largest displacement of the pile cap and are in inches. Positive values indicate upward movement, while negative indicates downward movement (settlement). The dashed lines are set up in a 2 ft by 2 ft grid, consistent with the grid that was painted on the soil surface before the test was performed. As can be seen from this figure, the maximum heave occurs about 6 ft from the face of the pile cap. At a given distance behind the pile cap, the contours indicate that heave is greatest near the center of the fill and lowest near the walls. This is likely a result of outward movement near the wall which reduces the heaving.

Figure 7-15 is a map showing the development of cracks observed for each pile cap displacement increment, with cracks for each increment identified by a separate color. The process by which cracks were mapped is described in greater detail in section 4.1.3. It should be observed that most of the cracks are perpendicular to the front face of the pile cap or parallel to the MSE wall panels. Most of the cracks that don't exhibit this behavior are those which developed after the applied load was reduced and the pile cap was pulled away from the backfill. Further away from the pile cap, the greatest concentration of cracks is in the center. This is likely a result of the outward movement of the wall panels as documented previously. The bar mats end about in the middle of the soil backfill. Thus, soil could be "riding" on these mats, pulling apart the soil in the center of the backfill. However, the cracks are fairly evenly distributed closer to the pile cap, and seem to spread from the middle toward the edges of the pile

cap. When compared to a compression test on concrete cylinders, there appears to be a remarkable similarity. One type of fracture in concrete cylinders is called a cone and split. The rough failure surface presented by the cracks mimics this cone and split failure type. The cone occurs at the top of the figure, with one side against the pile cap face, while the split begins about 10 ft from the pile cap face and follows the center of the backfill.

7.7 Mat Strains and Forces

This section will present the data gathered from the strain gauges placed on the bar mats, as described in section 4.4. The forces developed in the mats are also presented in this chapter along with a comparison of pressure on the wall panels relative to the pressure on the pile caps. Also, the development of the force in the bar mats will be compared to the outward displacement of the wall panels.

Figure 7-16 through Figure 7-23 are plots of the force in the bar mats along the length of the mats for selected displacement increments, obtained from the strain gauges. Each point along a curve represents the location of a set of strain gauges placed at that location on the bar mat. To obtain the force, F, for the entire bar mat, the strain from a set of strain gauges (located at the same distance from the panel face, on the top and bottom of the longitudinal bar) was averaged and the force was computed using the equation

$$F = \bar{\varepsilon} * E * A * B \qquad (7\text{-}2)$$

where F is the force in the entire mat at a location
$\bar{\varepsilon}$ is the average strain at a location
E is the modulus of elasticity of steel, 29000000 psi
A is the area of one longitudinal bar, in^2
B is the number of longitudinal bars minus 1

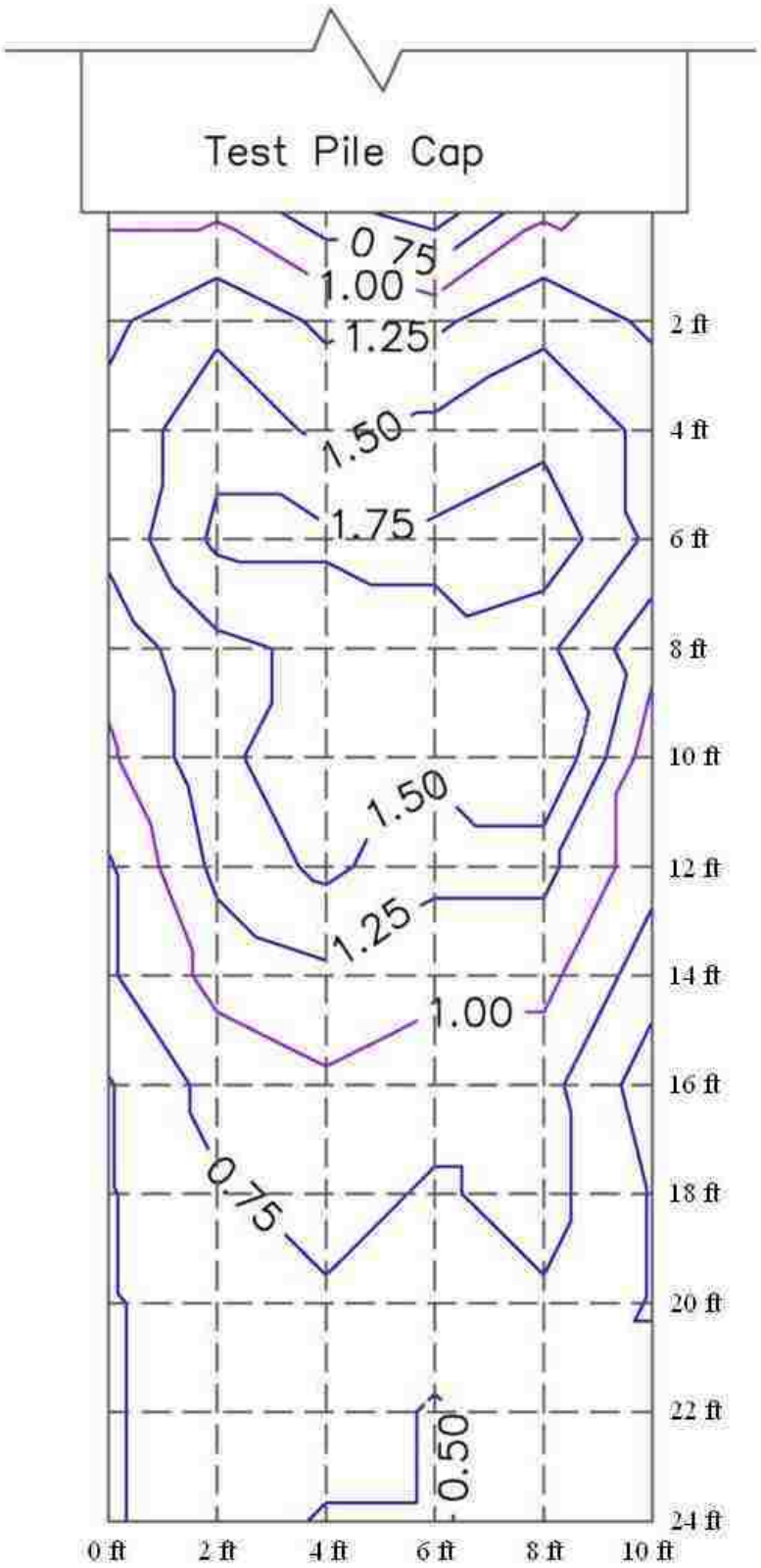

Figure 7-14: Soil heave contours (inches) for the backfill within MSE wall panels behind pile cap.

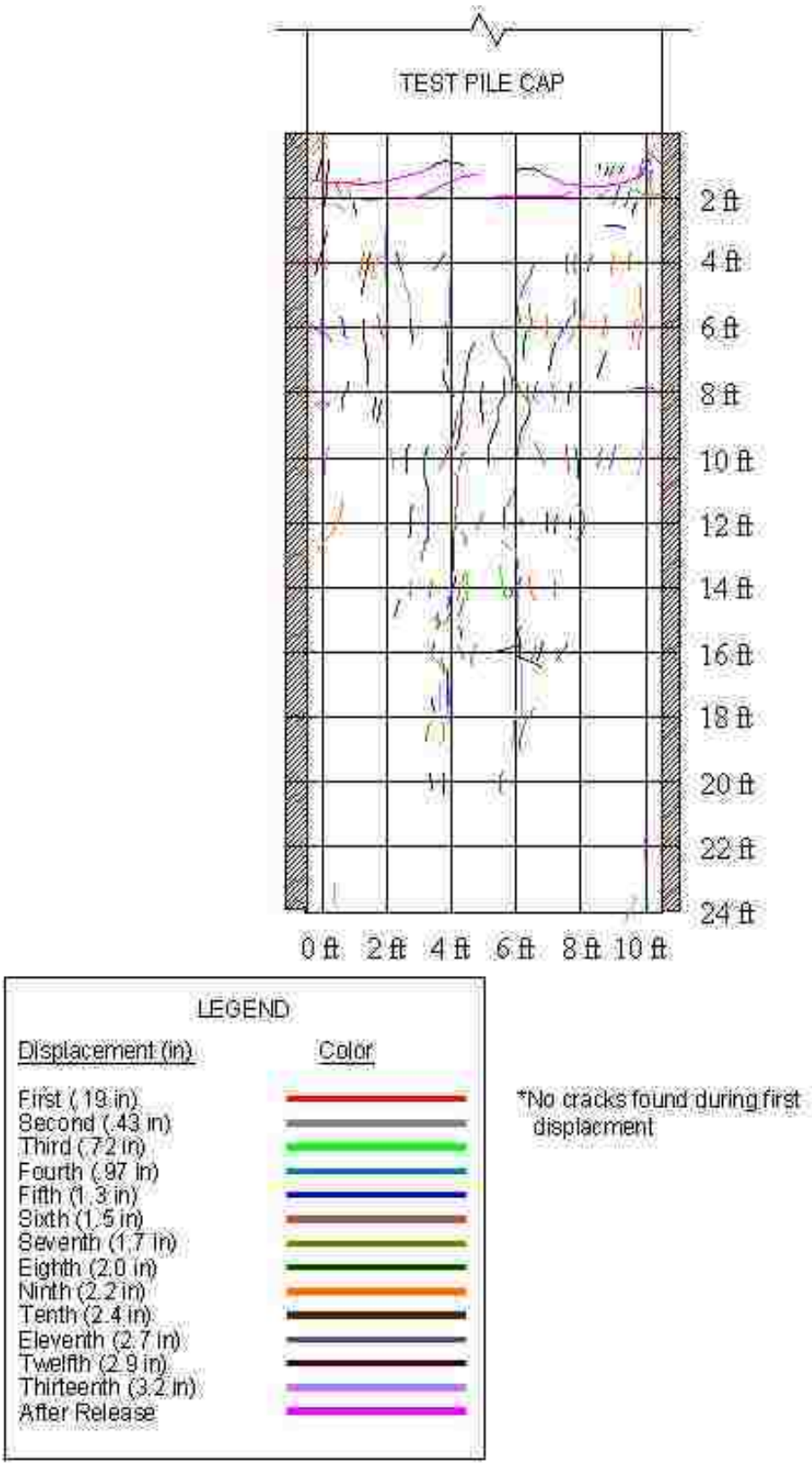

Figure 7-15: Crack map for the soil backfill between the MSE walls for each pile cap displacement increment.

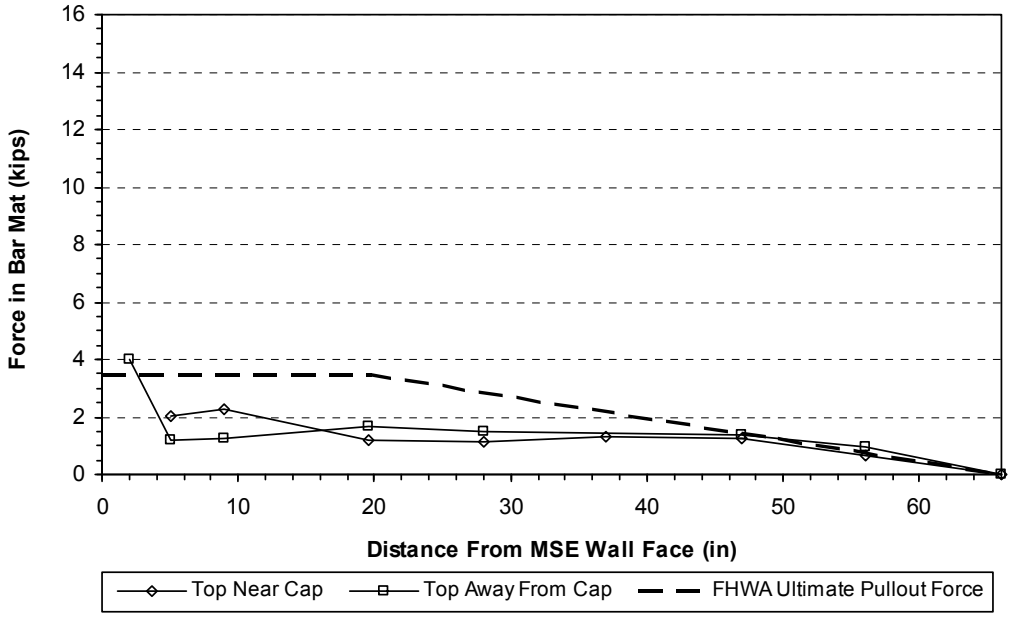

Figure 7-16: Force in top mats, 0.5 inch pile cap displacement.

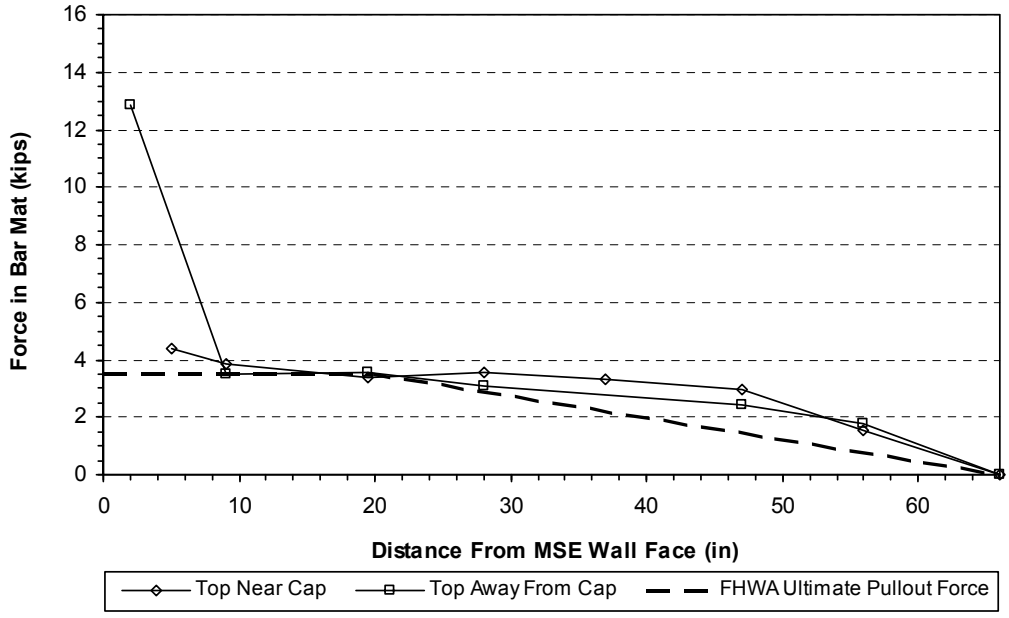

Figure 7-17: Force in top mats, 1.0 inch pile cap displacement.

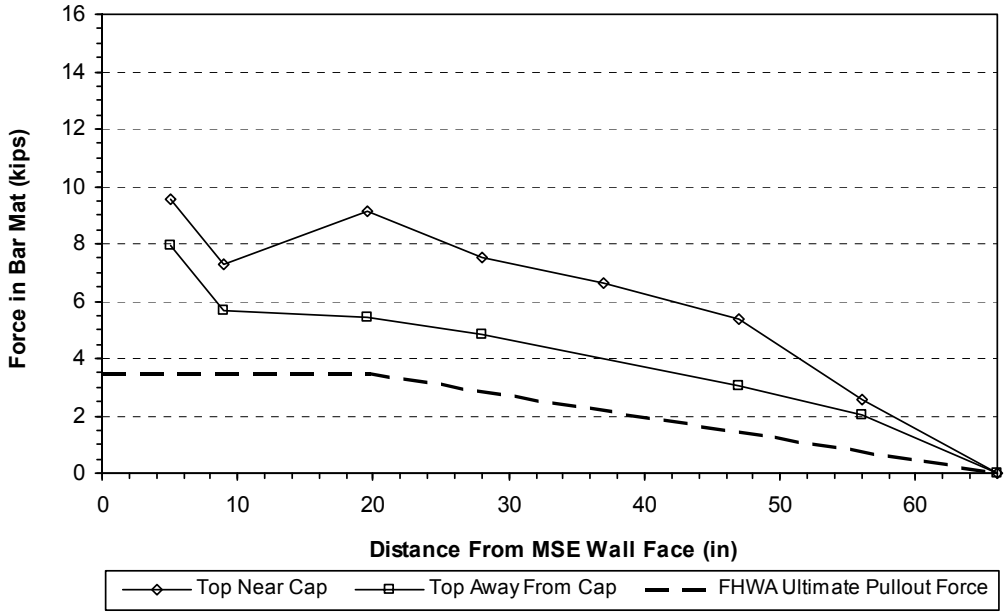

Figure 7-18: Force in top mats, 2.0 inch pile cap displacement.

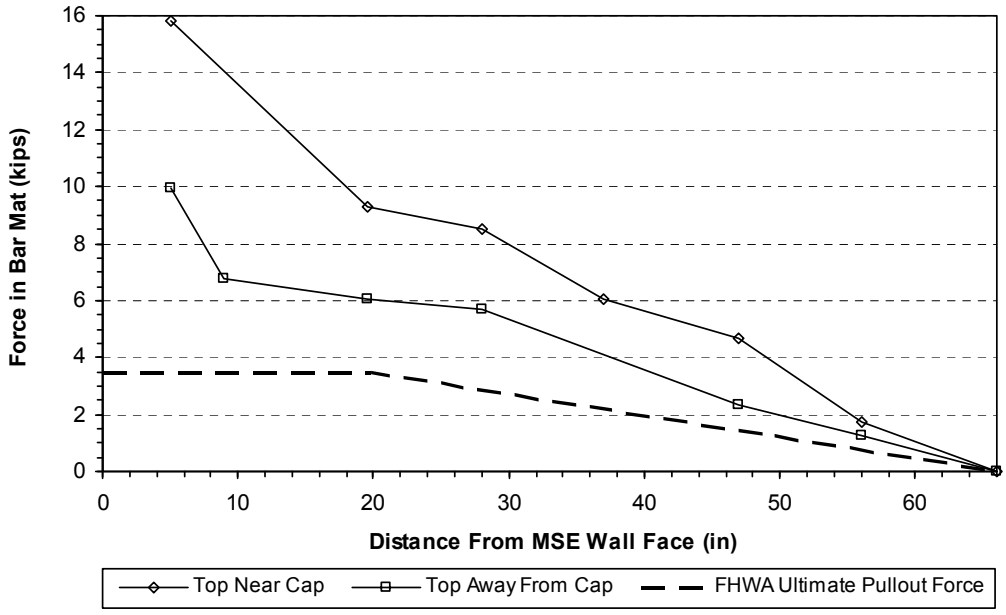

Figure 7-19: Force in top mats, 3.0 inch pile cap displacement.

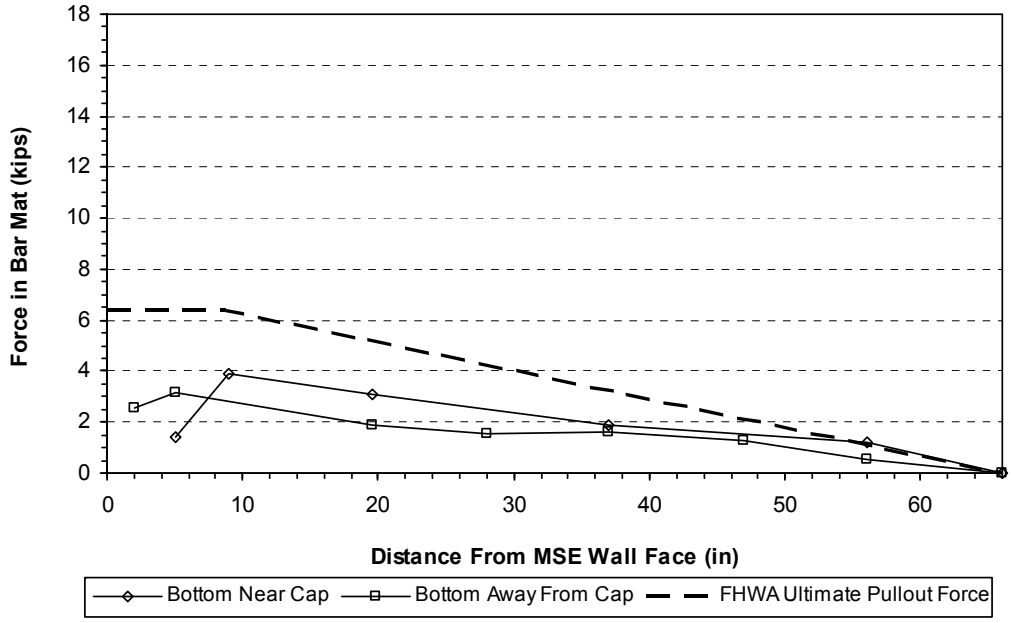

Figure 7-20: Force in bottom mats, 0.5 inch pile cap displacement.

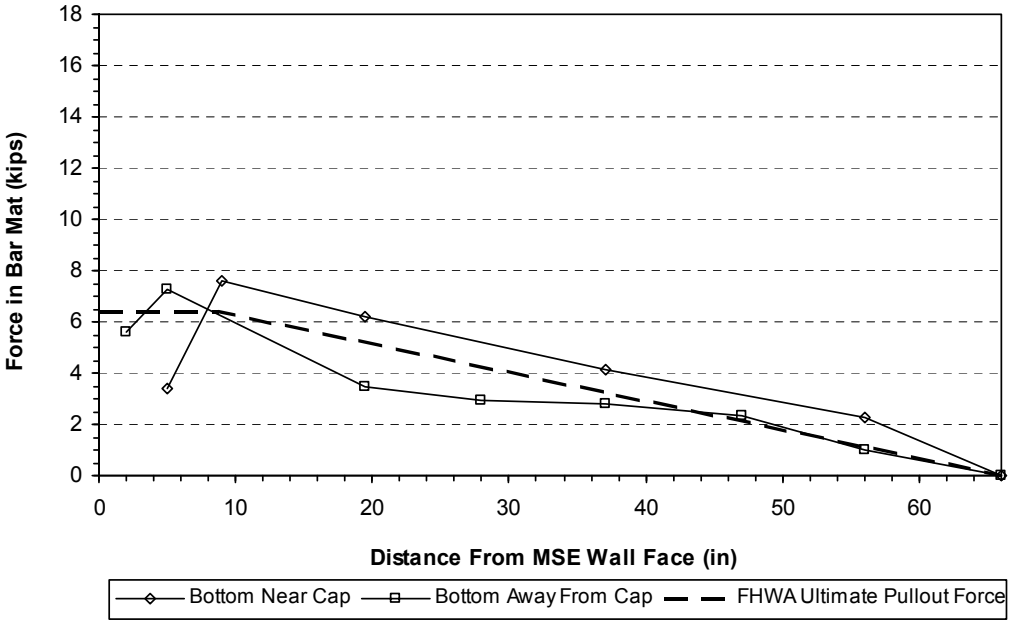

Figure 7-21: Force in bottom mats, 1.0 inch pile cap displacement.

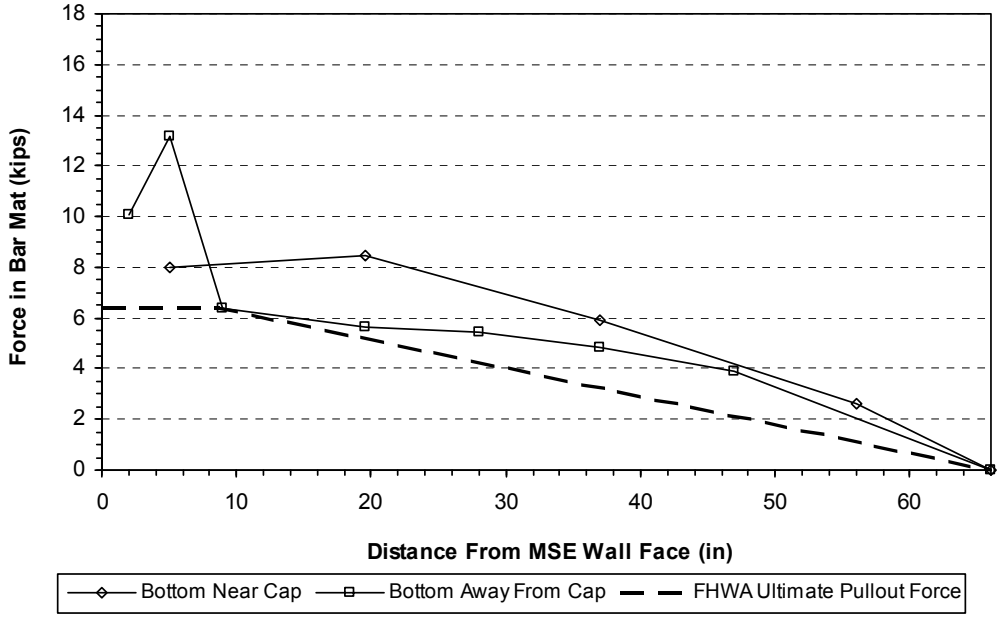

Figure 7-22: Force in bottom mats, 2.0 inch pile cap displacement.

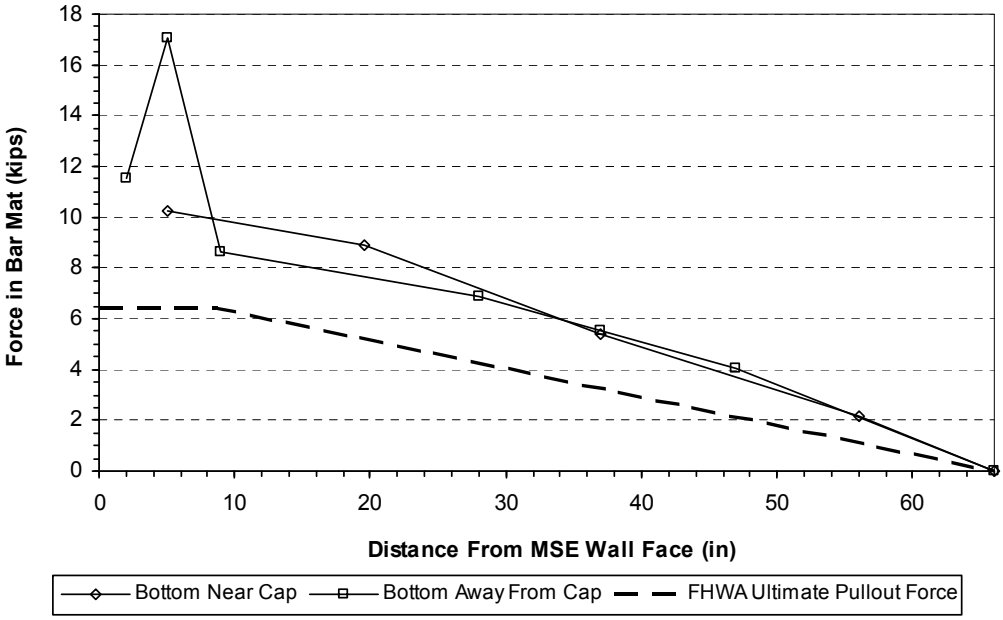

Figure 7-23: Force in bottom mats, 3.0 inch pile cap displacement.

The reason the total number of longitudinal bars in equation 7-2 is reduced by one is because the outer bars only carry half the tributary area of inner bars, so two halves are subtracted from the total number of bars. Great effort was made to separate useful data from the bad strain gauge data, however, not all of the strain gauges operated with complete reliability. When a strain gauge appeared to malfunction, its point on the graph was simply interpolated between adjacent gauges (indicated by a line), or nothing is graphed. Any point on the graph represents data from that location's gauges.

The forces shown in these figures are those developed during construction and during subsequent loading of the pile cap. The mats are carrying an initial load from construction. During construction, the data acquisition computers measured the increase in strain as the backfill was placed and force developed in the bar mats. The forces produced by construction of the backfill were also computed using Equation 7.2 and plotted against the design load. Based on this comparison, an equation was developed to represent the force in the mats due to construction.

The dashed line in each figure is the design pullout line. The flat portion of this line is the predicted total capacity of the mat according to the Federal Highway Administration (FHWA) design manual Mechanically Stabilized Earth Walls and Reinforced Soil Slopes Design and Construction Guidelines (National Highway Institute (NHI), 2001). The flat portion of the line extends from the face of the wall to a distance equal to the distance to the resistant zone for each mats respective location. From this point, the line slopes down to a force value of zero at a distance equal to the length of the mat.

As can be seen in the figures, the results between the sets of bar mats are pretty consistent with one another, despite individual variability. The measured force in the mats develops to

values greater than the design pullout force. This could be due to conservatism in the design equations, assumptions made concerning how uniformly force develops in the mats, and errors in the strain measurements. The values nearer to the wall face (2 inches to 9 inches) have a greater tendency to show unreasonable values. This is likely due to either bending effects near the wall face, or damage to strain gauges during construction. Strain gauges in this area are exposed to greater risk of damage due to construction and placement of the pins to connect the bar mats to the wall panel. To make comparison from push increment to push increment easier, the same scale is maintained for each level of mat. Figure 7-16 through Figure 7-23 show that the force in the bar mats develops roughly parallel to the design pullout line.

Figure 7-17 and Figure 7-21 are the plots corresponding to the 1 inch pile cap displacement increment. The force at this point appears to reach the design pullout line. Figure 7-24 and Figure 7-25 show the mat force plotted against the transverse MSE wall displacement. Also shown here are the design pullout lines for the respective levels. As can be seen in the figures, the force measured in the mats is greater than the capacity that was predicted in the design. However, in most cases, the lines seem to reach a peak, where the walls continue to displace, with little or no increases in force in the mats. The one exception is the bottom near mat in Figure 7-25. This was the string pot that is believed to have been faulty, as mentioned in Section 7.5.

Figure 7-26 shows the ratio of the pressure on the wall/pressure on the pile cap face, as a function of distance from the face of the pile cap. The pressure on the wall panels was taken as the load measured in the bar mat divided by the area of the wall panel that bar mat was designed to carry. The pressure on the face of the pile cap was determined by assuming the pressure developed in a simple triangular manner, so that the pressure multiplied by the area divided by

two equaled the passive load measured in the actuators. The level of pressure at the level of each bar mat was obtained by linear interpolation. The value of pressure on the wall was divided by the value of pressure on the pile cap at the depth of the bar mat for each pile cap displacement increment. The median values of all the displacement increments for each bar mat was plotted as a function of the distance of that mat from the face of the pile cap, and a line was fitted to the data points. As can be seen, the R^2 value for this line is very low.

Further analysis was performed to determine whether there was any apparent effect on the relationship shown in Figure 7-26 owing to the bar mats pulling out. As the force on the wall panel increases, the wall will eventually pull-out and this would limit the force on the wall. To make this assessment, the total force on each wall panel was plotted against the average displacement of the panel and the resulting curves are shown in Figure 7-27. These curves indicate that pull-out occurs at a displacement of 0.2 to 0.4 inches when the force on the wall becomes relatively constant with increasing displacement.

Figure 7-28 shows the same thing as Figure 7-26, except all values past 0.2 inches of transverse MSE wall panel displacement were eliminated from consideration. The justification for doing this is provided in 9.5. Doing this provided a slightly higher R^2 value. This data could possibly be used to predict the load on an MSE wall panel if a known transverse load were to be placed on an adjacent pile cap. The MSE wall could possibly be designed for this increased transverse load on the panels.

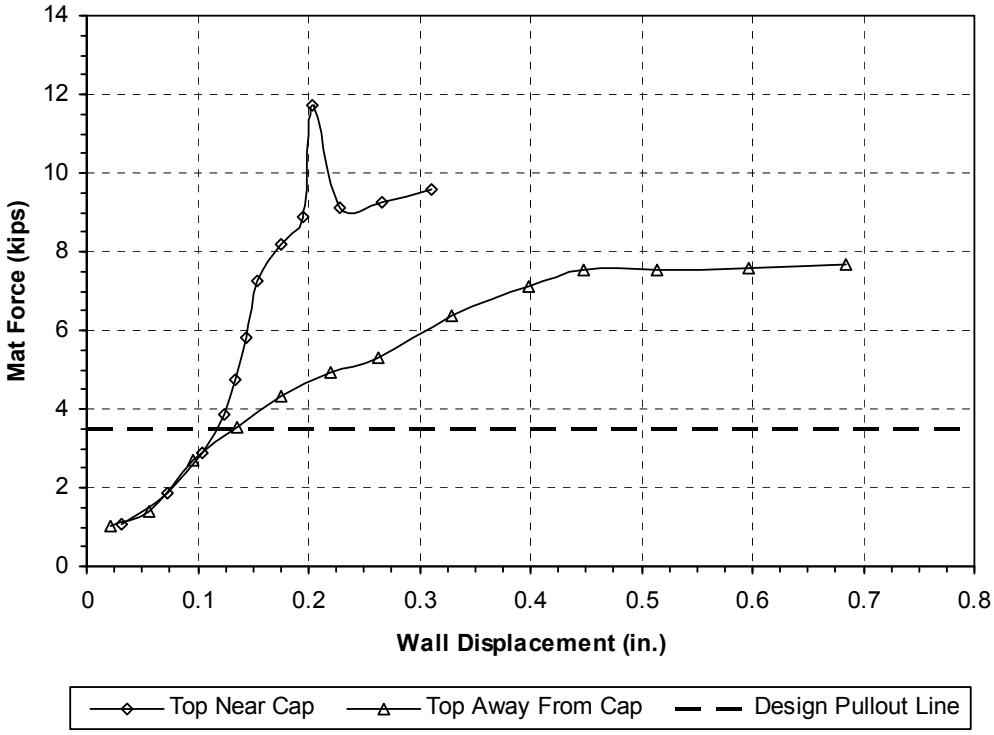

Figure 7-24: Wall displacement versus mat force, top mats.

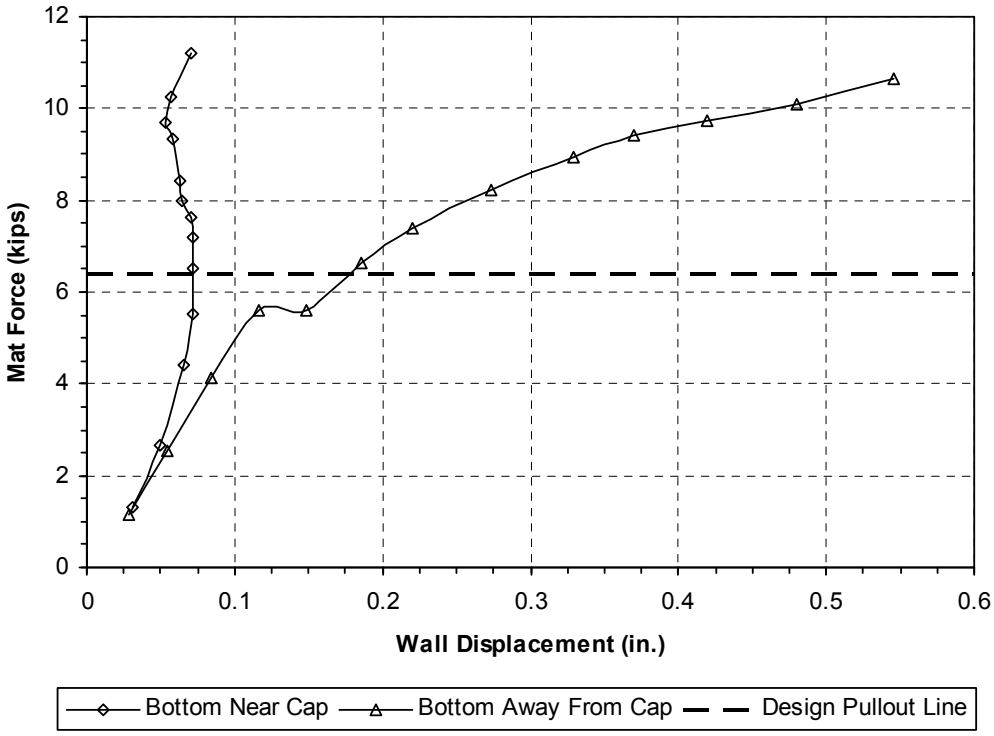

Figure 7-25: Wall displacement versus mat force, bottom mats.

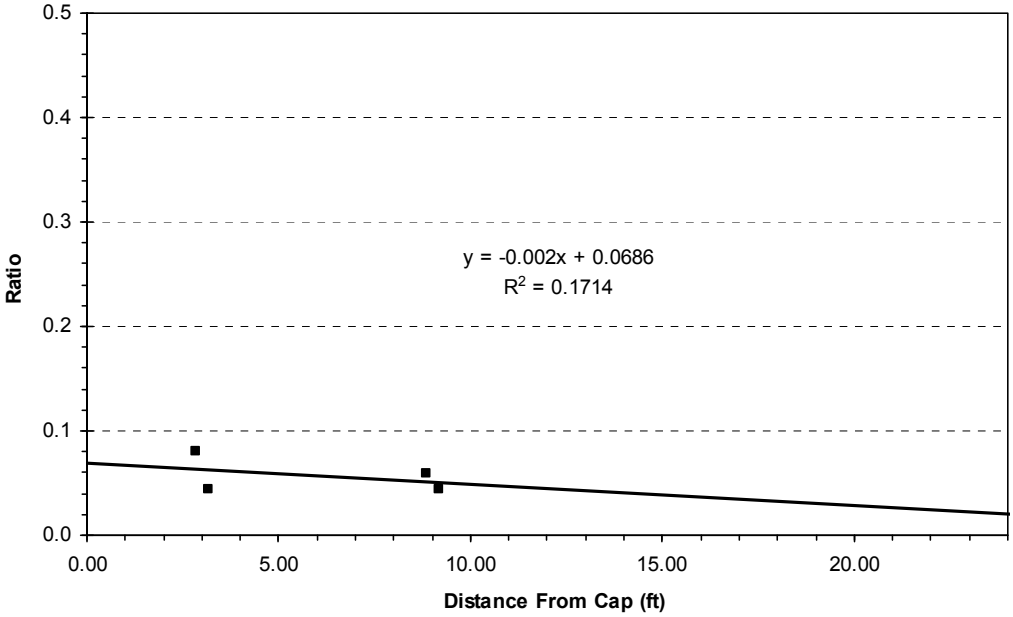

Figure 7-26: Ratio of pressure on wall/pressure on pile cap versus distance from pile cap.

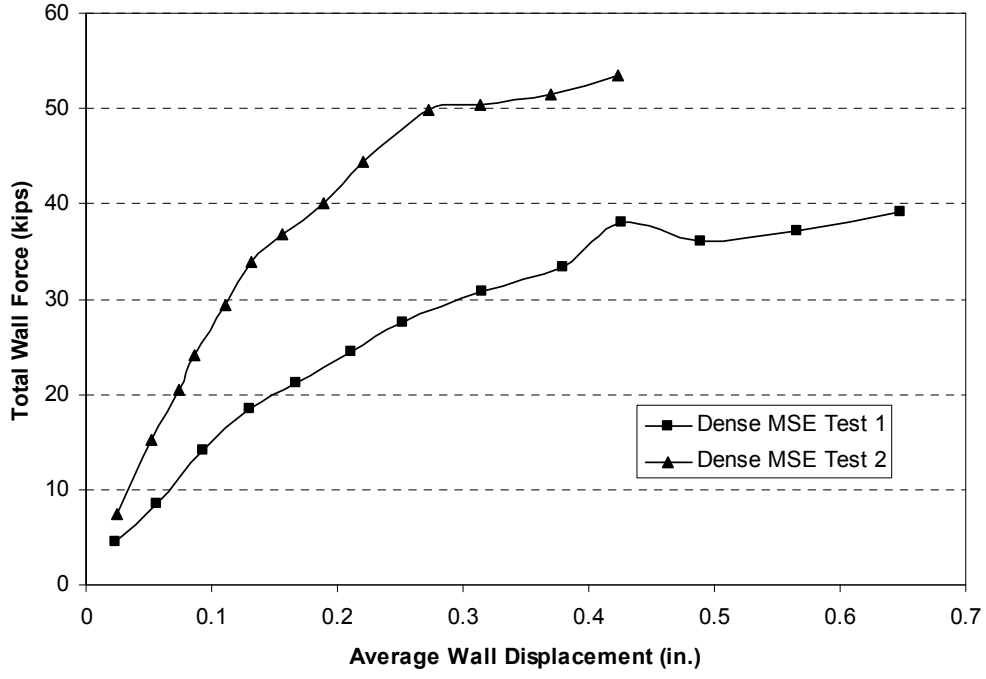

Figure 7-27: MSE wall force-displacement curves from MSE tests 1 and 2.

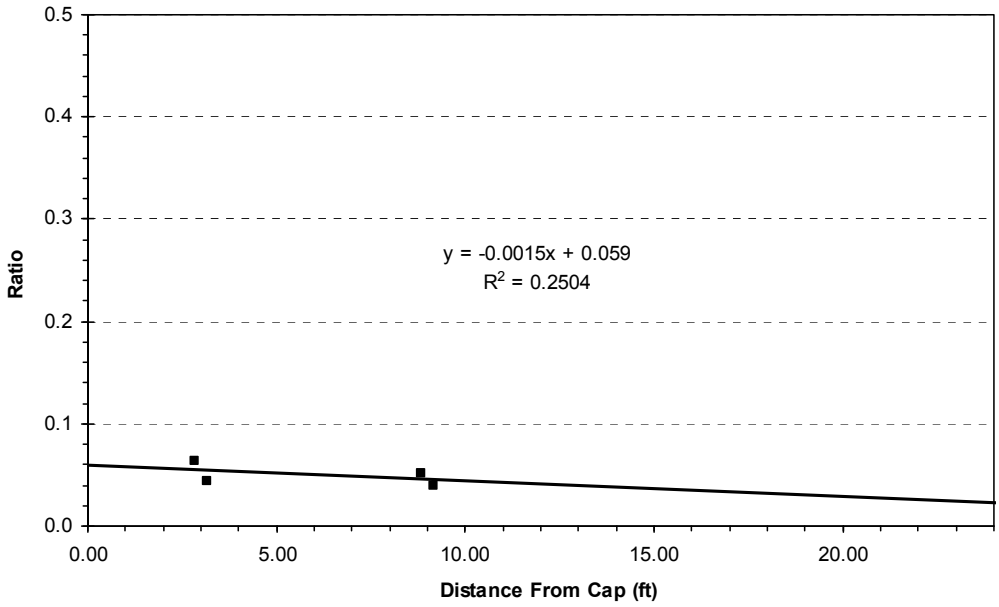

Figure 7-28: Ratio of pressure on wall/pressure on pile cap versus distance from pile cap, larger wall displacements deleted.

8 MSE Test 2 Results

This chapter presents the results of the second MSE test. These results are broken down into the following areas: force-displacement (force measured from actuators), force-displacement (force measured from pressure cells), inclinometer data, backfill displacement, transverse wall displacement, heave and cracking, and mat strains/forces. This test was designed to have an average static factor of safety against pullout of 2.5. The results of this test will be compared with other test results in this study and with test results from Heiner (2010) in a later chapter.

8.1 Load-Displacement Results

The measured total resistance versus deflection of the pile cap is shown in Figure 8-1. The graph was obtained by plotting the measured total force from the actuators versus the average displacement of the pile cap corresponding to the peak load. Figure 8-2 also shows the total measured response, along with the baseline response and the passive earth response. The baseline results were obtained by running the test with no backfill present. This allows researchers to subtract the resistance contributed by factors other than the backfill passive response (such as lateral pile resistance and base shears) from the total response measured during the test. The baseline curve is relatively linear with a stiffness of approximately 118 kips/in. In contrast, the passive resistance versus displacement curve exhibits a hyperbolic shape and approaches an ultimate resistance of about 530 kips asymptotically.

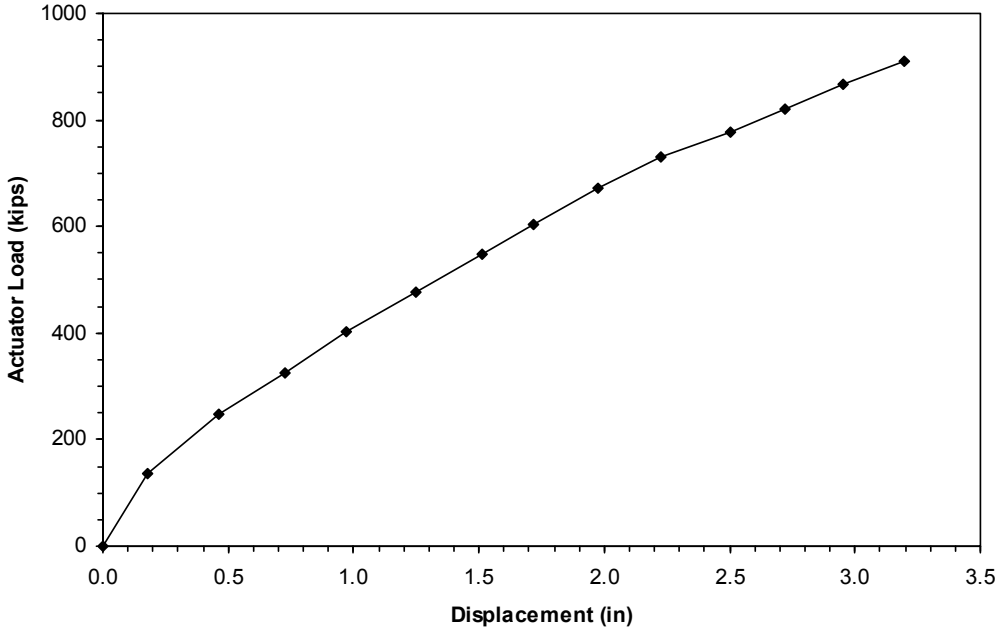

Figure 8-1: Total measured response versus displacement.

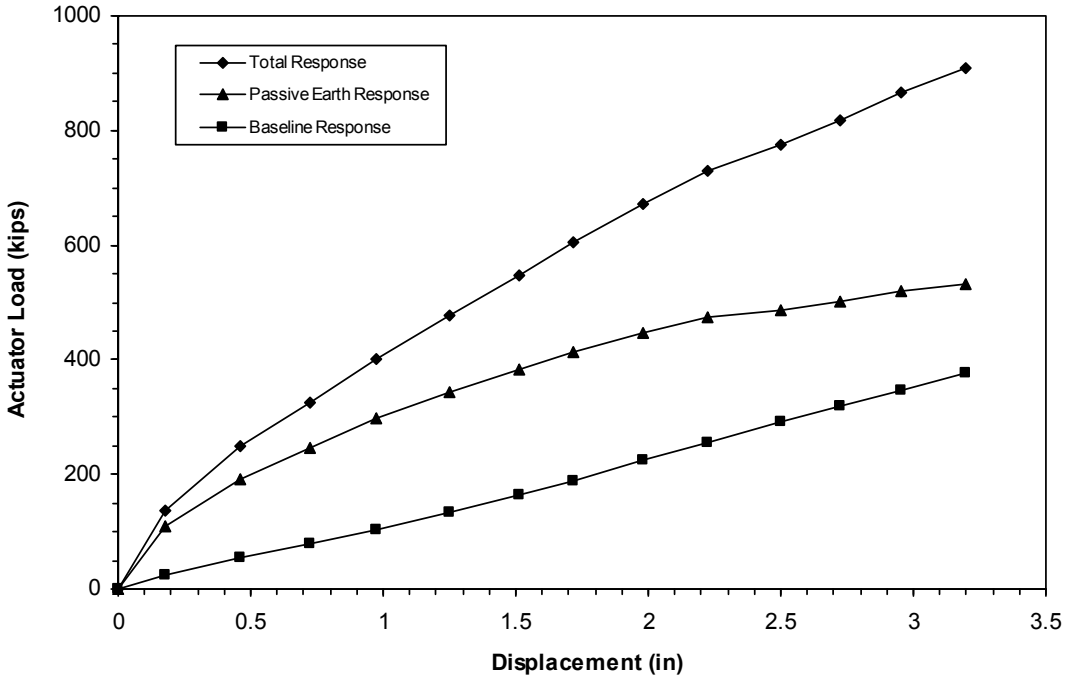

Figure 8-2: Passive resistance versus pile cap displacement.

8.2 Load-Displacement Results from Pressure Cells

Figure 8-3 shows the development of pressure on the pile cap face, with each reading corresponding to each displacement increment. Each point going down the pile cap face indicates the location of a pressure cell. The pressure in this test develops evenly in the top half of the pile cap, but much greater pressure develops in the bottom half. The values from the pressure plate at depths of 0.46 and 5.05 ft drop off beginning at about the 2.0 inch and 2.5 inch nominal pile cap displacement increment, respectively. These values have been adjusted to equal the maximum value reached at that depth; this is shown in Figure 8-4.

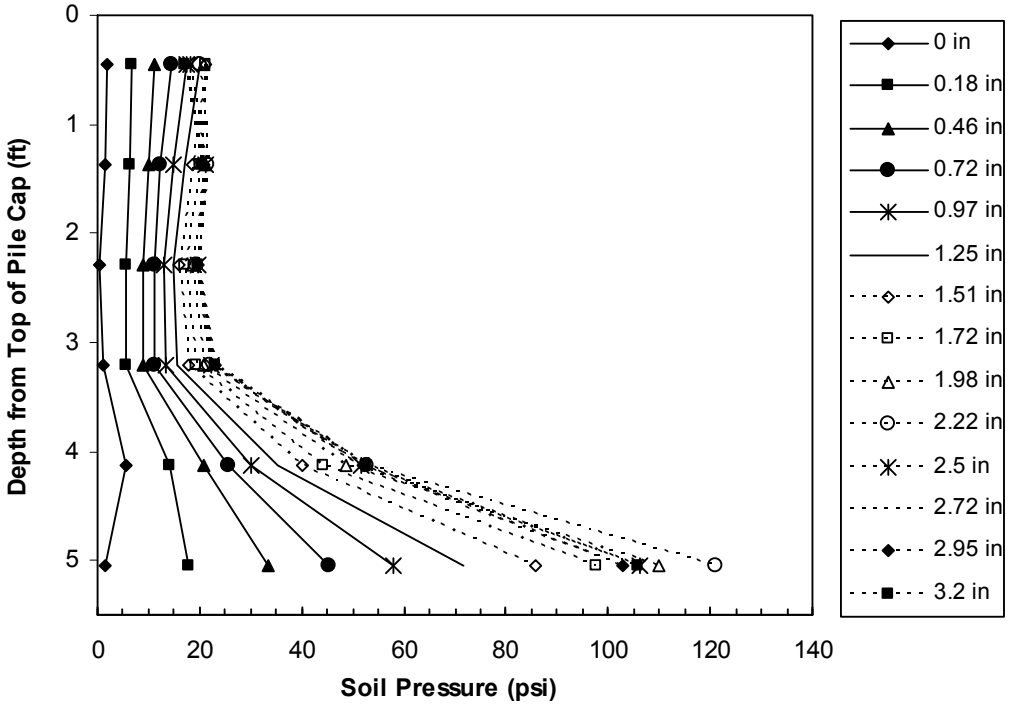

Figure 8-3: Development of pressure cell readings versus displacement.

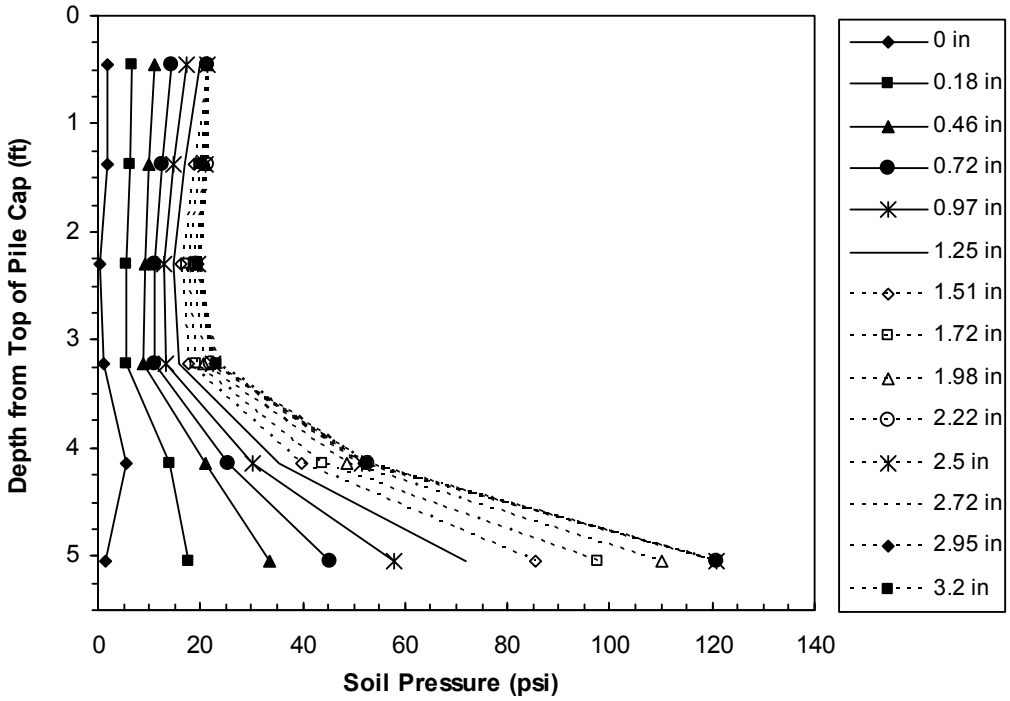

Figure 8-4: Development of pressure cell readings versus displacement, adjusted.

Figure 8-5 provides a comparison of the passive force-displacement curves obtained from the pressure cells with that from the actuators. The passive force from pressure cells was obtained by multiplying the measured pressure of each cell (as shown in Figure 8-4) by its tributary area. The tributary area is the distance from either the top of the pile cap or halfway to the adjacent pressure cell above the cell to the bottom of the pile cap or halfway to the adjacent pressure cell below the cell multiplied by the width of the pile cap. The passive earth response is the measured curve obtained from the actuators. The measured passive earth response from the pressure cells is multiplied by a factor of 1.3 to account for the end effects discussed in Section 5.2; these values are shown as the pressure cells with multiplier in Figure 8-5.

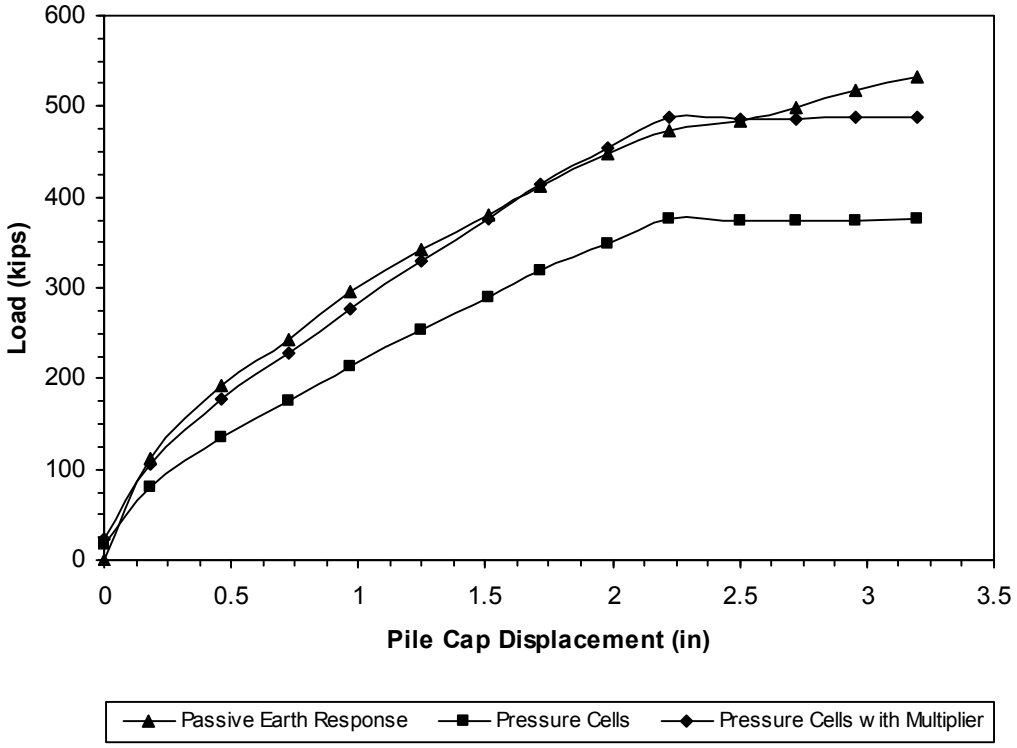

Figure 8-5: Load versus displacement from pressure cells.

As can be seen, the values for load from pressure cells with multiplier provides an excellent match to the load measured from the actuators for the initial part of the curve, then flat lines, falling below the ultimate passive resistance measured from the actuators. The portion that matches the actuator curve reinforces the values obtained from the actuators alone, and increases the confidence in results obtained from the actuators. It also qualifies the method of subtracting baseline response from total measured resistance to obtain the passive earth response described in Section 8.1.

8.3 Inclinometer Data

As discussed in Section 4.1.2, inclinometer readings were taken for each test. Figure 8-6 shows the deflection versus depth from these readings in both the north and south inclinometer

casings. The curve represents change in deflection of the inclinometer tubes in the direction of loading, (the baseline reading was subtracted from the reading taken at the maximum displacement of the pile cap). A depth of zero corresponds to the top of the pile cap. The curves from both the north and the south match each other very well as would be expected. Also shown in this figure is the displacement of the pile cap as measured by the string pots that were attached to the pile cap. As can be seen the displacement measured by the inclinometer matches the displacement measured from the string pots. The deflection in the pile reaches zero at a depth of about 21 ft, which corresponds to nearly 20 pile diameters. The points within the cap translate horizontally and remain nearly vertical, indicating very little rotation of the pile cap. This is consistent with a fixed head boundary condition.

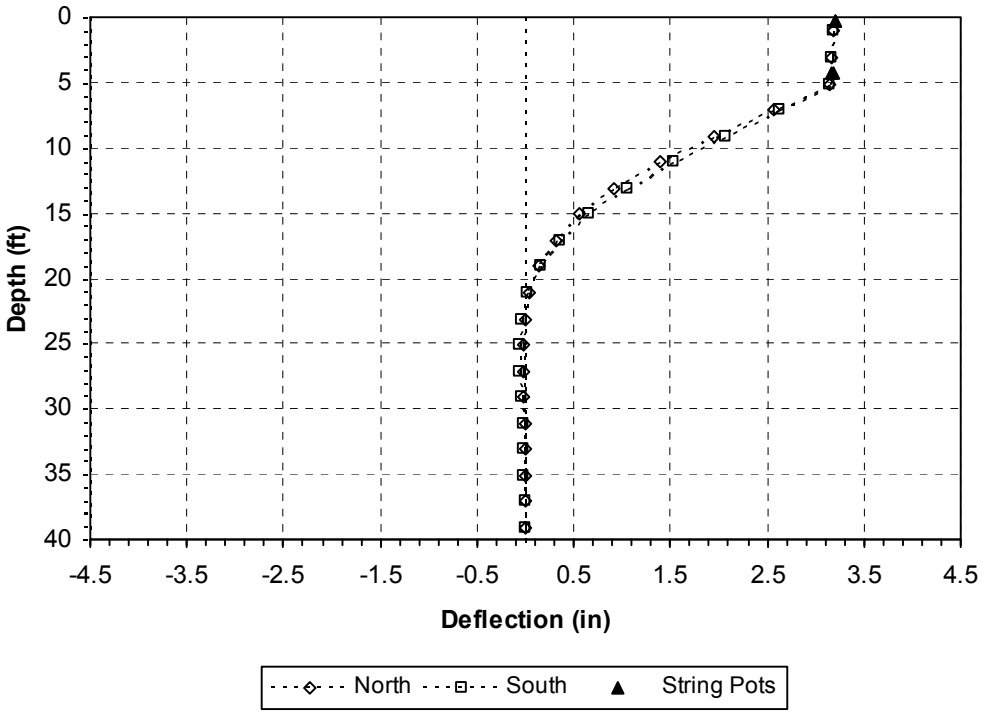

Figure 8-6: Deflection versus depth.

8.4 Backfill Soil Displacements

Figure 8-7 shows the absolute displacement of the backfill soil. The arrangement of string pots and stakes was discussed in section 4.1.3. These values were obtained by subtracting the displacement measured by each backfill string pot from the pile cap displacement at that loading increment. For example, if the backfill string pot at a distance of 2 ft from the face of the pile cap measured a displacement of 1 inch, and the loading increment was 2 inches, the value shown in Figure 8-7 would be 1 inch at 2 ft.

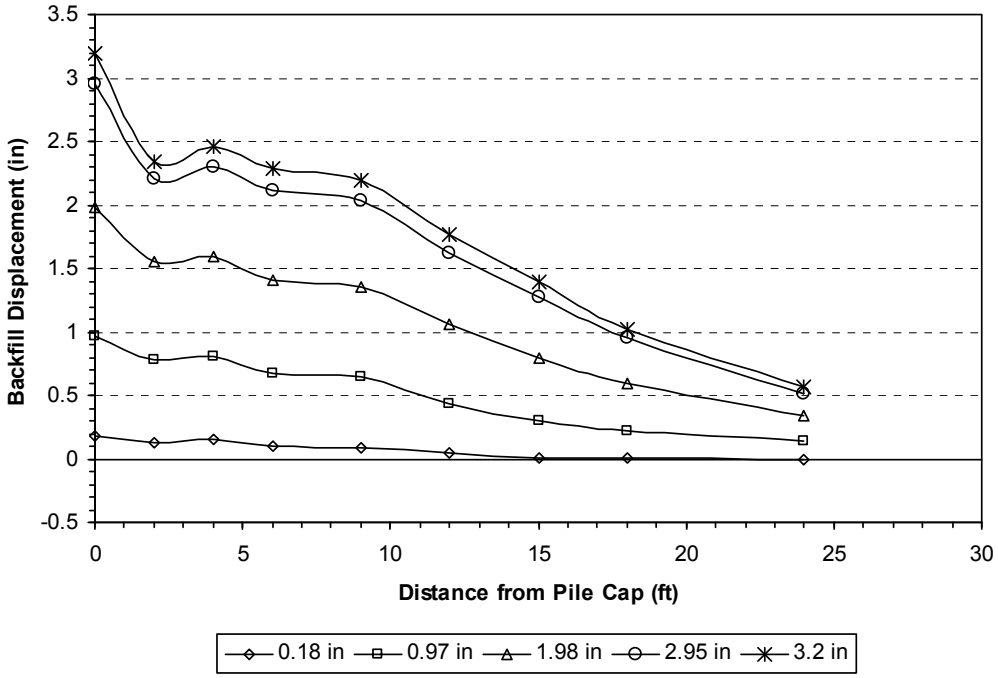

Figure 8-7: Displacement of backfill soil.

The compressive strain of the backfill is shown in Figure 8-8. In this figure each of the lines represents the compressive strain obtained from the corresponding string pot and stake. The strain values were obtained using the equation

$$\varepsilon = \Delta L / L \tag{8-1}$$

where ΔL = change in length from adjacent string pot
L = distance between adjacent stakes

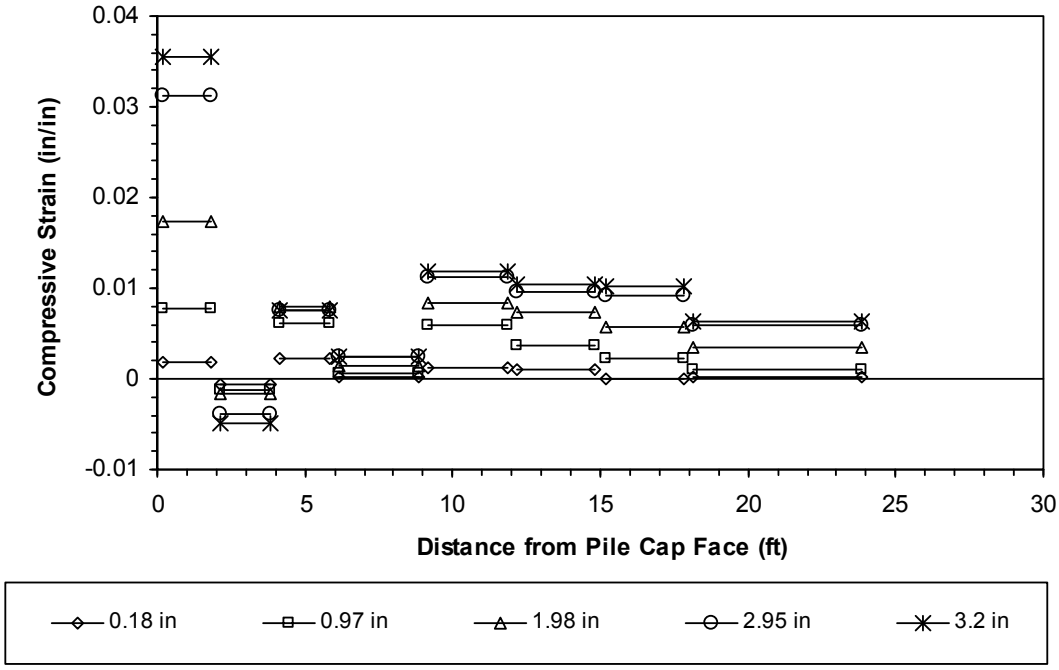

Figure 8-8: Compressive soil strain in backfill as a function of distance behind the cap for several displacement increments.

To simplify presentation of these results, only the first displacement increment, the nominal inch displacement increments, and the final displacement increment are shown in this figure. As can be seen, the greatest compressive strain occurs within the first couple feet of the cap face. The compressive strain fluctuates from 2 to 90 ft from the face of the pile cap, then the compressive strain increases to reach a local maximum value at 9 to 12 ft from the face of the pile cap, and decreases toward the back edge of the backfill zone. The predicted log-spiral failure profile surfaces at about 27.3 ft from the face of the pile cap. This appears consistent with the measured backfill strain in this figure.

8.5 Transverse Displacement of Wall Panels

Figure 8-9 shows the outward movement of the wall panel. This plot represents the data obtained from the LVDT's located 20 inches (1.67 ft) from the face of the pile cap. Figure 8-10 shows the same thing for the LVDT's located 103 inches (8.58 ft) from the face of the pile cap. The data was extrapolated linearly to demonstrate the movement of the wall from top to bottom, while the point on each line represents the location of each string pot. Each line represents values from each displacement increment, as indicated. The top of the wall is located at a depth of 0 inches. Figure 8-9 shows that the top of the wall is displacing outward more than the bottom, resulting in rotation of the wall. This result is harder to predict, due to the presence of three levels of bar mats. However, the top layer of mats does have much less extra capacity than the other mats; the lowest mat has about 7.5 times the extra capacity of the top mats, and the middle mats have about 5 times the extra capacity of the top mats. Figure 8-10 shows the opposite trend for most of the displacement increments, and then looks like what is expected toward the end of the test.

Figure 8-11 shows the rotation of the wall panel versus the actuator load. This is the measured rotation at a distance of 20 inches (1.67 ft) from the face of the pile cap. The rotation develops fairly smoothly until the actuator load approaches 700 kips. Then the rate of rotation of the wall seems to increase. The rotation of the wall at a distance of 103 inches is not shown, because it seems likely that one of the LVDT's at this distance malfunctioned for part of the test.

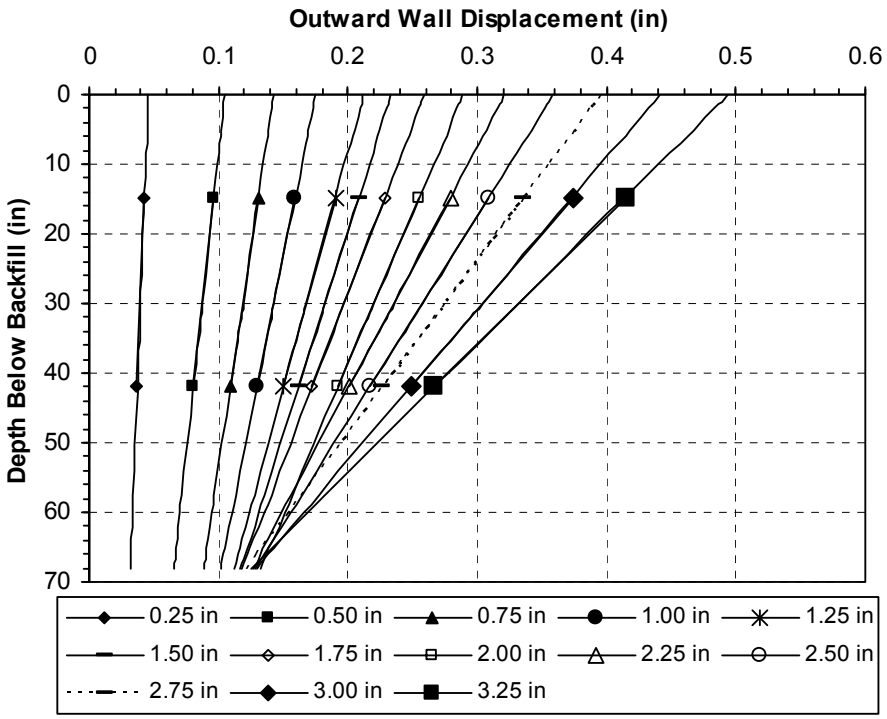

Figure 8-9: Outward movement of wall panel, top to bottom, 20 inches from pile cap face.

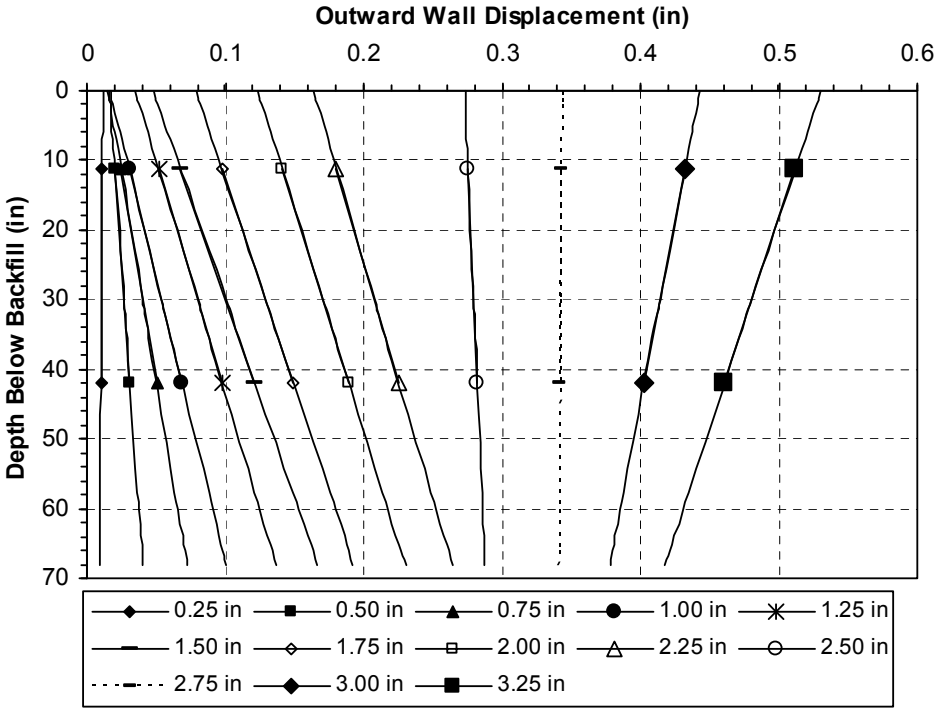

Figure 8-10: Outward movement of wall panel, top to bottom, 103 inches from pile cap face.

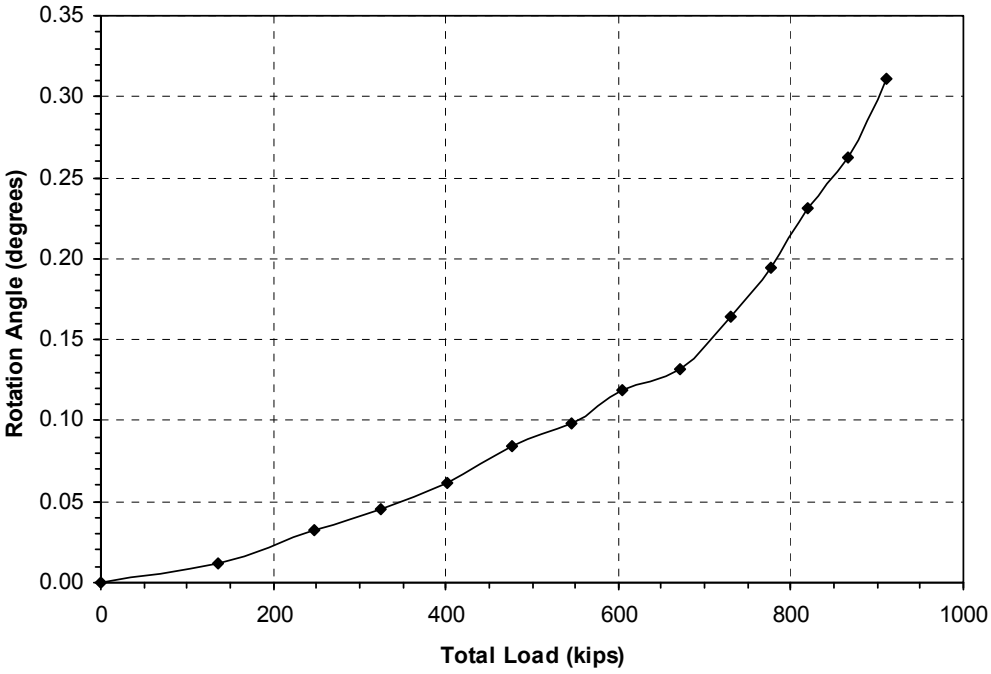

Figure 8-11: Rotation of wall panel versus actuator load.

Figure 8-12 shows the outward movement of the top of the wall versus distance from the pile cap. While Figure 8-9 and Figure 8-10 can be pictured as one standing at the end of the wall and looking along the wall (an elevation), Figure 8-12 is seen from above (plan view). For clarity, only data from every half inch of displacement is shown. This plot indicates that the point where the wall panels join moved out less than the end of the wall panel near the pile cap for the first couple inches of pile cap displacement, but more for the final inch of pile cap displacement. Again, this is likely the result of the LVDT that was discussed previously. The points on this plot indicate the location of the string pots.

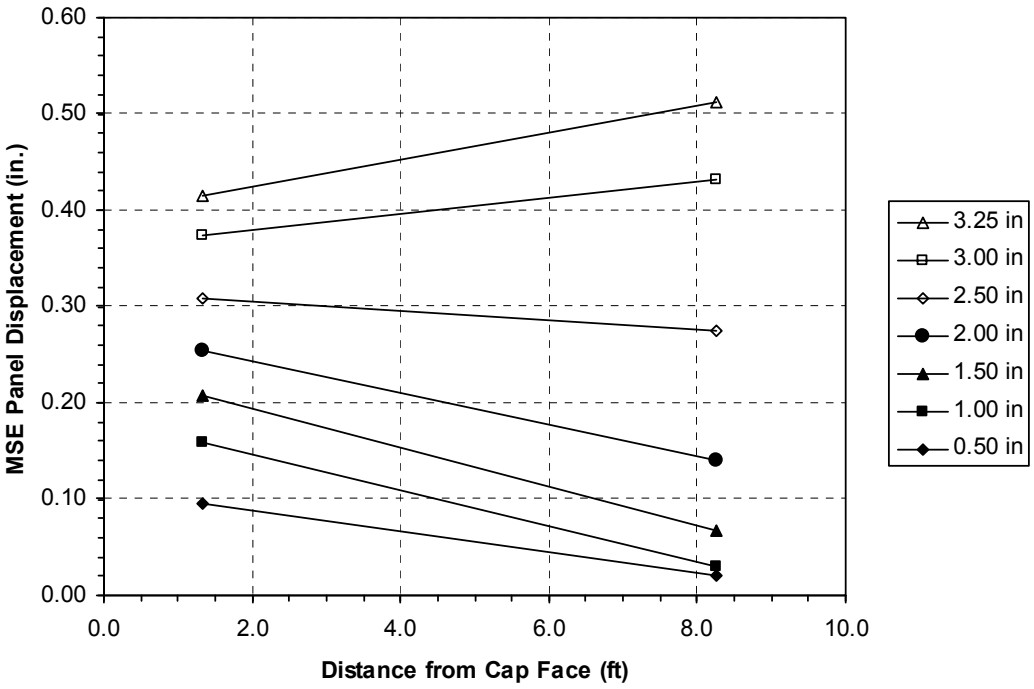

Figure 8-12: Outward movement of wall panel versus distance from pile cap.

Shown in Figure 8-13 is the outward movement of the top of the wall panel versus the measured load from the actuator. As can be seen from the shape of this plot, the wall begins to displace more rapidly, indicating diminishing returns from the wall panels. This data is from the top of the wall at distances of 20 and 103 inches from the pile cap face, along with the average of these two.

Figure 8-14 shows the transverse displacement of the wall panel versus the incremental displacement of the pile cap during the loading sequence. The displacement is for the top of the wall panels at distances of 20 and 103 inches from the pile cap face. This indicates that the wall panel is displacing outward at a constant rate at 20 inches from the face of the pile cap, while the rate the wall panels are displacing outward is increasing at 103 inches from the face of the pile cap.

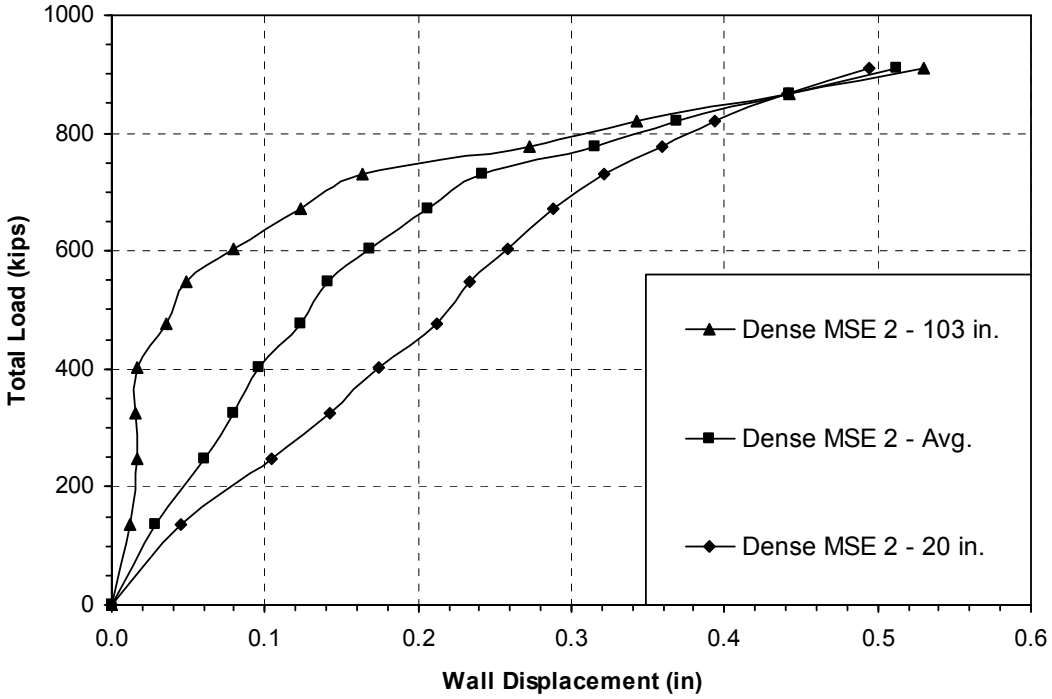

Figure 8-13: Outward displacement of wall panel versus actuator load.

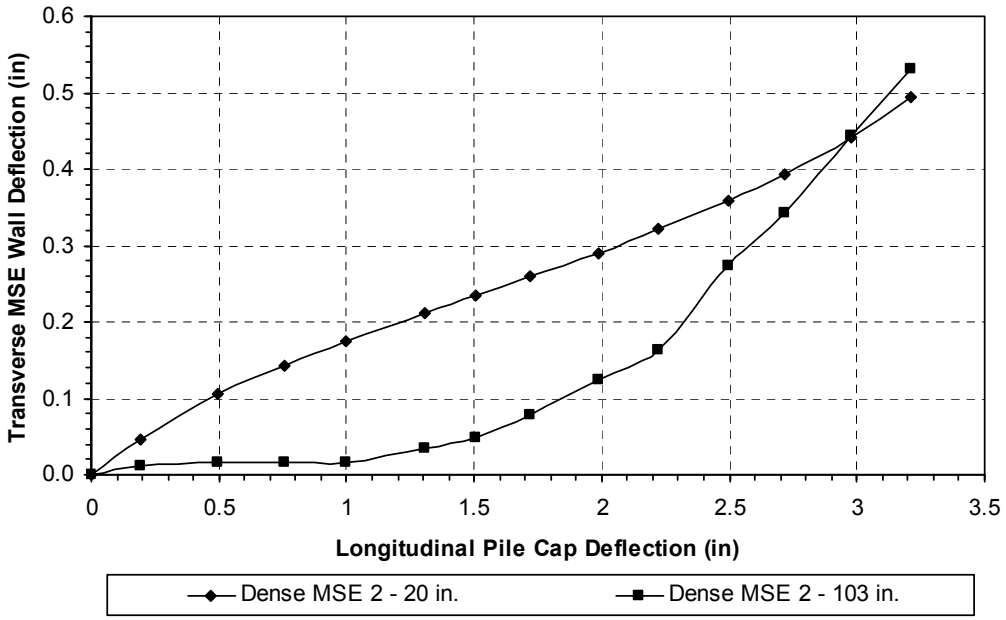

Figure 8-14: Transverse deflection versus longitudinal deflection.

8.6 Heave and Cracking of Soil Backfill

This section will present the data gathered regarding heaving and cracking of the backfill soil profile during and after testing. The methods that were used to gather this data are discussed in section 4.1.3. Figure 8-15 shows the soil heave profile for the test. The values represent the change in elevation from before the test to the largest displacement of the pile cap and are in inches. Positive values indicate upward movement, while negative indicates downward movement (settlement). The dashed lines are set up in a 2 ft by 2 ft grid, consistent with the grid that was painted on the soil surface before the test was performed. As can be seen from this figure, the maximum heave occurs about 6 ft from the face of the pile cap. At a given distance behind the pile cap, the contours indicate that heave is greatest near the center of the fill and lowest near the walls. This is likely a result of outward movement near the wall which reduces the heaving.

Figure 8-16 is a map showing the development of cracks observed for each pile cap displacement increment, with cracks for each increment identified by a separate color. The process by which cracks were mapped is described in greater detail in section 4.1.3. It should be observed that most of the cracks are perpendicular to the front face of the pile cap or parallel to the MSE wall panels. Most of the cracks that don't exhibit this behavior are those which developed after the applied load was reduced and the pile cap was pulled away from the backfill. Further away from the pile cap, the greatest concentration of cracks is in the center. During testing the cracks along the center of the backfill opened especially wide. This is likely a result of the outward movement of the wall panels as documented previously. The bar mats end about in the middle of the soil backfill. Also, in this test, the top layer of bar mats has only 6 inches of

soil above them. Thus, the tendency of the soil to ride on these mats would be greater than that for the first MSE test.

8.7 Mat Strains and Forces

This section will present the data gathered from the strain gauges placed on the bar mats, as described in section 4.5. The forces developed in the mats are also presented in this chapter along with a comparison of pressure on the wall panels relative to the pressure on the pile caps. Also, the development of the force in the bar mats will be compared to the outward displacement of the wall panels.

Figure 8-17 through Figure 8-27 are plots of the force in the bar mats along the length of the mats for selected displacement increments, obtained from the strain gauges. Each point along a curve represents the location of a set of strain gauges placed at that location on the bar mat. To obtain the force, F, for the entire bar mat, the strain from a set of strain gauges (located at the same distance from the panel face, on the top and bottom of the longitudinal bar) was averaged and the force was computed using the equation

$$F = \bar{\varepsilon} * E * A * B \tag{8-2}$$

where F is the force in the entire mat at a location
$\bar{\varepsilon}$ is the average strain at a location
E is the modulus of elasticity of steel, 29000000 psi
A is the area of one longitudinal bar, in^2
B is the number of longitudinal bars minus 1

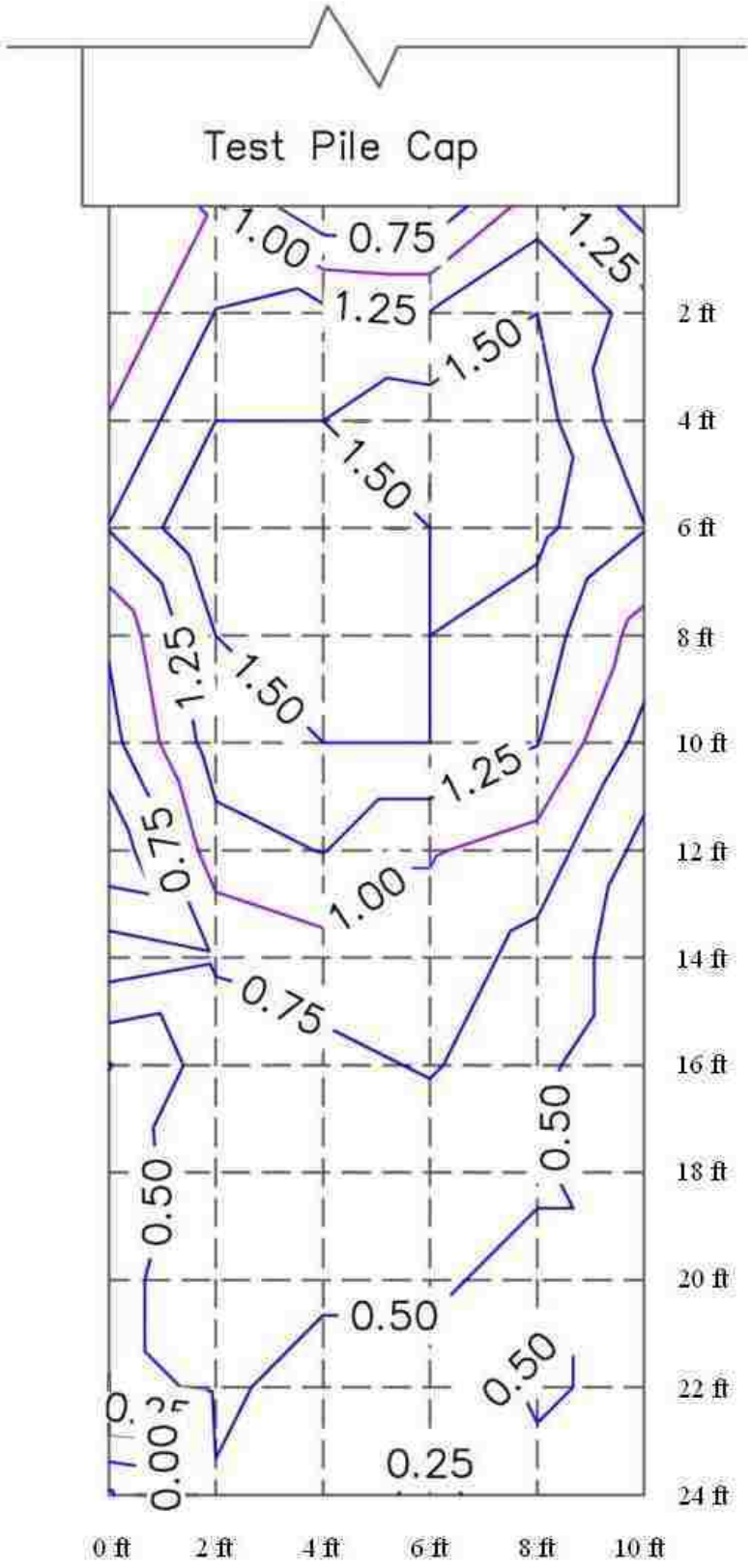

Figure 8-15: Soil heave contours (inches) for the backfill within MSE wall panels behind pile cap.

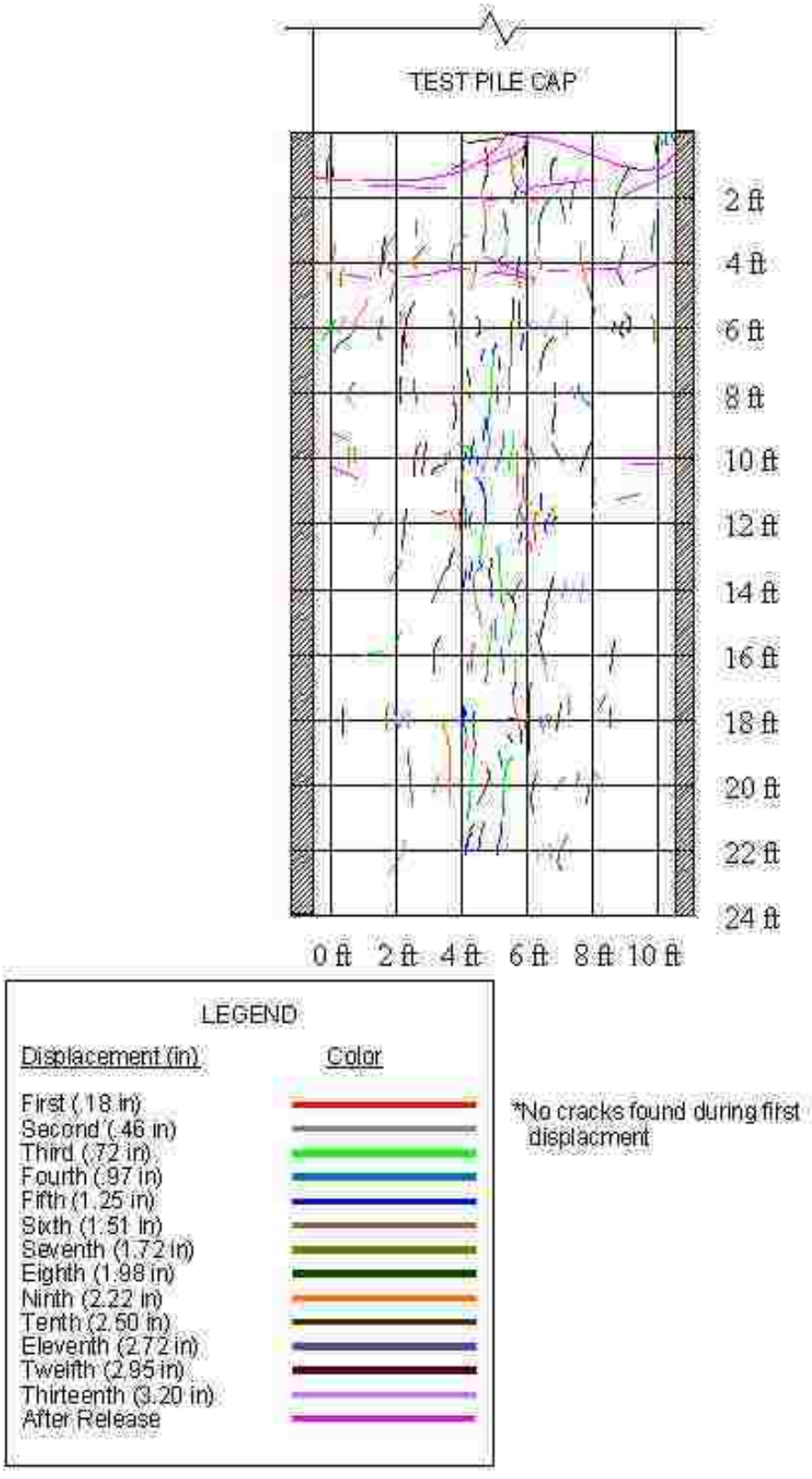

Figure 8-16: Crack map for the soil backfill between the MSE walls for each pile cap displacement increment.

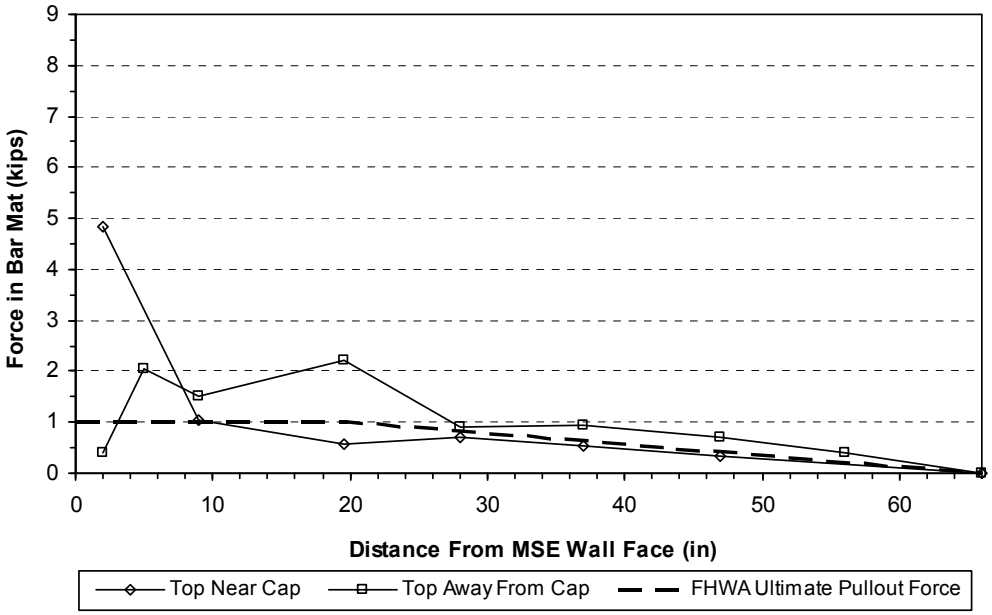

Figure 8-17: Force in top mats, 0.5 inch pile cap displacement.

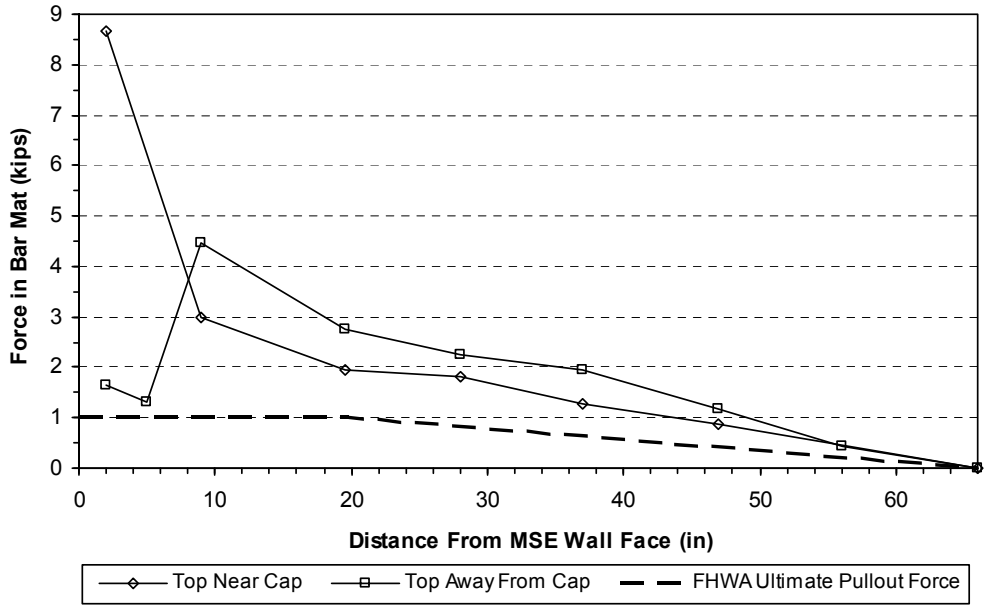

Figure 8-18: Force in top mats, 2.0 inch pile cap displacement.

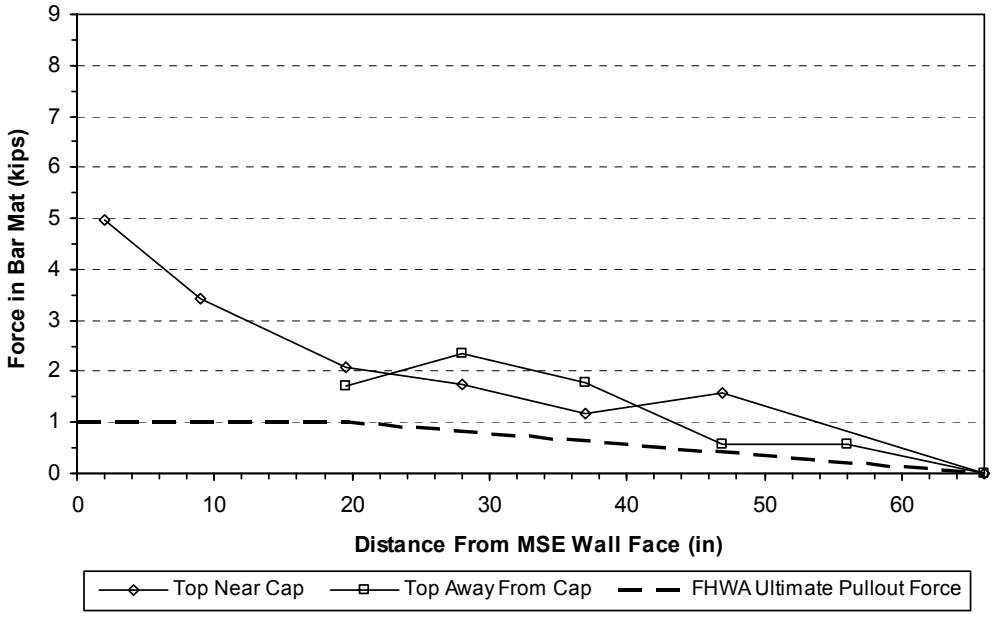

Figure 8-19: Force in top mats, 3.0 inch pile cap displacement.

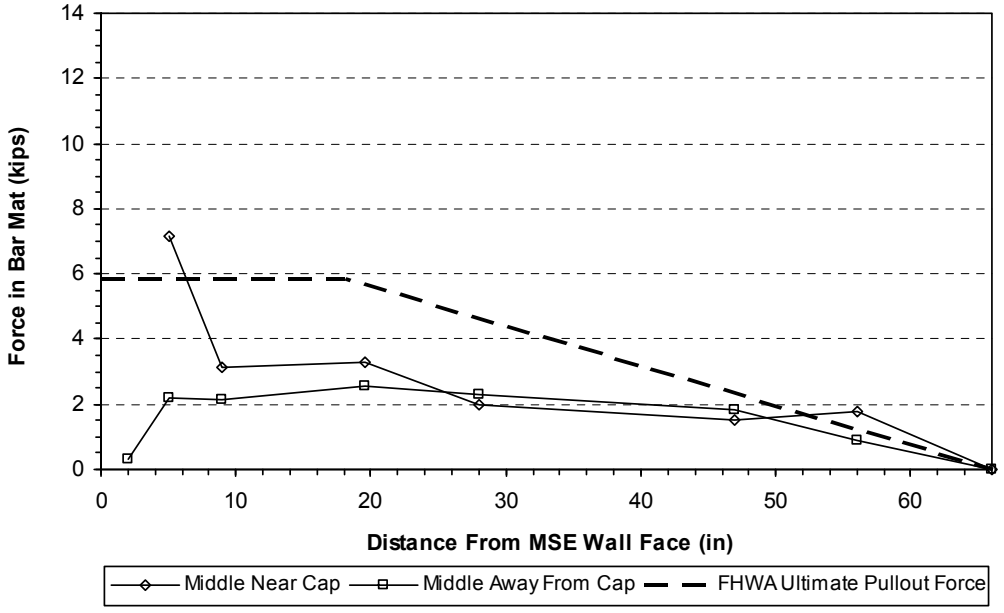

Figure 8-20: Force in middle mats, 0.5 inch pile cap displacement.

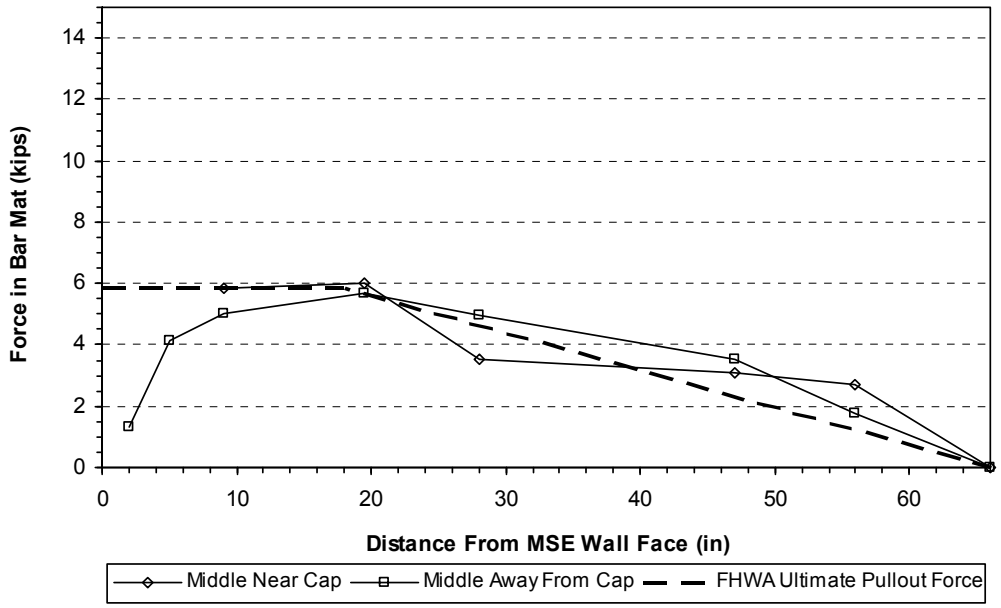

Figure 8-21: Force in middle mats, 1.25 inch pile cap displacement.

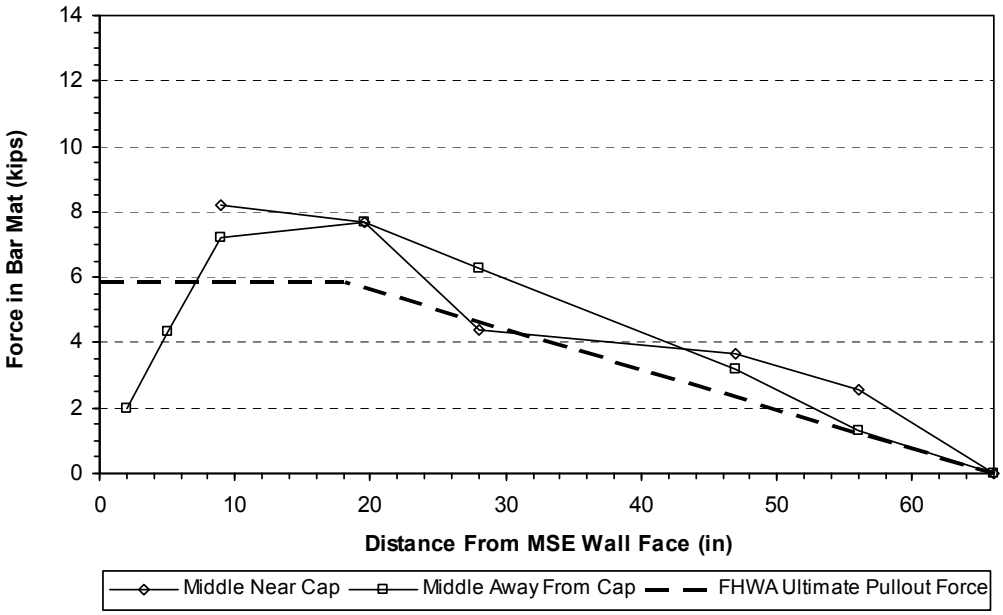

Figure 8-22: Force in middle mats, 2.0 inch pile cap displacement.

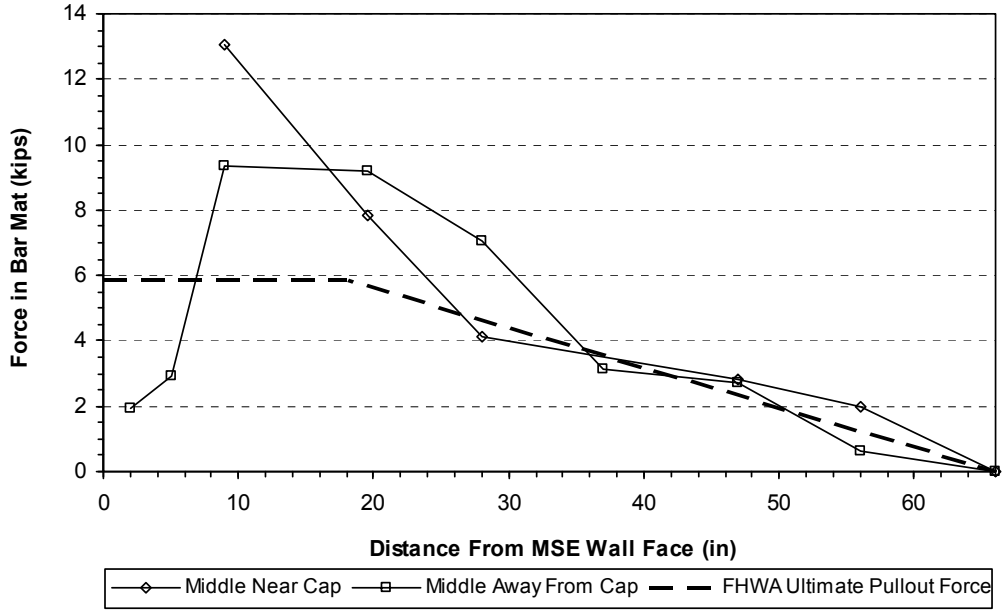

Figure 8-23: Force in middle mats, 3.0 inch pile cap displacement.

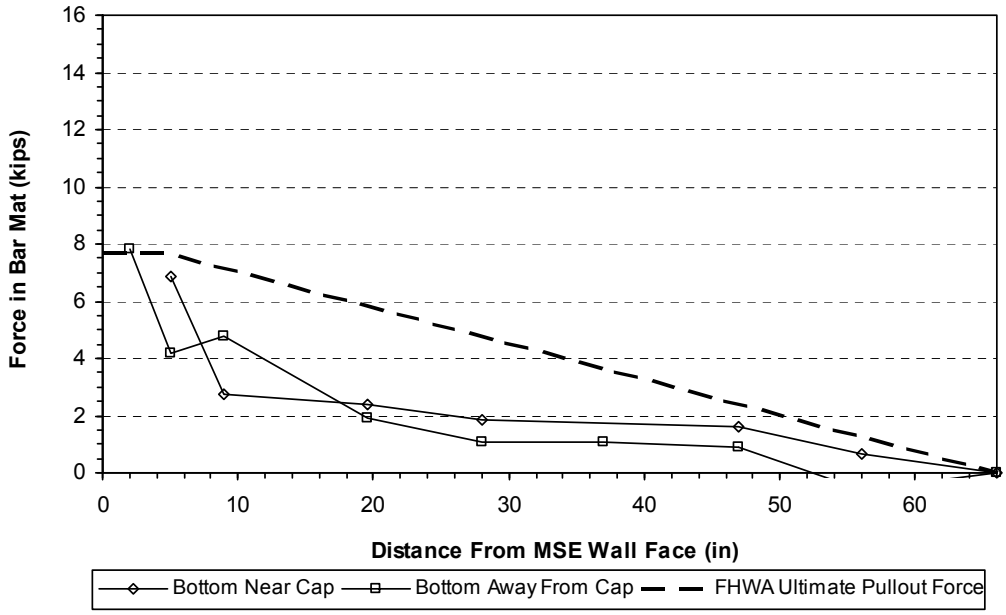

Figure 8-24: Force in bottom mats, 0.5 inch pile cap displacement.

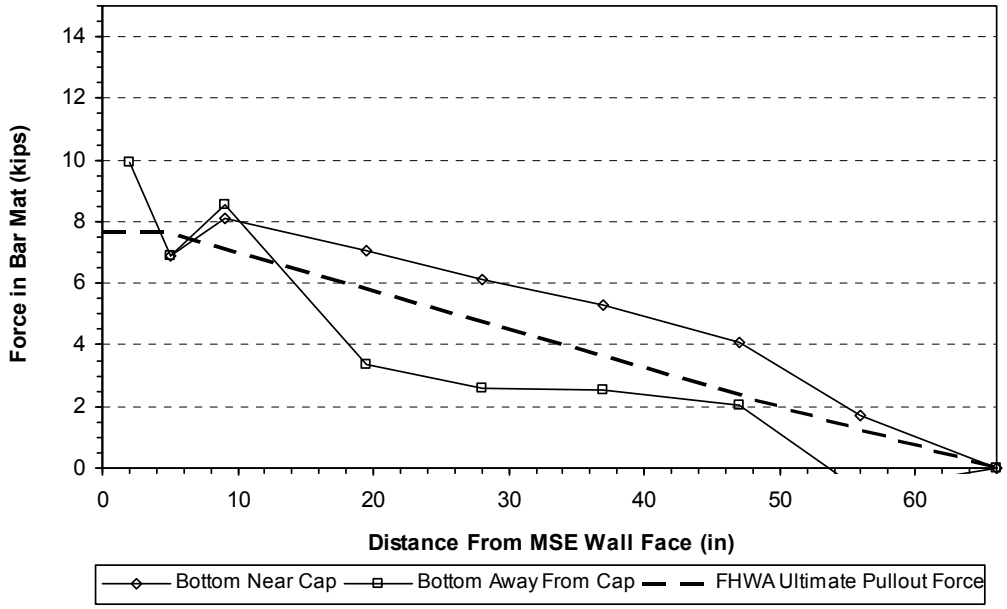

Figure 8-25: Force in bottom mats, 1.5 inch pile cap displacement.

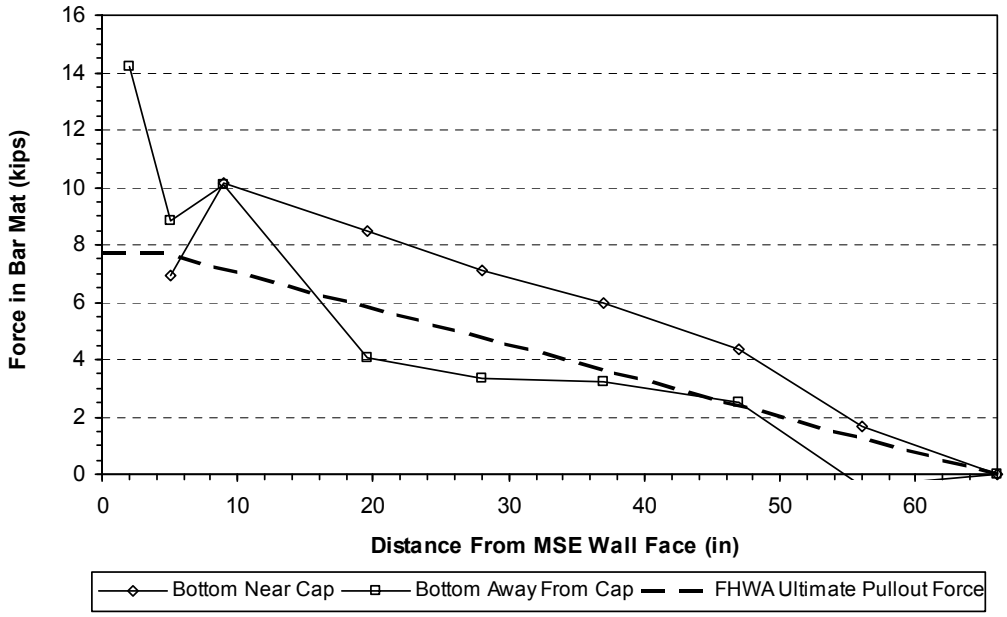

Figure 8-26: Force in bottom mats, 2.0 inch pile cap displacement.

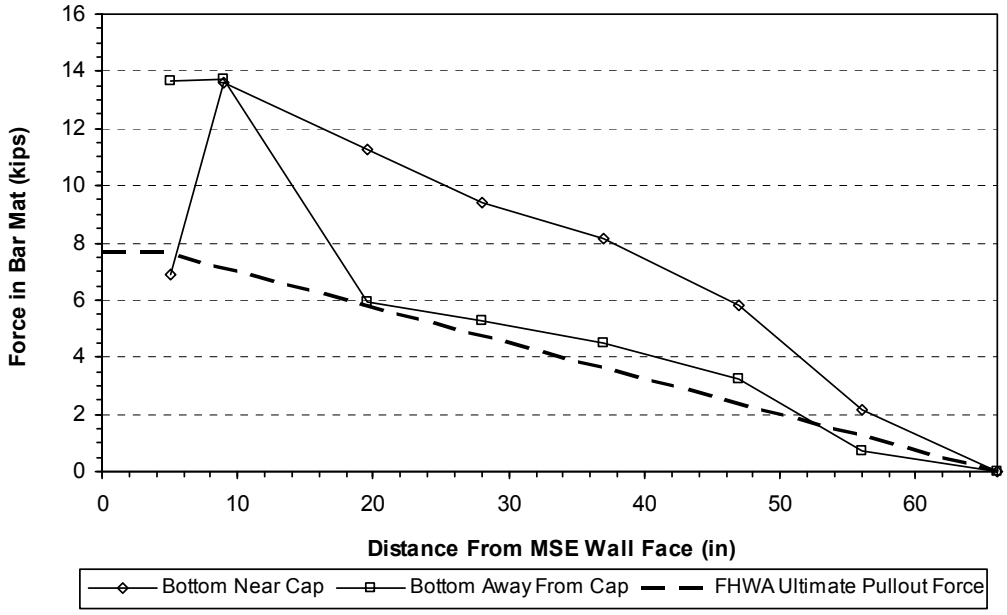

Figure 8-27: Force in bottom mats, 3.0 inch pile cap displacement.

The reason the total number of longitudinal bars is reduced by one is because the outer bars only carry half the tributary area of inner bars, so two halves are subtracted from the total number of bars. Great effort was made to separate useful data from the bad strain gauge data, however, not all of the strain gauges operated with complete reliability. When a strain gauge appeared to malfunction, its point on the graph was simply interpolated between adjacent gauges (indicated by a line), or nothing is graphed. Any point on the graph represents data from that location's gauges.

The forces shown in these figures are those developed during construction and during subsequent loading of the pile cap. The mats are carrying an initial load from construction. During construction, the data acquisition computers measured the increase in strain as the backfill was placed and force developed in the bar mats. The forces produced by construction of the backfill were also computed using Equation 8.2 and plotted against the design load. Based

on this comparison, an equation was developed to represent the force in the mats due to construction.

The dashed line in each figure is the design pullout line. The flat portion of this line is the predicted total capacity of the mat according to the Federal Highway Administration (FHWA) design manual Mechanically Stabilized Earth Walls and Reinforced Soil Slopes Design and Construction Guidelines (NHI, 2001). The flat portion of the line extends from the face of the wall to a distance equal to the distance to the resistant zone for each mats respective location. From this point, the line slopes down to a force value of zero at a distance equal to the length of the mat.

As can be seen in the figures, the results between the sets of bar mats are pretty consistent with one another, despite individual variability. The measured force in the mats develops to values greater than the design pullout force. This could be due to conservatism in the design equations, assumptions made concerning how uniformly force develops in the mats, and errors in the strain measurements. The values nearer to the wall face (2 inches to 9 inches) have a greater tendency to show unreasonable values. This is likely due to either bending effects near the wall face, or damage to strain gauges during construction. Strain gauges in this area are exposed to greater risk of damage due to construction and placement of the pins to connect the bar mats to the wall panel. To make comparison from push increment to push increment easier, the same scale is maintained for each level of mat. Figure 8-17 through Figure 8-27 show that the force in the bar mats develops roughly parallel to the design pullout line.

Figure 8-17, Figure 8-21, and Figure 8-25 are the plots corresponding to the 0.5, 1.25, and 1.5 inch pile cap displacement increments. The force at this point appears to reach the design pullout line for each respective level. The order that the mats appear to reach the design

pullout line proceeds from top to bottom, consistent with design capacities of each level. Figure 8-28, Figure 8-29, and Figure 8-30 show the mat force plotted against the transverse MSE wall displacement. Also shown here are the design pullout lines for the respective levels. As can be seen in the figures, the force measured in the mats is greater than the capacity that was predicted in the design. However, in most cases, the lines seem to reach a peak, where the walls continue to displace, with little or no increases in force in the mats. The wall displacement for the middle mats is taken as the average of the LVDT's above and below it.

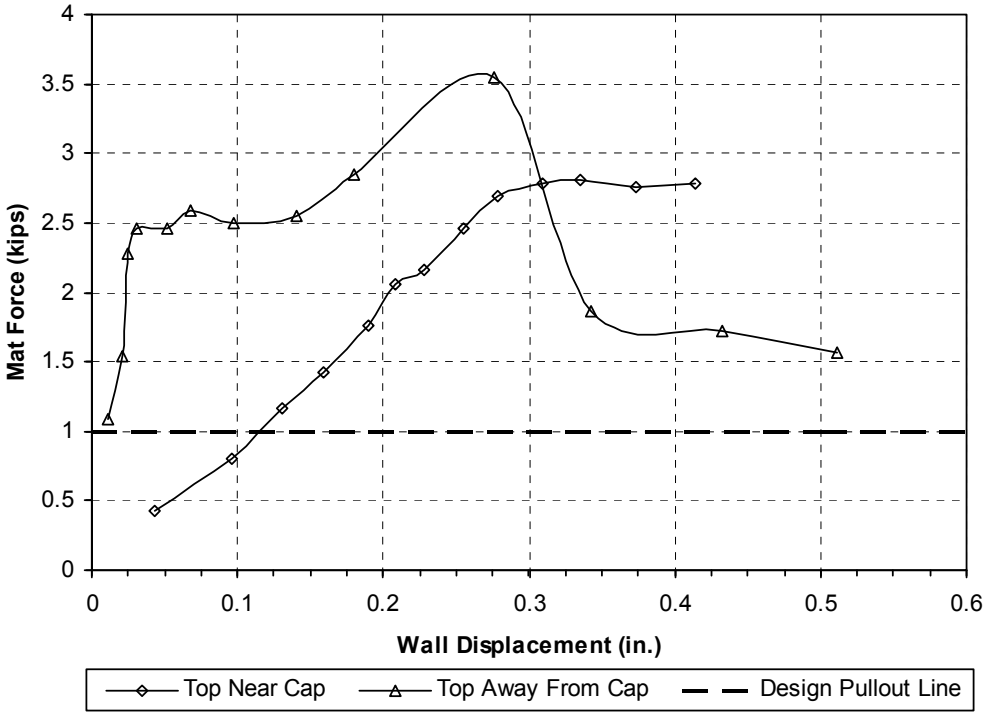

Figure 8-28: Wall displacement versus mat force, top mats.

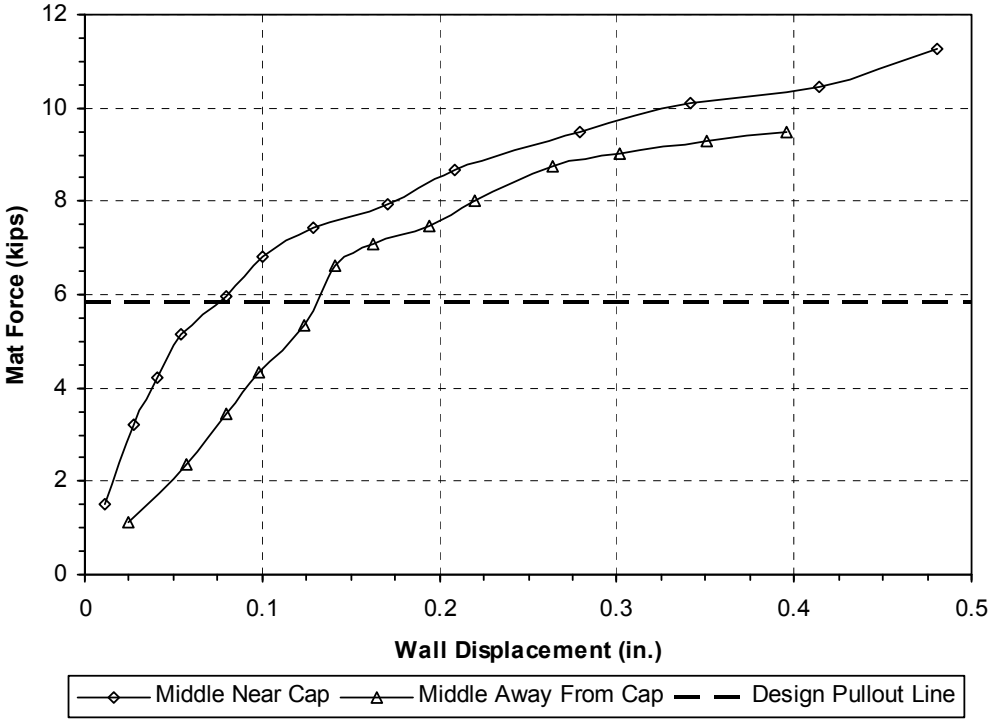

Figure 8-29: Wall displacement versus mat force, middle mats.

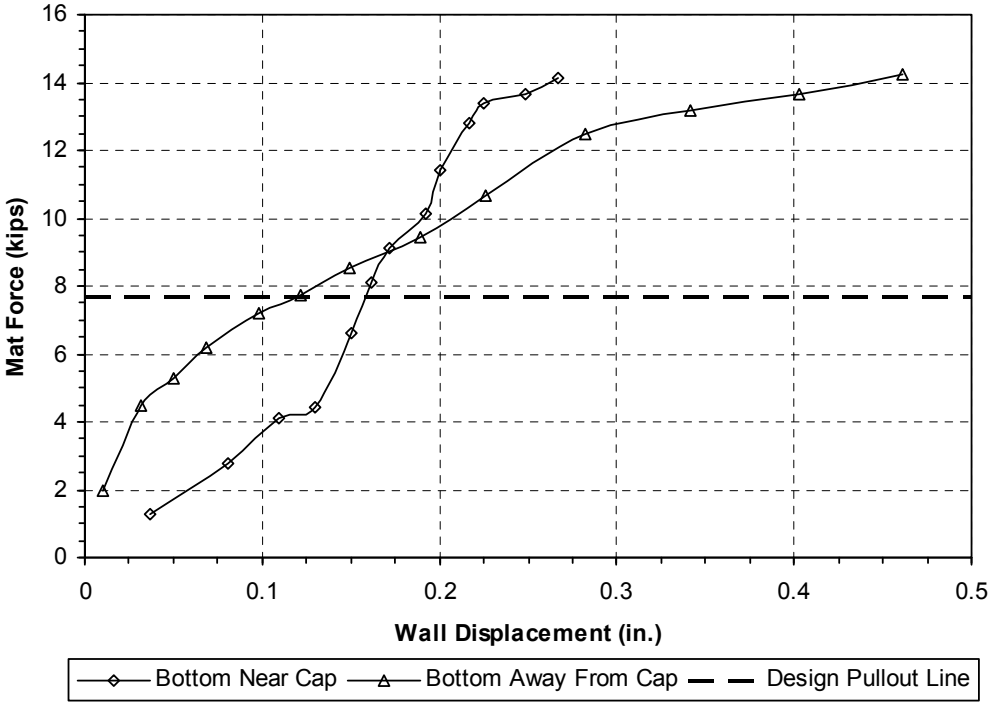

Figure 8-30: Wall displacement versus mat force, bottom mats.

Figure 8-31 shows the ratio of the pressure on the wall/pressure on the pile cap face, as a function of distance from the face of the pile cap. The pressure on the wall panels was taken as the load measured in the bar mat divided by the area of the wall panel that bar mat was designed to carry. The pressure on the face of the pile cap was determined by assuming the pressure developed in a simple triangular manner, so that the pressure multiplied by the area over two equaled the passive load measured in the actuators. The level of pressure at the level of each bar mat was obtained by linear interpolation. The value of pressure on the wall was divided by the value of pressure on the pile cap at the depth of the bar mat for each pile cap displacement increment. The median values of all the displacement increments for each bar mat was plotted as a function of the distance of that mat from the face of the pile cap, and a line was fitted to the data points. As can be seen, the R^2 value for this line is very low.

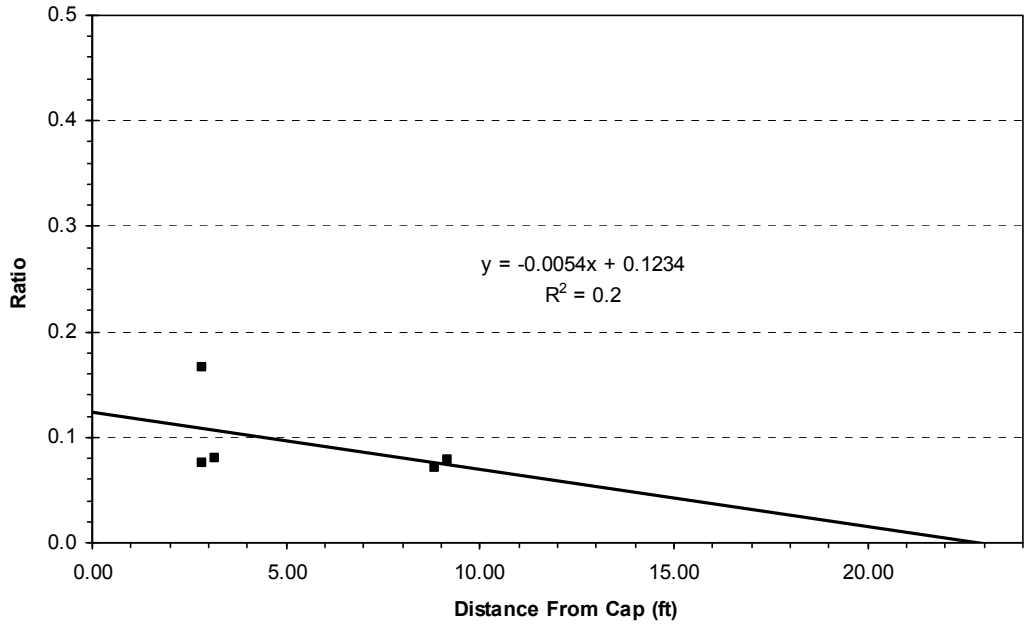

Figure 8-31: Ratio of pressure on wall/pressure on pile cap versus distance from pile cap.

Figure 8-32 shows the same thing as Figure 8-31, except the values beyond large displacements are not included, as discussed in Section 7.7. As can be seen in both of these figures, there is one data point near the pile cap that is larger in magnitude than the other data points. This data point comes from the top mat nearest the pile cap. Recall that this mat isn't very deep, so the pressure on the pile cap assuming a linear pressure distribution is comparatively small. The pressure on the tributary area of the top mats is less than that on rest of the wall, but due to the lesser pressure on the pile cap, both top mats have a higher pressure ratio than that of the deeper mats. The data point for the top mat further from the pile cap is not shown because its value is about three times that of the other values further from the pile cap. Without the higher point closer to the pile cap, the best-fit line would be closer to horizontal. This might be expected as long as the induced pressure on the wall panels caused the load on the mats to exceed the ultimate pullout capacity of the mats. More tests with mats instrumented further from the pile cap might show a decreasing pressure ratio with increasing distance from the pile cap.

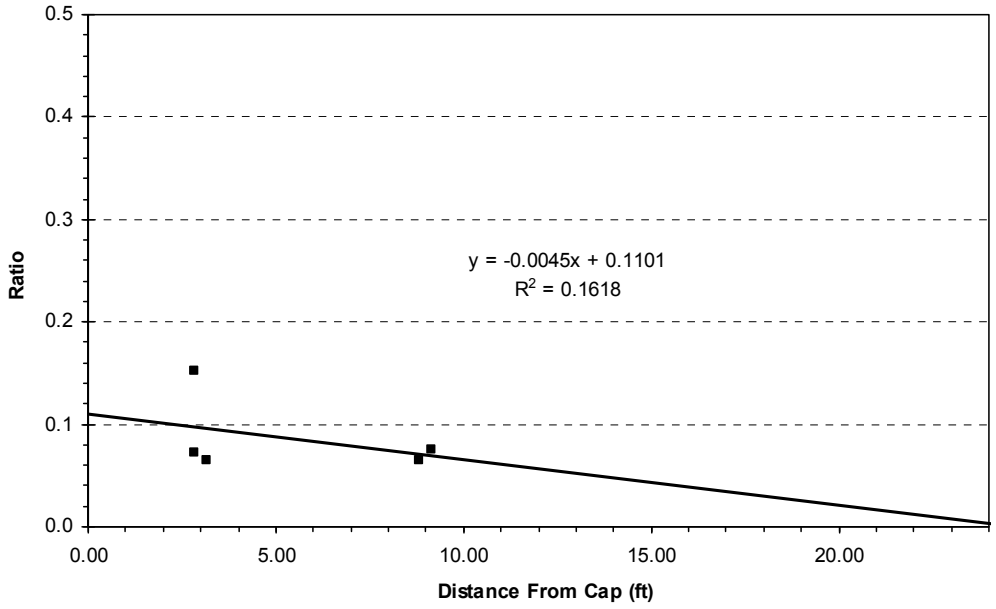

Figure 8-32: Ratio of pressure on wall/pressure on pile cap versus distance from pile cap, larger wall displacements deleted.

9 Comparison Of MSE Test Results

This chapter compares the results of the 3D or unconfined test, the 2D or plane strain test, both MSE tests, and the results from the MSE test reported by Rollins and Heiner (2010). These results are broken down into the following areas: force-displacement (force measured from actuators), backfill displacement, transverse wall displacement, heave and cracking, and mat strains/forces.

9.1 Load-Displacement Results

The measured passive resistance versus displacement curves for the various tests are shown in Figure 9-1. The unconfined 3D test provides the greatest passive resistance because the effective width of the pile cap (22 ft) is double the actual width of the cap. Despite the smaller effective width (11 ft), the plane strain or 2D test still produced about 83% of the resistance provided by the 3D test. This can be attributed to the higher plane strain friction angle applicable to the 2D test relative to the triaxial friction angle applicable to the 3D tests as discussed in Section 2.3 and subsequently in Chapter 10.

In these and other tests performed, we didn't necessarily reach the peak value of passive resistance due to limits on pile cap displacement. In addition, there is a potential for decreased ultimate resistance with additional displacement, due to the dilation of the dense sand.

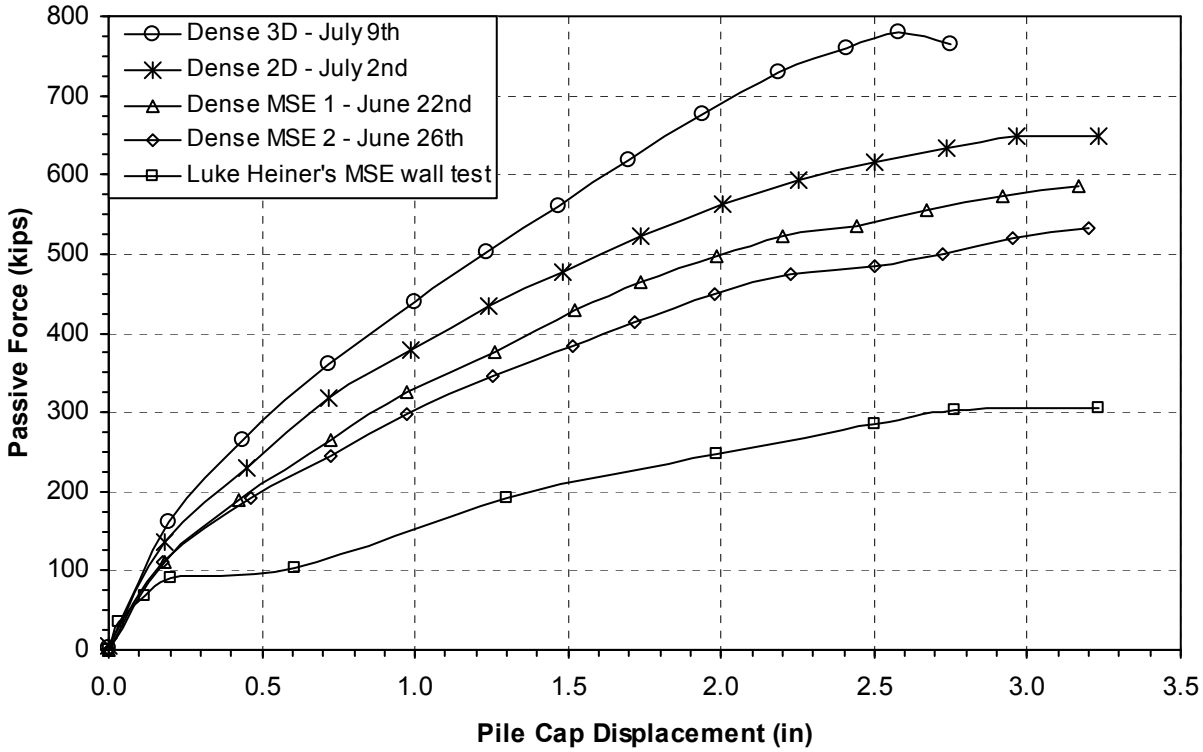

Figure 9-1: Measured passive force versus horizontal pile cap displacement.

The ultimate value of passive resistance of each test can be divided by the effective width for that test. These values for each case are shown in Table 9-1. As can be seen, the greatest force per effective width was realized with the plane strain case, with diminishing results in each wall case. Both MSE test 1 and 2 had higher forces per effective width than the unconfined case.

Table 9-1: Comparisons of Force per Effective Width

Test	P_u/Effective Width (kips/ft)
Unconfined (3D) Backfill	35.5
Plane Strain (2D)	59.1
MSE 1	53.2
MSE 2	48.4
Rollins and Heiner	27.7

Differences in backfill width and soil unit weights make direct comparison of the results difficult. To help circumvent this difficulty, the passive earth pressure coefficient versus displacement curves for the various tests are shown in Figure 9-2.

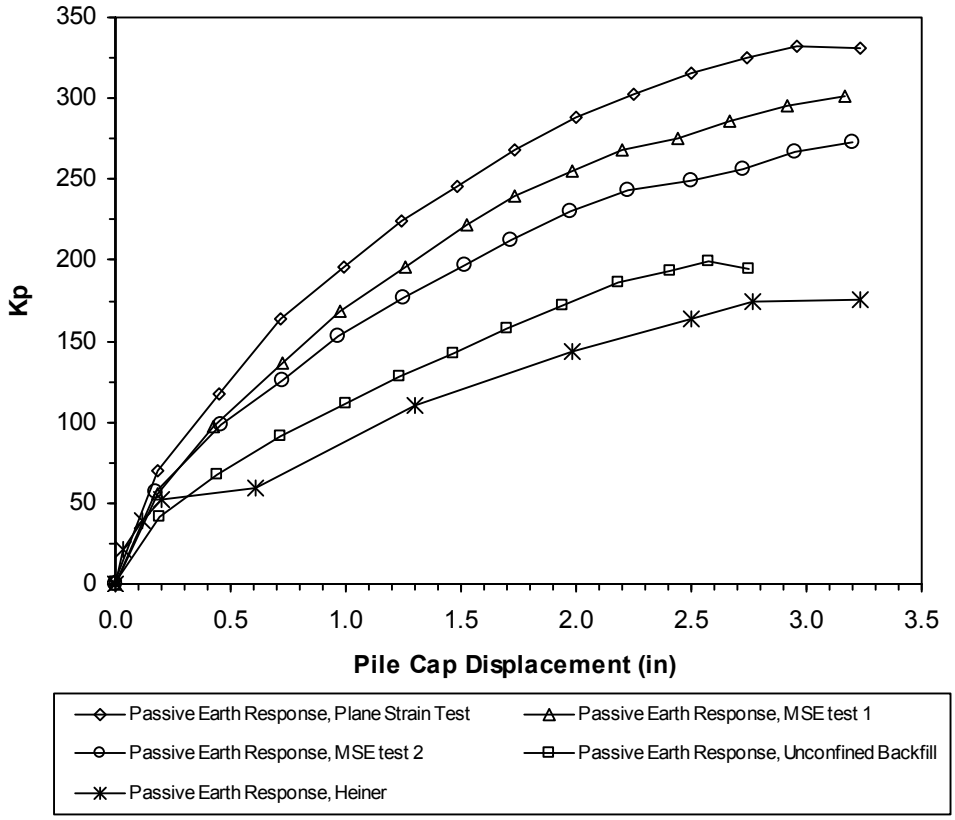

Figure 9-2: Measured passive earth pressure coefficient versus horizontal pile cap displacement.

The passive earth pressure coefficients were determined using the equation

$$K_p = P/(0.5\gamma_m H^2 B_e) \tag{9-1}$$

where K_p = passive earth pressure coefficient
P = measured passive resistance (lbs)
γ_m = soil unit weight (lbs/ft^3)
H = pile cap height (ft)
B_e = Brinch-Hansen 3D correction factor

The differing inputs for this equation for each of the tests are shown in Table 9-2. Whereas in Figure 9-1 the unconfined backfill has the largest values, in Figure 9-2 it is only higher than the results from Heiner et al (2010). This is mostly due to the unconfined values being divided by the Brinch Hansen 3D correction factor of 2 (1966). The order of the other tests remains the same. The results from Heiner et al are closer to the results from MSE 1 and MSE 2 due to the unit weights being divided out, but still fall far short of these values.

Table 9-2: Test Properties

Test	Soil Unit Weight (lb/ft^3)	Brinch-Hansen 3D Correction Factor
Unconfined (3D) Backfill	129.5	2
Plane Strain (2D)	129.3	1
MSE 1	128.7	1
MSE 2	128.8	1
Rollins and Heiner	114.7	1

The measured passive force-displacement curves for all the MSE tests are flatter and develop lower ultimate values than those for the plane strain test. This may be a result of the greater outward movement of the MSE wingwalls relative to the plane strain test. As can be seen in Figure 9-1, the curves for the MSE tests conducted during this study were significantly higher than the measured curve for the MSE test reported by Rollins and Heiner (2010). This could be a result of several factors. First, eccentric mass shakers were used during the Rollins and Heiner

test which may have softened the response. Second, the MSE wingwalls for this study had higher factors of safety against pull-out relative to the test conducted by Rollins and Heiner. Finally, the MSE wingwall in the Rollins and Heiner test translated and rotated outward more than the MSE wingwalls in this study. These factors may explain the unusual shape of the load-displacement curve for the Rollins and Heiner test relative to the hyperbolic curve shapes observed in the tests during this study.

One unexpected result was that the passive resistance for MSE test 1 was greater than for MSE test 2. The average factor of safety against pull-out in test 1 was about 1.5, compared to an average factor of safety of 2.5 in the second MSE test. This could be due to the shallow embedment of the top layer of mats in MSE test 2. As was mentioned, the top layer was only embedded 6 inches. This could have reduced the factor of safety of this mat, and caused the wall to rotate outwardly more. Also, the shallow embedment could have caused the top layer of soil to "ride" on the top mat, reducing the resistance of the top mat, as discussed in Section 8.6. As can be seen by comparing Figure 8-16 with Figure 7-15, more cracks are present in the center of the soil backfill near the face of the pile cap in MSE test 2 than MSE test 1.

Figure 9-3 shows the passive earth pressure coefficient divided by the maximum passive earth pressure coefficient for each test versus the pile cap displacement for each test. Such normalization makes it possible to compare the development of passive resistance relative to each test's maximum. As can be seen, the curves are so tightly grouped that it is difficult to distinguish between the tests. The jog in the results of Rollins and Heiner (2010) can still be seen in this plot. The curves for the plane strain, MSE test 1, and MSE test 2 plot nearly on top of one another.

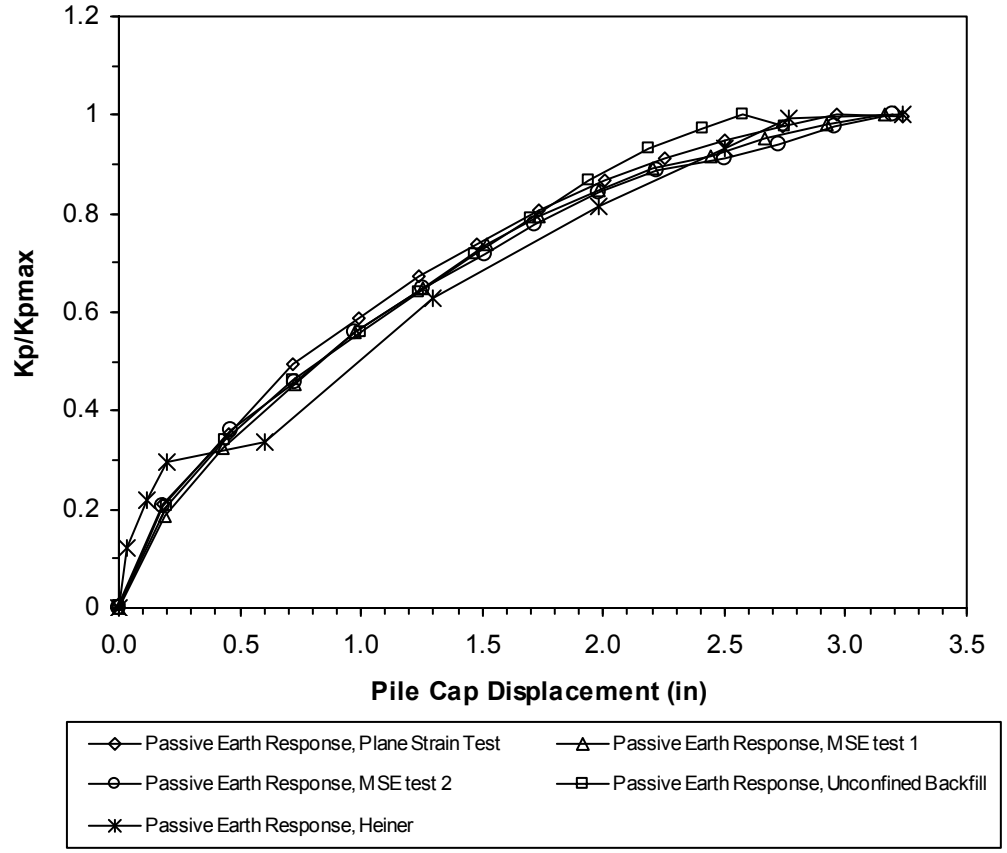

Figure 9-3: Measured passive earth pressure coefficient divided by each tests maximum passive earth pressure coefficient versus pile cap displacement.

9.2 Backfill Soil Displacements

Figure 9-4 through Figure 9-7 show the absolute displacement of the backfill soil for each of the tests performed, excluding Rollins and Heiner (2010). As can be seen, the backfill displacements for equal pile cap displacements are very close, and the shape of each of the curves is similar.

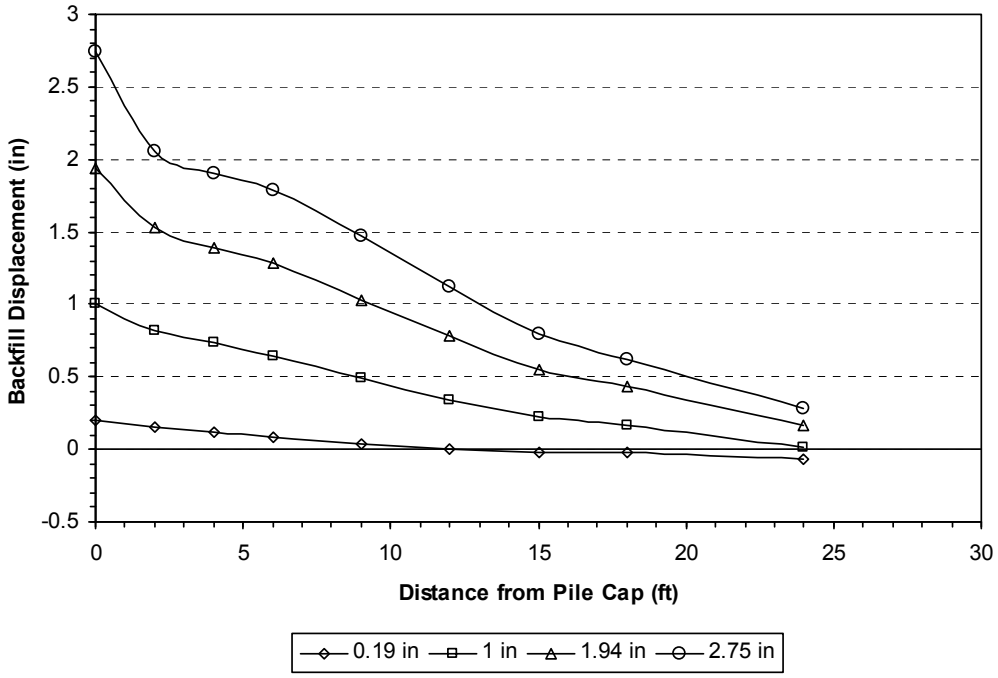

Figure 9-4: Displacement of backfill soil, unconfined backfill (repeat of Figure 5-7).

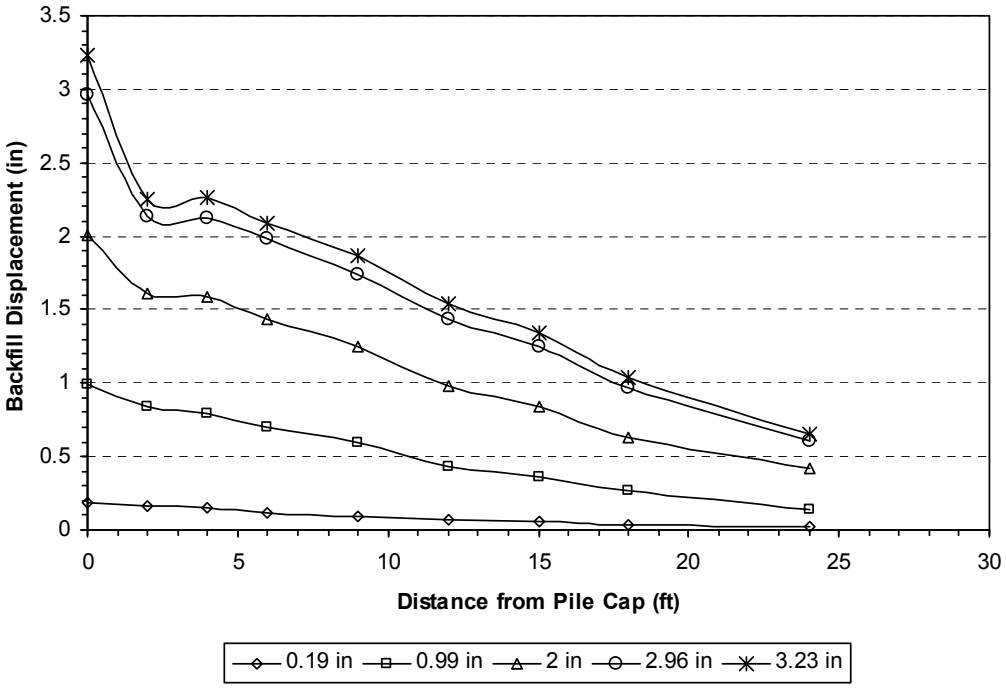

Figure 9-5: Displacement of backfill soil, plane strain (repeat of Figure 6-7).

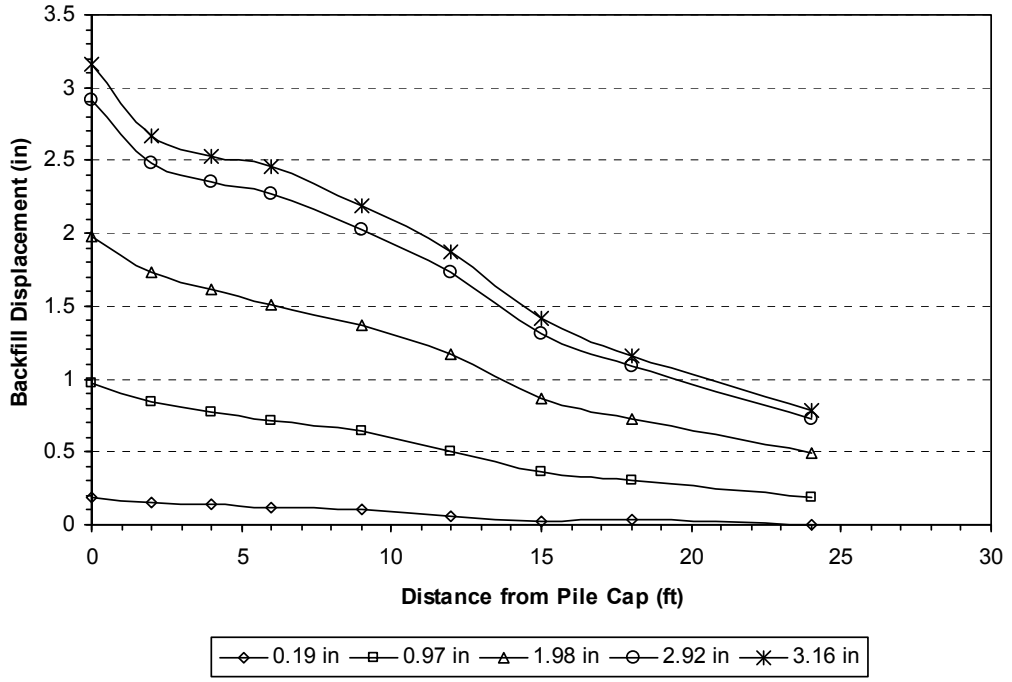

Figure 9-6: Displacement of backfill soil, MSE test 1 (repeat of Figure 7-7).

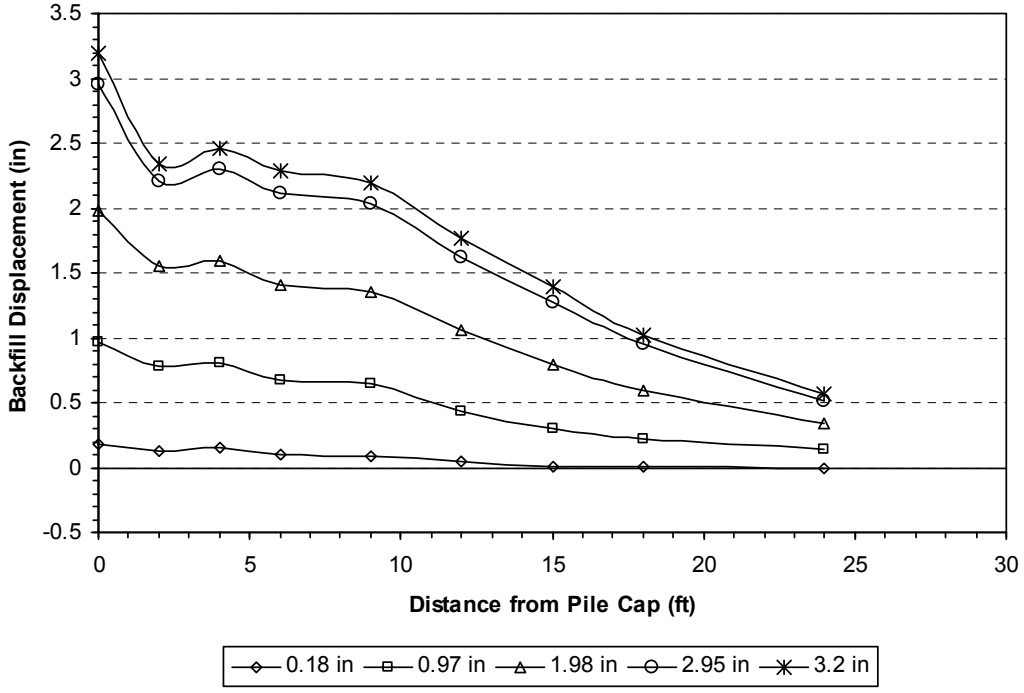

Figure 9-7: Displacement of backfill soil, MSE test 2 (repeat of Figure 8-7).

The compressive strain of the backfill for each of the cases is shown in Figure 9-8 through Figure 9-12. As can be seen in each case, the greatest compressive strain occurs within the first couple feet of the cap face. The value of strain then reaches a local minimum and then increases and decreases with increasing distance from the face of the pile cap. The magnitude of compressive strain developed varies from one case to another.

9.3 Transverse Displacement of Wall Panels

Figure 9-13 through Figure 9-15 show the outward movement of the wall panels for MSE tests 1 and 2. Plots from Rollins and Heiner (2010) were not available. These plots represent the data obtained from the string pots located at 102.5 inches from the face of the pile cap from the first test and at 20 and 103 inches from the face of the pile cap from the second test.

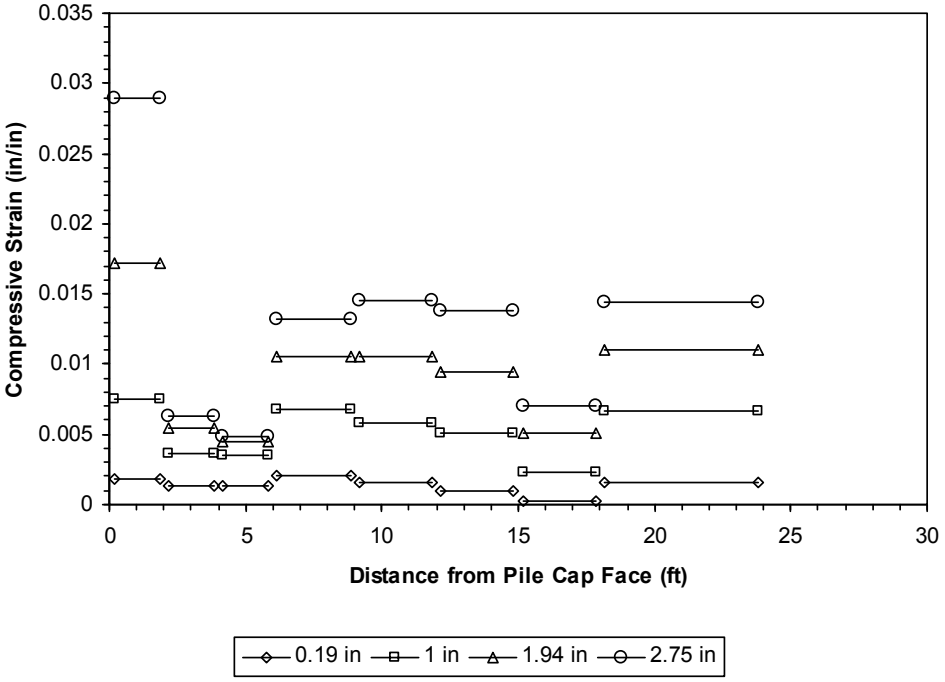

Figure 9-8: Compressive soil strain in backfill as a function of distance behind the cap for several displacement increments, unconfined backfill (repeat of Figure 5-8).

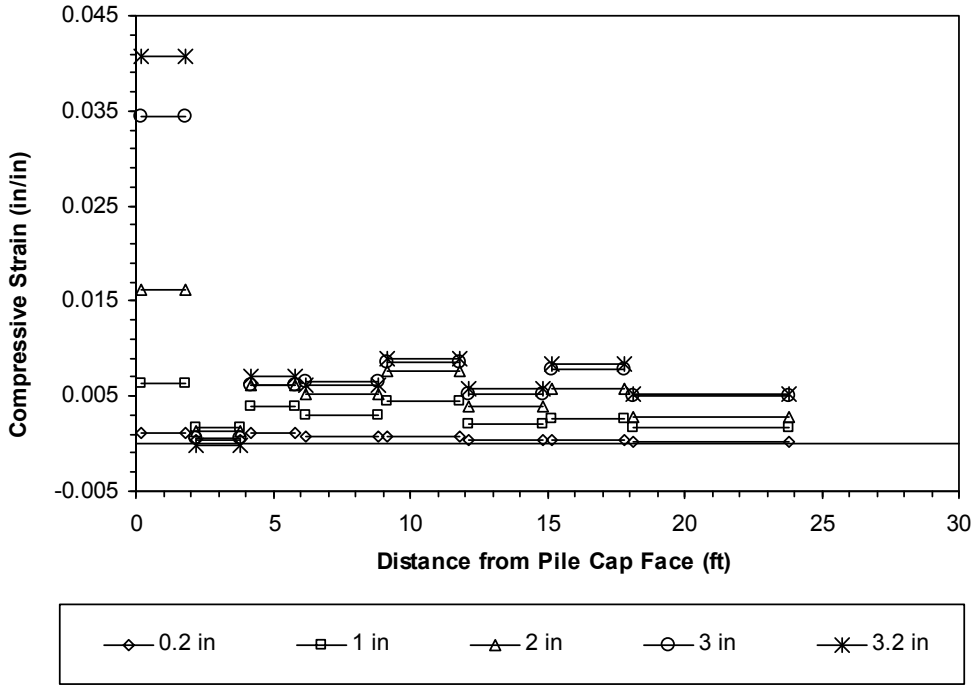

Figure 9-9: Compressive soil strain in backfill as a function of distance behind the cap for several displacement increments, plane strain backfill (repeat of Figure 6-8).

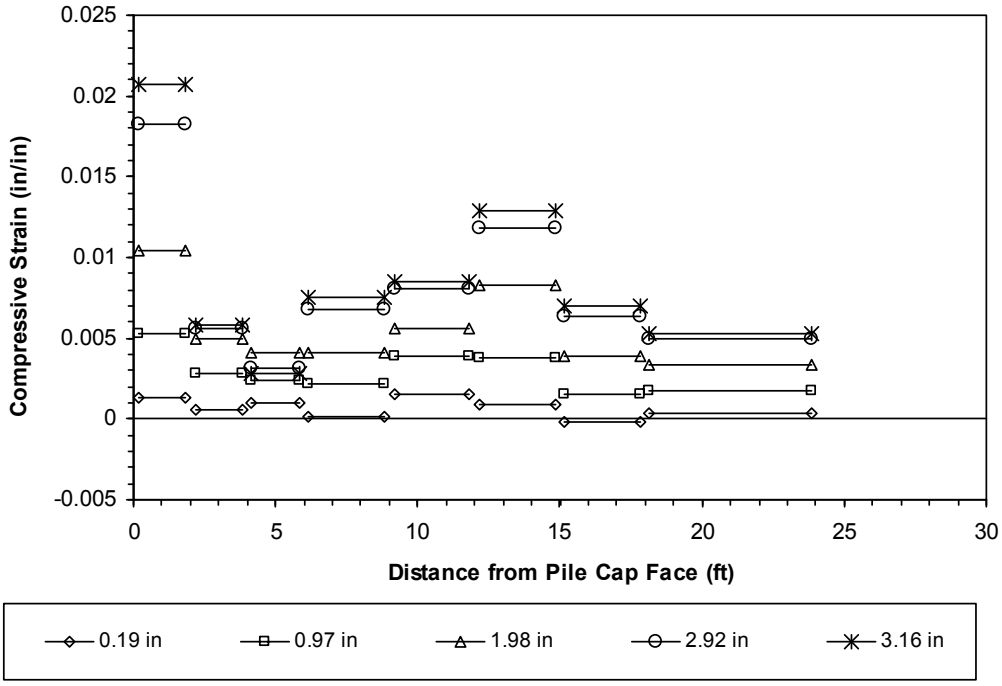

Figure 9-10: Compressive soil strain in backfill as a function of distance behind the cap for several displacement increments, MSE test 1 (repeat of Figure 7-8).

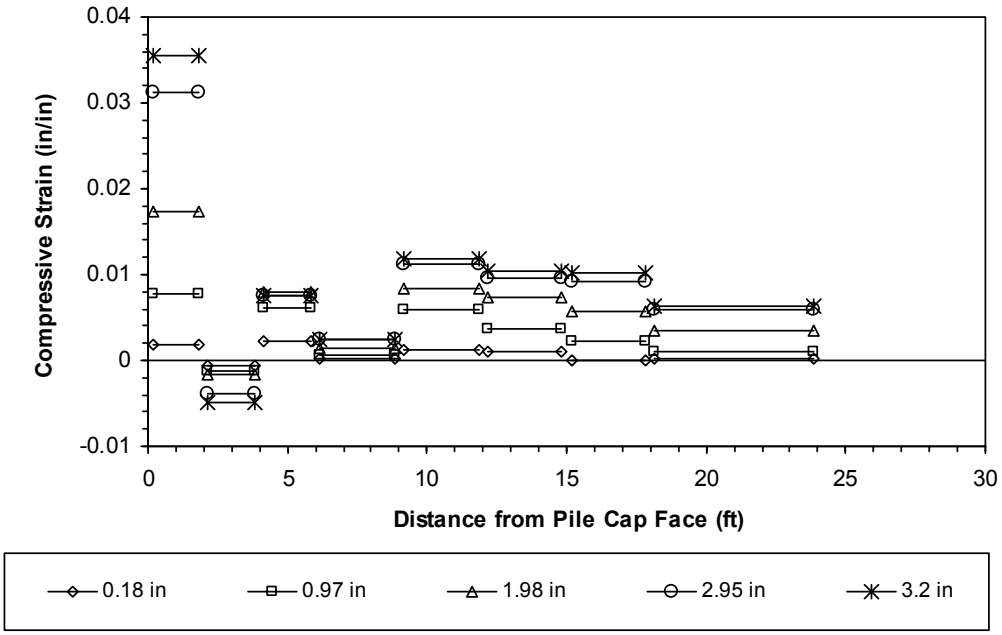

Figure 9-11: Compressive soil strain in backfill as a function of distance behind the cap for several displacement increments, MSE test 2 (repeat of Figure 8-8).

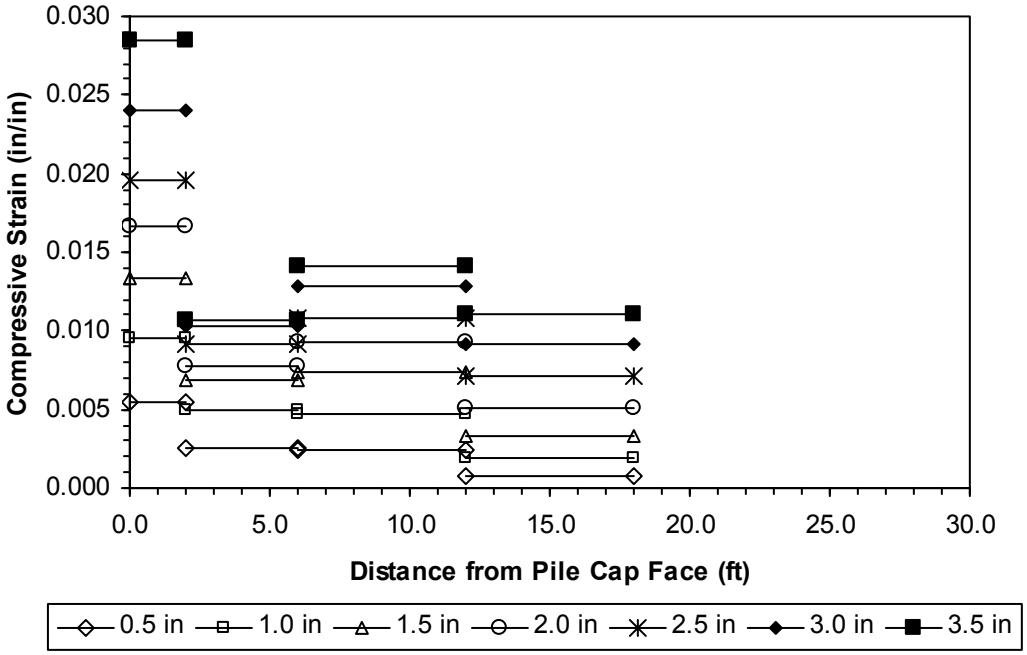

Figure 9-12: Compressive soil strain in backfill as a function of distance behind the cap for several displacement increments, Rollins and Heiner (2010).

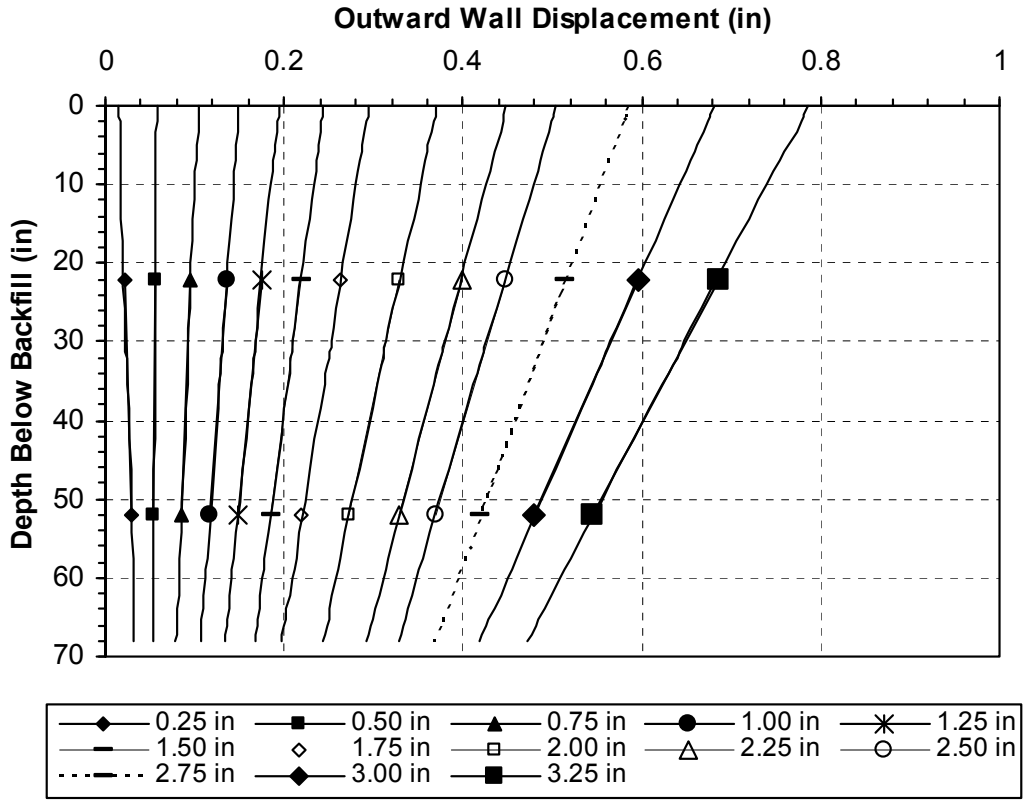

Figure 9-13: Outward movement of wall panel, top to bottom, 102.5 inches from pile cap face, MSE test 1 (repeat of Figure 7-9).

The data was extrapolated linearly to demonstrate the movement of the wall from top to bottom, while the point on each line represents the location of each string pot. Each line represents values from each displacement increment, as indicated. The top of the backfill is located at a depth of 0 inches, while the wall extended 9 inches above the backfill. Both Figure 9-13 and Figure 9-14 show that the top of the wall is displacing outward more than the bottom, resulting in rotation of the wall. At first glance, these figures look fairly comparable; however, with inspection of magnitudes it can be noticed that the wall in Figure 9-14 displaces outward about 0.3 inches less than the wall in Figure 9-13.

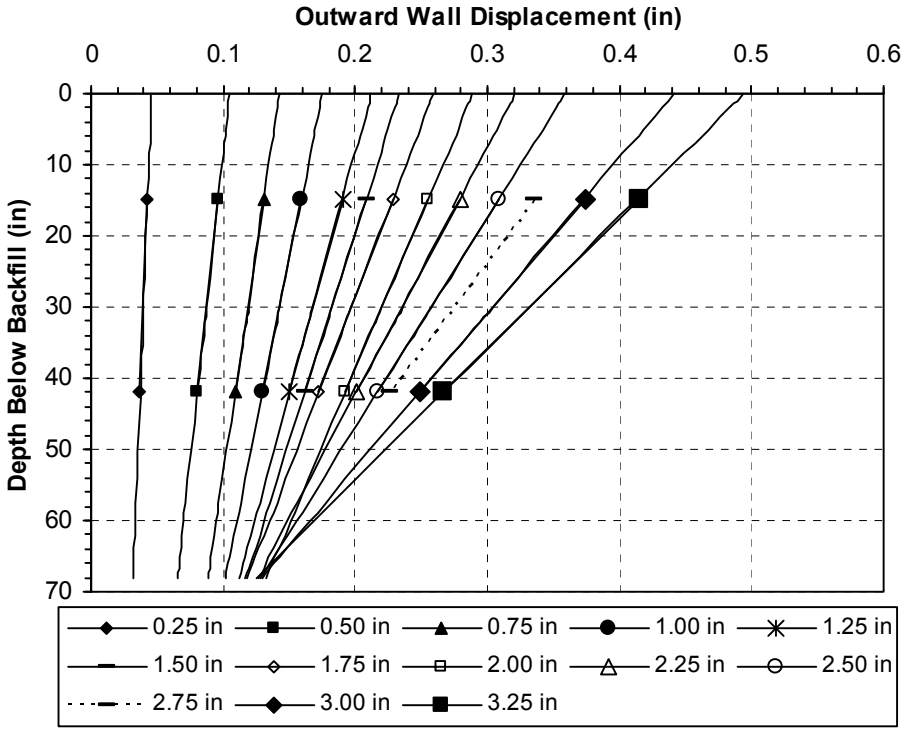

Figure 9-14: Outward movement of wall panel, top to bottom, 20 inches from pile cap face, MSE test 2 (repeat of Figure 8-9).

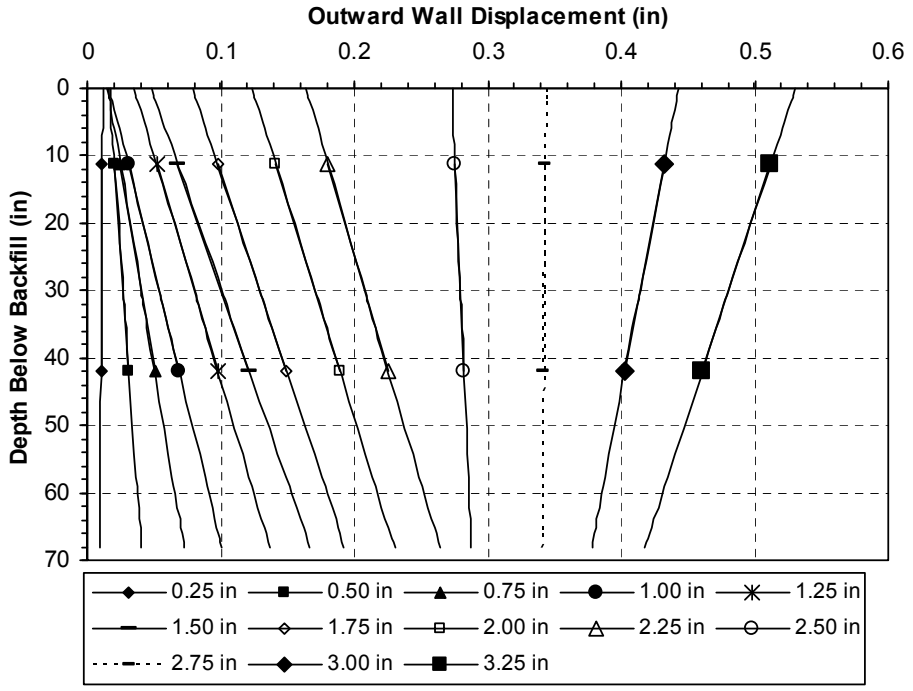

Figure 9-15: Outward movement of wall panel, top to bottom, 103 inches from pile cap face, MSE test 2 (repeat of Figure 8-10).

Figure 9-15 shows that the bottom of the wall moves out more first, then the top begins moving out. It seems likely that this is an error of some sort. As in test 1, it would be expected that the top moves more than the bottom, as the bottom reinforcing in test 2 has about 1600 lb more extra capacity beyond the construction loading than the reinforcing above it. Closer to the end of testing, it appears that the data begins to look more like what is expected, and the displacement magnitude for the upper string pot is similar to that shown in Figure 9-14.

Figure 9-16 shows the rotation of the wall panel versus the actuator load. While the magnitude of displacement in MSE test 1 was greater than that in MSE test 2, the wall panel actually rotated more in MSE test 2. This is likely attributable to the shallow depth of embedment in MSE test 2, as has been discussed.

Figure 9-17 through Figure 9-20 show the outward movement of the wall versus distance from the pile cap. While Figure 9-13 through Figure 9-15 can be pictured as one standing at the end of the wall and looking along the wall (an elevation), these figures are seen from above (plan view). For clarity, data from every half inch of displacement is shown. The way the panels move out is different in each test. In MSE test 1, the joint between panels moves out more than the portion of the wall panel near the pile cap. The opposite is true in MSE test 2, until near the end of testing. The magnitude of displacement is less in MSE test 2 than in test 1. Both MSE test 1 and 2 move out about twice as much as the wall panels from the plane strain (2D) test. The results from Rollins and Heiner test (2010) shows the panel moving out fairly evenly, but to a far greater magnitude: about double the greatest displacement experienced in MSE test 1 and 2. This is likely due to the shakers used and the slightly lower factor of safety in the upper mats for the Rollins and Heiner test.

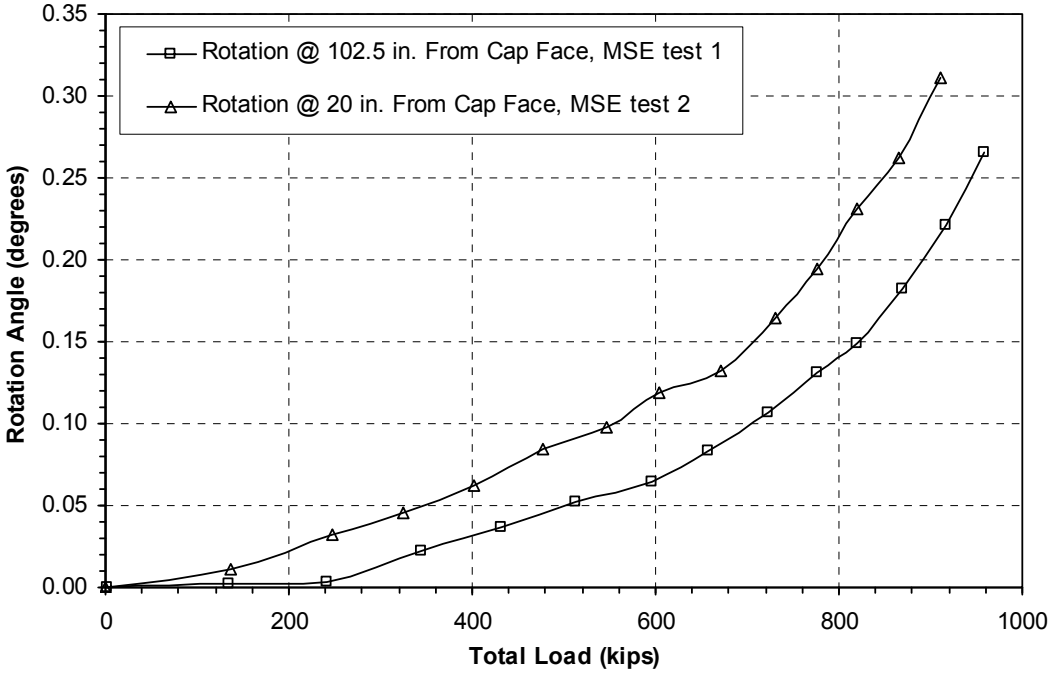

Figure 9-16: Rotation of wall panel versus actuator load.

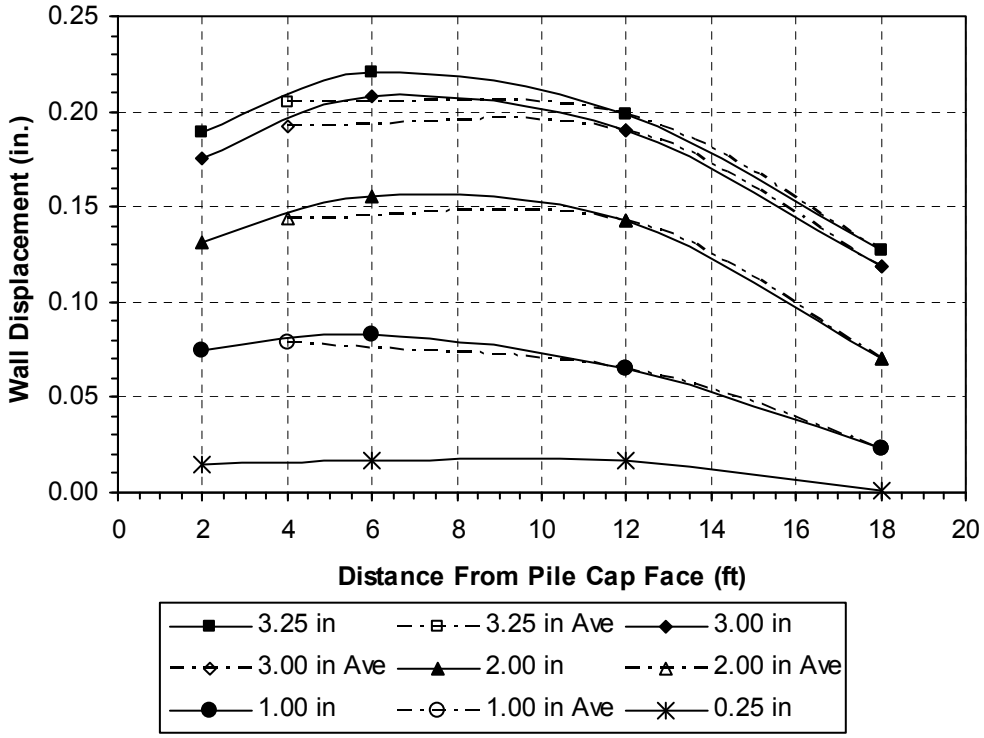

Figure 9-17: Outward movement of wall panel versus distance from pile cap, plane strain (2D) test (repeat of Figure 6-9).

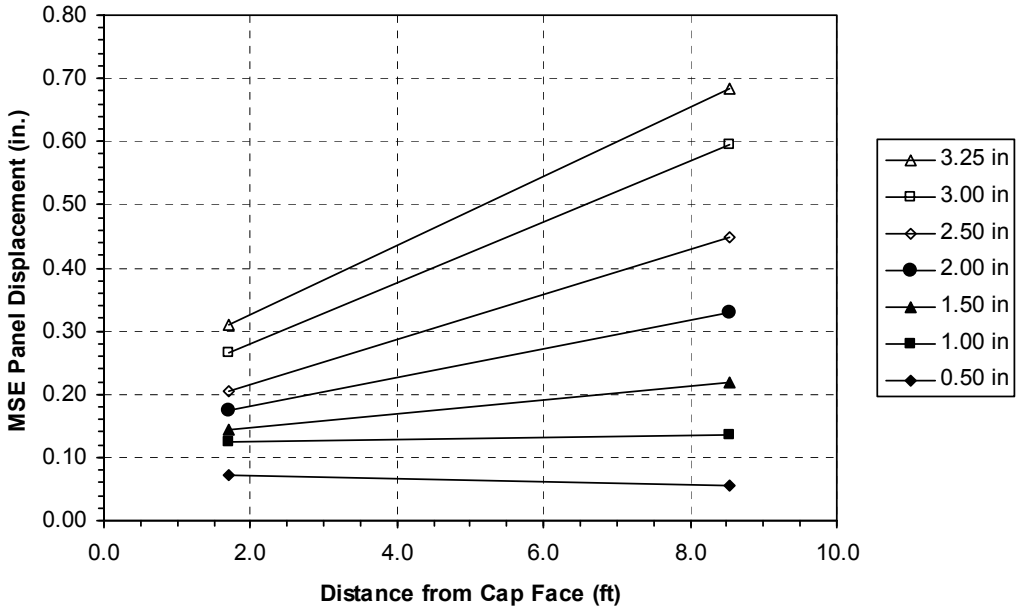

Figure 9-18: Outward movement of wall panel versus distance from pile cap, MSE test 1 (repeat of Figure 7-11).

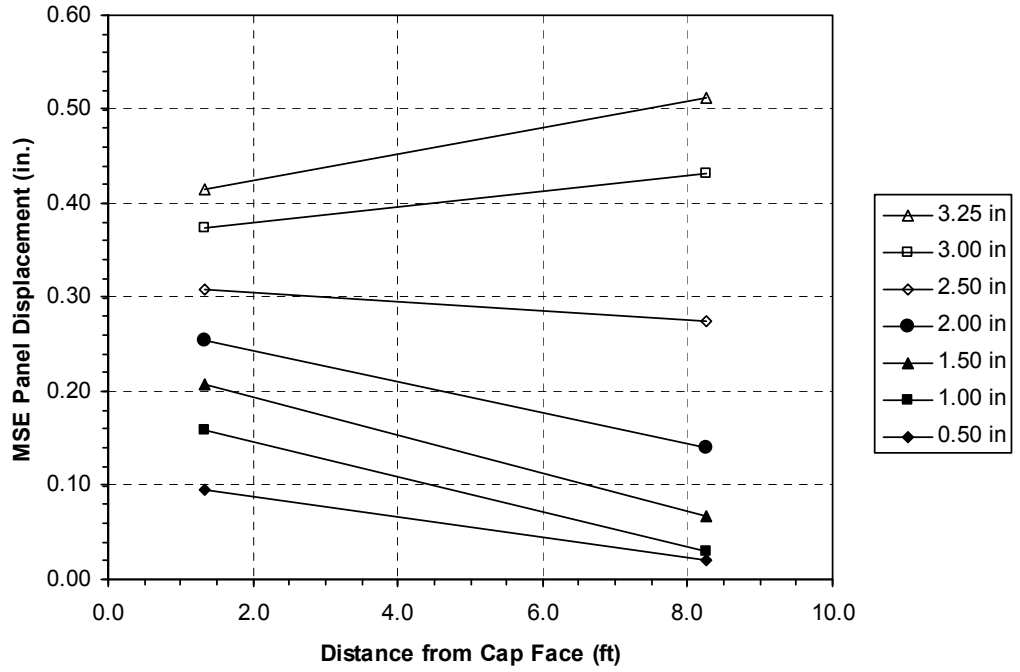

Figure 9-19: Outward movement of wall panel versus distance from pile cap, MSE test 2 (repeat of Figure 8-12).

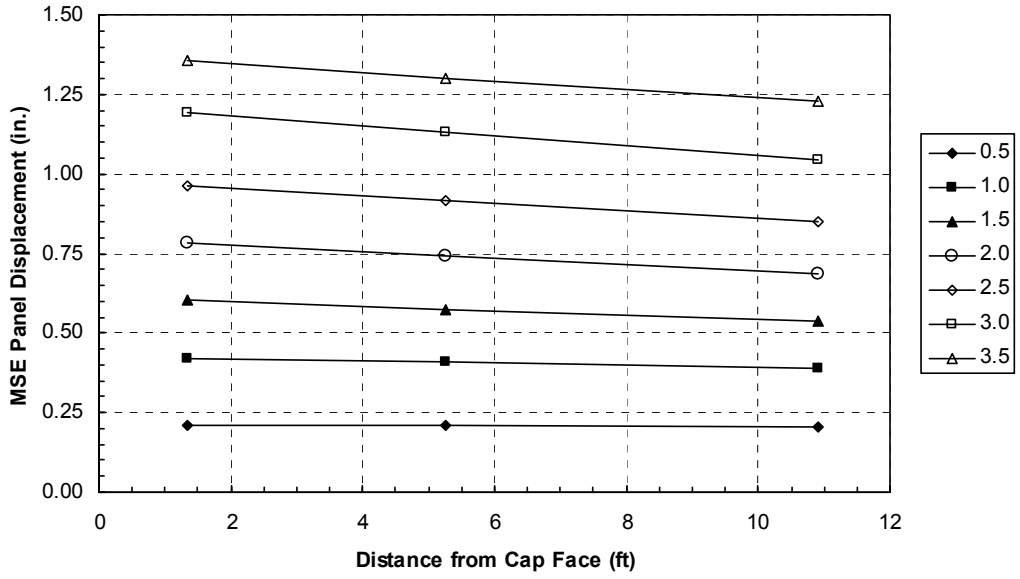

Figure 9-20: Outward movement of wall panel versus distance from pile cap, Rollins and Heiner (2010) MSE test.

Shown in Figure 9-21 is the outward movement of the top of the wall panel versus the measured load from the actuator. Each curve in this figure represents average values from each test, except that from MSE test 1, which didn't have values to average. As can be seen, the data from our MSE test 1 and 2 are roughly similar, but the load from these tests is greater than that obtained in the Rollins and Heiner (2010) tests, while the displacement of the wall panels in MSE test 1 and 2 is less than that from Rollins and Heiner (2010). Some of this increased load and decreased displacement is likely due to the absence of shakers as part of the test procedure. Figure 9-22 and Figure 9-23 show the transverse displacement of the wall panel versus the incremental displacement of the pile cap during the loading sequence. This is for the top of the wall panels at distances of 15-24 inches and 102-103 inches from the pile cap face for Figure 9-22 and Figure 9-23, respectively. The curves from the plane strain test and MSE test 1 and 2 are similar, with the plane strain case showing the least displacement, while the curve from Rollins and Heiner (2010) shows greater displacement.

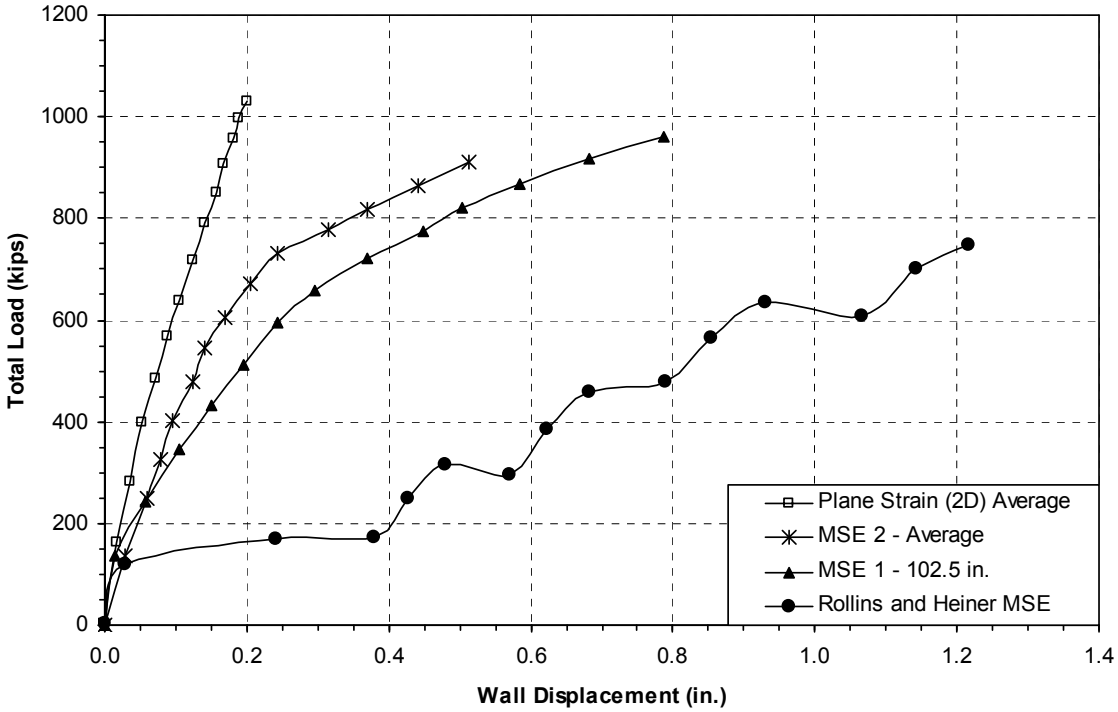

Figure 9-21: Outward displacement of wall panel versus actuator load.

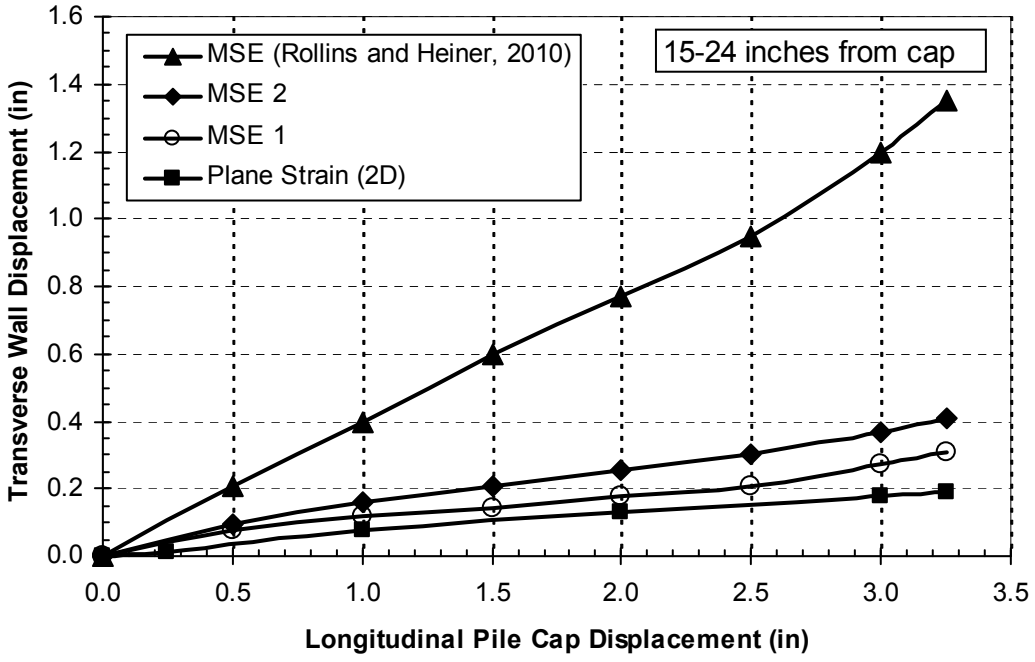

Figure 9-22: Transverse deflection versus longitudinal pile cap deflection, 15-24 inches from pile cap.

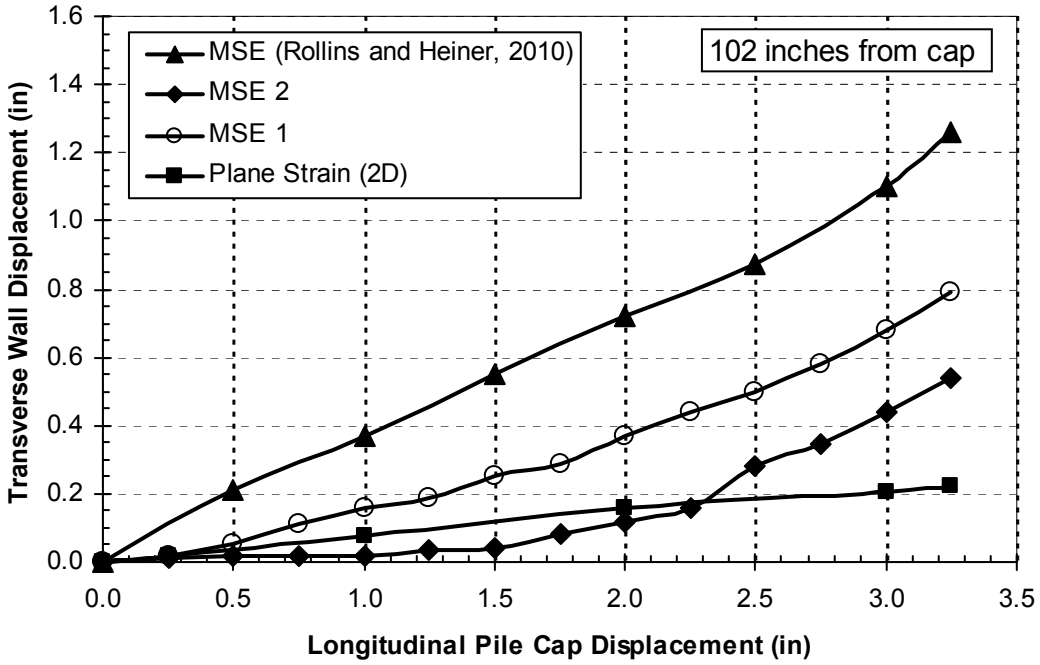

Figure 9-23: Transverse deflection versus longitudinal pile cap deflection, 102-103 inches from pile cap face.

9.4 Heave and Cracking of Soil Backfill

This section will compare the data gathered during the plane strain (2D) test and the two MSE backfill tests conducted during this study with data obtained from the MSE backfill test conducted by Rollins and Heiner (2010). The methods that were used to gather this data are discussed in Section 4.1.3. Figure 9-24 and Figure 9-25 show the soil heave profile for MSE test 1 and MSE test 2, respectively. The values represent the change in elevation from before the test was run to the largest displacement of the pile cap and are in inches. Positive values indicate upward movement, while negative indicates downward movement (settlement). The dashed lines represent the 2 ft by 2 ft grid that was painted on the soil surface before the test was run. In the first test, the maximum heave occurred at a distance of about 6 ft from the face of the pile cap, while in test 2 the maximum heave occurred from 4 to 8 ft from the face of the pile cap.

The distance to maximum heave from the second test bounds the distance to maximum heave of the first test. The shape of the heave contour lines in both tests is circular, as occurs with a plane strain backfill test, but they tend to be slightly stretched along the length of the wall panels.

Figure 9-26 through Figure 9-28 are maps of all the cracks observed after each displacement increment for the three tests conducted during this study and the MSE test reported by Rollins and Heiner (2010). The cracks developed for each increment are identified by a separate color. The process by which cracks were mapped is described in greater detail in section 4.1.3. As can be seen, the predominant crack direction in all three tests is perpendicular to the face of the pile cap. The major exception to this are the cracks which form after the pile cap is pulled back from the soil backfill after completion of the tests. Again, the longest and most predominant cracks occur toward the center of the backfill, between the two sides of the MSE walls. This is likely a result of the outward movement of the wall panels. The bar mats end about in the middle of the soil backfill. Thus, soil could be "riding" on these mats, pulling apart the soil in the center of the backfill.

9.5 Mat Strains and Forces

This section will compare the forces in the bar mat for the two tests conducted during this study and the MSE test reported in Rollins and Heiner (2010), based on the strain gauges placed on the bar mats as described in section 4.4. In addition, a comparison of pressure on the wall panels to the pressure on the pile caps is presented.

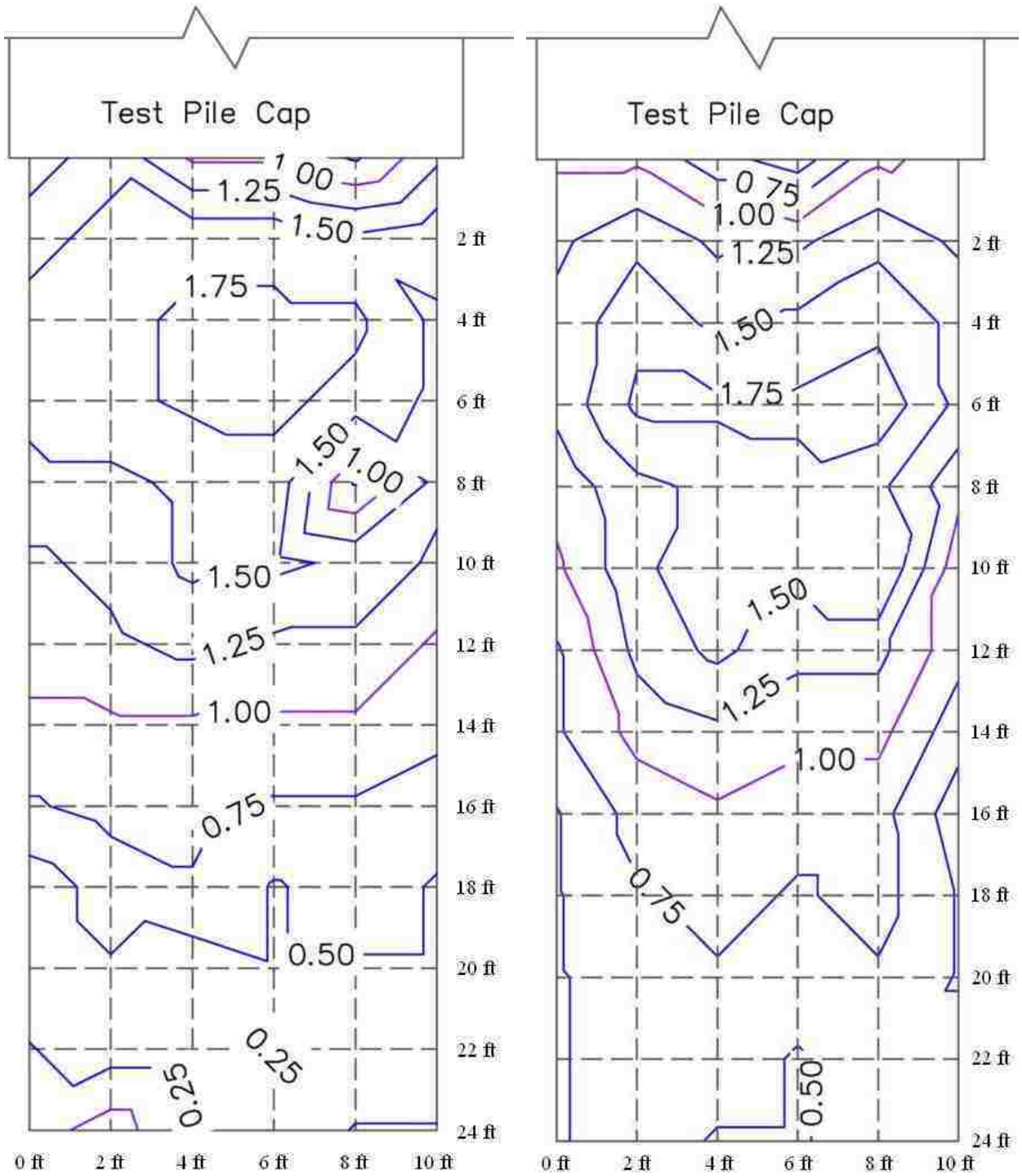

a. b.

Figure 9-24: Soil heave profile, a.) plane strain test (repeat of Figure 6-11), b.) MSE wingwall test 1 (repeat of Figure 7-14).

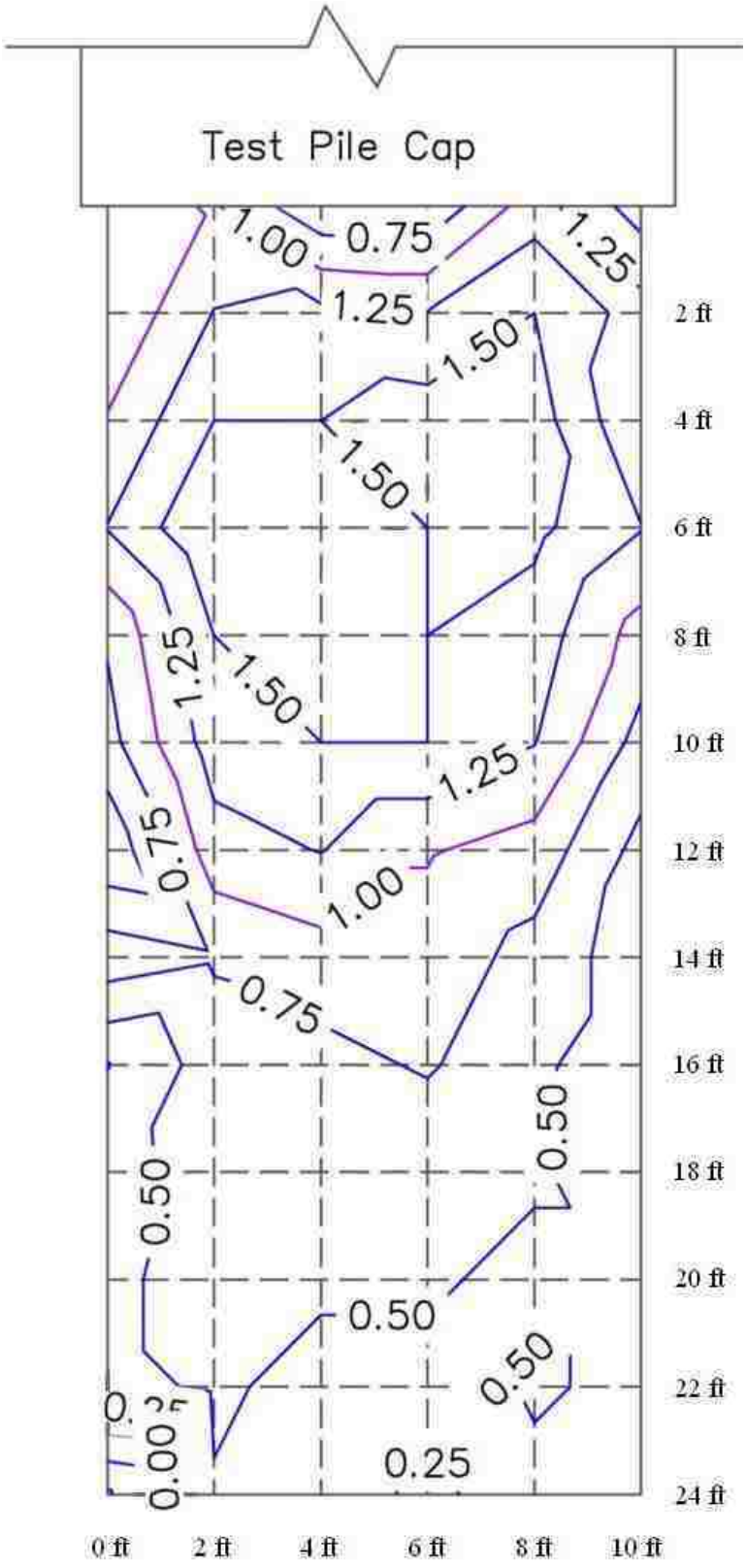

Figure 9-25: Soil heave profile, MSE wingwall test 2 (repeat of Figure 8-15).

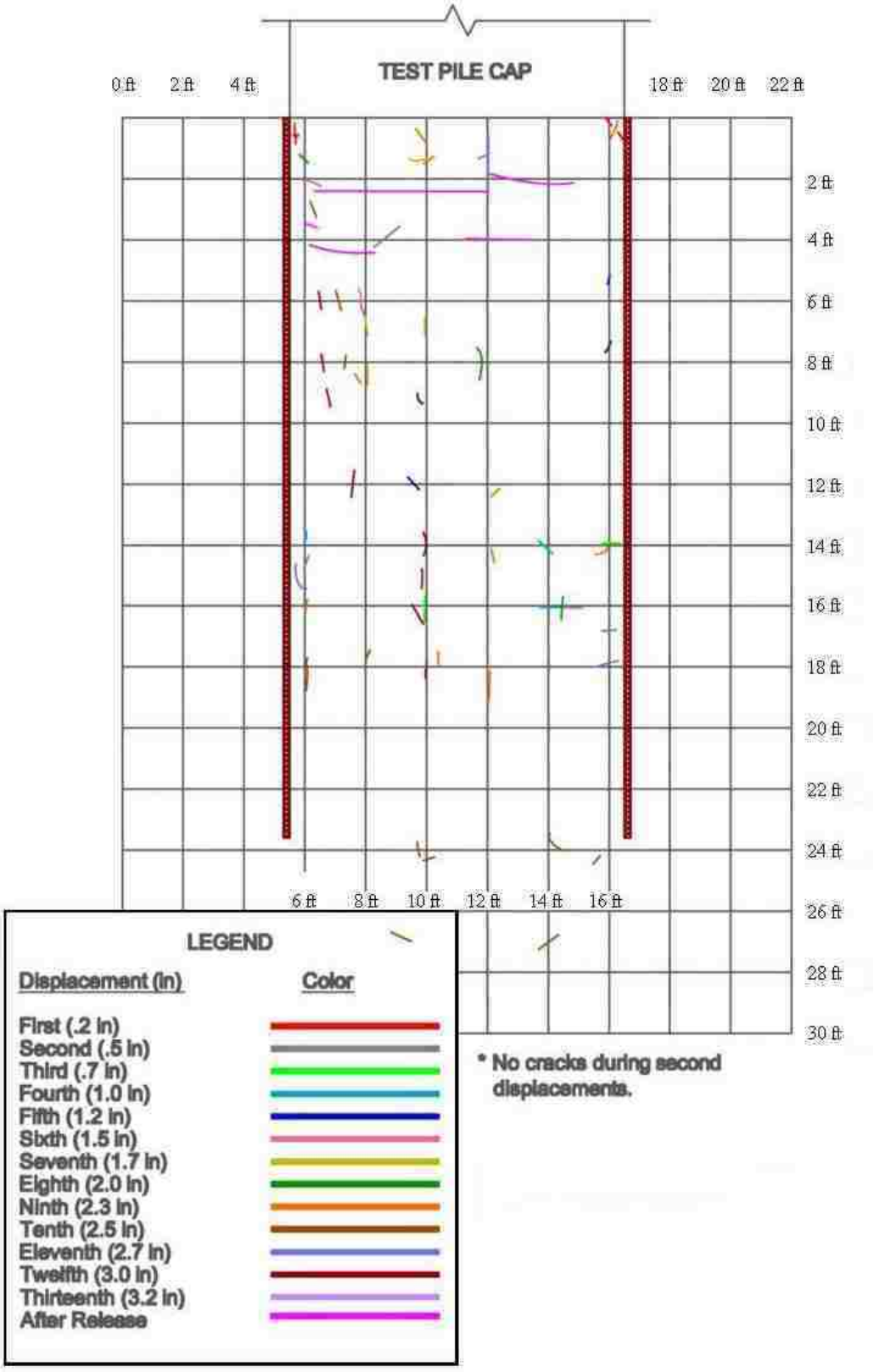

Figure 9-26: Crack map for plane strain test (repeat of Figure 6-12).

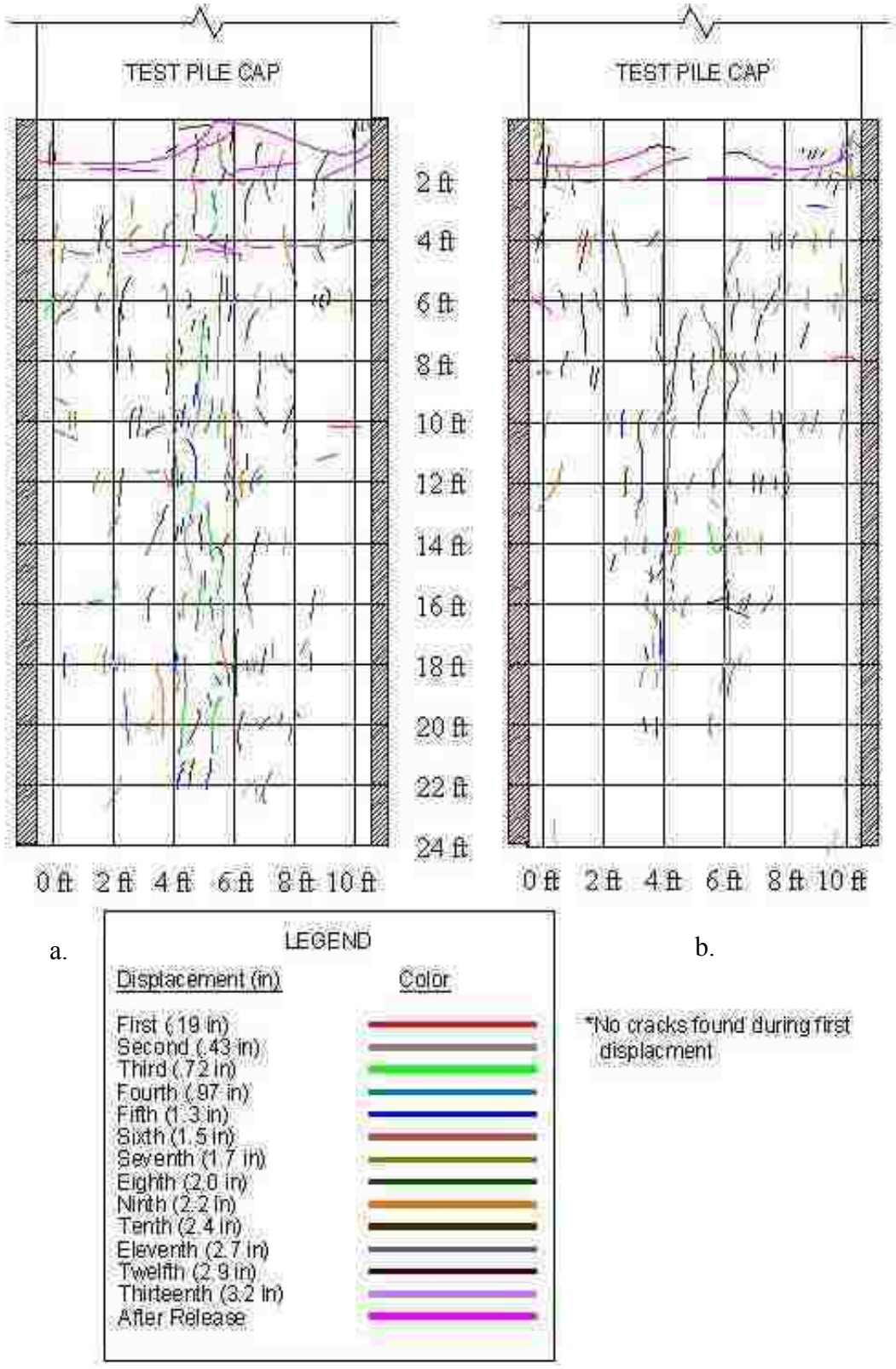

Figure 9-27: Crack map for a.) MSE wingwall test 2 (repeat of Figure 8-16) and b.) MSE wingwall test 1 (repeat of Figure 7-15).

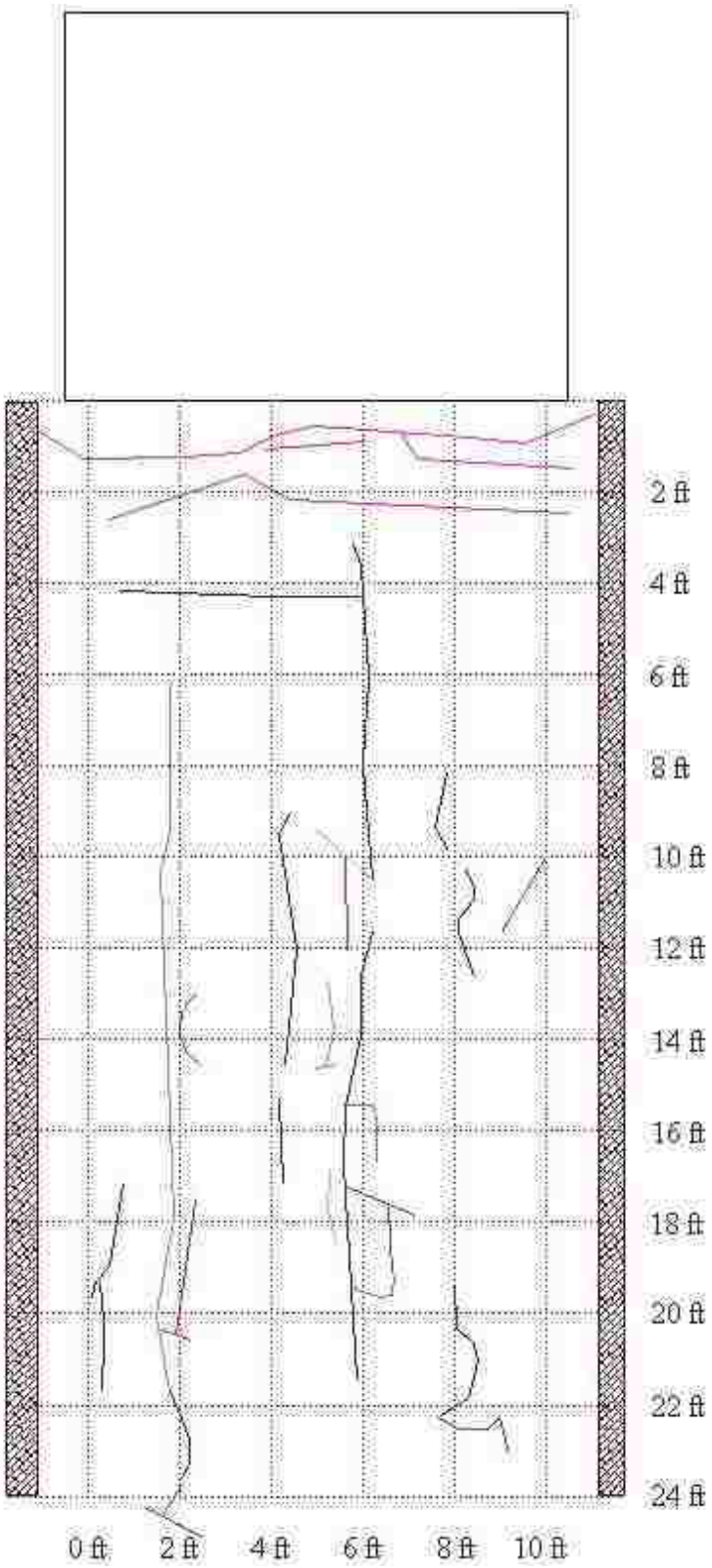

Figure 9-28: Crack map for MSE wingwall test (Rollins and Heiner, 2010).

Figure 9-29 through Figure 9-47 are plots of the force along the length of the mats for selected displacement increments, obtained from the strain gauges for both our tests. In these figures, a distance of zero is at the face of the wall, and 66 is the end of the mat. Each point in the lines represents the location of a set of strain gauges placed at that location on the bar mat. To obtain the force, the strain from a set of strain gauges (located at the same distance from the panel face, on the top and bottom of the longitudinal bar) was averaged, and multiplied as shown in Equation 7-2.

The value shown in Equation 7-2 is the force developed in the mats due to testing. The mats are also carrying an initial load from construction. During construction, the computers were hooked to the strain gauges and were gathering data. The values of these forces were computed using Equation 7-2 and plotted against the design load. Based on this comparison, an equation was developed to represent the force in the mats due to construction. This was done to "fill in" the gaps created by strain gauges that didn't work.

As can be seen from the figures, the measured force in the mats develops to values greater than the design pullout force. This could be due to conservatism in the design equations, assumptions made concerning how uniformly force develops in the mats, and errors due to the strain gauges. The values nearer to the wall face (2 inches to 9 inches) have a greater tendency to show unreasonable values. This is likely due to either bending effects near the wall face, or damage to strain gauges. Strain gauges in this area are exposed to greater risk of damage due to construction. To make comparison from push increment to push increment easier, the same scale is maintained for each level of mat.

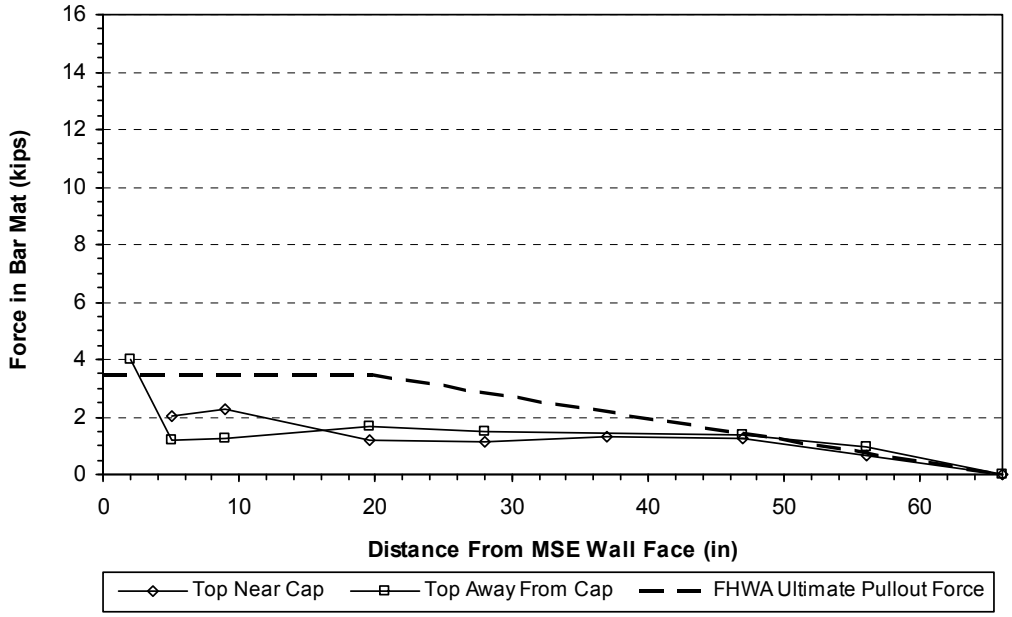

Figure 9-29: Force in top mats, 0.5 inch pile cap displacement, MSE test 1 (repeat of Figure 7-16).

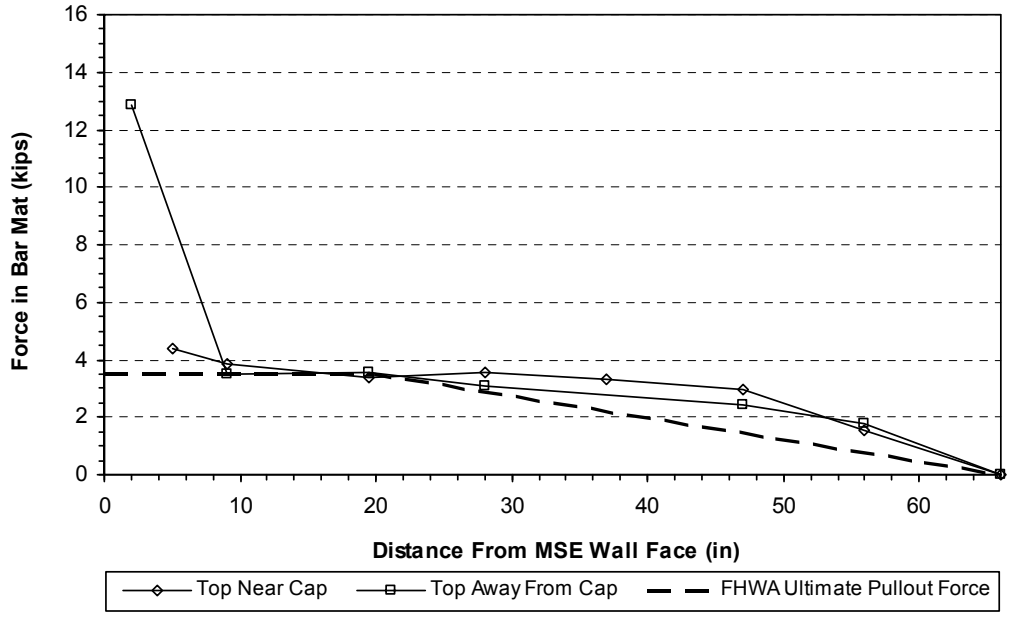

Figure 9-30: Force in top mats, 1.0 inch pile cap displacement, MSE test 1 (repeat of Figure 7-17).

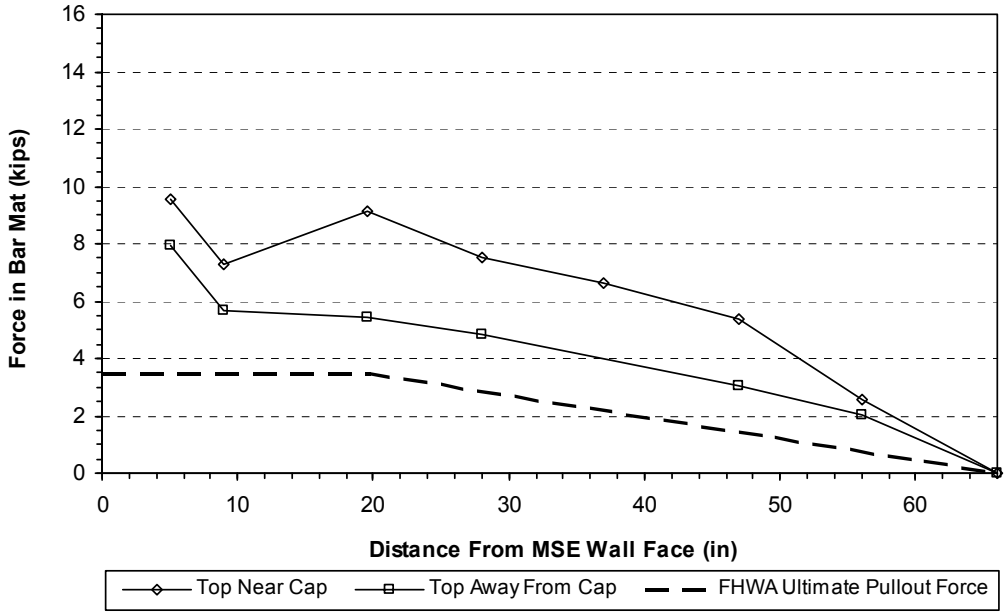

Figure 9-31: Force in top mats, 2.0 inch pile cap displacement, MSE test 1 (repeat of Figure 7-18).

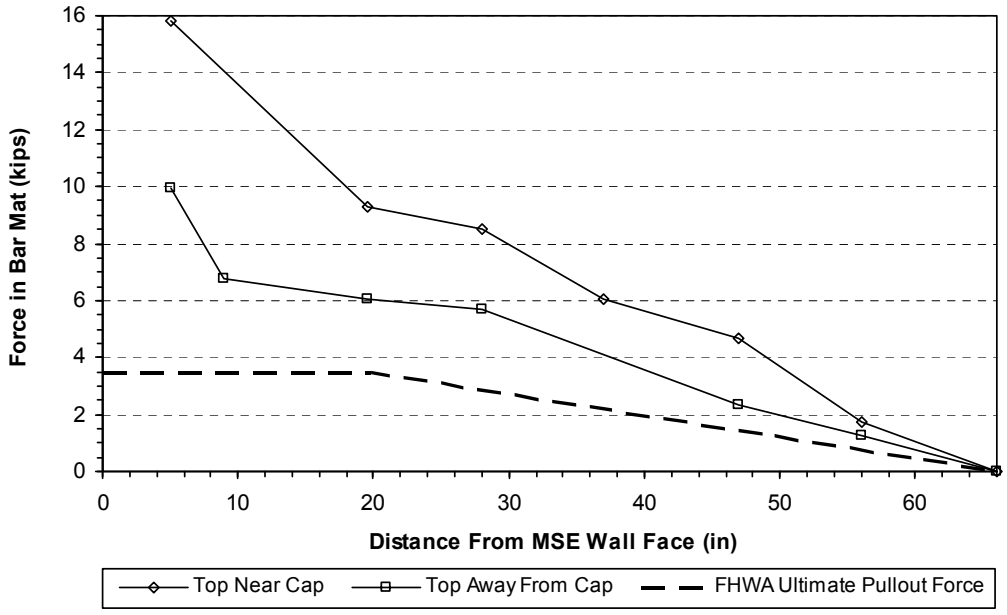

Figure 9-32: Force in top mats, 3.0 inch pile cap displacement, MSE test 1 (repeat of Figure 7-19).

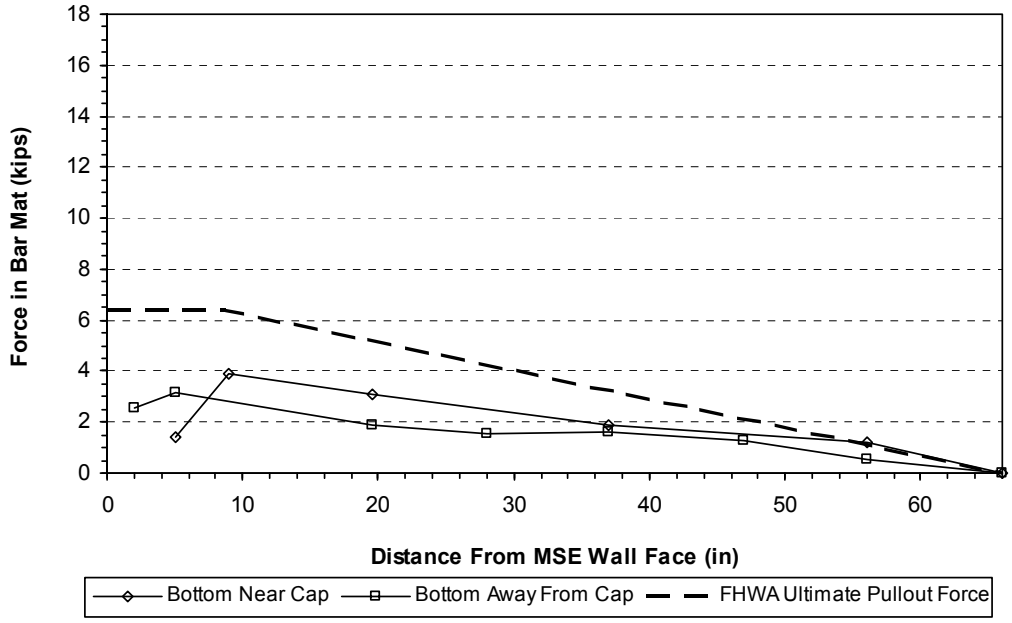

Figure 9-33: Force in bottom mats, 0.5 inch pile cap displacement, MSE test 1 (repeat of Figure 7-20).

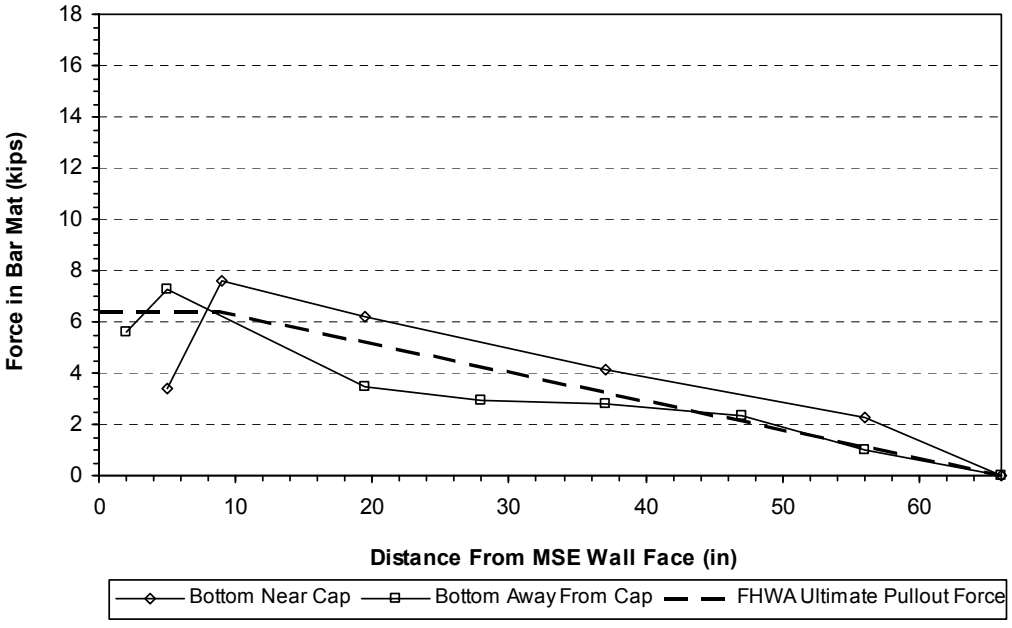

Figure 9-34: Force in bottom mats, 1.0 inch cap displacement, MSE test 1 (repeat of Figure 7-21).

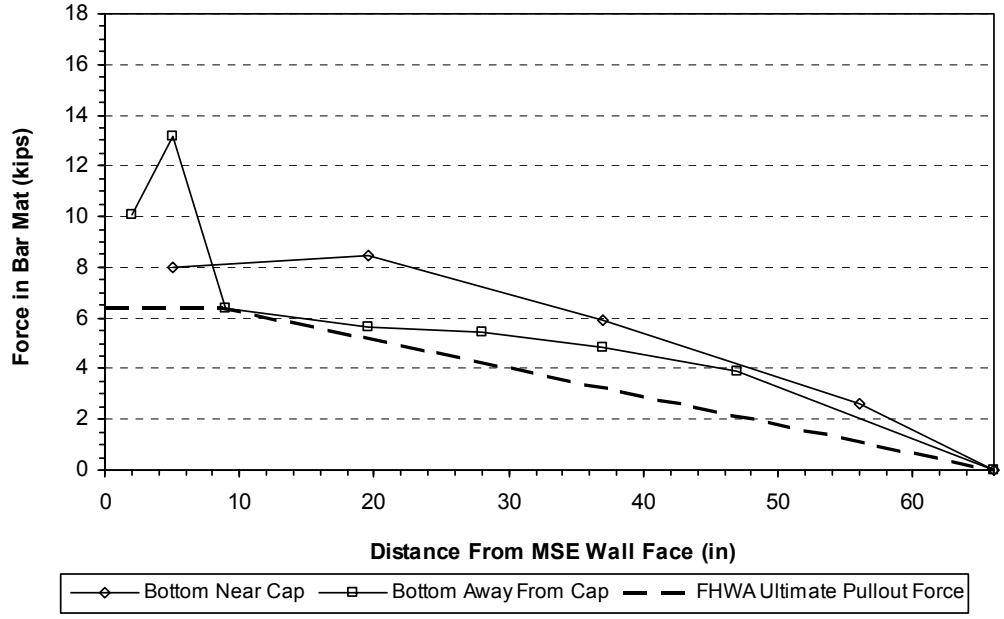

Figure 9-35: Force in bottom mats, 2.0 inch cap displacement, MSE test 1 (repeat of Figure 7-22).

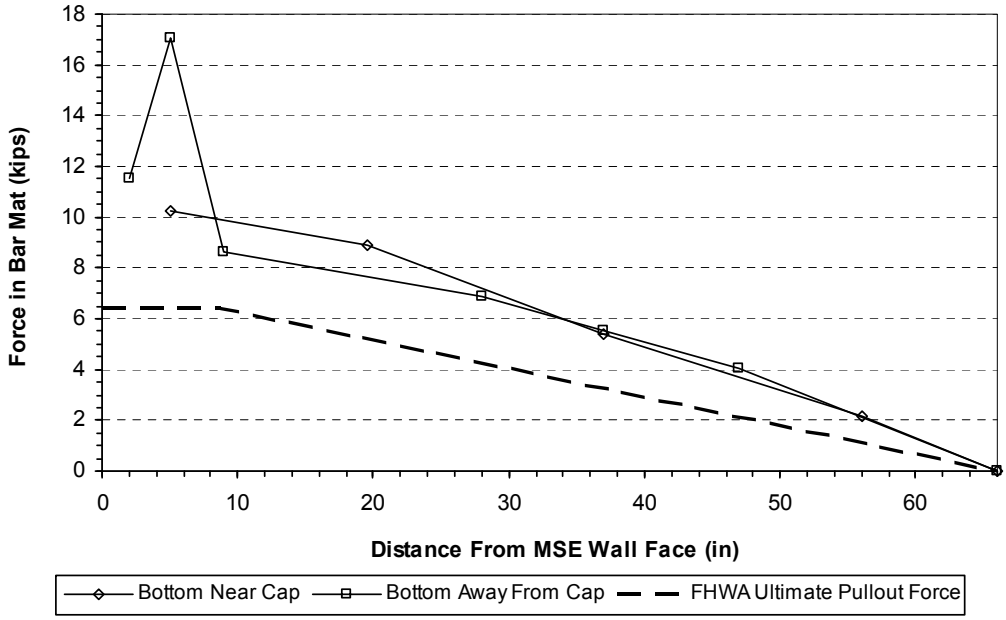

Figure 9-36: Force in bottom mats, 3.0 inch cap displacement, MSE test 1 (repeat of Figure 7-23).

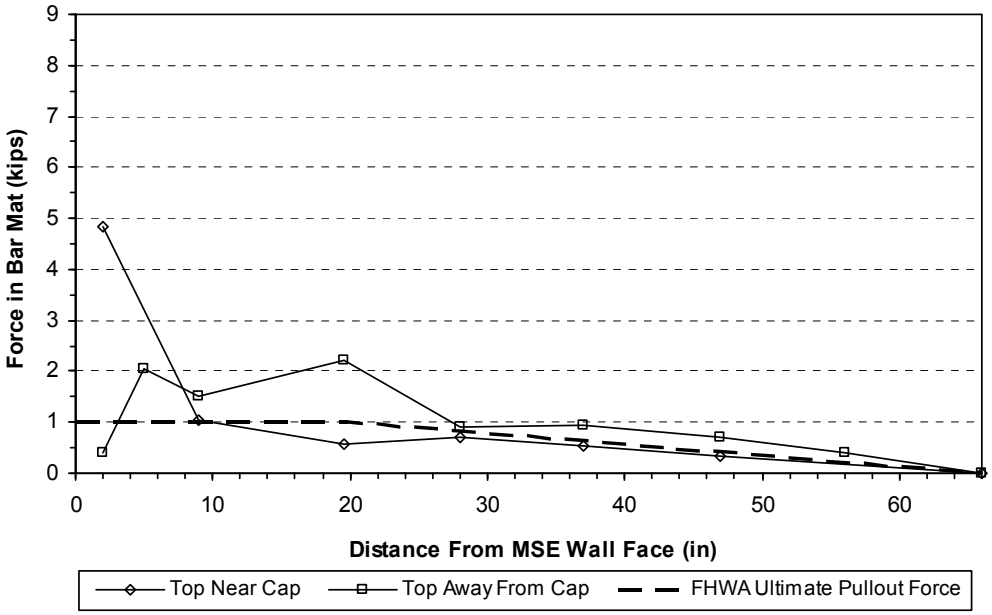

Figure 9-37: Force in top mats, 0.5 inch pile cap displacement, MSE test 2 (repeat of Figure 8-17).

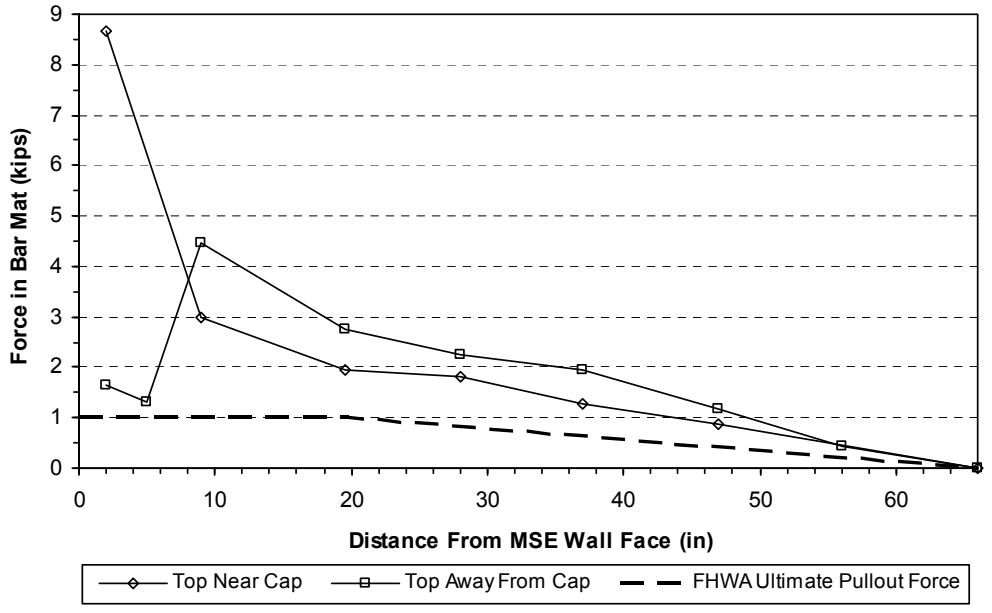

Figure 9-38: Force in top mats, 2.0 inch pile cap displacement, MSE test 2 (repeat of Figure 8-18).

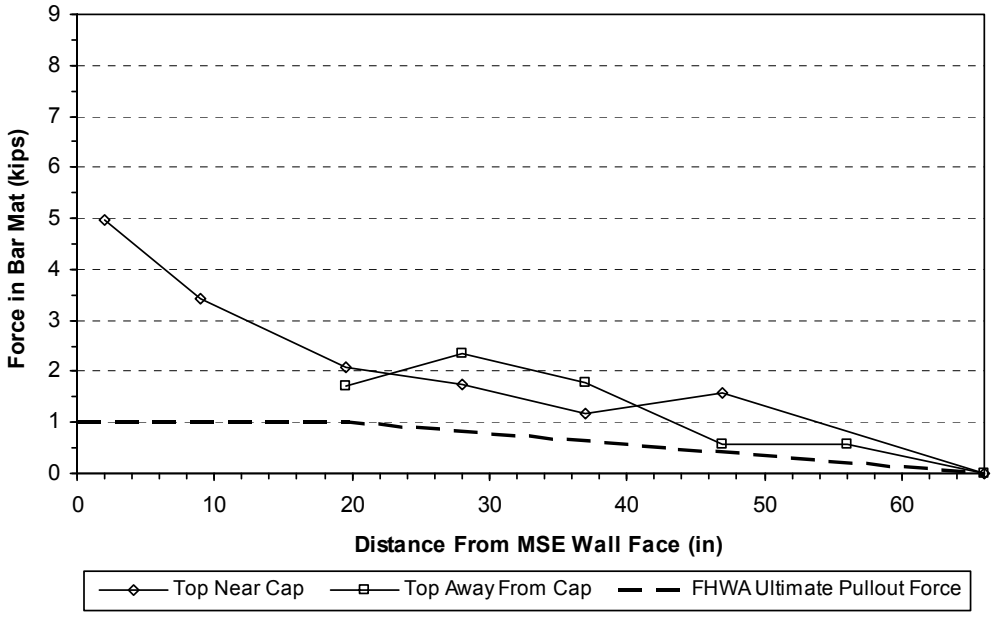

Figure 9-39: Force in top mats, 3.0 inch pile cap displacement, MSE test 2 (repeat of Figure 8-19).

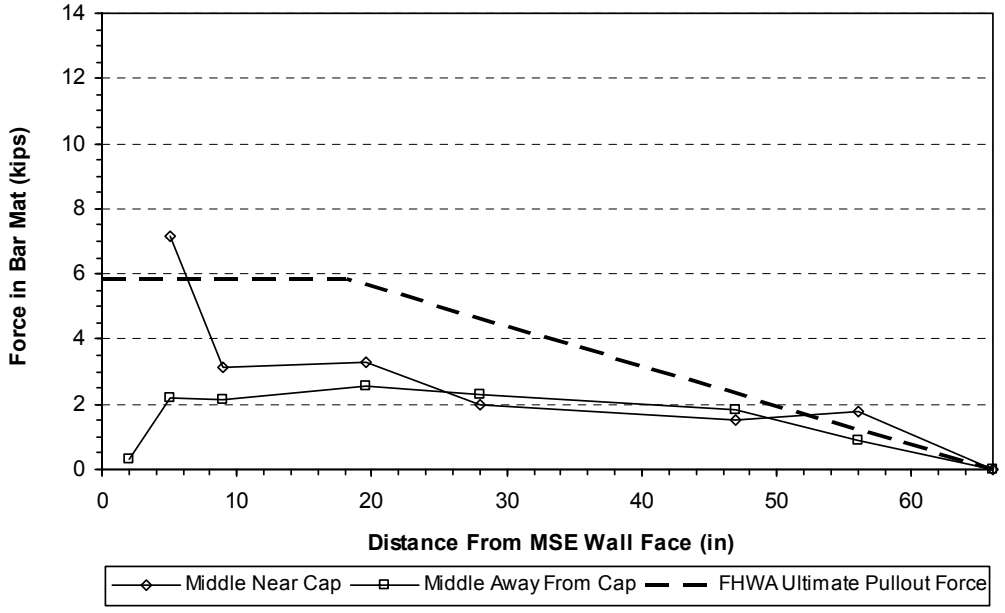

Figure 9-40: Force in middle mats, 0.5 inch pile cap displacement, MSE test 2 (repeat of Figure 8-20).

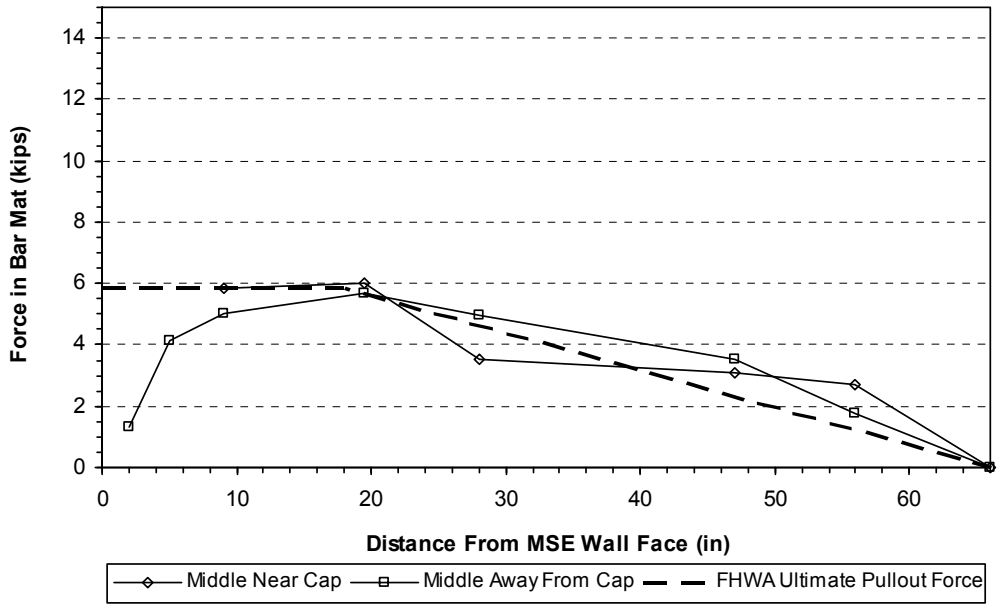

Figure 9-41: Force in middle mats, 1.25 inch pile cap displacement, MSE test 2 (repeat of Figure 8-21).

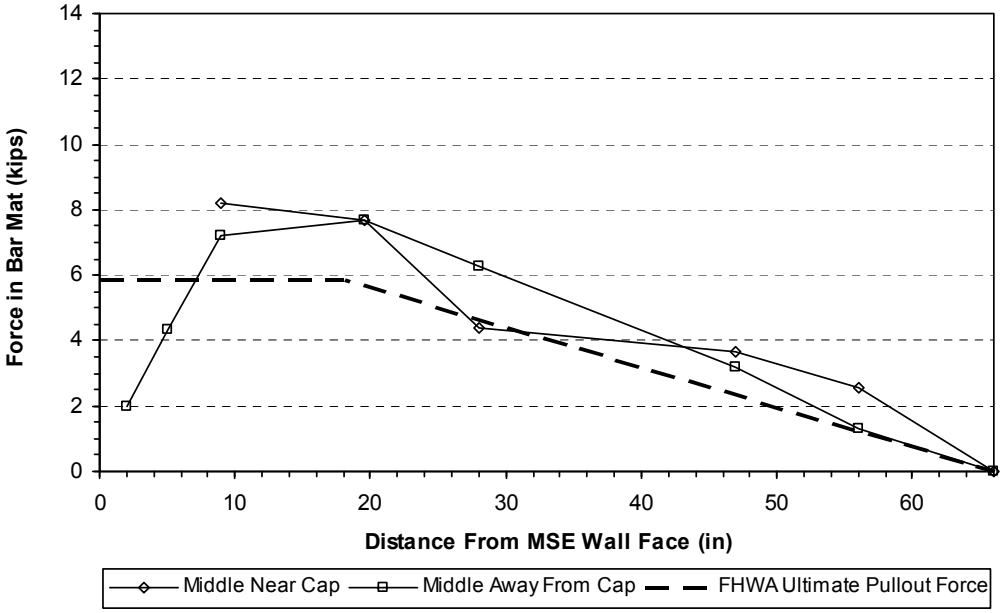

Figure 9-42: Force in middle mats, 2.0 inch pile cap displacement, MSE test 2 (repeat of Figure 8-22).

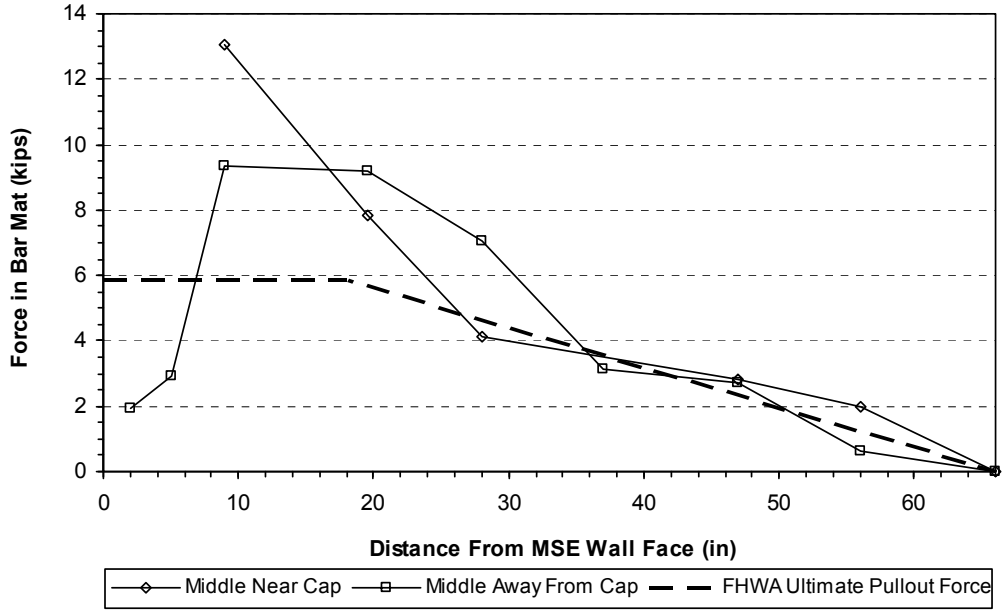

Figure 9-43: Force in middle mats, 3.0 inch pile cap displacement, MSE test 2 (repeat of Figure 8-23).

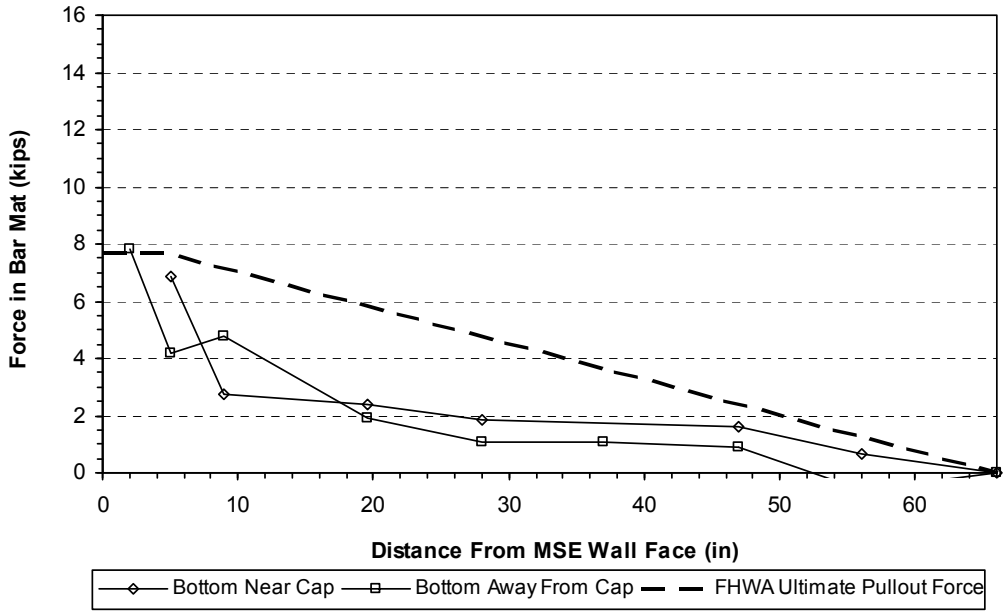

Figure 9-44: Force in bottom mats, 0.5 inch pile cap displacement, MSE test 2 (repeat of Figure 8-24).

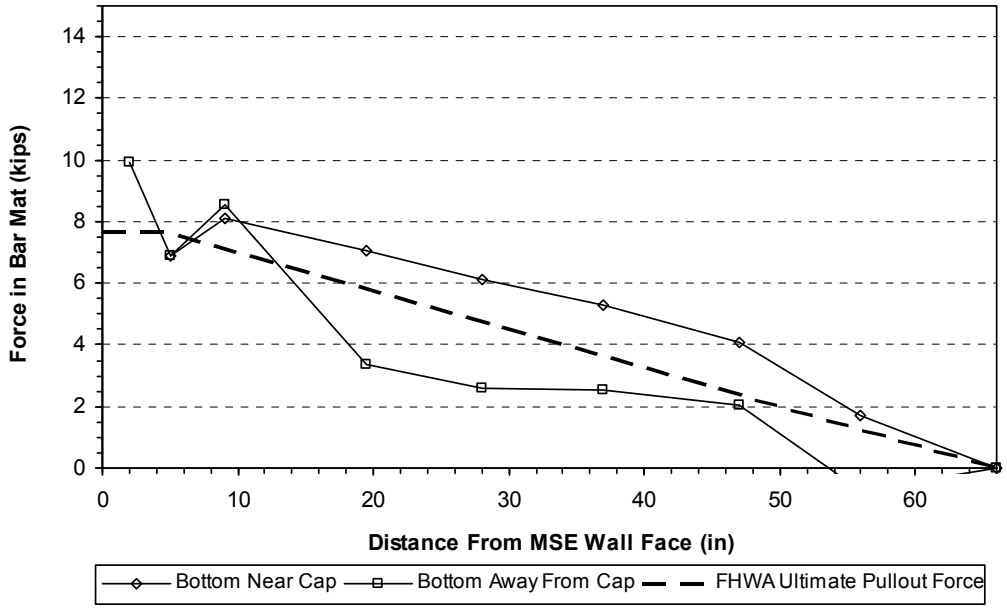

Figure 9-45: Force in bottom mats, 1.5 inch pile cap displacement, MSE test 2 (repeat of Figure 8-25).

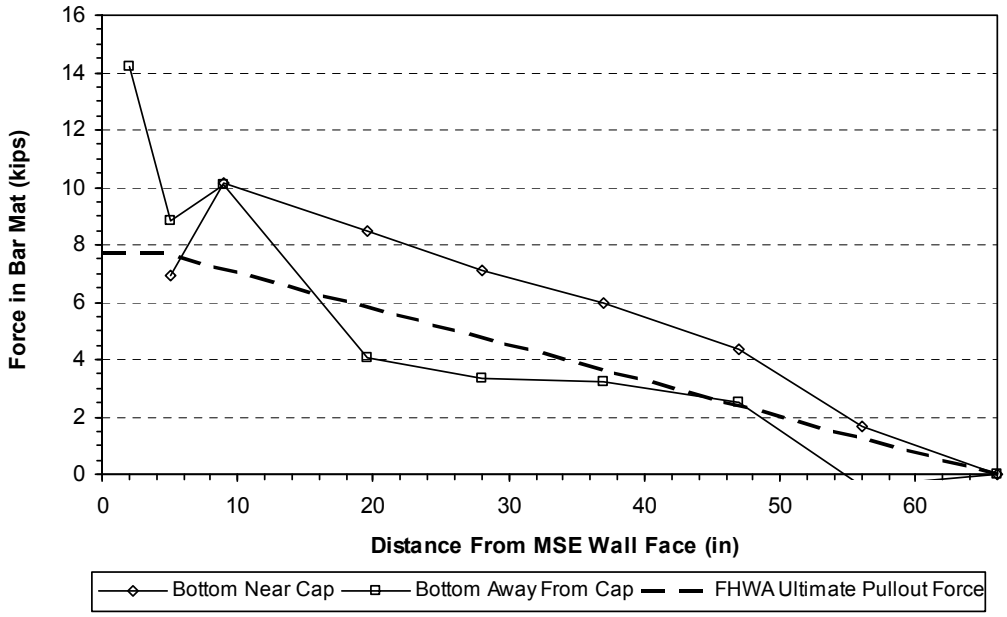

Figure 9-46: Force in bottom mats, 2.0 inch pile cap displacement, MSE test 2 (repeat of Figure 8-26).

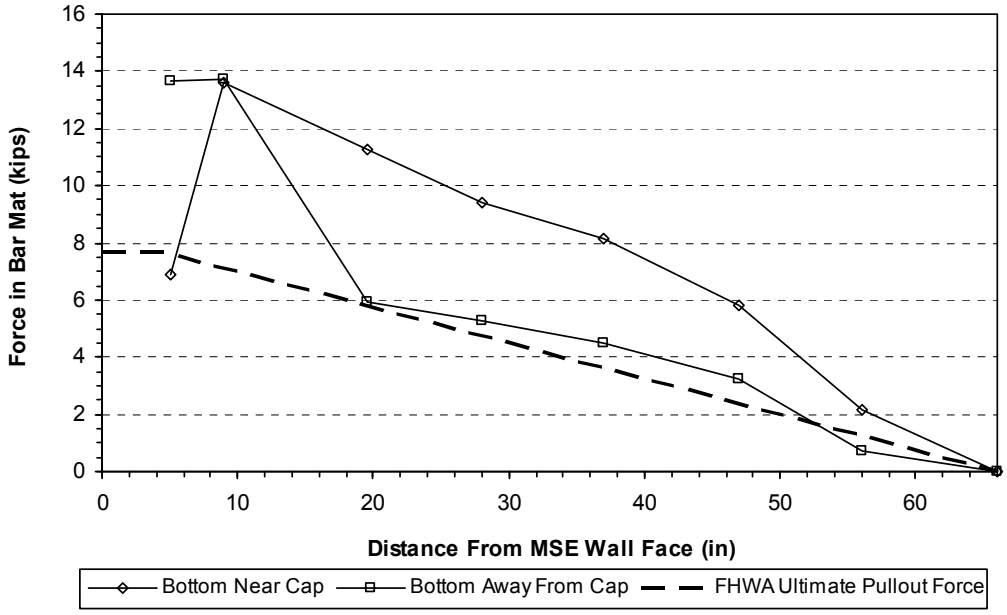

Figure 9-47: Force in bottom mats, 3.0 inch pile cap displacement, MSE test 2 (repeat of Figure 8-27).

Figure 9-29 through Figure 9-47 show that the force in the bar mats develops roughly parallel to the design pullout line. The flat portion of this line is the predicted total capacity of the mat according to the Federal Highway Administration (FHWA) guidelines (NHI, 2001). The flat portion of the line extends from the face of the wall to a distance equal to the distance to the resistant zone for each mats respective location. From this point, the line slopes down to a force value of zero at a distance equal to the length of the mat.

Figure 9-48 through Figure 9-53 show the force developed in the mats in the MSE test reported by Rollins and Heiner (2010). The concept in calculating the force from the strain gauges in the Rollins and Heiner study is similar to that in this study, however, strain gauges were placed on only one side of the bars. Thus, it was impossible to average the strain from the top and the bottom of the bar to cancel bending effects. This is apparent from the figures, as in most cases the force experiences extreme values near the face of the wall panel. Despite this, the

forces seem remarkably close to the expected values further along the bar mats. This is likely because bending effects are diminished further from the face of the wall panel.

From the force obtained in the mats from each of our tests, a pressure on the wall panel was derived by dividing by the area as shown in Equation 7-3. The boundary for the tributary area of each bar mat was taken as the midpoint between the center points of adjacent bar mats. The force was obtained by averaging the reasonable force values from the strain gauges that were within the flat-line portion of the design pullout line. The pressure on the pile cap was assumed to develop linearly from zero at the ground surface to a maximum value at the bottom of the pile cap. The pressure at the bottom of the pile cap was calculated based on the passive force and the pile cap area as shown in Equation 7-4. The pressure on the face of the pile cap at the depth of each of the bar mats was determined from linear interpolation.

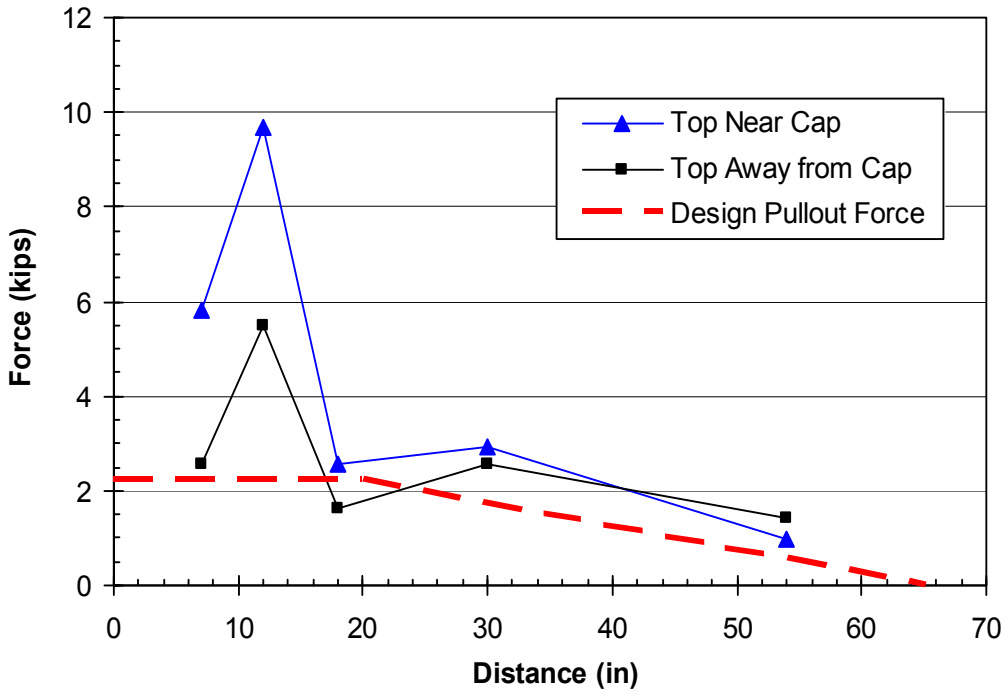

Figure 9-48: Force in top mats, 0.61 inch pile cap displacement, Luke Heiner's MSE test.

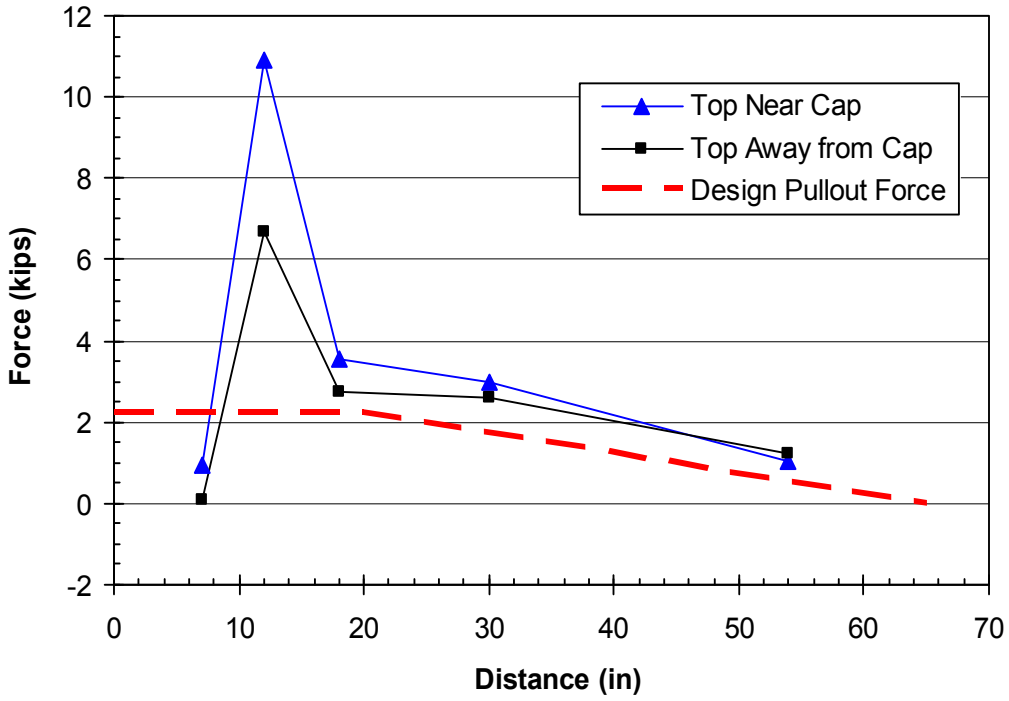

Figure 9-49: Force in top mats, 1.99 inch pile cap displacement, Luke Heiner's MSE test.

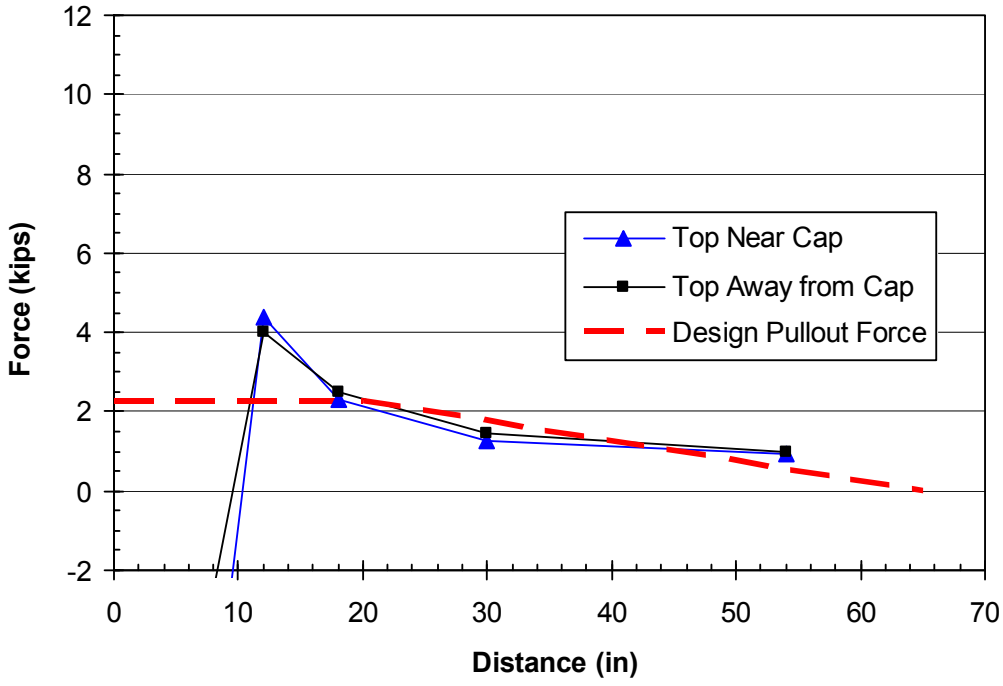

Figure 9-50: Force in top mats, 3.51 inch pile cap displacement, Luke Heiner's MSE test.

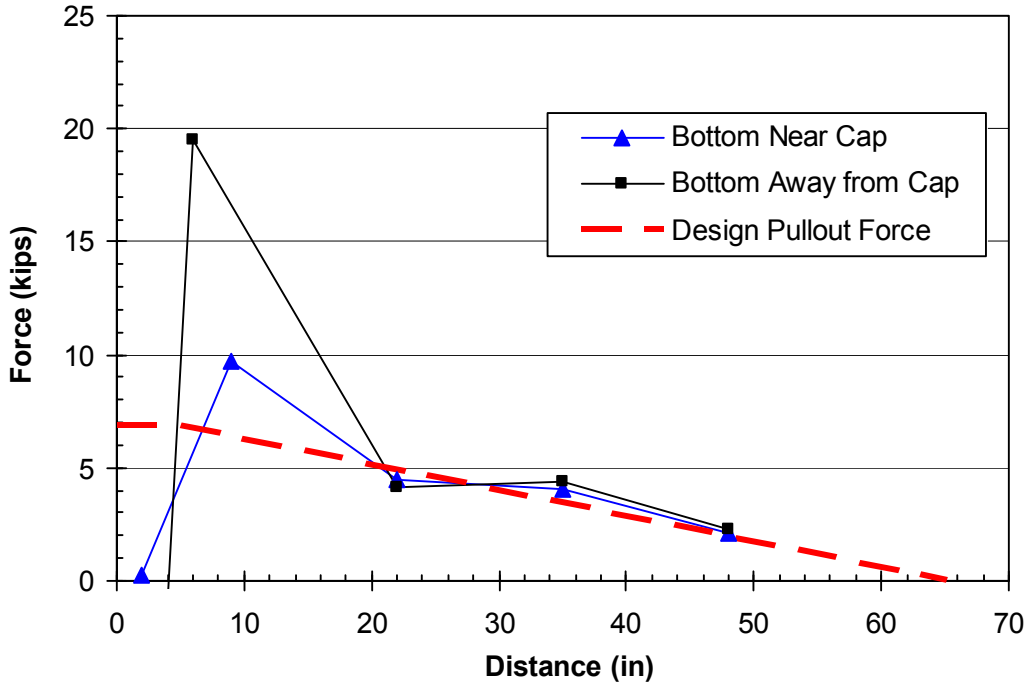

Figure 9-51: Force in bottom mats, 0.61 inch pile cap displacement, Luke Heiner's MSE test.

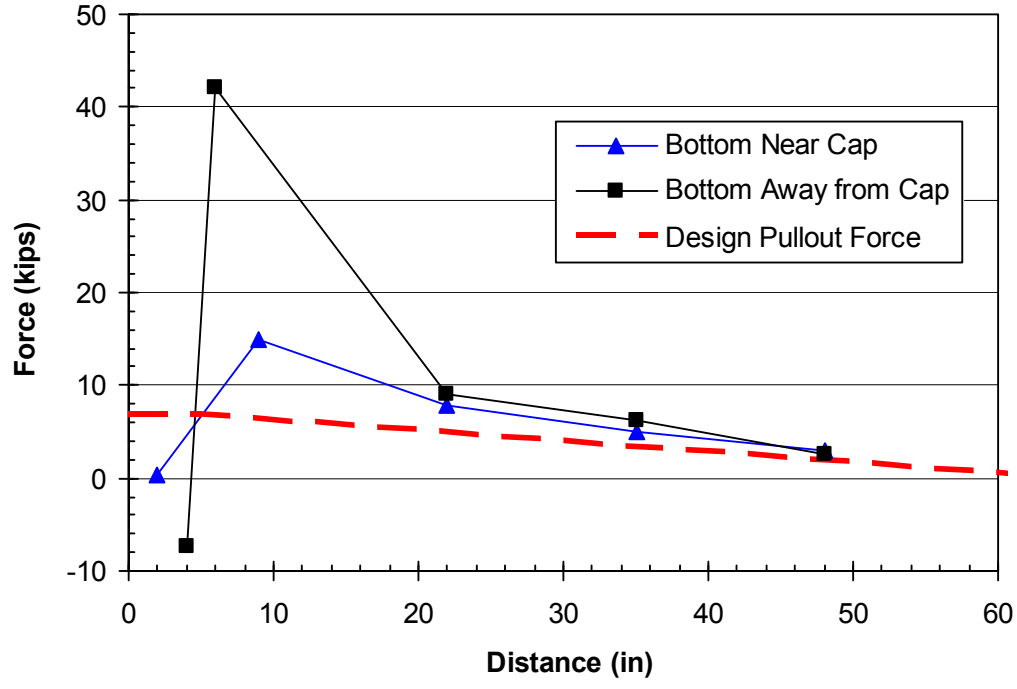

Figure 9-52: Force in bottom mats, 1.99 inch pile cap displacement, Luke Heiner's MSE test.

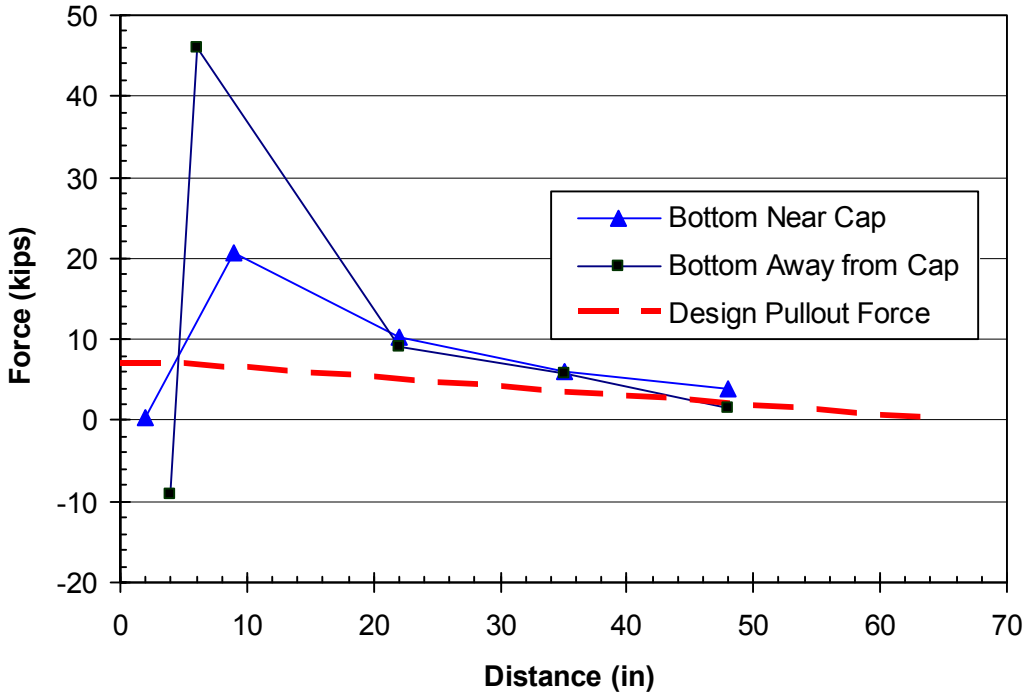

Figure 9-53: Force in bottom mats, 3.51 inch pile cap displacement, Luke Heiner's MSE test.

The ratio of the induced pressure on the wall panels to the pressure on the face of the pile cap at the depth of the bar mats was then computed for each displacement increment. These ratios are plotted as a function of distance from the pile cap face, and are shown for each bar mat in Figure 9-54. The induced pressure ratio typically ranges from 0.17 to 0.04 and generally decreases with distance from the pile cap as shown in Figure 9-54. A best-fit line defining the induced pressure ratio, Δp_r, as a function of distance from the pile cap face, x, is given by the equation

$$\Delta p_r = -0.0045x + 0.1029 \qquad (9\text{-}2)$$

This trendline is also shown in Figure 9-54 in comparison with the data. The R^2 of 0.1565 indicates a relatively poor correlation coefficient relative to distance.

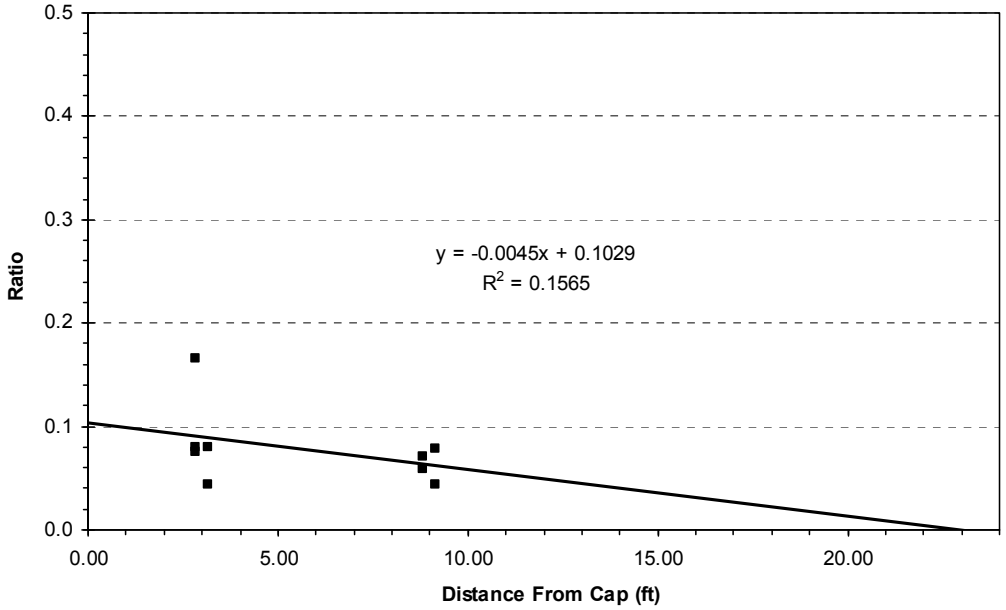

Figure 9-54: Ratio of induced MSE wall pressure to pile cap passive pressure versus distance from pile cap face.

Figure 9-55 shows the induced pressure to passive pressure relationship after excluding data points where pull-out has limited the induced force, as discussed in Section 7.7. Omitting these values doesn't change the R^2 value by much, and the line is essentially the same.

In the absence of additional data, Equation 9-2 can be used to estimate the average induced stresses on an MSE wingwall produced by passive force development on the abutment wall. These pressures can then be used to design the MSE wall to prevent bar mat pullout and excessive wingwall deflection. A more conservative estimate of the induced pressure could be obtained by using the mean plus one standard deviation equation. This is shown in Figure 9-56, where the trendline is fit to one standard deviation above the data points.

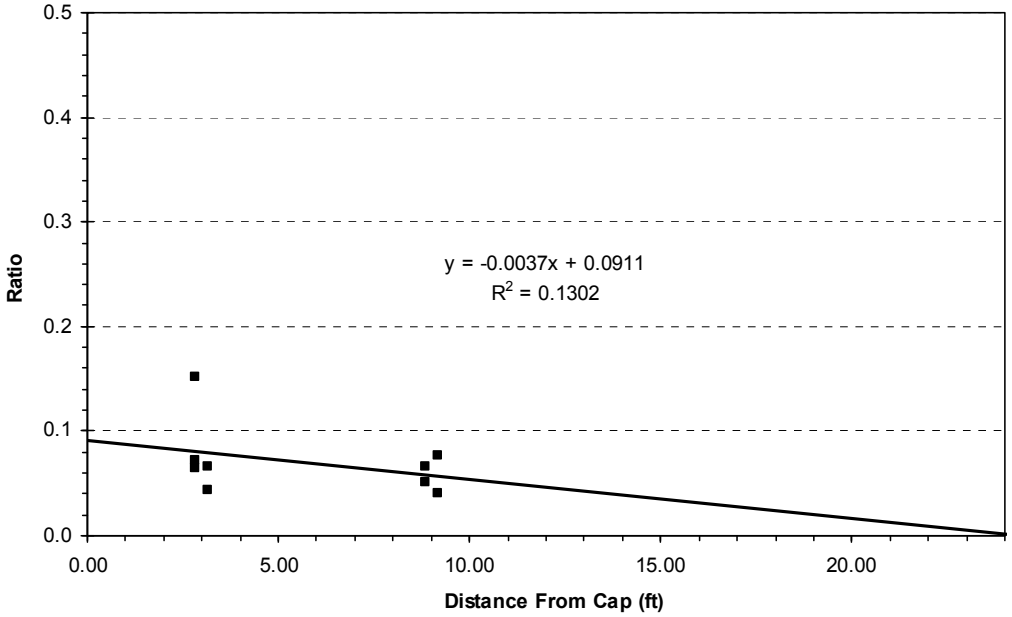

Figure 9-55: Ratio of induced MSE wall pressure to pile cap passive pressure versus distance from the pile cap face after omitting data points after MSE pull-out.

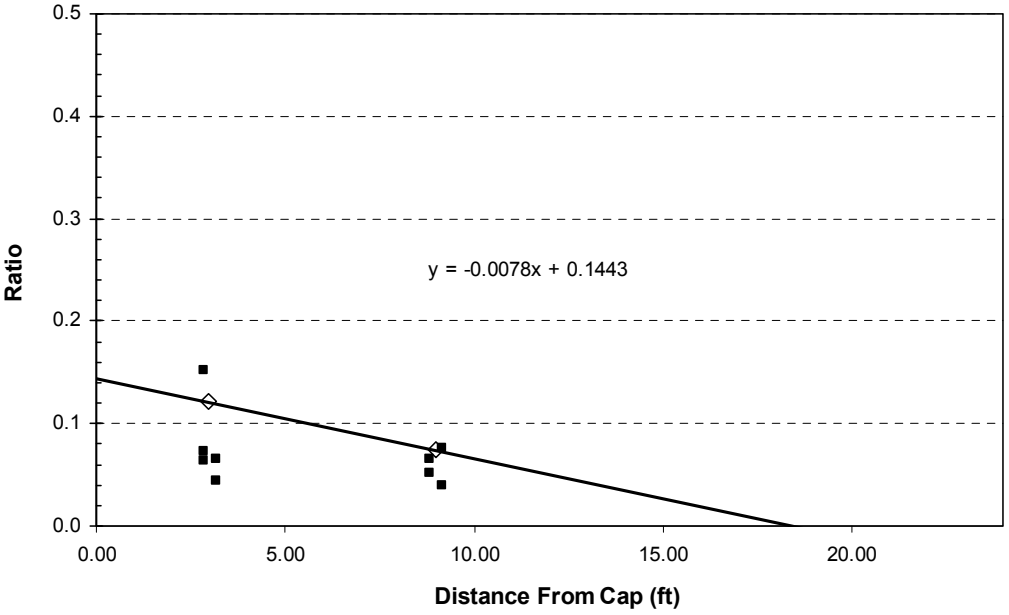

Figure 9-56: Ratio of induced MSE wall pressure to pile cap passive pressure versus distance from the pile cap face after omitting data points after MSE pull-out, plus one standard deviation.

Using the maximum force that develops in each mat, the anchorage factor can be calculated according to the equation

$$A_c = \frac{F * S_t}{\gamma * d * b * L_e * z} \tag{9-3}$$

where F = the measured force that developed in the mat
S_t = spacing of transverse bars
γ = unit weight of the soil
d = transverse bar diameter
b = bar mat width
L_e = bar mat effective length
z = depth of bar mat below fill

Equation 9.3 comes from Mitchell and Villet (1987), on page 248. The anchorage factor for each of the instrumented bar mats for MSE test 1 and 2 is shown in Figure 9-57. Figure 9-58 shows the same data at a different scale to separate the data. For comparison, data from Mitchell and Villet (1987) is shown in Figure 9-59.

It should be observed that the data from MSE test 1 and 2 fall within the data presented by Mitchell and Villet. Due to the break in scale in this data, it isn't possible to determine whether the data scattered at anchorage factors greater than 60 fall within the data presented by Mitchell and Villet.

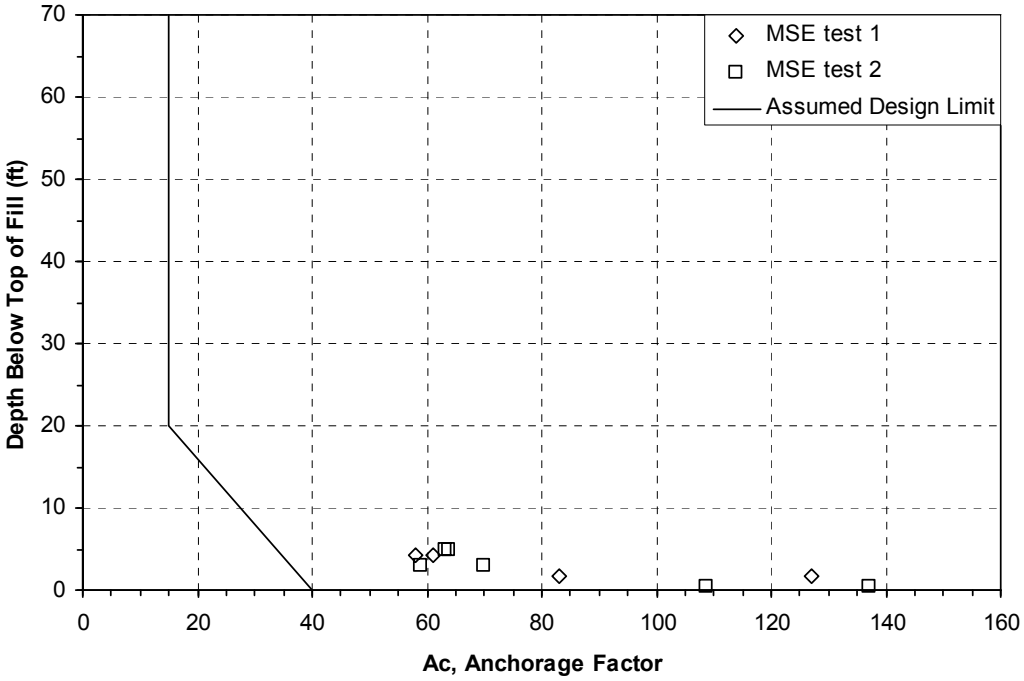

Figure 9-57: Anchorage factor versus depth for MSE test 1 and MSE test 2.

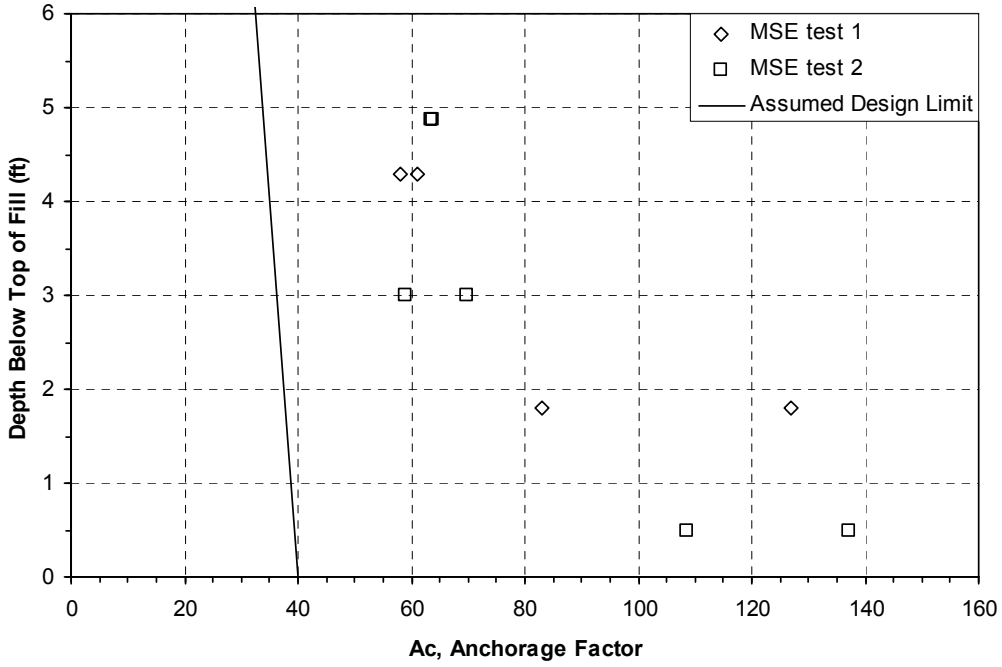

Figure 9-58: Anchorage factor versus depth for MSE test 1 and MSE test 2.

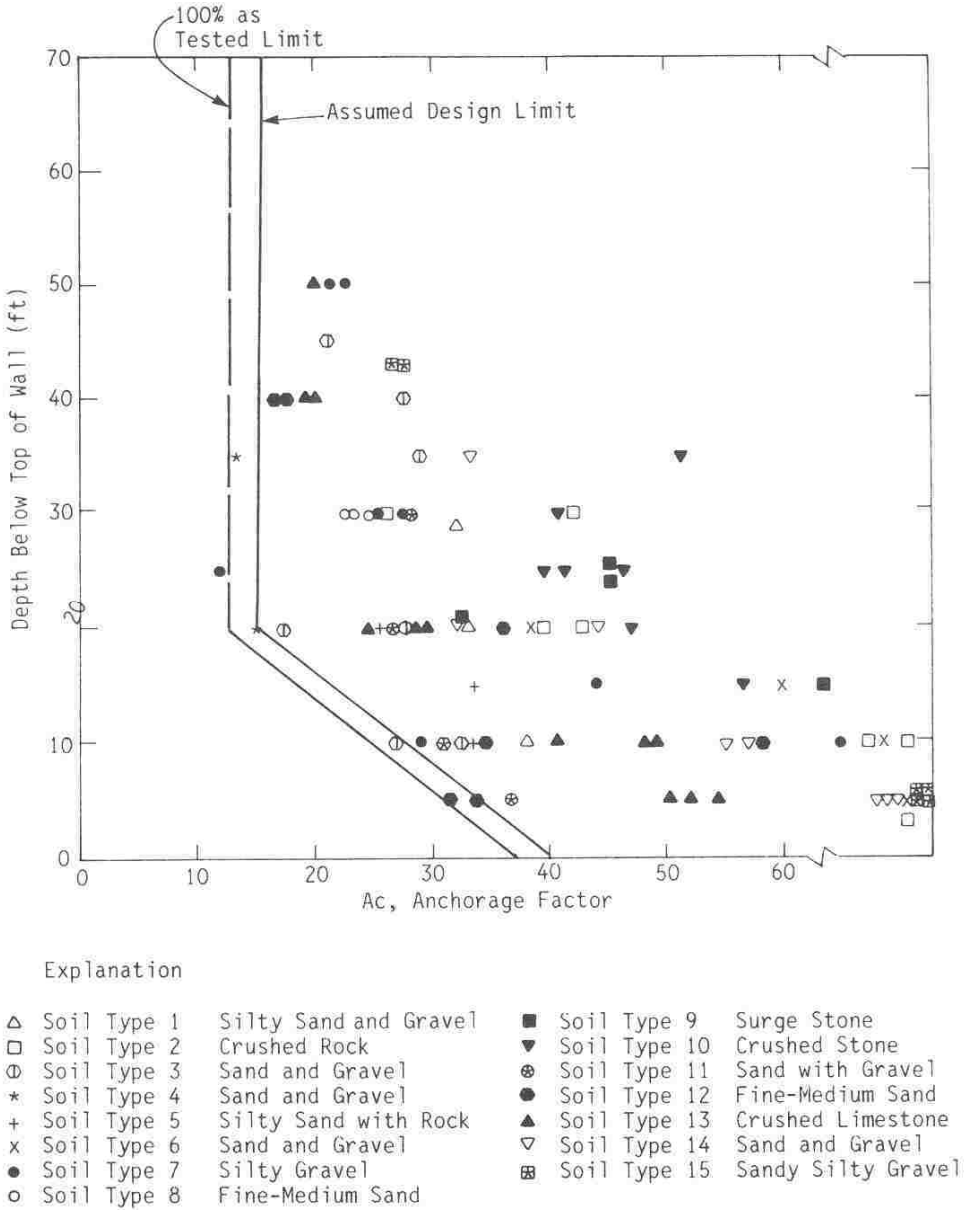

Figure 9-59: Anchorage factor versus depth, Mitchell and Villet (1987).

10 Computer Analysis

This chapter will compare the results from the field tests to common methods for predicting the ultimate passive force as wells as the passive force-displacement curve in use today. These methods include the classical Rankine, Coulomb, and Log-Spiral approaches as well as the empirical design method developed by Caltrans to predict the ultimate force. The force-displacement curves were computed using the computer programs ABUT, and PYCAP which use the Log-Spiral approach to compute passive force along with the Caltrans design procedure and a comparison to the AASHTO LRFD bridge design approach.

10.1 Analyses Using PYCAP Computer Model

The load-displacement curves have also been compared to results predicted using PYCAP, a spreadsheet analysis program developed by Duncan and Mokwa (2001). PYCAP computes the ultimate passive force using the log-spiral approach based on moment equilibrium. The program then develops a hyperbolic load-displacement curve using the ultimate passive force and the initial stiffness as fitting parameters. Figure 10-1 compares the computed curves from PYCAP with the measured curves from the unconfined backfill or 3D backfill test, while Figure 10-2 shows the same curves for the plane strain or 2D test. The input parameters used for each of these comparisons are shown in Table 10-1. For the 3D test, the computed passive resistance for the 2D case was multiplied by the Brinch-Hansen 3D correction factor. However,

for the plane strain (2D) test and MSE wall tests, no 3D adjustment factors were necessary in computing the passive force-displacement curves.

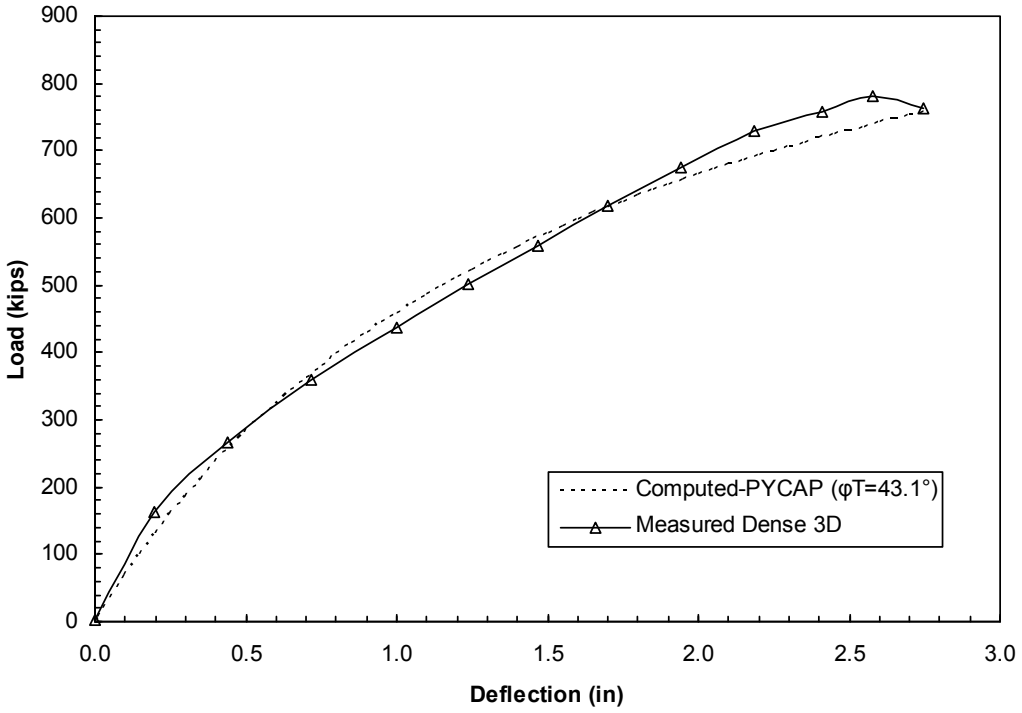

Figure 10-1: Comparison of load-displacement curve computed by PYCAP with measured curve for unconfined backfill test.

Table 10-1: PYCAP Input Values

Test	Unconfined Backfill	Plane Strain, φ_T=43.1°	Plane Strain, φ_{PS}=48.3°
Cohesion (psf)	60	60	60
Soil Friction Angle	43.1°	43.1°	48.3°
δ/φ	0.72	0.72	0.72
Initial Soil Modulus (kip/ft^2)	450	680	680
Poisson's Ratio	0.23	0.23	0.23
Soil Moist Unit Weight (lb/ft^3)	129.5	129.3	129.3
Δ_{max}/H	0.042	0.049	0.049
φ / Triaxial Friction Angle	1.00	1.00	1.12

As can be seen in Figure 10-1, a friction angle slightly higher than the measured triaxial friction angle (φ=43.1°) is needed to obtain good agreement with the load-displacement curve for the unconfined backfill test. However, use of this same friction angle leads to significant underprediction of the ultimate passive force for the plane strain test. In this case the computed force is about 42% lower than the measured ultimate force as shown in Figure 10-2. To obtain reasonable agreement with the measured plane strain (2D) test results using PYCAP, it is necessary to use a plane strain friction angle. As discussed in Section 2.3, the plane strain friction angle (φ=48.3°) was estimated by increasing the triaxial friction angle by 12%. When the plane strain friction angle is used, the agreement between the measured and computed load-displacement curves is very good as shown in Figure 10-2. These results highlight the importance of using the plane strain friction angle when the geometry constrains the soil to fail in plane strain.

A soil modulus 34% lower than the initial soil modulus for the plane strain is necessary to match the load-displacement curve for the unconfined backfill case relative to the plane strain backfill case. It is possible that greater movement is necessary to develop the full three-dimensional failure surface than the plane strain failure surface. The initial soil moduli used for the unconfined tests are at the lower end of the range recommended by Duncan and Mokwa (2001).

Figure 10-3 shows the measured load-displacement curve for MSE test 1, along with three load-displacement curves computed using PYCAP. One curve was computed using the triaxial friction angle (43.1°), one was computed using the plane strain friction angle (48.3°) calibrated from the 2D test, and the third was computed with back-calculated friction angle of 47.2° which produced the best agreement with the measured curve.

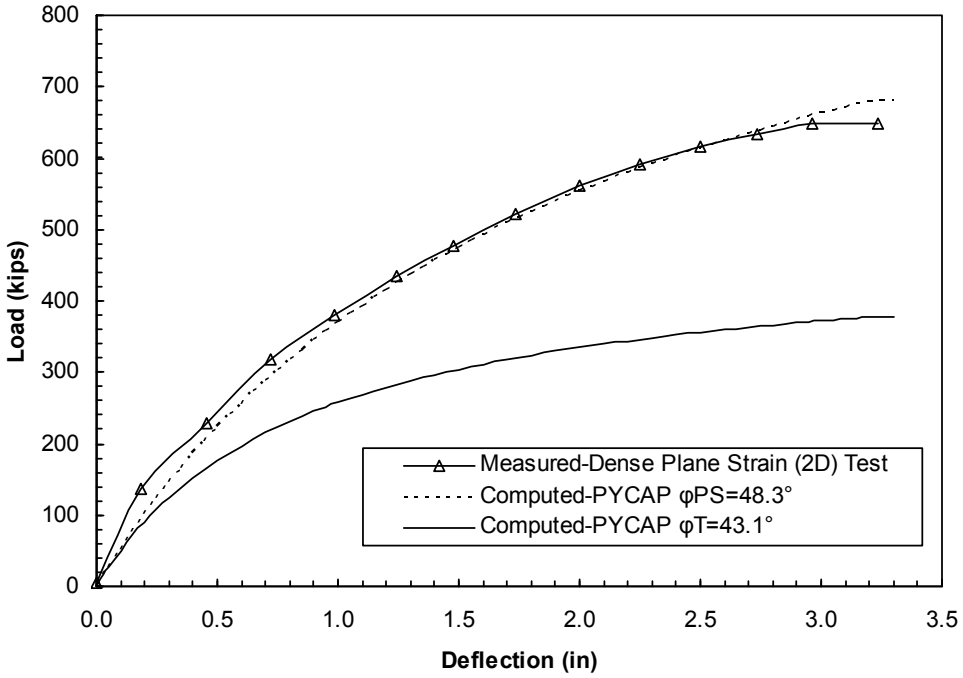

Figure 10-2: Comparison of load-displacement curve computed by PYCAP with measured load-displacement curve for plane strain test.

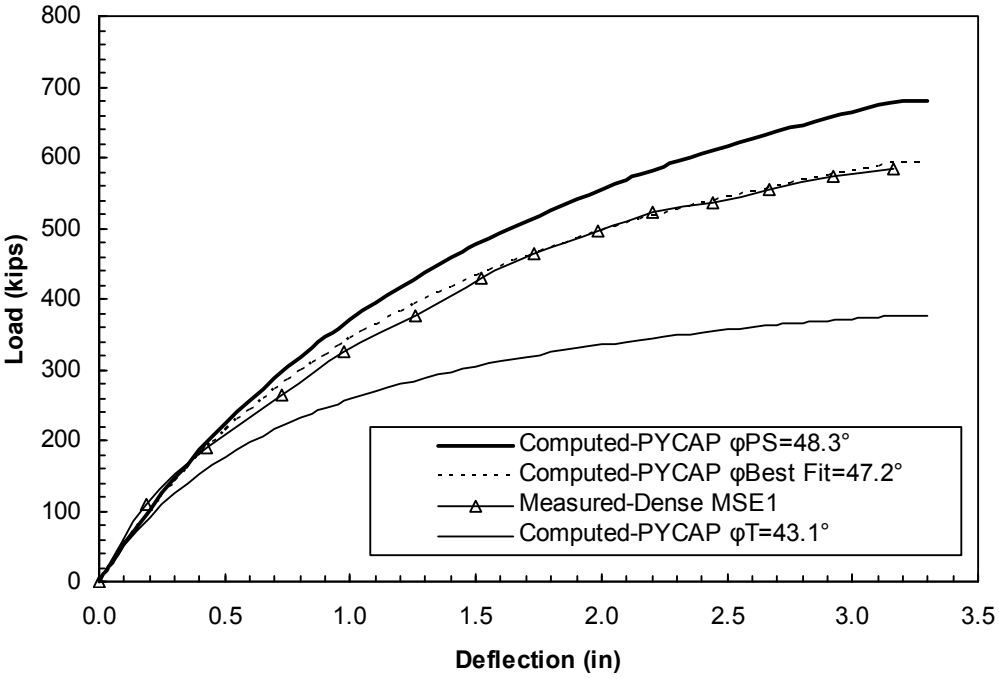

Figure 10-3: Comparison of PYCAP to measured results, MSE test 1.

Figure 10-4 shows similar computed and measured curves for MSE test 2. For this test, the best fit was obtained with a friction angle of 46.3°. For both of these tests, the curve computed with the triaxial friction angle is considerably softer than the measured load-displacement curve (29-36% lower), while the measured load-displacement curve is slightly softer (16-28% lower) than the curve obtained with the plane strain friction angle. The best fit friction angles may be slightly lower than the plane strain friction angle because the MSE walls translate outward during the load testing as described previously. As a result, the failure geometry is no longer a true plane strain or 2D geometry, but becomes a little more 3D in orientation. Nevertheless, it should be recognized that the best-fit friction angles are still 1.095 and 1.074 times higher, respectively, than the triaxial friction angle which is within observed range of $\varphi_{ps}/\ \varphi_{triax}$ values (1.07 to 1.18) as discussed in Section 2.3. Therefore, the lower back-calculated friction angles may simply be variations resulting from differences in soil compaction or composition. The inputs for Figure 10-3 and Figure 10-4 are shown in Table 10-2 and Table 10-3, respectively.

Table 10-2: PYCAP Input Values for Figure 10-3, MSE Test 1

Test	Plane Strain	Triaxial	Best Fit
Cohesion (psf)	60	60	60
Soil Friction Angle	48.3°	43.1°	47.19°
δ/φ	0.72	0.72	0.72
Initial Soil Modulus (kip/ft^2)	680	680	680
Poisson's Ratio	0.23	0.23	0.23
Soil Moist Unit Weight (lb/ft^3)	128.7	128.7	128.7
Δ_{max}/H	0.048	0.048	0.048
φ / Triaxial Friction Angle	1.12	1.00	1.09

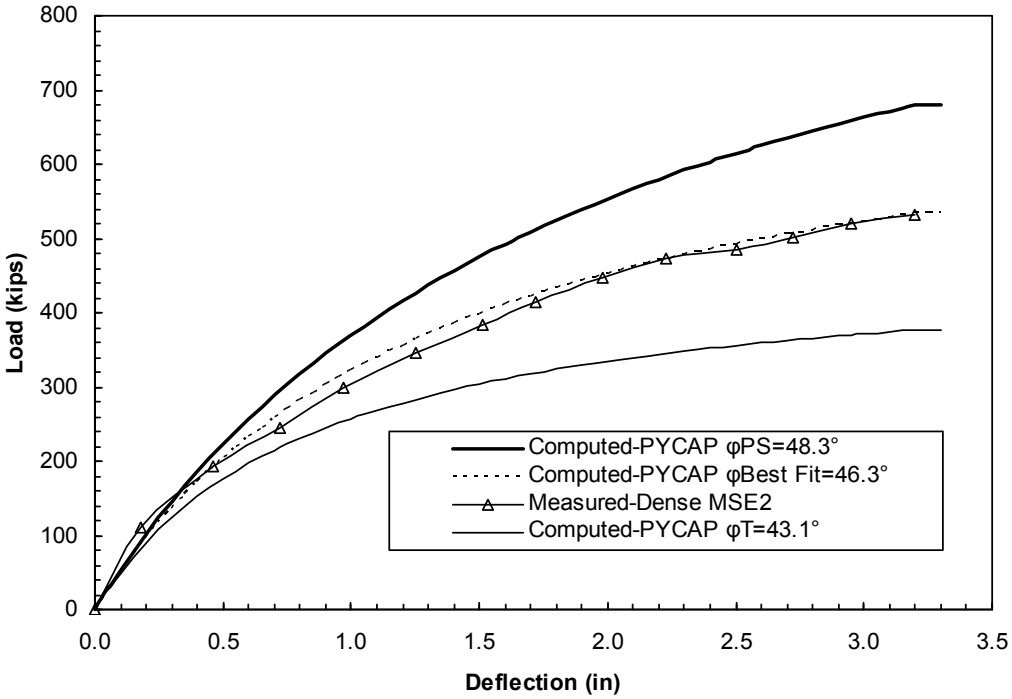

Figure 10-4: Comparison of PYCAP to measured results, MSE test 2.

Table 10-3: PYCAP Input Values for Figure 10-4, MSE Test 2

Test	Plane Strain	Triaxial	Best Fit
Cohesion (psf)	60	60	60
Soil Friction Angle	48.3°	43.1°	46.3°
δ/φ	0.72	0.72	0.72
Initial Soil Modulus (kip/ft^2)	680	680	680
Poisson's Ratio	0.23	0.23	0.23
Soil Moist Unit Weight (lb/ft^3)	128.82	128.82	128.82
Δ_{max}/H	0.048	0.048	0.048
φ / Triaxial Friction Angle	1.12	1.00	1.07

10.2 Caltrans Seismic Design Approach

The load-displacement curve from the unconfined backfill test is compared to the design load-displacement curve recommended by the Caltrans seismic design method (Caltrans, 2004) in Figure 10-5.

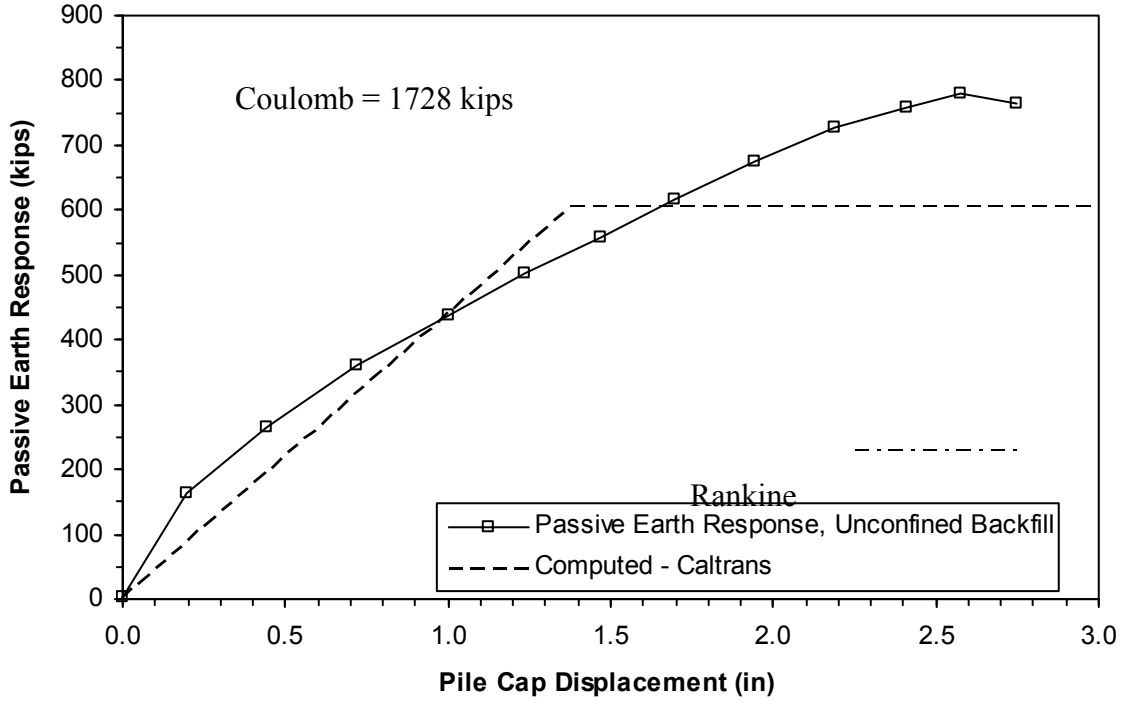

Figure 10-5: Comparison of load-displacement curve for 3D backfill to Caltrans seismic design method, Coulomb method, and Rankine method, 22 ft effective width, φ=43.1°.

The results are also compared with the Rankine and Coulomb methods of fully developed passive resistance in this figure. On average, the Caltrans method provides a somewhat reasonable representation of the measured curve during much of the development portion of the curve, but ultimately underestimates the passive resistance from the field tests by 22.5%. The Coulomb and Rankine values were computed using a friction angle of 43.1°, and a wall friction angle of 0.72 times the soil friction angle. The unit weight of soil used was 128.8 pcf, a rough

average of the moist unit weight of the soil backfill from all the tests. The friction angle used here is the triaxial friction angle. Assuming an effective pile cap width of 22 ft based on the Brinch-Hansen method, the Coulomb method overestimates the ultimate passive resistance by a factor of 2.2 while the Rankine method underestimates the measured resistance by a factor of 3.4.

Figure 10-6 shows the measured load-displacement curves for the plane strain and MSE wingwall tests along with the design curve based on the Caltrans method. The ultimate passive force was also computed using the Rankine and Coulomb methods using a plane strain friction angle (48.3°) and the actual width of the pile cap. The plane strain friction angle was obtained by increasing the triaxial friction angle of 43.1° by 12%, as explained in Section 2.3.

In this case, the Coulomb method over-predicts the passive force in the MSE tests by about 7.75-8.5 times, and the passive force in the Plane Strain test by about 7.0 times. The value predicted by the Rankine method underestimates the ultimate value of the MSE tests by about 3.6-4.0 times, and underestimates the value for the Plane Strain test by about 4.4 times. The Caltrans method underestimates the ultimate values of the MSE tests by about 1.76-1.94 times, and underestimates the value for the Plane Strain test by about 2.15 times. The best fit line is similar to the Caltrans methodology, but is adjusted to an increased slope and maximum value. The moist unit weight of soil in our tests was higher than the tests upon which the Caltrans curve is based. The best fit maximum is based on a soil pressure of 8 psf, and a slope of 26 kips/in/ft.

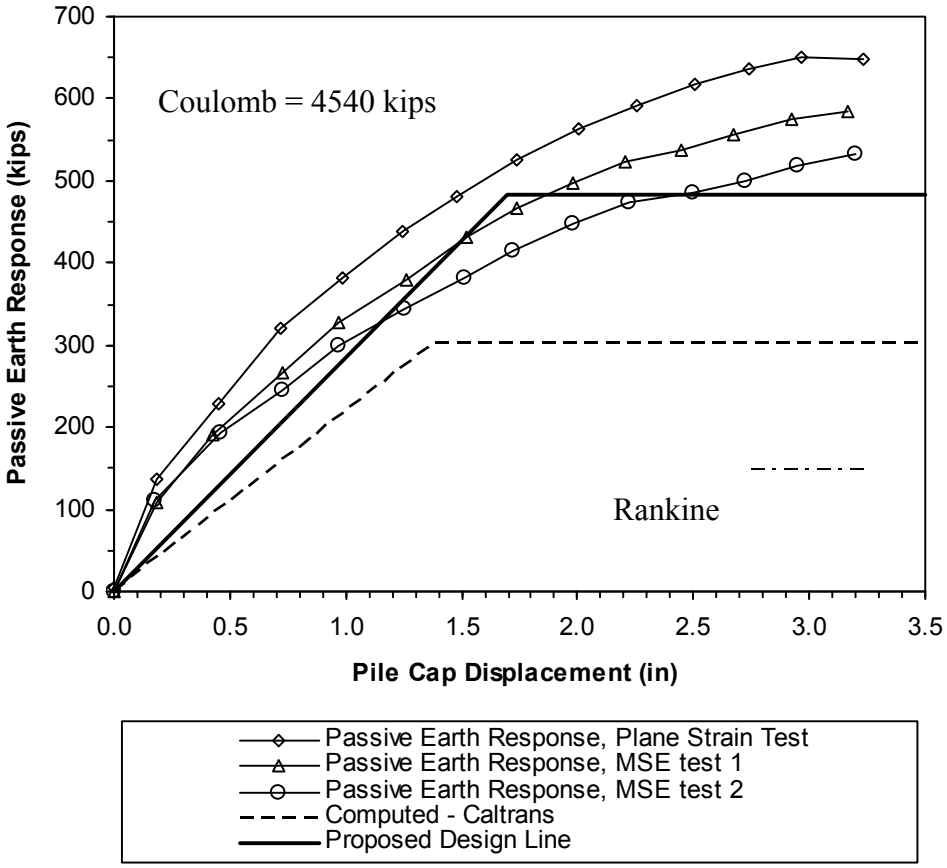

Figure 10-6: Comparison of load-displacement curves for MSE tests and Plane Strain test to Caltrans seismic design method, Coulomb method, and Rankine method, 11 ft effective width, φ=48.3°.

In addition to the possible extra resistance available in MSE reinforcements, consideration should also be given to whether the wall-reinforcement connection is adequately designed for the additional force that could develop beyond the FHWA ultimate design forces. As shown in Figure 9-29 through Figure 9-47 and mentioned in Section 9.1, these forces could be significant when dealing with full-scale walls and very large soil deformations. This study did not deal with larger deflections due to the limited deformations that could be applied by the actuators.

10.3 Comparison to AASTHO LRFD Bridge Design Specifications

A plot showing the normalized wall displacement versus passive force for the plane strain and MSE wall tests is shown in Figure 10-7. It can be seen that in these tests that more than the 1% of wall height recommended in Table C3.11.1-1 of AASHTO (2010) is needed to develop the ultimate passive resistance. The displacement as a percentage of wall height needed in these tests is closer to the 5% recommended in the commentary on page 3-105. The greater displacement needed in these tests could be a result of limited the width of the backfill.

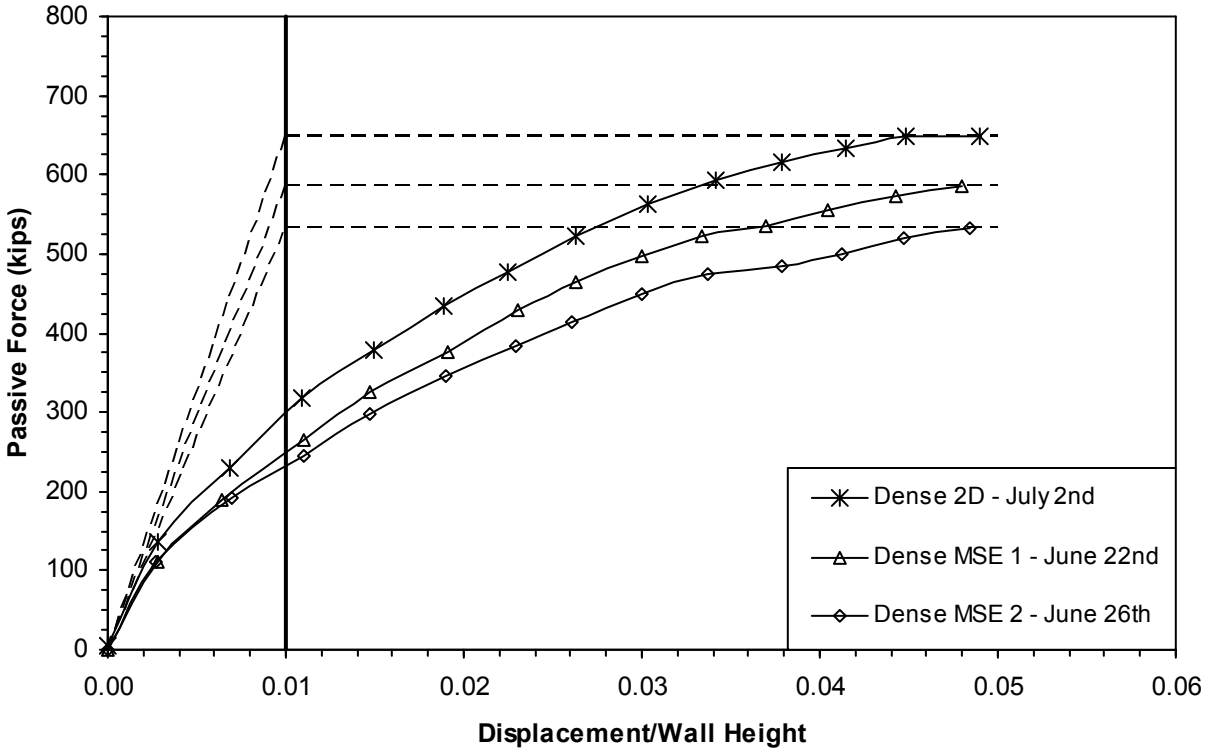

Figure 10-7: Normalized wall displacement, Δ/5.5 ft, versus passive force.

10.4 Analyses Using ABUT Computer Model

The measured results from all of the tests were also compared to results computed using the program ABUT which employs the method proposed by Shamsabadi et al (2007). The inputs for the unconfined and plane strain tests are shown in Table 10-4 and Table 10-5, respectively. In every instance in these tables, the failure ratio, R_f, is calculated to produce a final strain of 0.1. Both the presumptive values of ε_{50} and best fit values were used. The load-displacement curves obtained with best fit values for the unconfined test are shown in Figure 10-8 in comparison with the measured load-displacement curve. In general, the agreement is reasonably good.

Table 10-4: ABUT Input Values, Unconfined

	Unconfined	
	Best Fit Values	Presumptive Values
Internal Friction Angle, φ	42.1	43.5
Wall Friction Angle, δ	30.312	31.32
Cohesion (ksf)	0.06	0.06
Adhesion (ksf)	0.06	0.06
Soil Weight, γ (kcf)	0.1295	0.1295
ε_{50}	0.0055	0.0035
Failure Ratio, R_f	0.935	0.95
Poisson Ratio, ν	0.23	0.23
Surcharge	0	0
Wall Height, H (ft)	5.5	5.5
Wall Width, W (ft)	11.0	11.0

Table 10-5: ABUT Input Values, Plane Strain

	Plane Strain	
	Best Fit Values	Presumptive Values
Internal Friction Angle, φ	49.9	48.3
Wall Friction Angle, δ	35.928	34.776
Cohesion (ksf)	0.06	0.06
Adhesion (ksf)	0.06	0.06
Soil Weight, γ (kcf)	0.1293	0.1293
ε_{50}	0.007	0.0035
Failure Ratio, R_f	0.93	0.965
Poisson Ratio, ν	0.23	0.23
Surcharge	0	0
Wall Height, H (ft)	5.5	5.5
Wall Width, W (ft)	11.0	11.0

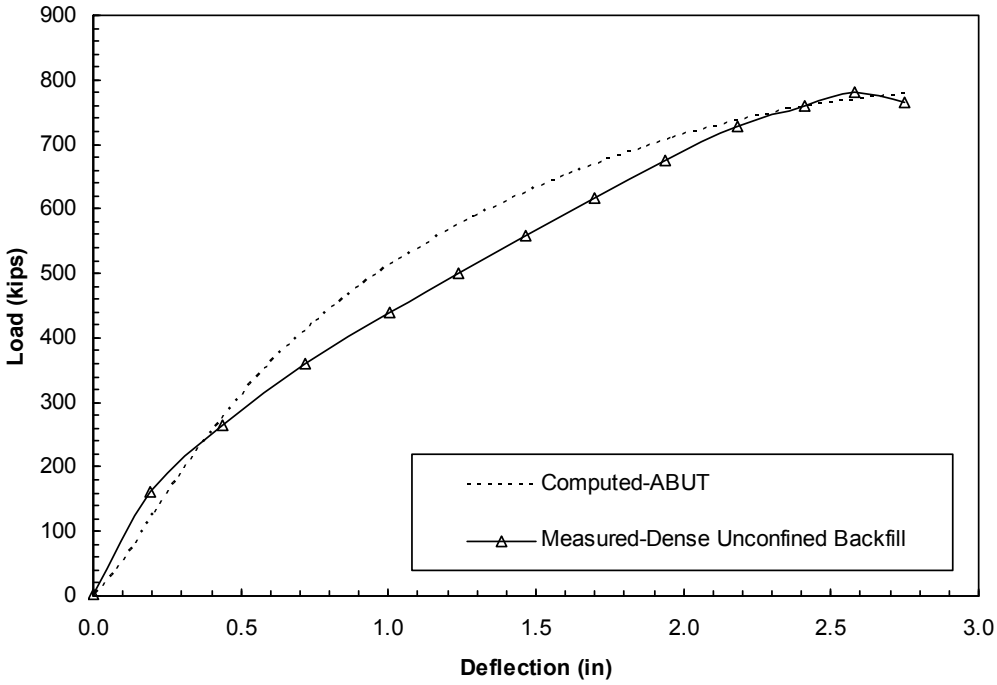

Figure 10-8: Measured load-displacement curve along with ABUT calculated best fit curve for the unconfined backfill test.

The best fit friction angle is 1.4° lower than the measured triaxial value. The values used for ε_{50} and R_f lie higher for the former and lower for the latter of the presumptive values from Shamsabadi et al (2007). The value of ε_{50} used is just outside the ranges recommended in Shamsabadi et al (2007), as shown in Table 2-1, which stretches the computed curve horizontally providing a better fit with the measured curve.

Figure 10-9 shows the measured load-displacement curves compared with the ABUT calculated values using the presumptive value of ε_{50} and the measured triaxial friction angle. The ultimate passive resistance predicted using the triaxial friction angle in this case is about 20% higher than the measured results, and the predicted load-displacement curve arches significantly above the measured curve.

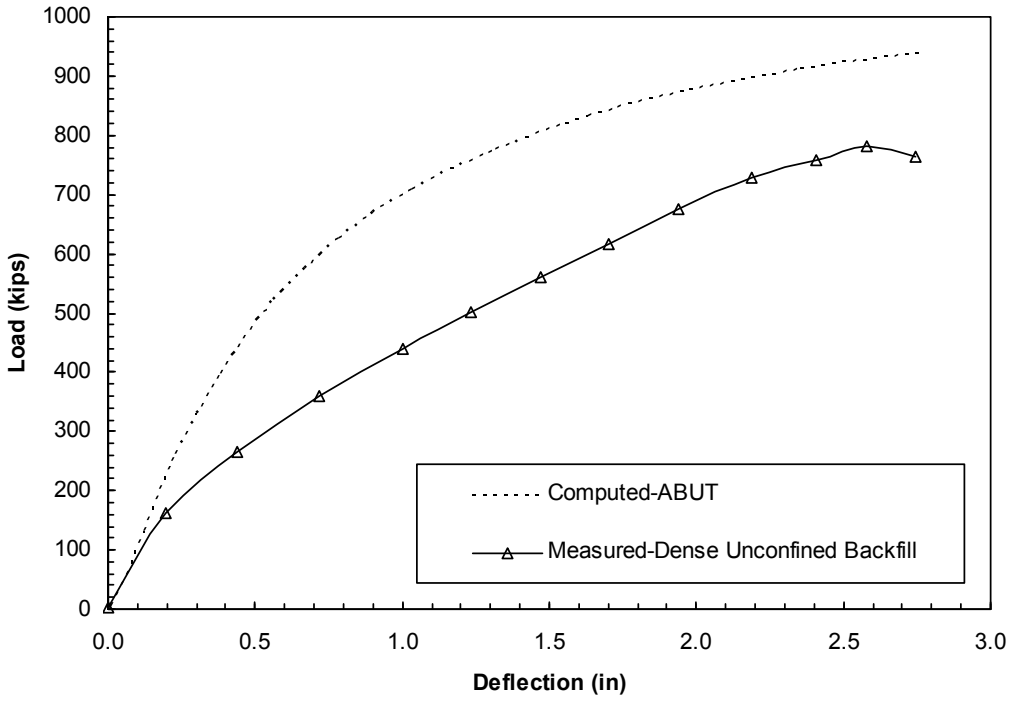

Figure 10-9: Measured load-displacement curve with ABUT calculated presumptive curve for the unconfined backfill test.

The best fit values for the plane strain test are shown in Figure 10-10. Here the values of ε_{50} and R_f are still higher and lower, respectively, than the presumptive values, and ε_{50} is farther outside the range recommended by Shamsabadi et al (2007) as shown in Table 2-1. To obtain reasonable agreement with the measured curve it was necessary to increase the friction angle by a factor of 1.18 times the angle used to obtain best fit curve for the unconfined backfill case. This factor is at the upper end of the range for $\varphi_{ps}/\ \varphi_{triax}$ values and produces a friction angle 1.6° higher than that used for the plane strain calculations with the PYCAP program.

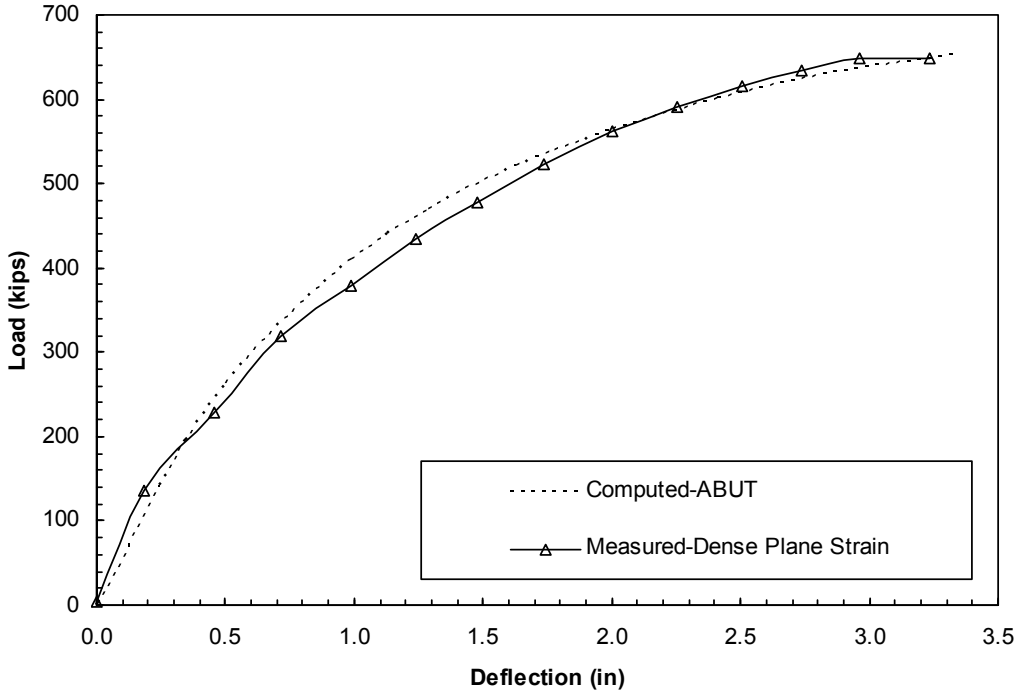

Figure 10-10: Measured load-displacement curve along with ABUT calculated best fit curve for the plane strain test.

Figure 10-11 shows the measured load-displacement curve along with the ABUT calculated curve using the presumptive value of ε_{50}. The friction angle used in this figure is the triaxial friction angle increased by 12% to obtain the plane strain friction angle. The ultimate passive resistance is under predicted using the presumptive values, but the initial stiffness is greater than that which was measured.

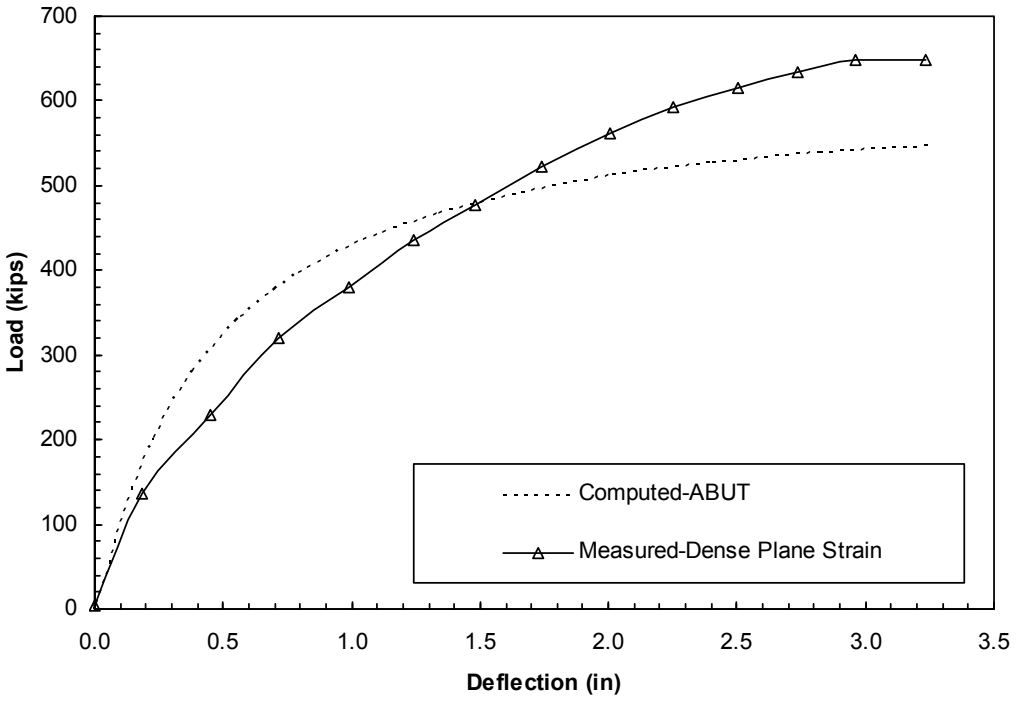

Figure 10-11: Measured load-displacement curve along with ABUT calculated presumptive curve for the plane strain test.

The ABUT input values used for MSE tests 1 and 2 are shown in Table 10-6 and Table 10-7, respectively. Values are shown for best-fit and presumptive inputs in both tables. The measured load-displacement curve is compared with the curve computed with the best fit values for MSE test 1 in Figure 10-12. The value used for ε_{50} is about 2.5 times higher than the presumptive value based on the ranges recommended in Shamsabadi et al (2007), while the R_f is

somewhat lower than recommended. The best fit friction angle (49°) is somewhat smaller than the plane strain friction angle back-calculated from the plane strain (2D) test (49.9°) using ABUT, but still substantially higher than the back-calculated triaxial friction angle from the unconfined backfill case (42.1°). Figure 10-13 shows the measured load-displacement curve along with the ABUT calculated load-displacement curve using the presumptive value of ε_{50} and a friction angle of 48°. While the computed ultimate passive resistance in this instance is in good agreement with the measured value, the load-displacement curve is arched high above the measured results.

Table 10-6: ABUT Input Values, MSE 1

	MSE 1	
	Best Fit Values	Presumptive Values
Internal Friction Angle, φ	49	49
Wall Friction Angle, δ	35.3	35.3
Cohesion (ksf)	0.06	0.06
Adhesion (ksf)	0.06	0.06
Soil Weight, γ (kcf)	0.1287	0.1287
ε_{50}	0.009	0.0035
Failure Ratio, R_f	0.91	0.965
Poisson Ratio, ν	0.23	0.23
Surcharge	0	0
Wall Height, H (ft)	5.5	5.5
Wall Width, W (ft)	11.0	11.0

Table 10-7: ABUT Input Values, MSE 2

	MSE 2	
	Best Fit Values	Presumptive Values
Internal Friction Angle, φ	48	48
Wall Friction Angle, δ	34.56	34.56
Cohesion (ksf)	0.06	0.06
Adhesion (ksf)	0.06	0.06
Soil Weight, γ (kcf)	0.12882	0.12882
ε_{50}	0.009	0.0035
Failure Ratio, R_f	0.91	0.965
Poisson Ratio, ν	0.23	0.23
Surcharge	0	0
Wall Height, H (ft)	5.5	5.5
Wall Width, W (ft)	11.0	11.0

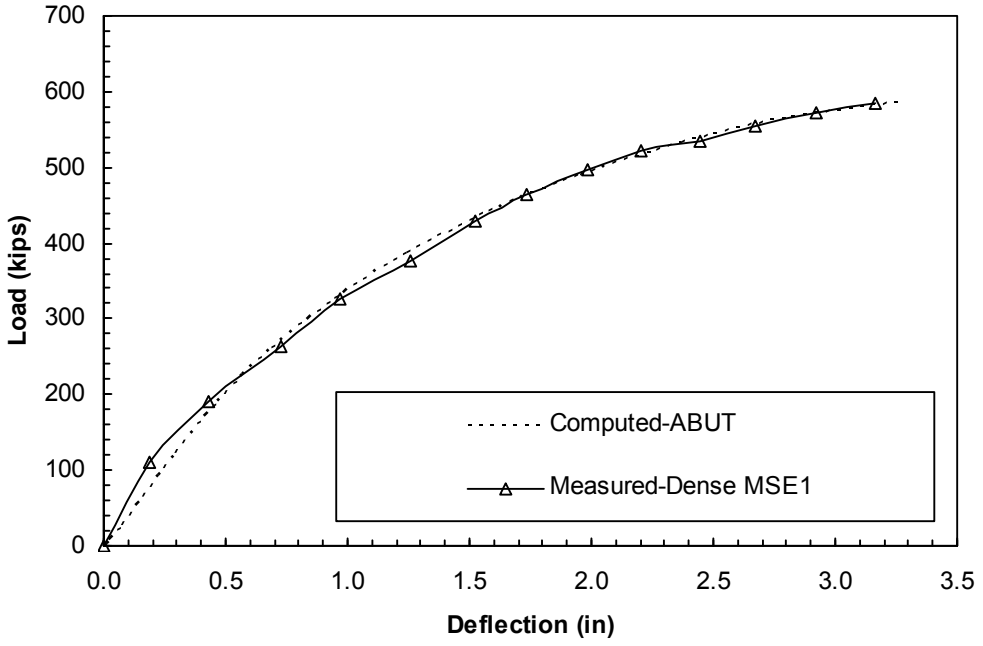

Figure 10-12 Measured results versus ABUT calculated best fit, MSE 1

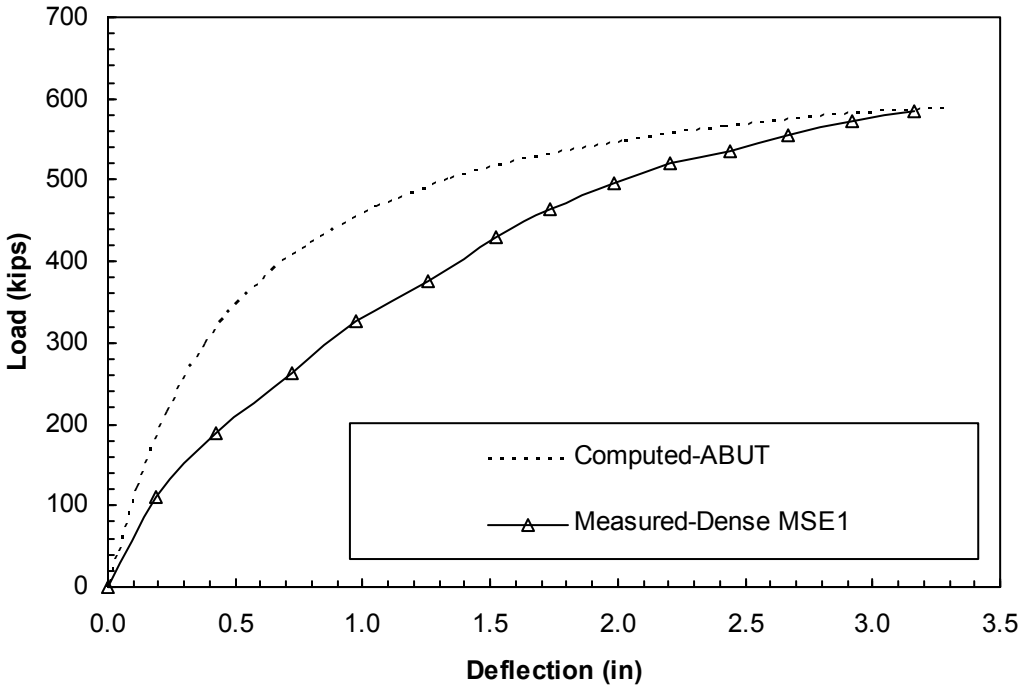

Figure 10-13: Measured results versus ABUT calculated presumptive values, MSE 1.

Similar trends were observed for the results obtained for MSE test 2. Figure 10-14 presents the measured load-displacement curve along with the curve computed by ABUT using back-calculated best fit values. Figure 10-15 provides the measured load-displacement curve calculated by ABUT using the presumptive values. Once again the best fit ε_{50} value was 2.5 times higher than the recommended value and the best fit friction angle (48°) was somewhat lower than the plane strain friction angle (49.9°) back-calculated from the plane strain test by ABUT. Therefore, both ABUT and PYCAP indicate that a friction angle greater than the triaxial friction angle but slightly less than the plane strain is required to match the measured load-displacement curves. This appears to be a result of the "plane strain" geometry imposed by the MSE wing walls.

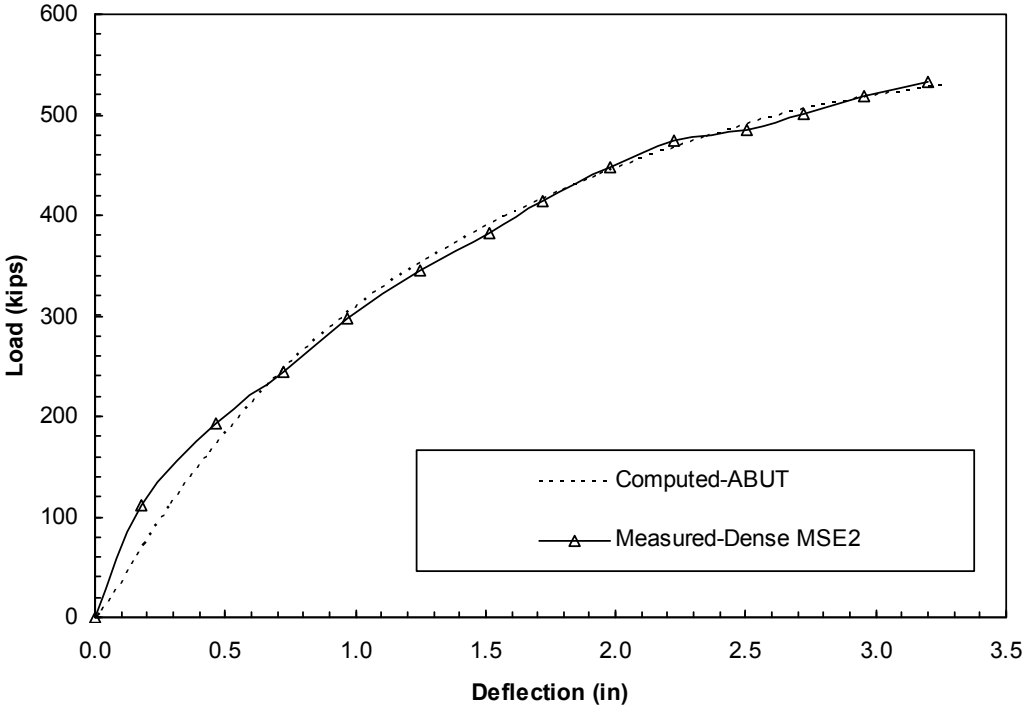

Figure 10-14: Measured results versus ABUT calculated best fit values, MSE2.

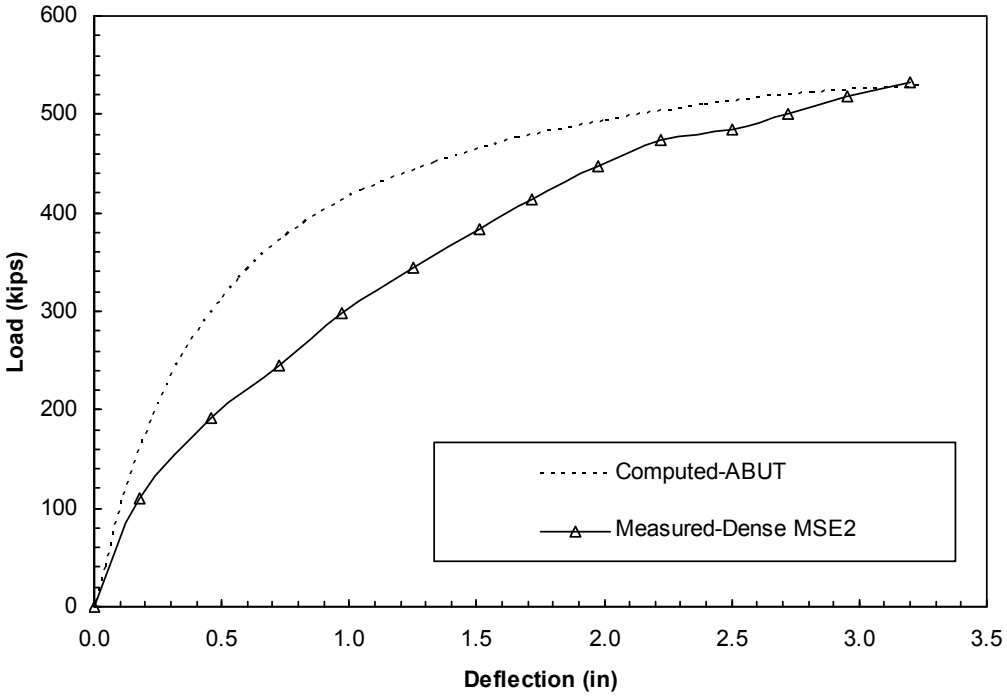

Figure 10-15: Measured results versus ABUT calculated presumptive values, MSE 2.

11 Conclusions

This thesis presents the results of a series of lateral load tests on a full-scale pile cap with dense backfill soil conditions and varying constructed setups, namely: unconfined (full width), plane strain (slip planes), and two MSE setups with varying factors of safety. This chapter lists the conclusions drawn and recommendations based on the analysis of the test results. They are as follows.

1. When an abutment backfill is confined with an MSE wall with a reasonable factor of safety against pull-out (FS=1.5 to 2.0), the passive force geometry approaches that of a 2D or plane strain configuration.
2. Limiting the backfill width with a longitudinal MSE wingwall decreases the ultimate passive resistance of the backfill; however, confining the backfill in a plane strain configuration increases the passive resistance per unit width above that for an unconfined backfill loading.
3. Passive resistance in the presence of MSE wingwalls can be calculated with reasonable accuracy using a log-spiral approach, such as that employed in the computer programs PYCAP or ABUT; however, the plane strain friction angle must be used. The plane strain friction angle is typically 7 to 14% higher (3° to 6°) than the triaxial friction angle and leads to a significant increase in computed passive force. The authors recommend using a log-spiral approach to determine the passive resistance of an abutment confined with MSE wingwalls, with a

friction angle 5% higher than the triaxial friction angle. The authors also recommend considering possibility of additional load on wall-reinforcement connections.

4. As the abutment wall is pushed longitudinally into the backfill soil a transverse pressure is induced on the MSE wingwalls. The transverse pressure on the MSE wing wall panels decreases as distance from the pile cap increases and can be computed as a function of the passive pressure on the backwall of the abutment.
5. The transverse force on the wall can cause the MSE reinforcements to pull-out from the soil. Based on the measurements in these tests, the FHWA MSE design manual (NHI, 2001) provided reasonable estimates of pullout resistance of bar mats in the dense sand.

REFERENCES

American Association of State Highway and Transportation Officials (AASHTO) (2010). *LRFD Bridge Design Specifications*, 5th Ed., AASHTO, Washington, D.C., Section 3: Loads and Load Factors, 100-105

AASHTO (2009). *Guide Specifications for LRFD Seismic Bridge Design*, 1st Ed., AASHTO, Washington, D.C.

Bathurst, R. J., Nernheim, A., and Allen, T. M. (2009). "Predicted loads in steel reinforced soil walls using the AASHTO simplified method." *Journal of Geotechnical and Geoenvironmental Engineering*, 177

Brinch Hansen, J. (1966). "Resistance of a rectangular anchor slab." *Bull. No. 21*, Danish Geotechnical Institute, Copenhagen, 12-13.

Caltrans (2004). *Seismic Design Criteria*. Caltrans, Sacramento, CA, Section 7: Design, 28-30.

Christensen, D. S. (2006). "Full scale static lateral load test of a 9 pile group in sand." M.S. thesis, Dept. of Civil and Environ. Eng., Brigham Young Univ., Provo, UT.

Cole, R. T., Rollins, K. M. (2006). "Passive earth pressure mobilization during cyclic loading." *J. Geotech. Geoenviron. Eng.*, 132(9), 1154-1164.

Cummins, C. R. (2009). "Behavior of a full-scale pile cap with loosely and densely compacted clean sand backfill under cyclic and dynamic loadings." M.S. thesis, Dept. of Civil and Environ. Eng., Brigham Young Univ., Provo, UT.

Das, B. M. (2006). *Principles of Geotechnical Engineering, Sixth Edition*, Thompson.

Douglas, D. J., Davis, E. H. (1964). "The movement of buried footings due to moment and horizontal load and the movement of anchor plates." *Geotechnique*, London, 14(2), 115-132.

Duncan, J. M., Mokwa, R. L. (2001). "Passive earth pressures: theories and tests." *J. Geotech. Geoenviron. Eng.*, 127(3), 248-257.

Heiner, L., Rollins, K. M., Gerber, T. G. (2008). "Passive force-deflection curves for abutments with MSE confined approach fills." *Proc., 6th National Seismic Conference on Bridges and Highways (6NSC)*, Federal Highway Administration (FHWA), Charleston, SC.

Kulhawy, F. H., Mayne, P. W. (1990). *Manual on Estimating Soil Properties for Foundation Design*, Electric Power Research Inst. (EPRI), Palo Alto, CA, Section 4: Strength, 12-14.

Ladd, C. C., Foott, R., Ishihara, K., Schlosser, F., Poulos, H. G. (1977). "Stress-deformation and strength characteristics." *Proc., 9th International Conference on Soil Mechanics and Foundation Eng. (ICSMFE)*, ISSMFE, Tokyo, Vol. 2, 421-494.

Lee, K. L., Singh, A. (1971). "Relative Density and Relative Compaction." *J. Soil Mechanics and Foundations Division*, 97(7), 1049-1052.

Maroney, B. (1995). "Large scale bridge abutment tests to determine stiffness and ultimate strength under seismic loading." Ph.D. dissertation, Univ. of Cal., Davis, CA.

Mitchell, J. K., and Villet, W. C. B., (1987). "Reinforcement of Earth Slopes and Embankments." *NCHRP Report 290, Transportation Research Board*, Washington, DC.,

Mokwa, R. L., Duncan, J. M. (2001). "Experimental evaluation of lateral-load resistance of pile caps." *J. Geotech. Geoenviron. Eng.*, 127(2), 185-192.

National Highway Institute (NHI), FHWA, (2001). *Mechanically Stabilized Earth Walls and Reinforced Soil Slopes Design and Construction Guidelines*. NHI, FHWA, Washington, D. C.

Peterson, K. T. (1996). "Static and dynamic lateral load testing of a full-scale pile group in clay." M.S. thesis, Dept. of Civil and Environ. Eng., Brigham Young Univ., Provo, UT.

Potyondy, J. G. (1961). "Skin friction between various soils and construction materials." *Geotechnique*, London, 11(1), 339-353.

Rollins, K. M., Cole, R. T. (2006). "Cyclic lateral load behavior of a pile cap and backfill." *J. Geotech. Geoenviron. Eng.*, 132(9), 1143-1153.

Rollins, K. M., Sparks, A. (2002). "Lateral resistance of full-scale pile cap with gravel backfill." *J. Geotech. Geoenviron. Eng.*, 128(9), 711-723.

Romstad, K., Kutter, B., Maroney, B., Vanderbilt, E., Griggs, M., Chai, Y. H. (1996). "Longitudinal strength and stiffness behavior of bridge abutments." Dept. of Civil and Environ. Eng., Univ. of Cal., Davis, CA.

Rowe, P. W. (1969). "The relation between the shear strength of sands in triaxial compression, plane strain and direct shear." *Geotechnique*, London, 19(1), 75-86.

Shamsabadi, A., Rollins, K. M., Kapuskar, M. (2007). "Nonlinear soil-abutment-bridge structure interaction for seismic performance-based design." *J. Geotech. Geoenviron. Eng.*, 133(6), 707-720.

Shamsabadi, A., Yan, L. (2008). "Closed-form force-displacement backbone curves for bridge abutment-backfill systems." *Proc., Geotech. Earthquake Eng. and Soil Dynamics (GEESD) IV*, ASCE, Reston, VA, 1-10.

Snyder, J. L. (2004). "Full-scale lateral load tests of a 3x5 pile group in soft clays and silts." M.S. thesis, Dept. of Civil and Environ. Eng., Brigham Young Univ., Provo, UT.

Strassburg, A. N. (2010). "Influence of Relative Compaction on Passive Resistance of Abutments with Mechanically Stabilized Earth (MSE) Wingwalls." M.S. thesis. Dept. of Civil and Environ. Eng., Brigham Young Univ., Provo, UT.

U.S. Navy (1982). *Foundations and Earth Structures Design Manual 7.2*, Dept. of the Navy, Naval Facilities Engineering Command (NAVFAC), Alexandria, VA.